PART I

ELECTRIC BIREFRINGENCE STUDIES OF DEOXYRIBONUCLEIC ACIDS

PART II

SELECTIVE DISSOCIATION OF NUCLEOHISTONE COMPLEXES

Thesis by

Heiko H. Ohlenbusch

In Partial Fulfillment of the Requirements

For the Degree of

Doctor of Philosophy

California Institute of Technology

Pasadena, California

1966

(Submitted December 10, 1965)

Dedicated to

Janet

and

Mr. and Mrs. Thomas E. McKnight

Acknowledgements

Throughout the years of my studies at Caltech under the patient guidance of Prof. Norman Davidson, I have become deeply indebted to his advice and suggestions. My association with him and his research group has been highly rewarding to me through the enthusiasm and cooperation, which have been a constant moral support.

Concerning the work described in part I, I should like to acknowledge the contributions of Mr. Richard Jones in the construction of the electronic system for the birefringence apparatus, and of Dr's W. F. Dove, R. F. Stewart and R. H. Jensen for their donation of DNA samples. Special thanks is due Dr. W. Huber for his discussions concerning some of the theoretical aspects of electric birefringence. I wish to thank Prof. C. T. O'Konski of the Department of Chemistry of the Univeristy of California (Berkeley) for communicating their research findings before publication and for sending us the design of his quarter wave prism.

The studies presented in the second part of this thesis were carried out in close cooperation with the research staff of Prof. James Bonner. Their previous investigations stimulated the present work of the dissociation behavior of nucleohistones. The studies would not have been con-

cluded so quickly, had it not been for the invaluable contributions made by Dr. Ru-Chih C. Huang, who furnished most of the nucleohistone samples and who performed the biological assays, and Mr. Douglas Fambrough, Jr., who constructed the Amberlite column and instructed me in its operation.

Furthermore, I should like to express my indebtedness to Mr. Baldomero M. Olivera for his contributions to the characterization of the nucleohistone samples by electrophoresis and melting behavior.

Aside from the more tangible evidence of the close collaboration which made this work possible, I should like to acknowledge the constructive criticism and fruitful discussions by all those, who contributed to this work. In this regard I am especially thankful to Professor James Bonner.

Abstract

Part I

The electric birefringence of dilute DNA solutions has been studied in considerable detail and on a large number of samples, but no new and reliable information was discovered concerning the tertiary structure of DNA. The large number of variables which effect the birefringence results is discussed and suggestions are made for further work on the subject.

The DNA molecules have been aligned in a rapidly alternating (10 to 20 kc/sec) square wave field confirming that the orientation mechanism is that of counterion polarization. A simple empirical relation between the steady state birefringence, Δn_{st}, and the square of the electric field, E, has been found: $\Delta n_{st} = E^2/(a\,E^2 + b)$, where $a = 1/\Delta n_s$ and $b = (E^2/\Delta n_{st})_{E \to o}$. Δn_s is the birefringence extrapolated to infinite field strength.

The molecules show a distribution of relaxation times from 10^{-4} to 0.2 sec, which is consistent with expectations for flexible coil molecules. The birefringence and the relaxation times decrease with increasing salt concentrations. They also depend on the field strength and pulse duration

in a rather non-reproducible manner, which may be due in part to changes in the composition of the solution or in the molecular structure of the DNA (other than denaturation). Further progress depends on the development of some control over these effects.

Abstract

Part II

The specificity of the dissociation of reconstituted and native deoxyribonucleohistones (DNH) by monovalent salt solutions has been investigated. A novel zone ultracentrifugation method is used in which the DNH is sedimented as a zone through a preformed salt gradient, superimposed on a stabilizing D_2O (sucrose) density gradient. The results, obtained by scanning the quartz sedimentation tubes in a spectrophotometer, were verified by the conventional, preparative sedimentation technique. Procedures are discussed for the detection of microgram quantities of histones, since low concentrations must be used to prevent excessive aggregation of the DNH.

The data show that major histone fractions are selectivly dissociated from DNH by increasing salt concentrations: Lysine rich histone (H I) dissociates gradually between 0.1 and 0.3 F, slightly lysine rich histone (H II) dissociates as a narrow band between 0.35 and 0.5 F, and arginine rich histone (H III, H IV) dissociates gradually above 0.5 F $NaClO_4$.

The activity of the partially dissociated, native DNH in sustaining RNA synthesis, their mobility and their unusual heat denaturation and renaturation behavior are described. The two-step melting behavior of the material indicates that the histones are non-randomly distributed along the DNA, but the implications are that the uncovered regions are not of gene-size length.

TABLE OF CONTENTS

TABLE OF CONTENTS

I. Introduction

The work presented in the first part of this dissertation was undertaken to determine the feasibility of using electric birefringence to measure molecular parameters of deoxyribonucleic acids (DNA) in dilute salt solutions. The need for new methods to study the behavior of DNA in solution exists despite Watson and Crick's proposal of a detailed structure for the DNA molecule more than a decade ago (1).

This structure, deduced from X-ray scattering of semicrystalline DNA, describes the primary and secondary configuration of DNA as a basepaired double helix in sufficient detail, but does not shed much light on its overall configuration (tertiary structure) in solutions, which might conceivably be influenced by infrequent single strand breaks or other as yet undetected interruptions of the secondary structure (2). Or it may be, that the observed flexibility of the DNA double strand is a direct result of an intrinsic non-rigidity of the helix.

The results of the investigation were disappointing, in that no new and reliable information was discovered concerning the tertiary structure of DNA. Nevertheless,

we believe that electric birefringence does have promise of ultimate utility and are therefore setting forth our results in considerable detail for the benefit of future workers.

In addition, the results include many suggestions of possibly interesting differences between one DNA sample and another, which will yield structurally significant information, once more reproducible and confirmable results can be obtained. For the benefit of those readers who do not wish to peruse the detailed description, a brief summary is presented here:

Native DNA molecules in solutions at low concentration can be oriented in an electric field. They show the expected negative birefringence. The molecules can be aligned in a rapidly (10 to 20 kc/sec) alternating square wave field. They do not reorient if the field is rapidly reversed, showing that the orientation mechanism is that of counterion polarization.

The birefringence is a function of the square of the electic field, which can be approximated by a simple empirical equation (Eqn. 21).

The molecules show a distribution of relaxation times from about 10^{-4} to close to 0.2 sec. The observed complex relaxation behavior is consistent with expectations for flexible coil molecules.

The birefringence and the relaxation times decrease with increasing salt concentration in a fairly reproducible way.

The distribution of relaxation times is a function of field strength, but rather non-reproducible results were obtained in the investigation of this variable. There are suggestions of differences between bacterial DNA's and Calf Thymus and viral DNA's with regard to this property and also with regard to melting behavior as observed by electric birefringence.

It is believed that some of the observed non-reproducibility is due to effects of the electric field pulses themselves in causing changes in the composition of the solution and in the state of aggregation or in the molecular structure of the DNA. Further progress depends on the development of some control over these effects.

II. Electric Birefringence

In recent years, electric birefringence has been used to determine electrical, optical and structural parameters characterizing polyionic macromolecules in solution (3). These studies have shown that rod-like polyelectrolytes like Tobacco Mosaic Virus (TMV) (4) are easily oriented in strong electric fields due to their large electric polarizability. Several investigators have studied the electric birefringence of dilute DNA solutions (5) and found that orientation in electric fields is possible.

The advantages which this method offers are its sensitivity to small changes in the length of rod-like particles, the small amount of sample required for experiments, and the fact that external forces are applied for only a fraction of a second, thus minimizing breakdown and uncontrolled structural changes of delicate molecules like DNA.

In order to understand this phenomenon and to analyze the experimental data, it is necessary to clearly distinguish the three basic, simultaneously occurring phenomena - optical anisotropy, electric polarizability and orientation-disorientation - which make electric birefringence possible.

1. Optical Anisotropy

A material is optically anisotropic, if it exhibits different optical properties along different directions relative to the direction of light propagation, due to differences in optical polarizabilities along these directions. An easily measurable quantity related to this optical anisotropy is the birefringence, defined by $\Delta n = n_{\parallel} - n_{\perp}$. Here $n_{\parallel}$ and $n_{\perp}$ are the refractive indices along the parallel and perpendicular directions relative to a specific direction, in our case the direction of the electric field which is used to align the molecules.

Langevin (6), Born (7), Gans (8), and Peterlin and Stuart (9) were the first to treat the optical anisotropy, Δg, of macromolecules theoretically. A simplified version of the derivation of the Peterlin-Stuart relation shows that the theoretical equation

$$\Delta g = \frac{\beta_{\parallel} - \beta_{\perp}}{\bar{v}} \qquad (1a)$$

gives rise to the following relation (Appendix I):

$$\Delta g = \frac{3\, n\, \Delta n_s}{(n^2 + 2)\, 2\pi\, \sigma_v} \qquad (1b)$$

Here β = optical polarizability, $\bar{v}_1$ = molecular volume of the solute, n = refractive index of the solution, C_v = volume fraction of anisotropic molecules and Δn_s = birefringence at infinite field strength, an experimentally measurable quantity.

The fact that the birefringence of DNA is negative ($n_\perp > n_\parallel$) is a result of the optical anisotropy and the mode of alignment of the DNA. Since the optical polarizability varies with the strength of binding of an electron cloud, it is expected that the optical polarizability parallel to the base pairs of DNA is larger than that perpendicular to them. It is mainly by virtue of the stacking of base pairs, which causes a difference in the optical properties between any direction perpendicular to the molecular axis (cylindrical symmetry) and that parallel to it, that the DNA molecule is an optically anisotropic substance. Light waves vibrating parallel to this axis experience a smaller change in velocity (have a lower refractive index) than those vibrating perpendicularly. Thus, alignment of the DNA with its axis parallel to the electric field will result in negative birefringence (Eqn. 1a with $\beta_\perp > \beta_\parallel$).

In order to determine the amount of birefringence of an anisotropic medium it is best to use monochromatic light, which is plane polarized at 45° to the molecular axis. Such light will have equal vectors parallel and perpendicular to this axis. If a phase difference δ develops in the medium, as a result of differences in refractive indeces, the emerging light vectors will add up to give elliptically polarized light, which can be thought of as a superposition of two perpendicular harmonic vibrations, 90° out of phase.

In order to determine the degree to which the emerging light is elliptically polarized, indicating the birefringence of the medium, a quarter wave prism and an analyzer prism are used. The quarter wave prism introduces a 90° shift of one of the vectors of the elliptically polarized light and brings both vectors into phase with each other, thus creating plane polarized light again, which, however, will be turned by a certain angle $\delta/2$ from the original 45° plane. This angle is a function of the ellipticity of the light and is therefore related to the birefringence of the molecules in solution:

$$\Delta n = \lambda \delta / 2 \, l \, \pi \qquad (2)$$

Here λ is the wavelength of the incident light and l is the light path through the birefringent medium. The angular displacement $\delta/2$ may be clockwise or counterclockwise. Looking against the light source such shifts are regarded as

positive or negative birefringence respectively.

However, instead of measuring this angle by means of turning the analyzer prism to the new extinction position, it is less time-consuming to keep the analyzer at a predetermined position and to measure the change of intensity of the transmitted light.

In order to find in this stationary setup the sign of the birefringence, indicating which vector had been retarded or accelerated, the analyzer is moved a few degrees off the crossed position. If the analyzer prism is moved counterclockwise (looking against the light source) and the birefringence is positive, a decrease in the intensity of the transmitted light would be observed. If it were negative, the intensity would increase.

2. Determination of the Birefringence

In appendix II a relation between the light signal transmitted, I_A, and the phase difference, δ, due to the birefringent medium is derived, giving

without quarterwave prism:

$$I_A = I_o[\sin^2\beta + \sin^2(\delta/2)(1 - 2\sin^2\beta)] \qquad (3)$$

and with quarterwave prism:

$$I_A = (I_o/2)(1 - \sin 2\beta \sin\delta \cos\phi - \cos 2\beta \cos\delta). \qquad (4)$$

Here I_o is the incident light intensity, β the angle by which the analyzer prism is offset from the crossed position and ϕ an angle correcting for an imperfect quarterwave prism. In case ϕ is close to zero, which holds for a well designed quarterwave prism, equation (4) reduces to

$$I_A = (I_o/2)\left[1 - \cos(2\beta - \delta)\right]. \qquad (5)$$

Since only the change in transmitted light intensity, I_δ, is measured, which results from the birefringence of the solution after the field is turned on, a more convenient form of equation (4) is given by

$$\frac{I_\delta}{I_{A_o}} = \frac{\cos 2\beta(1 - \cos\delta) - \sin 2\beta \sin\delta \cos\phi}{2\sin^2\beta} \qquad (6)$$

where I_{A_o} is the transmitted signal before application of the electric field corrected for the stray light, I_s, at extinction. A plot of I_δ / I_{A_o} versus δ (Fig. 1) is used to convert the measured intensities into δ.

The angle β determines the amount of transmitted light, I_{A_o}, according to the relation

$$I_{A_o} = I_o \sin^2\beta. \tag{7}$$

The imperfection of the quarterwave prism, ϕ, can be calculated from

$$I_A = \frac{I_o}{2}[1 + \sin\phi\,(2\sin^2\beta - 1)] \tag{8}$$

by letting $\beta = 0^\circ$ or 90°, for which

$$\sin\phi = \frac{2\,I_A}{I_o} - 1 \quad \text{or} \quad \sin\phi = 1 - \frac{2\,I_A}{I_o} \tag{9}$$

respectively.

By minimizing the difference between the minimum and maximum transmitted light signal, the quarterwave prism can be set to its optimum position. The intensities at this optimum position are then used to calculate ϕ. The ϕ's for several Polaroid quarterwave plates and a prism were determined. They range from 31.4° for the plates to $10.1 \pm 2.7^\circ$ for the prism which we designed.

Figure 1

Plot of the intensity ratio, I_δ/I_{A_o}, versus the negative phase difference, δ^o, due to birefringence (Eqn. 6 with $\beta = +10^o$, $\phi = 0^o$).

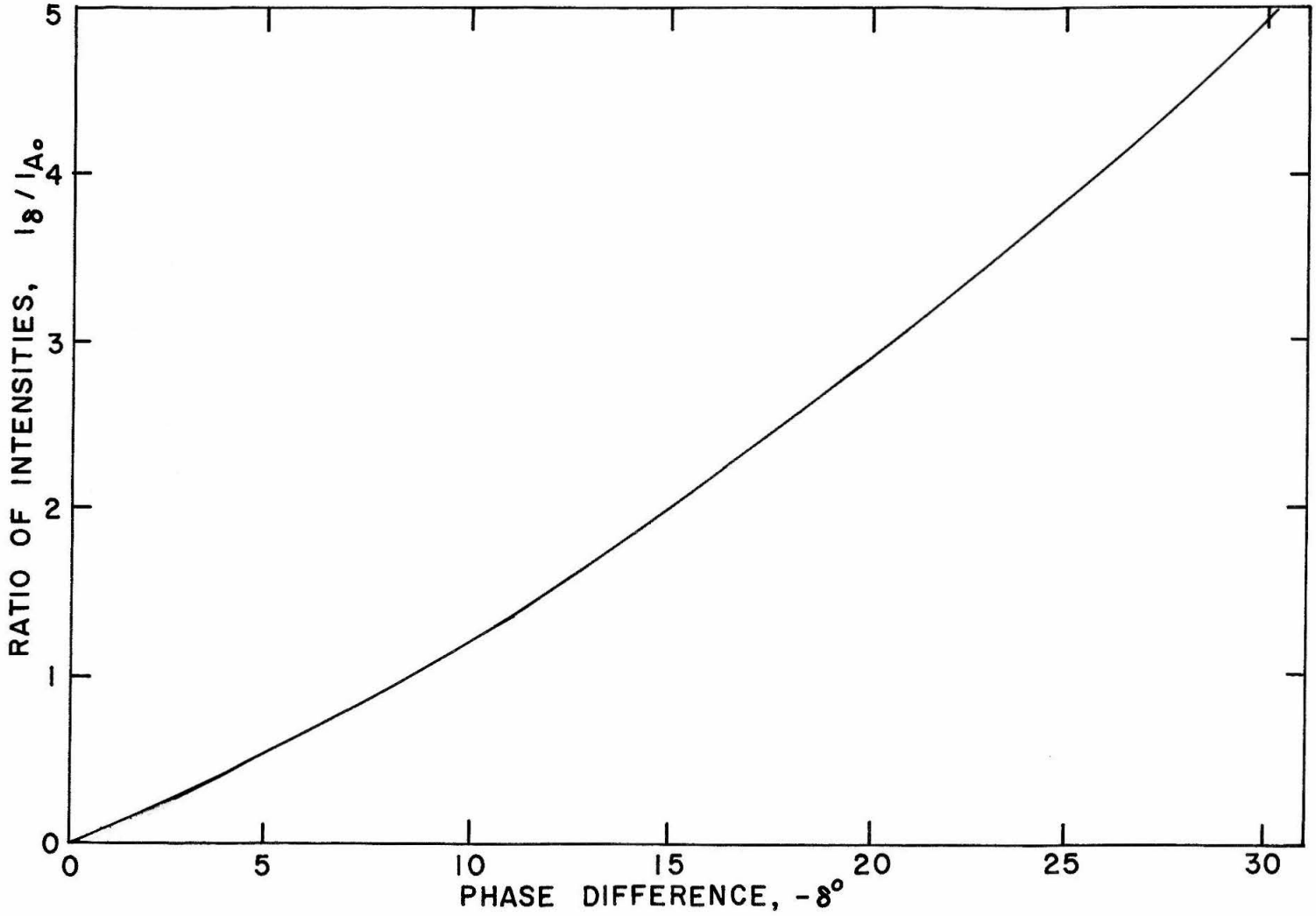
RATIO OF INTENSITIES, I_δ / I_{A_o}
0
1
2
3
4
5
0
5
10
15
20
25
30
PHASE DIFFERENCE, $-\delta^\circ$

Figure 1

Finally, in order to eliminate ϕ altogether, a prism designed by O'Konski (see Appendix III) was used, which could be adjusted so as to make the imperfection essentially zero.

3. Electric Polarizability

Experimentally it is as yet impossible to measure the optical anisotropy of a single molecule and therefore some means of alignment of a large collection of DNA molecules must be used. To this end concentrated DNA preparations have been drawn into fibers (10) or aligned by streaking between glass slides (11). DNA molecules in dilute solutions have been oriented in flow systems by means of hydrodynamic forces (12) or in an electric field (5).

Due to the rather high charge density of the DNA polyion (two negative charges per base pair every 3.4 Å), a dense counterion atmosphere is formed at the polymer surface, and the ions have sufficient mobility to move along the surface of the polymer in response to an external electric field. This in turn causes the polyions to be oriented along the field direction, just as for dipoles.

Thus, the alignability of DNA in solution by an electric field is a consequence of an induced charge distribution along the polyion surface, expressed as electric polarizability, α. According to an equation due to Maxwell (13) for long conducting ellipsoids of rotation, the magnitude of the electric polarizability is proportional to the third power of the particle length, l:

$$\alpha_{\parallel} = f(\epsilon_{\parallel}, P) \frac{\epsilon_o l^3}{24 \ln(2P)} \qquad (10)$$

where P is the ratio of long to short dimension of the polymer, ϵ_o the dielectric constant of the solvent and

$$f(\epsilon_{\parallel}, P) = \frac{\epsilon_{\parallel} \ln(2P)}{\epsilon_o P^2 + \epsilon_{\parallel} \ln(2P)}, \qquad (10a)$$

which equals unity under the assumption of completely free movement of charges along the ellipsoid (metallic conductor).

The equation for $\alpha_{\parallel}$ further assumes, that diffusion effects for the mobile charges are negligible and that, due to the l^3 factor, the induced dipole along the main axis is so large compared to that of the small axis, that the polarizability perpendicular to the field can be neglected. Thus, $\alpha_{\parallel}$ is the upper limit for the polarizability.

The energy of interaction of an induced dipole with the external electric field is proportional to the square of the field strength, E. Therefore, it should be independent of the sign of the field, which acts as if it were always in the same direction tending to orient the polyions.

Since the charge transfer along the polyion surface is rapid enough (about 10^{-5} sec), alternating fields of up to 10 kc/sec can be used for alignment of the molecules.

which takes place in about 10^{-3} sec. This is desirable, for it decreases electrochemical reactions and electrode polarization. A more detailed treatment of the charge transfer along the polyion is given by O'Konski (14).

The orientation of the polyions has, furthermore, the effect of increasing the conductivity along the electric field direction, decreasing it perpendicular to the field. This property of polyions is known as electric anisotropy and was investigated by Eigen and Schwarz (15).

4. Orientation - Disorientation

The changes in molecular parameters related to the size and shape of the DNA molecule become of prime importance in regard to the determination of the degree and mode of structural changes during DNA denaturation. The optical polarizability can give us information with respect to the internal structure of the DNA. Electric polarizability on the other hand is a very sensitive function of the length of the molecule, but it also varies with the dielectric constant of the solvent and the ease of movement of the counterion atmosphere, making its dependence on molecular parameters rather obscure.

However, the rate of orientation of the polyions by the electric field as well as their rate of disorientation as the field is turned off are also sensitive functions of the particle dimensions. Especially the randomization process, which occurs free of electric field effects and is due only to Brownian motion, can be easily related to the rotational diffusion constant, Θ , a parameter which involves the desired structural factors. Exact relations between Θ and the particle structure are of course dependent upon the model chosen. Of the

various relations available (16) we have chosen that of a rigid rod for DNA in want of a better theory for kinked chain or wormlike chain models, which would be more realistic. The relation of Θ to the length, (2a), of a rigid rod was derived by Burgers (16c) and is given by

$$a^3 = \frac{3\,kT}{8\,\pi\,\eta\,\Theta}\left(\ln\frac{2a}{b} - 0.80\right) \qquad (11)$$

where η is the viscosity of the solution and b the radius of the rod. kT has its usual meaning. A plot of 2a versus Θ is shown in figure 2.

Figure 2

A plot of the rotational diffusion coefficient, Θ, versus the length, 2a, of rigid, rod-like molecules (Eqn. 11 with T = 273.16°K, b = 15 Å, n = 0.01792 poise).

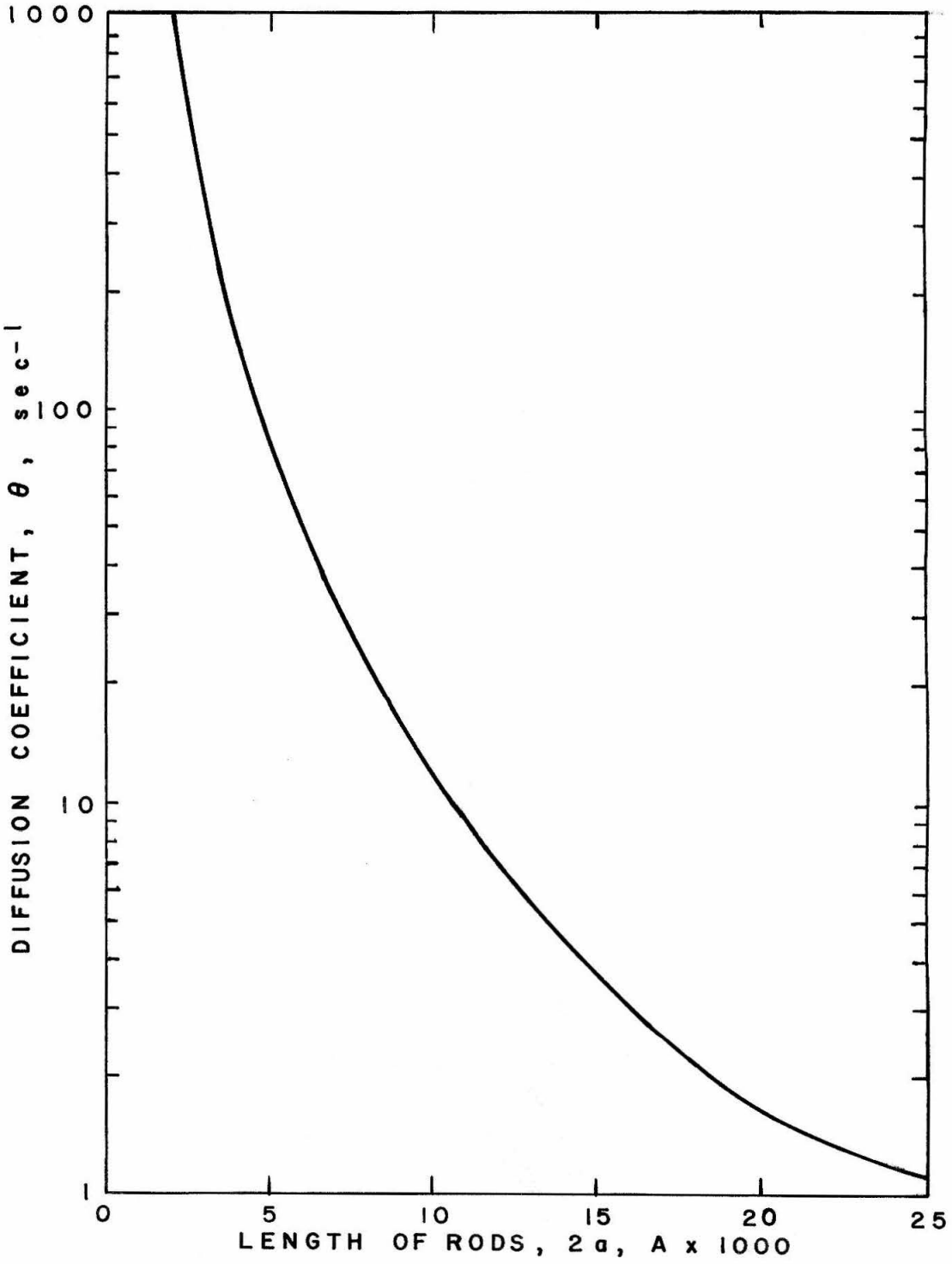
1000
100
10
1
DIFFUSION COEFFICIENT, θ, sec⁻¹
0
5
10
15
20
25
LENGTH OF RODS, 2a, A x 1000

Figure 2

5. Birefringence Theory

Early papers on electric birefringence (17) considered the effect of small fields. Gans (8) considered arbitrarily large fields for pure induced and pure permanent dipole moments, but obtained only a birefringence saturation function for pure permanent dipoles. O'Konski (14) developed a birefringence theory recently for the case of mixed orientation mechanisms, presenting methods of analyzing experimental data.

Three main phases are to be considered:

1. The rise of the birefringence signal due to the orientation of the molecules by the electric field.

2. The steady state, time independent birefringence signal.

3. The decay of the birefringence signal due to Brownian motion alone.

Complications arise, since complete orientation of the polyions cannot be achieved, due to the disorienting effect of Brownian motion. It becomes therefore necessary to extrapolate the data to infinite field strength.

Saturation functions for appropriate models have been calculated. Assuming hydrodynamic, electric and optical axes of symmetry, rigidity of structure, high dilution of the monodisperse polymer, the fundamental orientation distribution function for birefringence has been derived by Peterlin and Stuart (18)

$$\Delta n = \frac{2\pi C_v}{n} (g_{\parallel} - g_{\perp}) \int_0^{\pi} F(\theta) \frac{3\cos^2\theta - 1}{2} 2\pi \sin\theta \, d\theta . \quad (12)$$

This equation relates the birefringence, Δn, to the volume fraction of polyions, C_v, the optical anisotropy factor, Δg, and the angular orientation distribution function $F(\theta)$. The expression after the integral sign is called the orientation factor and θ is the average angle that the polymer axes make with the electric field direction.

Computation of $F(\theta)$ requires an expression for the energy of interaction of the particles with the external electric field, E. O'Konski (14) has calculated this function for the steady state distribution of axially symmetric particles having either a permanent dipole moment along the symmetry axis, an induced dipole moment, or both and has evaluated the orientation factor for this generalized case.

For pure induced dipole orientation, the appropriate mechanism for the alignment of DNA, O'Konski's steady state solutions of the fundamental equations for two limiting cases become:

a) for weak fields ($\Delta\alpha E^2/2 \ll kT$)

$$\left(\frac{\Delta n_{st}}{\Delta n_s}\right)_{E\to o} = \frac{\Delta\alpha\, E^2}{15\ kT}\ , \qquad (13)$$

b) for strong fields ($\Delta\alpha E^2/2 \gg kT$)

$$\left(\frac{\Delta n_{st}}{\Delta n_s}\right)_{E\to\infty} = 1 - \frac{3\ kT}{\Delta\alpha\ E^2}\ . \qquad (14)$$

Here, Δn_{st} is the steady state birefringence, $\Delta n_s = \frac{2\pi \Delta g\, C_v}{n}$ is the saturation birefringence, and $\Delta\alpha = (\alpha_{\parallel} - \alpha_{\perp})$ is the electric polarizability.

Thus, knowing C_v and n and having measured the saturation value of the birefringence, we can evaluate the specific Kerr constant

$$K_{sp} \equiv \frac{(\Delta n/E^2)_{E\to o}}{n\, C_v} \tag{15}$$

from equation (13), the optical anisotropy

$$\Delta g \equiv \frac{\Delta n_s\, n}{C_v\, 2\pi} \tag{16}$$

from Δn_s given by equation (14), and the electric polarizability

$$\Delta\alpha = \frac{kT\ 15\ K_{sp}\ n^2}{4\pi\ \Delta g} = \frac{15\ kT}{\Delta n_s} \left(\frac{\Delta n_{st}}{E^2}\right)_{E\to o} \tag{17}$$

from the ratio of equations (15) and (16), and the temperature.

The rise of the birefringence signal with time was first evaluated by Benoit (3a) for the two cases of low and high electric fields. O'Konski (14) derived a relation, which holds for any electric field. If

$$\gamma = 2(\alpha_{\parallel} - \alpha_{\perp})E^2\Theta t/kT \tag{18a}$$

is small, the result is

$$\left(\frac{d\Delta n}{dt}\right)_{t\to o} = \frac{4}{5} \frac{(\alpha_{\parallel} - \alpha_{\perp})\ E^2}{2\ kT}\ \Theta\ \Delta n_s\ . \tag{18b}$$

The molecular parameters are most easily obtained from the field free decay of the steady state birefringence by Brownian motion, which for monodisperse solutions is given by Benoit (3a) as

$$\Delta n/\Delta n_o = e^{-6\Theta t} = e^{-t/\tau} \qquad (19)$$

where Δn_o is the birefringence at the beginning of the disorientation and $\tau = 1/6\Theta$ is the relaxation time. The slope of a plot of $(-1/6)\ \ln(\Delta n/\Delta n_o)$ versus time, t, gives Θ. Figure 3 shows a graph of the particle length of a rigid rod as a function of the experimentally determined ratio $\Delta t/\Delta \log(\Delta n/\Delta n_o)$.

For polydisperse systems the decay depends on the field strength and is not exponential. O'Konski (14) derived the expression for the case where the optical anisotropy is the same for all components disorienting from a saturating field:

$$\frac{\Delta n}{\Delta n_s} = \sum_i \phi_i\ e^{-6\Theta_i t} \qquad (20)$$

where the sum is over all components i, ϕ_i is the volume fraction of component i, and Θ_i its rotational diffusion constant.

In summary, the length of a rigid, rod-shaped polyelectrolyte molecule can be determined from the decay rate of the signal, I_δ/I_{A_o}. Using figure 1, this ratio

Figure 3

Plot of the slope of monodisperse birefringence decay, $\Delta t / \Delta \log(\Delta n / \Delta n_o)$, versus the length, 2a, of rigid, rod-like molecules.

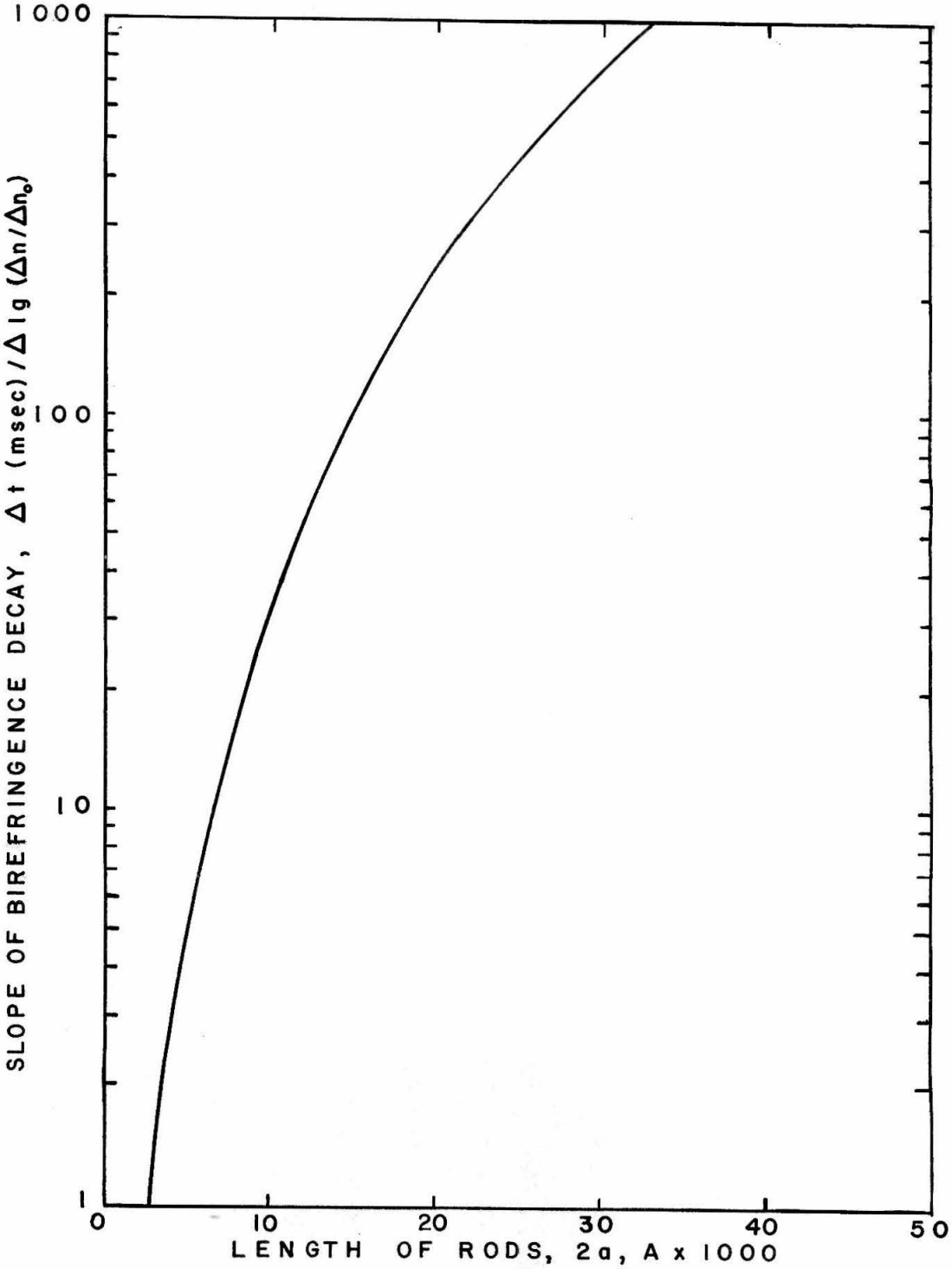
1000
100
10
1
SLOPE OF BIREFRINGENCE DECAY, Δt (msec) / Δ lg (Δn/Δn₀)
0
10
20
30
40
50
LENGTH OF RODS, 2a, A x 1000

Figure 3

is converted to δ. A plot of $-\lg(\delta / \delta_o) = -\lg(\Delta n / \Delta n_o)$ against t, the decay time, should be a straight line for a monodisperse system, and its slope should give the desired length of the particles by means of figure 3.

6. Birefringence Apparatus

The apparatus used to measure the electric birefringence is essentially that described by O'Konski (14). The overall set-up is shown in figure 4 and 6.

a. The Optical System

As light source a Sylvania Concentrated Arc lamp (100 W, DC) was found to be suitable. It was supplied by 54 V DC, which could be regulated by means of a 10 Ohm resistor. The operating voltage was about 15 V at 6.25 amp. A choke facilitated starting of the arc by means of a Tesla coil.

The light beam then passed through a Nivoc biconvex lens (f 100^h, dia. 48^h) which rendered it parallel. Two filters selected the wavelengths around 5250 Å (Fig. 5) and a polarizing prism polarized the light at an angle of 45° to the electric field direction in the birefringence cell containing the DNA solution. The beam then passed through a quartz window into the cell holder and was confined by a slit in front of the birefringence cell to 2 x 1 mm. It passed through the cell and out the other quartz window of the cell holder and through a quarterwave prism, whose fast axis was parallel to the plane of polarization

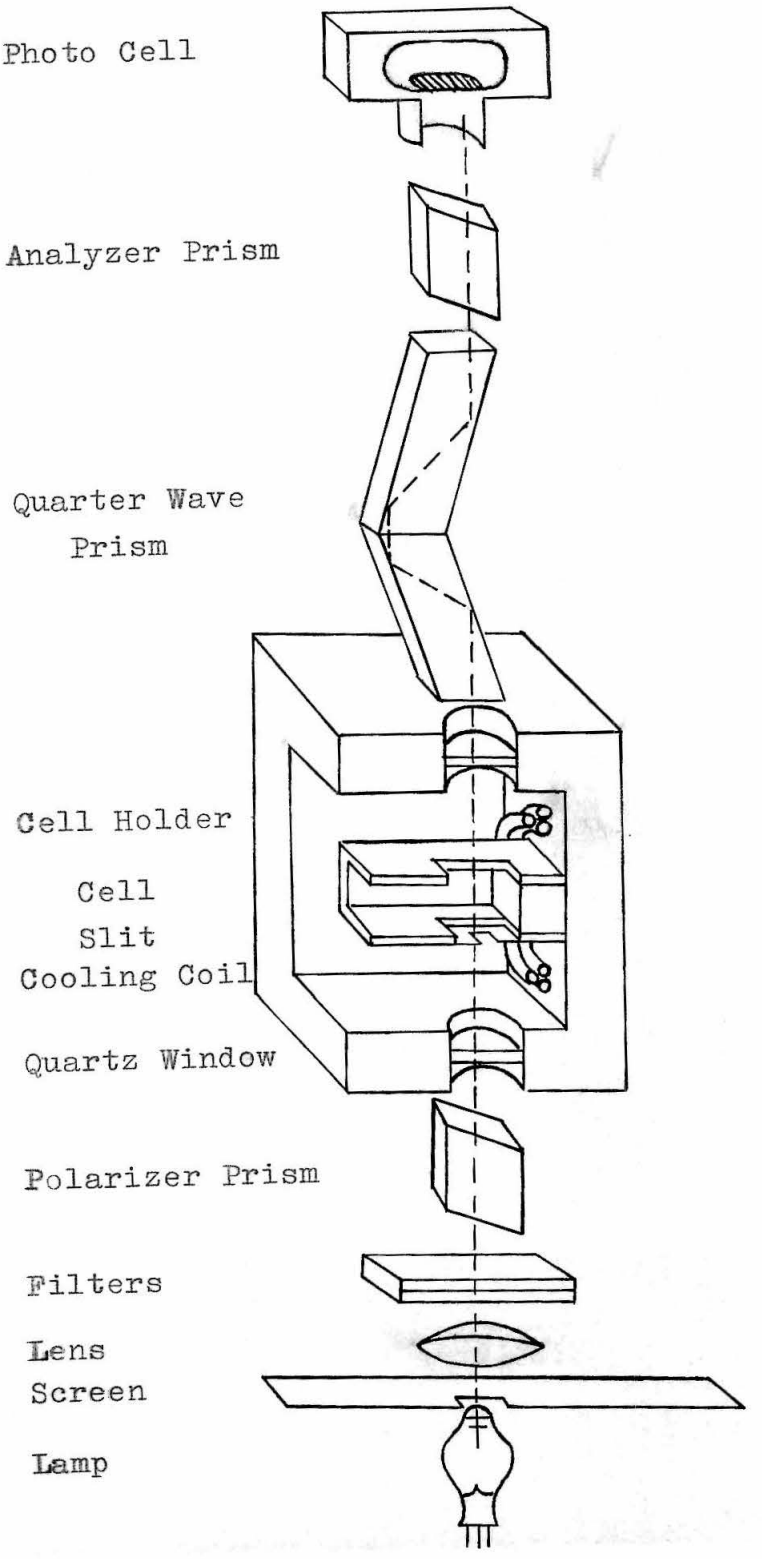

Figure 4: Cross section of optical system.
The main axes of all prisms are at 45° to the vertical.

Figure 5

Visible spectrum of the two filters used to select the light for our birefringence experiments.

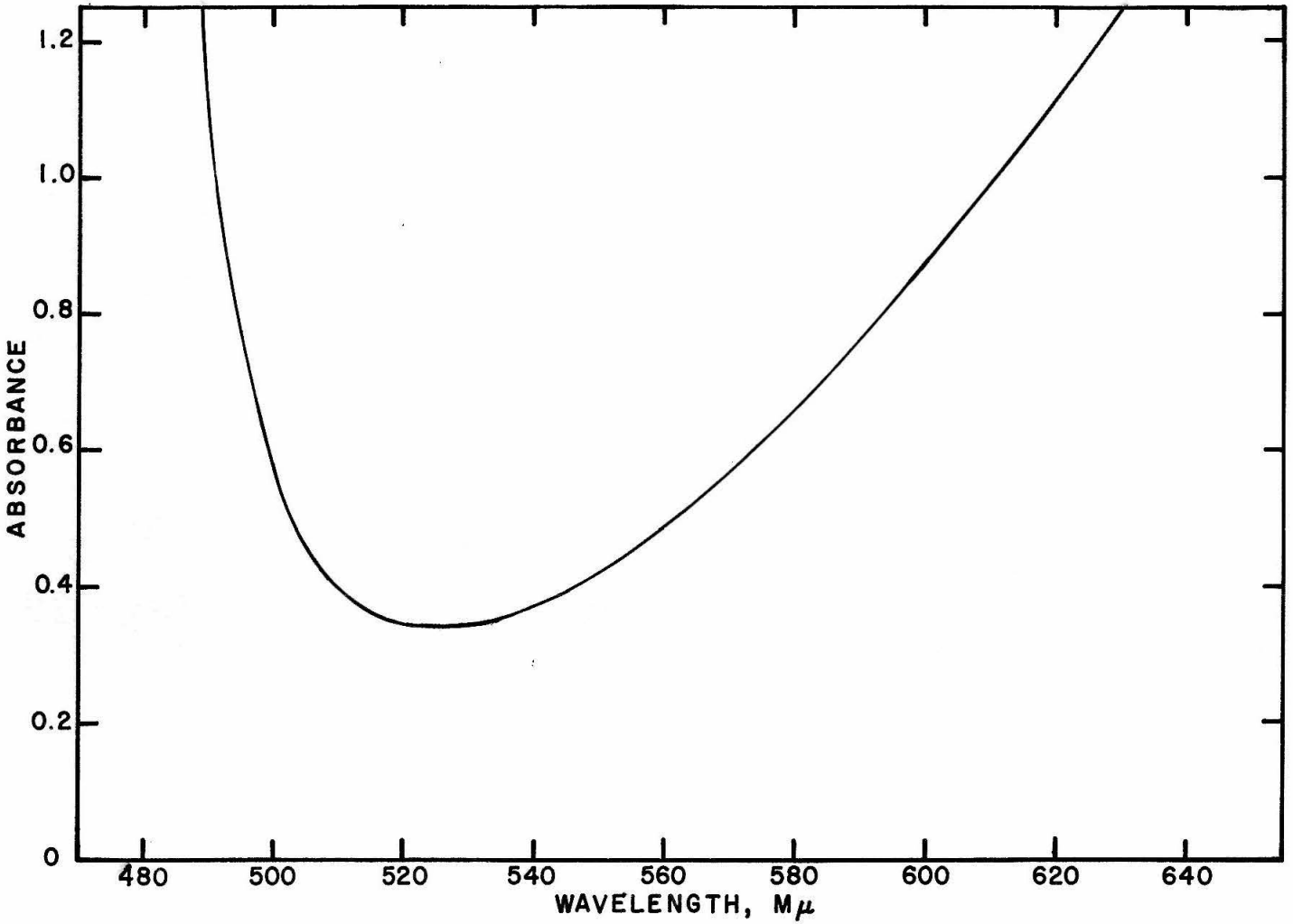
ABSORBANCE
1.2
1.0
0.8
0.6
0.4
0.2
0
480
500
520
540
560
580
600
620
640
WAVELENGTH, Mμ

Figure 5

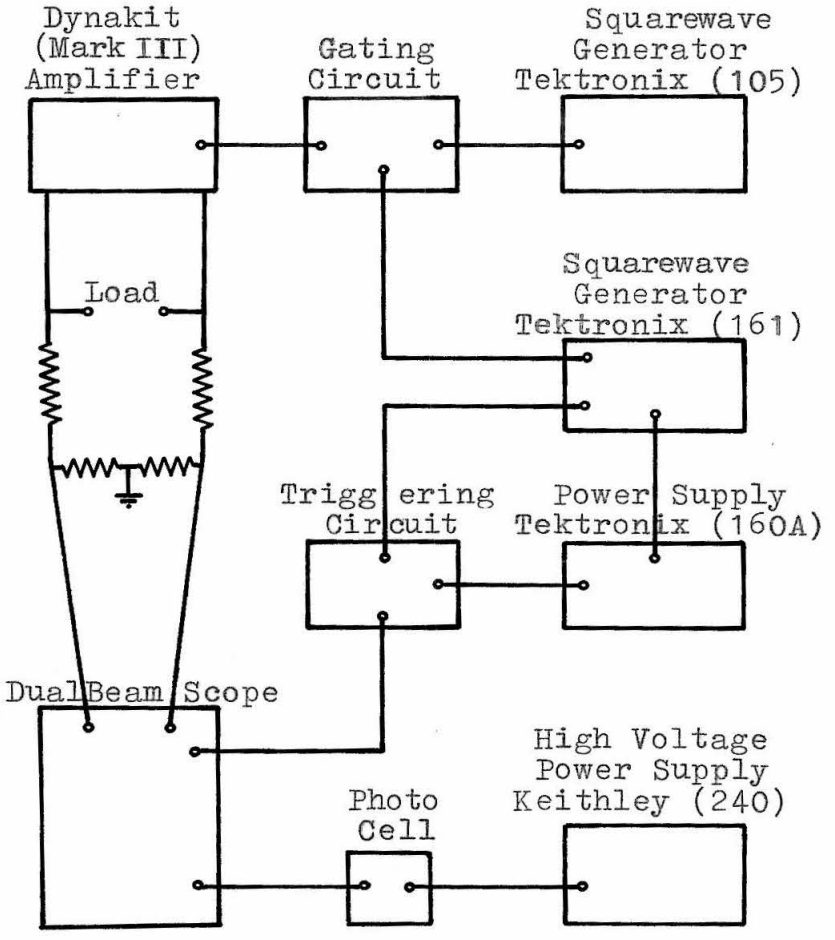

Figure 6: Block Diagram of Electrical System

of the incident light. The light was then analyzed by a prism, which was offset from the 45° plane by the angle β (usually 10°).

A phototube (No. GE 931 A) detected the intensity of the transmitted light, which was recorded on a dualbeam oscilloscope (Tektronix Type 502) simultaneously with a signal of the electric field applied across the cell.

b. The Electrical System (19, 20)

The electrical system (Fig. 6) was designed so as to make possible simultaneous measurement of birefringence and pulse signal. It was constructed by A. R. Jones (21) and was novel in that it was capable of generating a pulse of square waves of well-defined, variable duration and field strength. Since the duration of the impulses is of the order of 10 to 100 msec, an oscilloscope is required from which photographs of the signals can be obtained.

The birefringence signal was generated by the photomultiplier tube (Fig. 7) which was supplied with its dynode voltages by a Keithley (Model 240) regulated power supply with maximum output of ± 1000 V. For most purposes, the applied voltage has -500 volts. This gave oscilloscope signals of the birefringence of between 20 to 100 mV (Fig. 8).

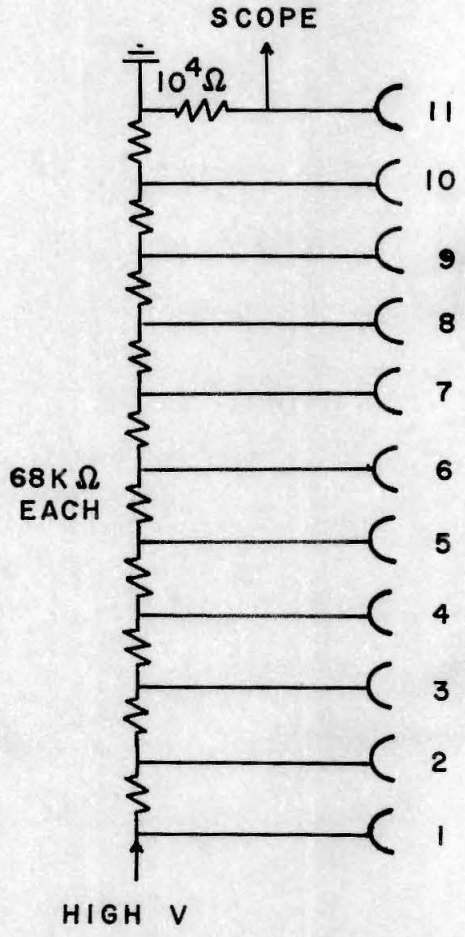

Figure 7

PHOTO CELL CIRCUIT

Figure 8

Oscilloscope trace of a typical birefringence signal. The sample shown here is T4-DNA (A_{260} = 0.564) in 1.26×10^{-4} μ at 4.0°C in response to a 10 Kc/sec alternating electric field of 2375 V/cm.
Pulse duration: 51 msec.
Maximum birefringence: 9.55°
I_{Ao}: 62 mV.

DNA sample number 25. The Mg-T4-DNA was dialysed versus water.

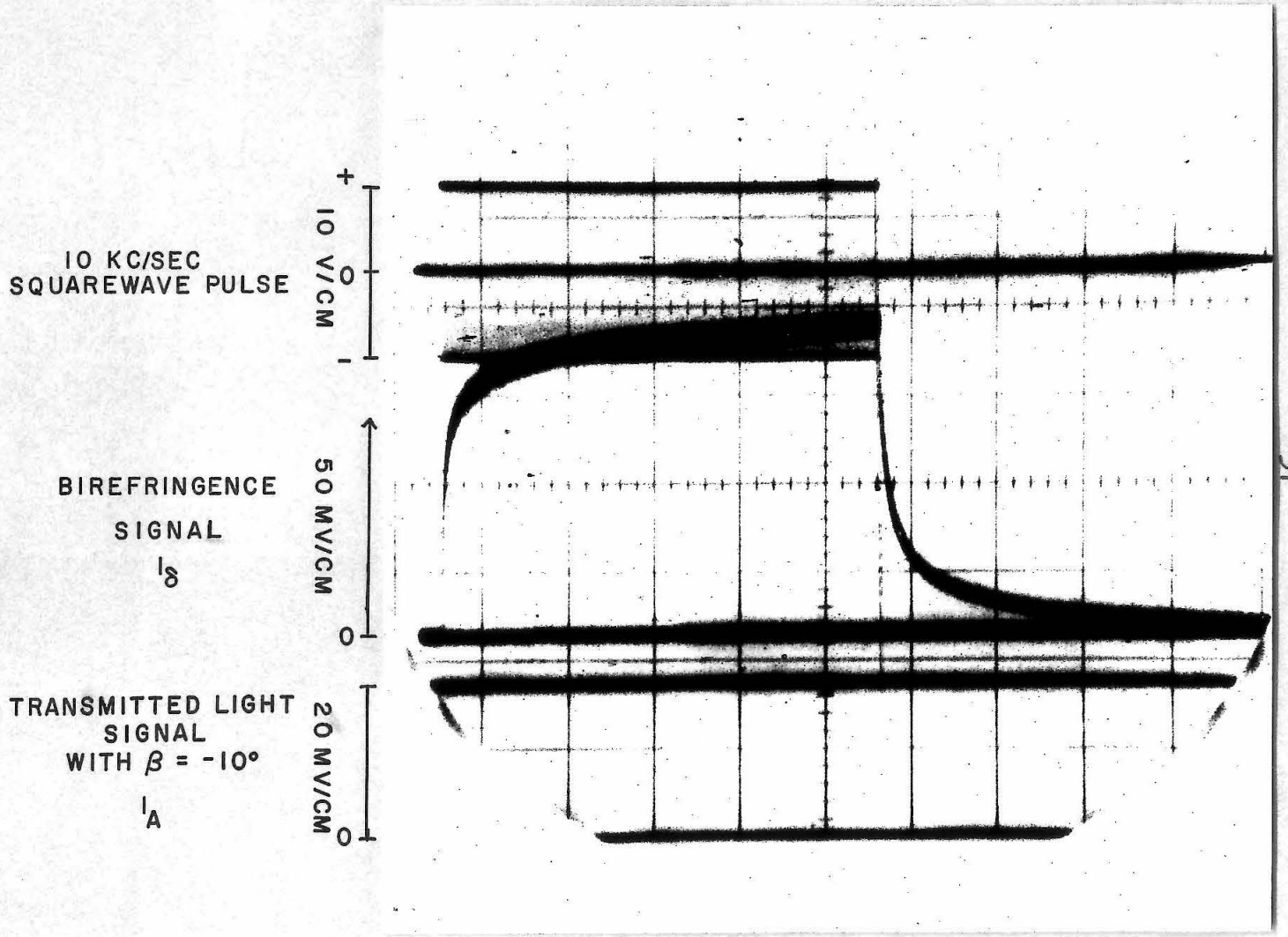
10 KC/SEC
SQUAREWAVE PULSE
+
10 V/CM
0
-
BIREFRINGENCE
SIGNAL
I_δ
50 MV/CM
0
TRANSMITTED LIGHT
SIGNAL
WITH β = -10°
I_A
20 MV/CM
0
TIME, 10 MSEC/CM

Figure 8

The pulse that was applied across the birefringence cell was generated by a square wave generator (Tektronix Type 105) with a variable frequency range from 0.1 kc/sec to 1000 kc/sec. A 10 kc/sec frequency was best for most purposes. The square wave generator out-put signal, variable from 4.1 to 100 V (38.5 V were generally used), was fed into a gating circuit (Fig. 9) which coupled the signal with the pulse (20 to 30 V) from another pulse generator (Tektronix Type 161) to facilitate the exact timing of its duration. This pulse generator was powered by a Tektronix (Type 160A) power supply with an out-put voltage of 160 V. (The actual power in-put into "PG 161" was 90 V).

The gating circuit out-put (less than 5 V) was amplified by a Dynakit (Mark III) power supply to about 1000 V and applied to the electrodes of the birefringence cell. Part of the pulse was tapped and fed to the other beam of the oscilloscope.

The triggering of the scope (Fig. 10) was coupled with that of the pulse generator, which started the electric field across the birefringence cell, causing alignment of the polyions.

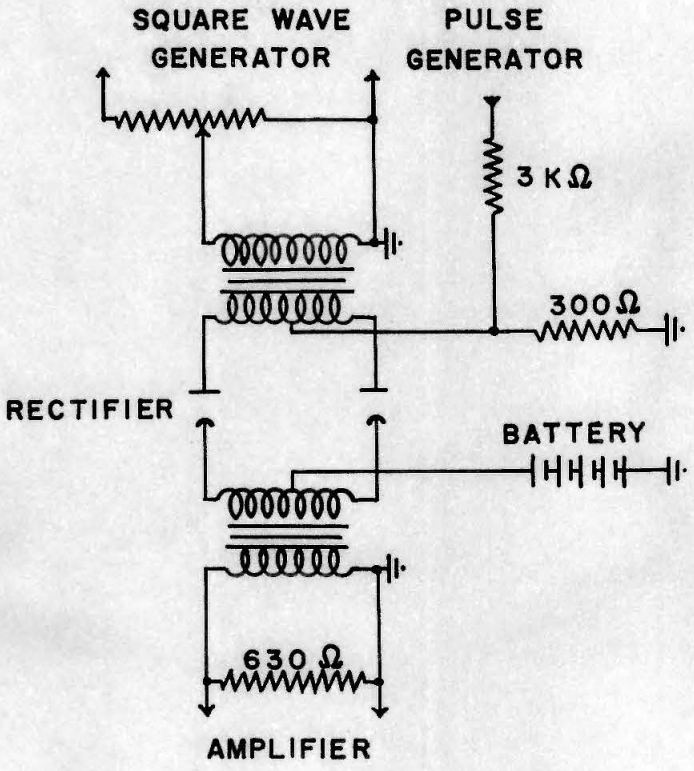

Figure 9

GATING CIRCUIT

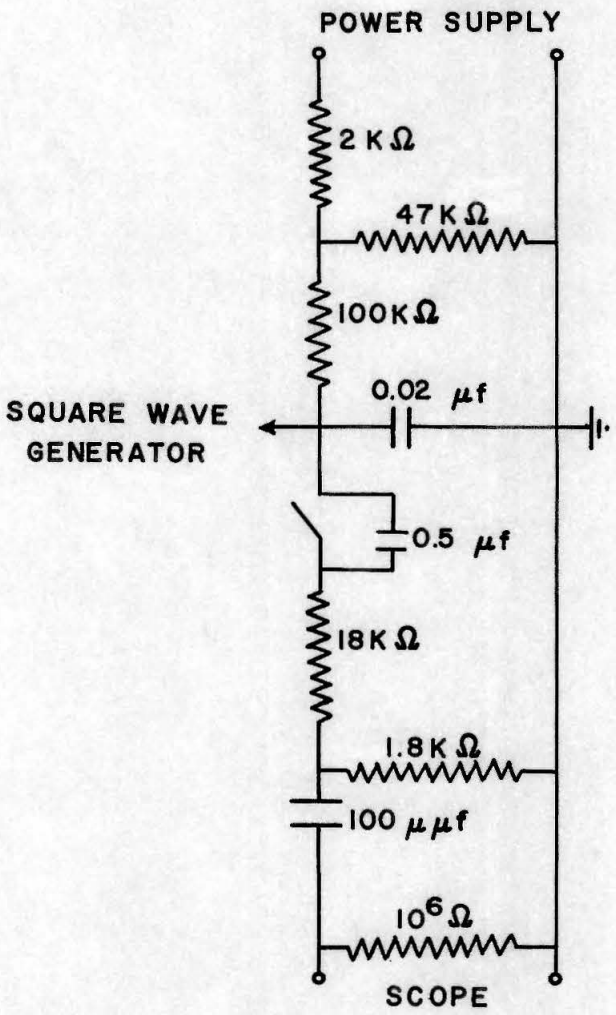

Figure 10

TRIGGERING CIRCUIT

c. The Birefringence Cell

Since DNA at low concentration and ionic strength is unstable at room temperature it was necessary to provide for cooling of the birefringence cell. Thus, a watertight cell holder (Fig. 4) was constructed with two quartz windows at opposite sides for the light beam. A constant stream of air, dried over $CaCl_2$ kept the windows from fogging. A cooling coil, immersed in the water or ethanol bath, which surrounded the birefringence cell in the center, was used to lower the bath temperature to between 0 and 5° C.

Several birefringence cells were designed to minimize the heating effects of the electric pulse as well as the volume of DNA solution required. The most satisfactory cell was constructed out of two platinum electrodes fitting snugly into a micro Beckman quartz cell. The electrodes were held to the inside cell walls by means of a removable teflon spacer facilitating easy cleaning. The volume of DNA solution required for an experiment was 0.25 ml, the pathlength 1 cm and the distance between the electrodes 2 mm.

7. Experimental Procedures

a. Absorbance Measurements

Ultraviolet absorption spectra of the DNA solutions were recorded by a Cary spectrophotometer (Model 14) and showed the characteristic absorption maximum at 2575 Å with a minimum at 2310 Å. However, all absorption data and calculations are based on the absorption at 2600 Å (A_{260}), which was routinely corrected for solvent blanks and normalized to zero absorption at 3600 Å (Fig. 11).

Using an extinction coefficient of 6600 at 2600 Å and an average molecular weight per basepair of 648, an absorbance of 1 corresponds to 49×10^{-6} g DNA/ml.

The ratio of the absorbance of 2600 Å to that of 2300 Å was used as an indication of the amount of contamination of the DNA by proteins etc., the higher ratio showing a purer DNA. Most of our samples had ratios of approximately 2, the highest being 2.4. DNA samples with ratios below 1.7 were considered too contaminated to give meaningful results.

The absorbances of all DNA solutions containing low salt concentrations were measured at less than 5° C in an icewater cooled cell holder designed by Wm. Dove (22).

Figure 11

UV absorption spectrum of a solution of "pure" Worthington calf thymus DNA in 0.90 x 10^{-3} F NaCl and 0.1 F Na-cacodylate (pH 7.1) corrected for the solvent blank and adjusted to zero absorption at 3600 Å (R_{230} = 2.4, R_{220} = 1.5).
Dashed curves represent solvent and uncorrected DNA solution.

Figure II

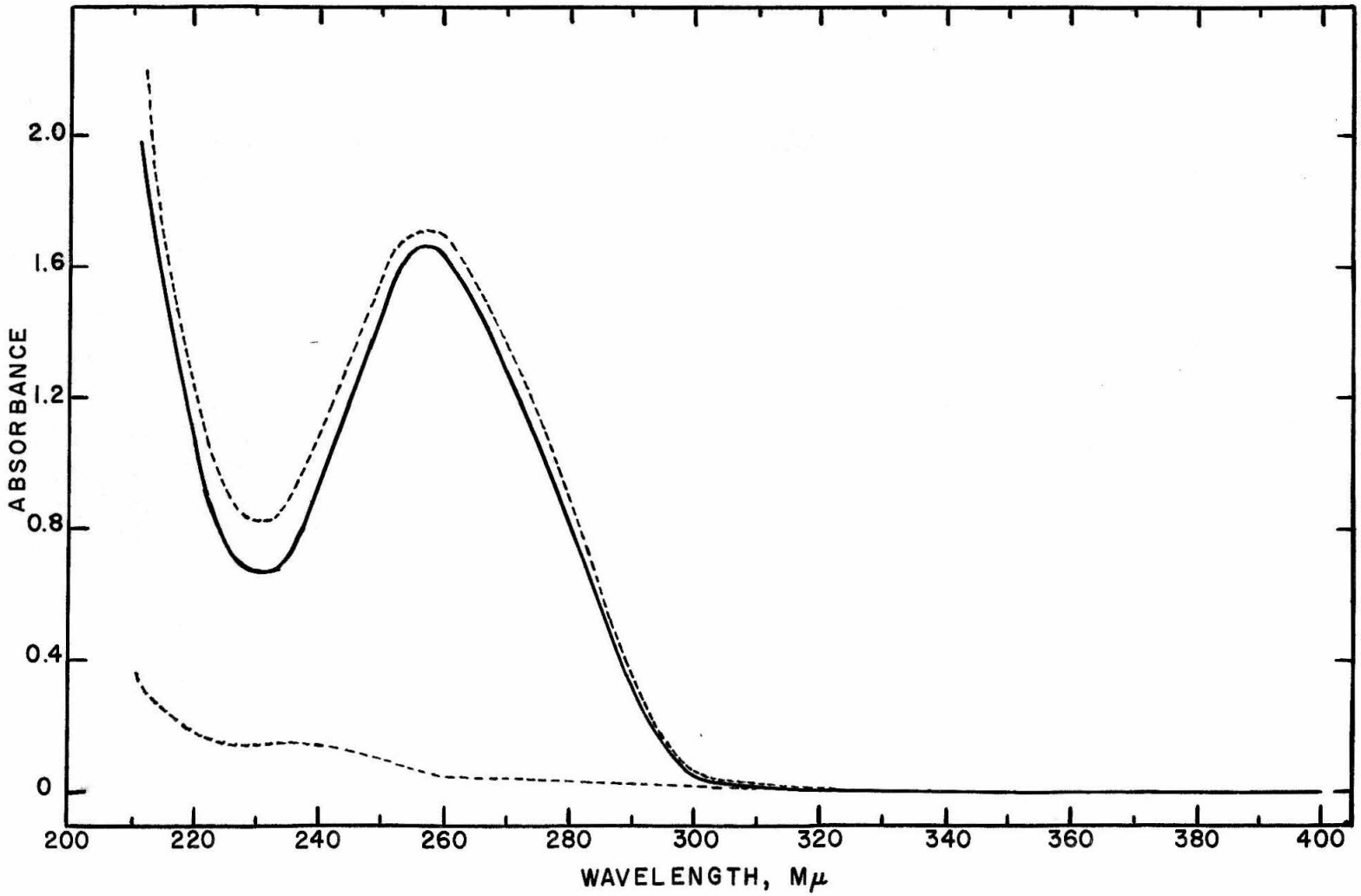
2.0
1.6
1.2
0.8
0.4
0
ABSORBANCE
200
220
240
260
280
300
320
340
360
380
400
WAVELENGTH, Mμ

b. Dialysis

Since we relied heavily on the absorbance measurements to determine the concentration as well as the purity of the DNA samples, it was essential that UV absorbing impurities were kept to a minimum. Thus, it was necessary to pretreat the Visking dialysis tubing, which was known to release UV absorbing impurities into the DNA solution. To this end the tubing was boiled in a concentrated $NaHCO_3$ solution for 15 minutes, rinsed with redistilled water, especially on the inside, boiled in two changes of redistilled water for 15 minutes each, rinsing on the inside after each boiling, and then stored at 4° C in redistilled water. The tubing was handled only with plastic gloves. The dialysis was carried out in a cold room at about 4° C.

When necessary, dilute versene (EDTA) solutions were used instead of redistilled water to eliminate divalent ions.

Similar cleaning procedures were used on all glassware used for storage or handling of the DNA solutions.

c. Resistance Measurements

The ionic strength of the DNA solutions was monitored by measuring their resistance directly in the birefringence cell using a Leeds and Northrup variable resistor. The cell was calibrated against standard KCl solutions, as well as the actual salt solutions used for the preparation of the DNA samples. A plot of the log of the resistance versus the negative log of the normality (Fig. 12) was used to determine the normality from the resistances measured before and after the birefringence experiments.

d. Viscosity Measurements

The viscosity of the DNA solutions was measured in the elegant, low shear viscometer designed by Zimm and Crothers (23).

Figure 12

Calibration curves of resistance versus ionic strength using the micro electric birefringence cell described in the text.
The data for 1/2 $MgCl_2$ and $NaClO_4$ are calculated from the cell constant and the values from the International Critical Tables.
The Li-cacodylate curve was determined experimentally.

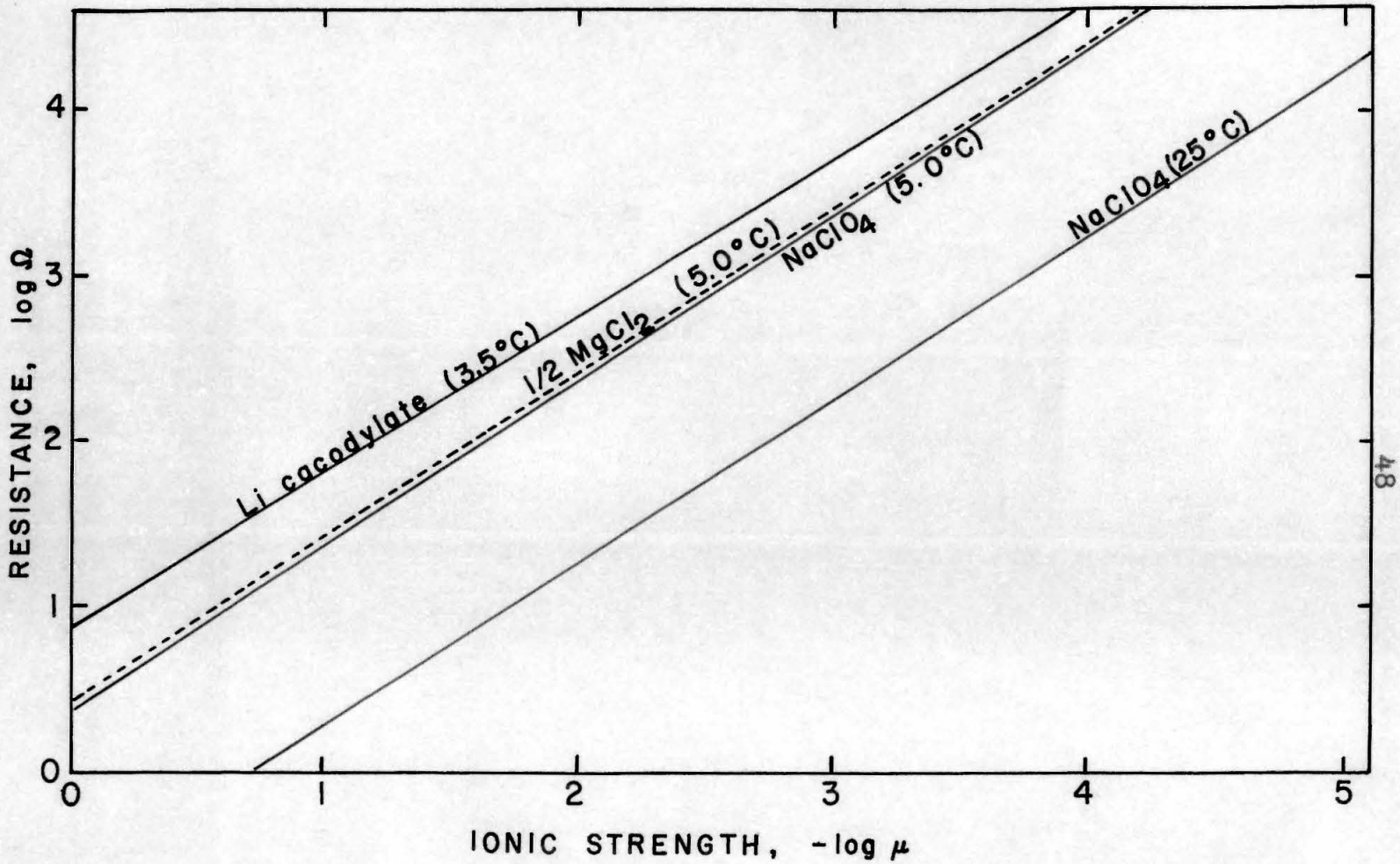
RESISTANCE, log Ω
IONIC STRENGTH, -log μ
Li cacodylate (3.5°C)
1/2 MgCl2 (5.0°C)
NaClO4 (5.0°C)
NaClO4 (25°C)
0
1
2
3
4
5

Figure 12

e. Preparation of DNA Samples

Because much of our work was directed toward finding a homogeneous DNA preparation for which we expected a simple decay behavior, a large number of DNA samples was studied which we obtained from various sources. It is therefore most convenient to present the pertinent data characterizing the preparations in a table.

This table lists the kind of DNA and its source (S), which may be either an industrial supplier (W = Worthington Biochemical Corp., Freehold, N. J., N = Nutritional Biochemicals Corp., Cleveland, Ohio) or a standard preparative procedure (M = Marmur procedure (24), P = phenol extraction (25)); it lists the investigators who prepared and donated the DNA solutions (P. B. = P. Brooks, E. C. = E. Carusi, W. H. = W. Huber, R. H. J. = R. H. Jensen, R. J. = R. Jones, H. O. = H. Ohlenbusch, B. O. = B. Olivera, R. S. = R. Stewart, B. Z. = B. Zimm), the approximate DNA concentration in mg/l, the type of salt solution and its normality in which the DNA was supplied, and the approximate age (storage at 0 to 5 °C) of the preparation before it was diluted or dialysed (indicated by *) to the final concentration used in the birefringence experiments. Similarly, the DNA concentration, salt type and normality and storage age of the diluted samples are listed.

Origin and Characteristics of DNA Preparations

#	Type of DNA	S	Donor	Appr. Conc. mg/l	Salt Type	N x 10^3	Age	Conc. mg/l	Salt Type	N x 10^4	Age	Av. μ x 10^4
1	C.T.	W	P. B.	772	NaIm	1.	60	93.3	NaIm	1.23	25	-
2	"	"	"	"	"	"	"	"	"	"	31	-
3	"	"	H. O.	742	NaPC	1.01	8	58.4	NaPC	1.24	0	
4	"	"	"	-	-	-	-	26.8	NaCac	1.	48	1.30
5	"	"	"	-	-	-	-	"	"	"	56	1.35
6	"	"	"	320	LiCac	100	33	24.2	LiCac*	1.00	2	2.14
7	"	"	"	"	"	"	"	"	"	"	24	2.82
8	"	"	"	"	"	"	"	"	"	"	42	2.85
9	"	"	R. J.	5000	NaPC	1.0	60	72.2	$MgCl_2$*	H_2O*	1	1.38
					NaCac	1.24						
10	"	"	"	"	"	"	"	"	"	"	18	2.18
10	"	"	"	"	"	"	"	"	"	"	"	5.08
11	"	"	"	"	"	"	"	58.0	"	"	17	3.73
12	"	"	"	"	"	"	"	35.4	"	"	9	1.0
13	"	N	H. O.	62	$MgCl_2$	20	5	28.2	$MgCl_2$	H_2O*	2	1.26
14	"	W	R. J.	5000	NaPC	1.0	60	24.4	$MgCl_2$*	H_2O*	7	0.79
					NaCac	1.24						
15	"	"	"	"	"	"	"	21.9	"	"	11	2.79
16	"	"	"	"	"	"	"	15.4	"	"	14	0.68
17	"	"	"	"	"	"	"	7.0	"	"	16	0.68
18	"	N	R.H.J.	3000	NaCac*	1.0	93					
				208	Ag	1.1	2	49.8	Ag	2.2	0	-
19	T-4	P	W. H.	400	NaPC	100		51.4	NaPC*	1.0	9	1.82
20	"	"	"	"	"	"		"	"	"	287	2.43
21	"	"	"	"	"	"		19.9	"	"	7	1.57
21	"	"	"	"	"	"		"	"	-	"	4.16
21	"	"	"	"	"	"		"	"	-	"	9.38
22	"	"	R. S.	275	Li			35.4	Li		0	3.38
23	"	"	B. O.	100	NaCl	10	53	17.0	LiCac*	0.5	0	9.10

Origin and Characteristics of DNA Preparations
Continued

#	Type of DNA	S	Donor	Appr. Conc. mg/l	Salt Type	N x 10^3	Age	Conc. mg/l	Salt Type	N x 10^4	Age	Av. μ_{20} x 10^4
24	T-4	P	W. H.	400	NaPC	100		27.7	MgPC*	H_2O*	13	1.18
25	"	"	"	"	"	"		"	"	"	2	1.26
26	"	"	"	"	"	"		27.6	"	"	13	0.88
27	T-2		B. Z.	375	NaP NaCl	20 180	138					
				375	LiCac*	0.10	9	21.9	LiCac	1.00	0	5.95
28	λ		W. D.	70	Tris	10		28.5	LiCac* Tris	8.6	2	11.87
29	Coli	M	"	250	NaPC	100	24	155.2	NaPC*	1.00	21	-
30	"	"	"	"	"	"	"	151.8	"	"	26	-
31	"	"	"	"	"	"	"	148.5	"	"	23	-
32	"	"	"	"	"	"	"	147.2	"	"	38	-
33	"	"	"	"	"	"	"	118.8	"	"	25	-
34	"	"	"	490	"	"	146	45.6	NaPC*	1.02	1	-
35	"	"	"	"	"	"	"	"	"	"	9	1.27
36	Lyso	"	"	1000	NaCl NaCit	150 60	19	72.1	NaPC*	1.00	54	1.09
37	"	"	"	"	"	"	"	56.5	"	"	66	2.24
38	"		E. C.	310				23.0	LiCac*	0.50	0	2.52
39	"		"	"				"	"	"	30	3.9
40	"		"	"				20	"	1.00	77	2.75
41	"	M	W. D.	1000	NaCl NaCit	150 60	19	72.9	MgPC NaPC*	0.92 0.50	66	1.50
42	B.M.	"	"	830	NaPC	100	3	63.7	Mg NaCac	1.0 0.5	0	3.54
43	"	"	"	"	"	"	"	18.8	"	"	72	2.88
44	"	"	"	"	"	"	"	15.6	"	"	12	-

The normality of each sample is given in terms of the salt concentrations of the media and does not include the contribution of the DNA and its counterions. In those cases in which the ionic strength was measured by conductivity determinations (Fig. 12), the total ionic strength is given in the last column (μ_Ω).

f. Storage of DNA Solutions

If DNA solutions are stored at low temperature and at high DNA and salt concentrations they are stable against denaturation for extended periods. Enzyme activity and bacterial growth may be retarded by adding poisonous buffers like cacodylate or a few drops of chloroform.

At low ionic strengths and DNA concentrations degradation of the DNA is enhanced (26). Although we have not investigated the effect of storage on the birefringence behavior explicitly, the available data indicate (Table V) that degradation is not a very important factor accounting for the observed variations of the data.

One sample of Na-T4 DNA in 10^{-4} N $NaClO_4$, which had been frozen and stored for 287 days (sample # 20, Table V) behaved very much like the original sample. Although the ionic strength was slightly higher ($2.43 \times 10^{-4}\ \mu$ instead of $1.82 \times 10^{-4}\ \mu$), the characteristic relaxation time

was nearly the same (2.3 ± 0.5 msec versus 1.45 ± 0.5 msec for the original sample).

III. Experimental Results

1. General Considerations

In order to calculate the theoretically meaningful electrical and optical parameters Δg, Ksp and $\Sigma \phi \alpha$, it is necessary to measure the steady state birefringence of a number of orienting pulses of increasing field strength, so that extrapolation to zero and infinite field strength is possible. Since the steady state is reached at anywhere from 1 to 100 ms pulse duration depending upon the field strength, the DNA sample, the temperature etc., it was important to verify that the DNA did not undergo denaturation or degradation during the treatment. Optical density measurements before and after a birefringence experiment showed that no denaturation occurred within experimental error (changes in absorbance at 2600 Å were generally less than ± 3 %).

To determine the extent of more subtle changes, e. g. breakage of strands, the viscosity of solutions of Lysodeikticus DNA was measured before and after birefringence. Six 0.25 ml aliquots of a solution (A_{260} = 1.6, less than 10^{-4} F Li-cacodylate buffer, pH 7) were each subjected at 4° C to ten high field (3140 ± 72 V/cm) 50 ms pulses at a rate of one per minute. The combined aliquots were then

diluted with 0.2 F Li-cacodylate to A_{260} = 0.8 and 0.10 F Li-cacodylate for a viscosity determination at 25.2° C. A plot of specific viscosity versus DNA concentration (Fig. 13) indicated that considerable structural changes had taken place during this drastic treatment.

In a follow-up experiment, eleven 0.25 ml aliquots of a dilute Lysodeikticus DNA solution (A_{260} = 0.77) in the same dilute buffer were subjected to only five high field (3020 ± 30 V/cm) 50 ms pulses at a rate of one every two minutes. The combined aliquots gave a more normal viscosity behavior (Fig. 14), but again a significantly lower intrinsic viscosity than the original sample. (The viscosity was determined at 4.92° C in the dilute buffer).

It is clear from the above, that an excessive number of high field pulses does cause changes in the DNA structure making it important to use as few pulses as possible and to begin with the low field strengths in order to get meaningful birefringence results.

In addition to measuring the absorbance of the DNA solutions in the birefringence cell before and after an experiment, the resistance was measured as well to determine any change in the ionic strength due to absorption or desorption of ions from the electrodes. Despite thorough cleaning of the birefringence cell in boiling redistilled water, the resistance did at times decrease appreciably

Figure 13

Plot of specific viscosity divided by the concentration of DNA (dl/g) versus DNA concentration in terms of absorbance.
Open circles represent data of Lysodeikticus DNA in 0.10 F Li-cacodylate buffer (pH 7).
Full circles represent data of a similar sample which had been subjected to ten high field 50ms pulses (see text).

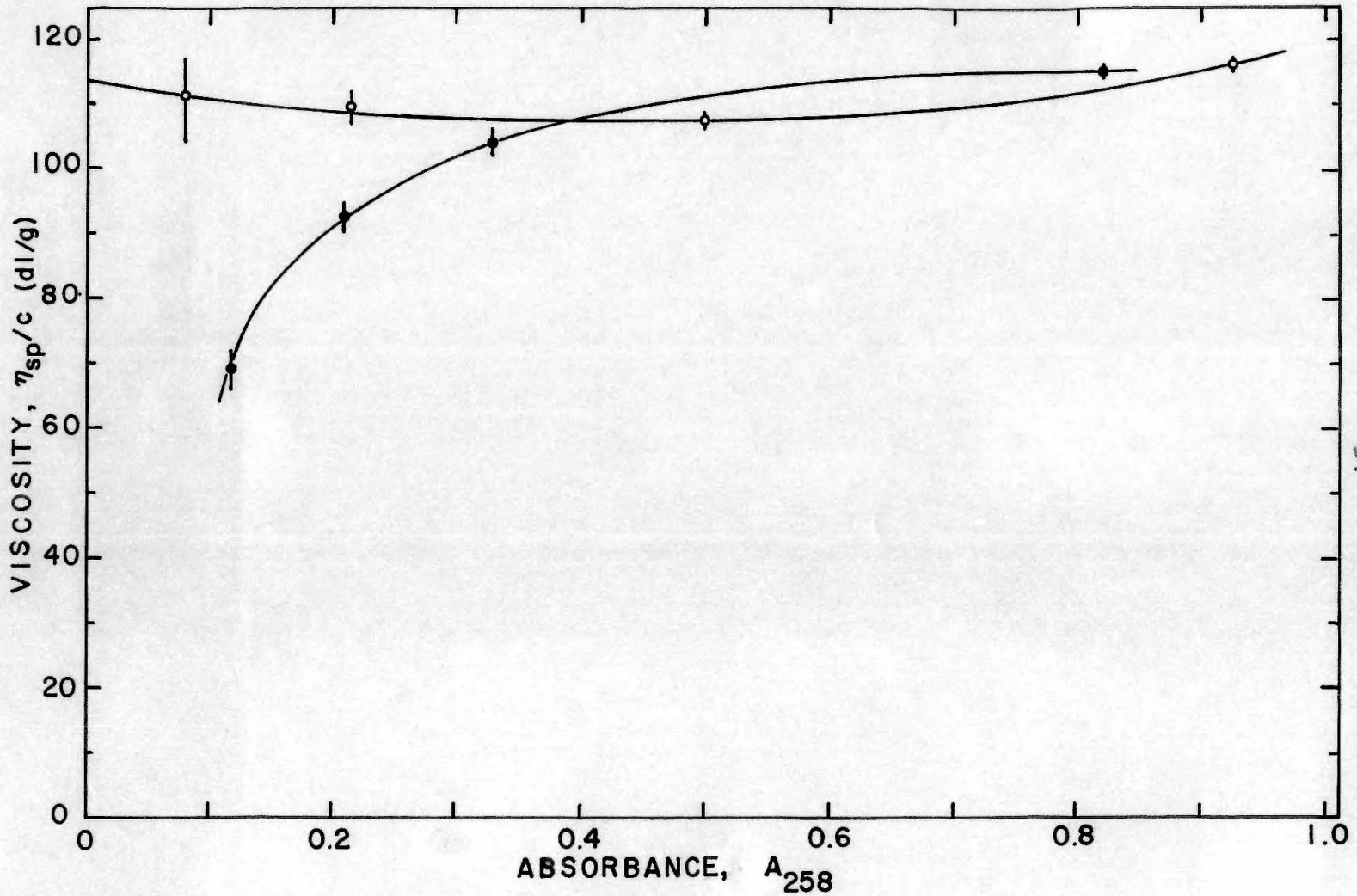
120
100
80
60
40
20
0
VISCOSITY, η_{sp}/c (dl/g)
0
0.2
0.4
0.6
0.8
1.0
ABSORBANCE, A_{258}

Figure 13

Figure 14

Plot of specific viscosity divided by the concentration of DNA (dl/g) versus DNA concentration in terms of absorbance.
Open circles represent data of Lysodeikticus DNA in 10^{-4} F Li-cacodylate buffer (pH 7) at 4.92° C.
Full circles represent data of a similar sample which had been subjected to five high field 50 ms pulses (see text).

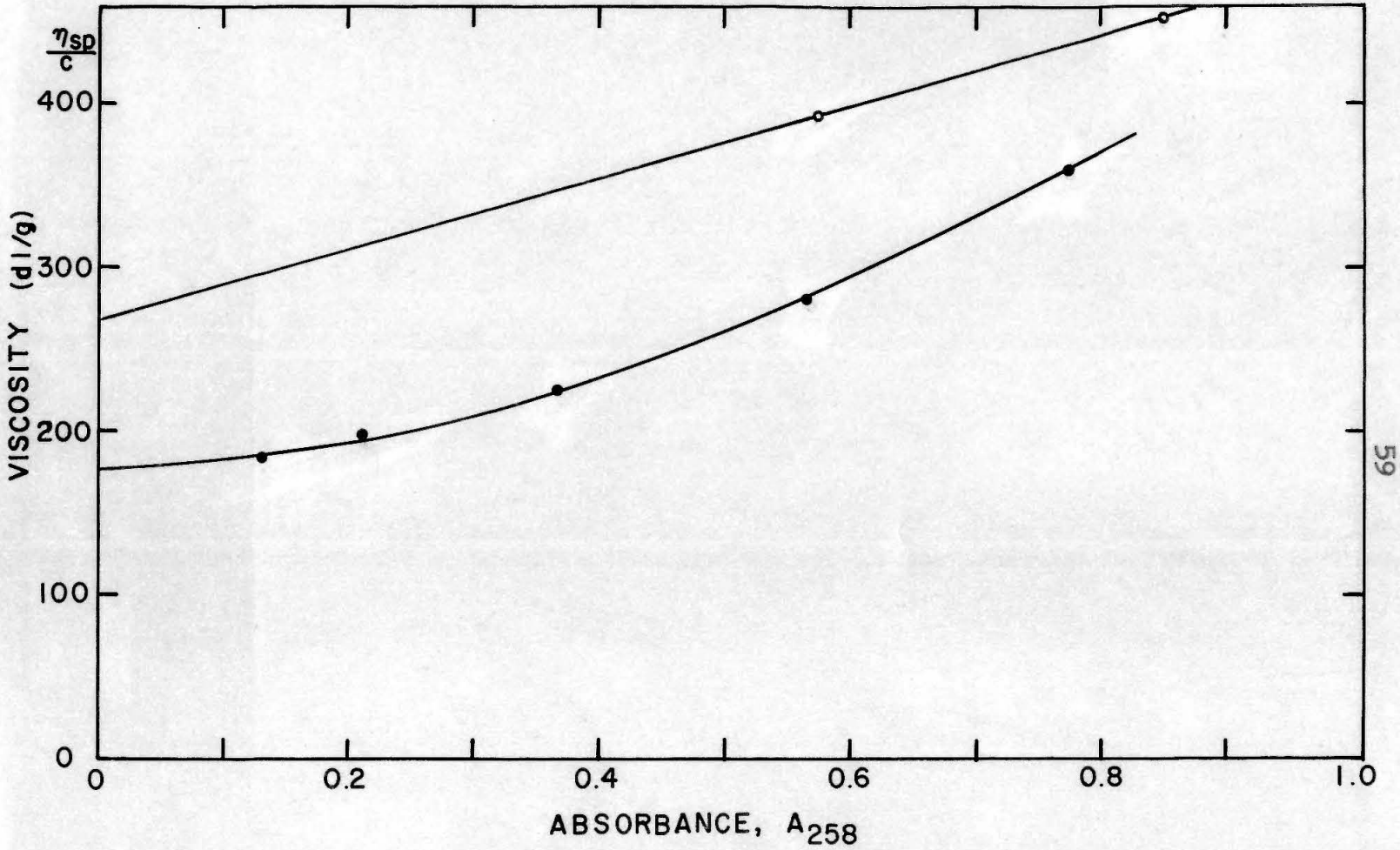
$\frac{\eta sp}{c}$
400
300
200
100
0
VISCOSITY (dl/g)
0
0.2
0.4
0.6
0.8
1.0
ABSORBANCE, A_{258}

Figure 14

during application of a few high field pulses. This makes the interpretation of the data ambiguous, for, as will be shown (Table III), Δg, $\Sigma \phi a$ and especially Ksp decrease significantly with increasing ionic strength.

2. Relation of Field Strength and Birefringence

Early attempts to correlate the field strength and the magnitude of the steady state birefringence in terms of O'Konski's equations (Eqns. 13 and 14) were unsuccessful. Instead it was found (Fig. 15 and 16) that the data could be plotted as $1/\delta_{st}$ versus $1/E^2$ and E^2/δ_{st} versus E^2 resulting in straight lines, both being represented surprisingly well by the following empirical relation:

$$\delta_{st} = E^2/(aE^2 + b). \qquad (21)$$

with the corresponding straight line equations

$$1/\delta_{st} = a + b/E^2 \quad \text{and} \quad E^2/\delta_{st} = b + aE^2 \qquad (22, 23)$$

where $a = 1/\delta_s$ and $b = (E^2/\delta_{st})_{E\to o}$.

The agreement between slope and intercept of the two plots, which were calculated by the least mean squares method, was generally within ± 5 % and independent of the kind of DNA or the counterion used (Table I). Nevertheless, in calculating Δg and Ksp only the corresponding intercepts were used and not the slopes, assuming the validity of O'Konski's limiting equations (Eqns. 15 to 17). The data are summarized in table II.

Figure 15

Birefringence data for various DNA samples demonstrating the straight line dependence of the inverse of the steady state birefringence to the inverse of the square of the field strength.

Sample Number	Type of DNA	Ionic Strength x 10^4	Concentration mg/l	R_{230}	Temperature °C
23	Li-T4	9.10	17.0	1.78	4.2
43	Mg-B.M.	2.88	18.8	(1.32)	4.8
27	Li-T2	5.95	21.9	1.86	5.6
28	Li-λ	11.87	18.5	1.98	3.7
38	Li-Lyso	2.52	23.0	1.94	4.3
19	Na-T4	1.82	51.4	2.28	3.8
29	Na-Coli	1	155.2	-	4.0

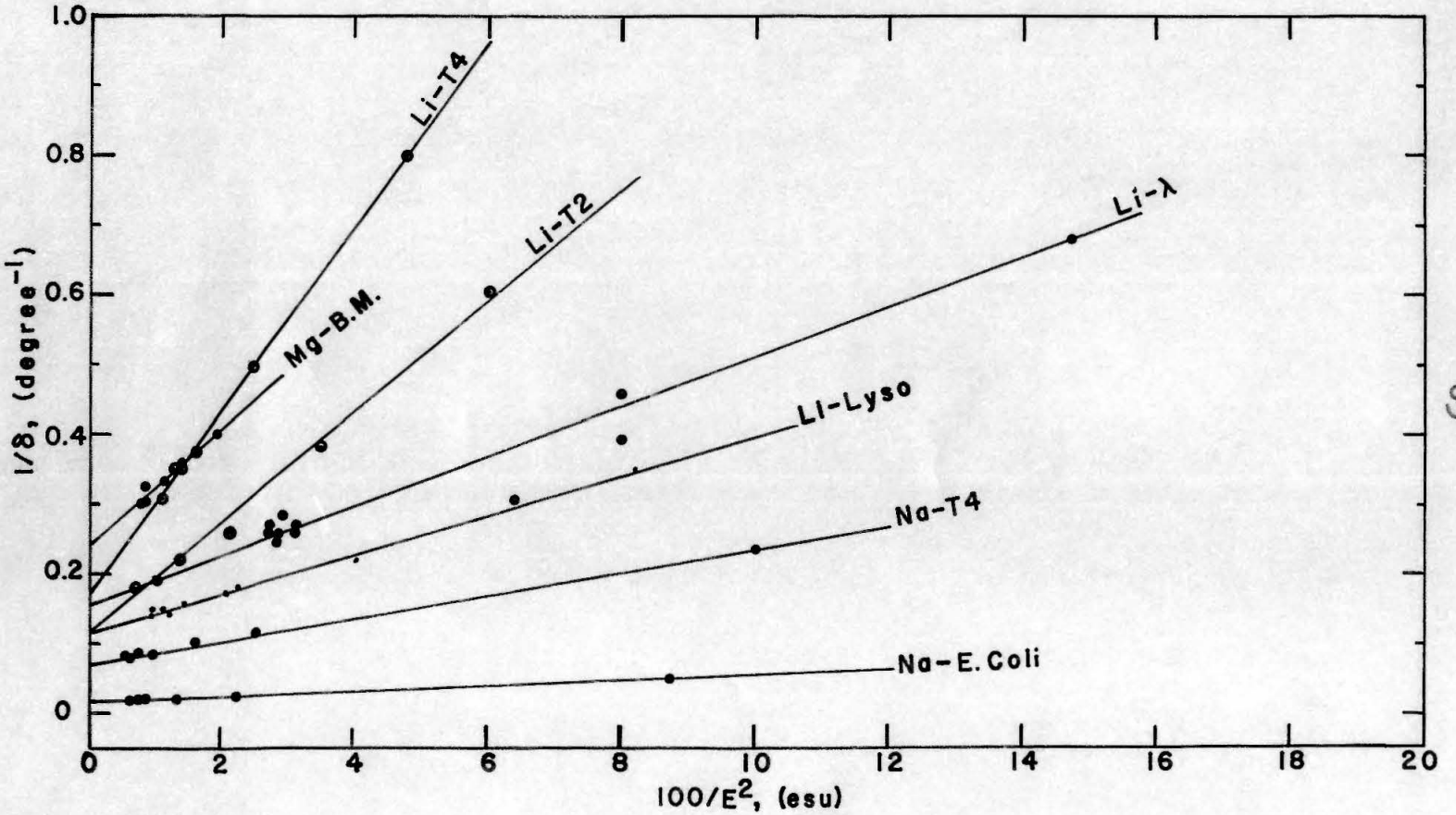
1.0
0.8
0.6
0.4
0.2
0
1/δ, (degree⁻¹)
Li-T4
Mg-B.M.
Li-T2
Li-λ
Li-Lyso
Na-T4
Na-E. Coli
0
2
4
6
8
10
12
14
16
18
20
100/E², (esu)

Figure 15

Figure 16

Birefringence data for various DNA samples demonstrating the straight line dependence of E^2/δ versus E^2, where δ is the steady state birefringence.
DNA samples are the same as in figure 15.

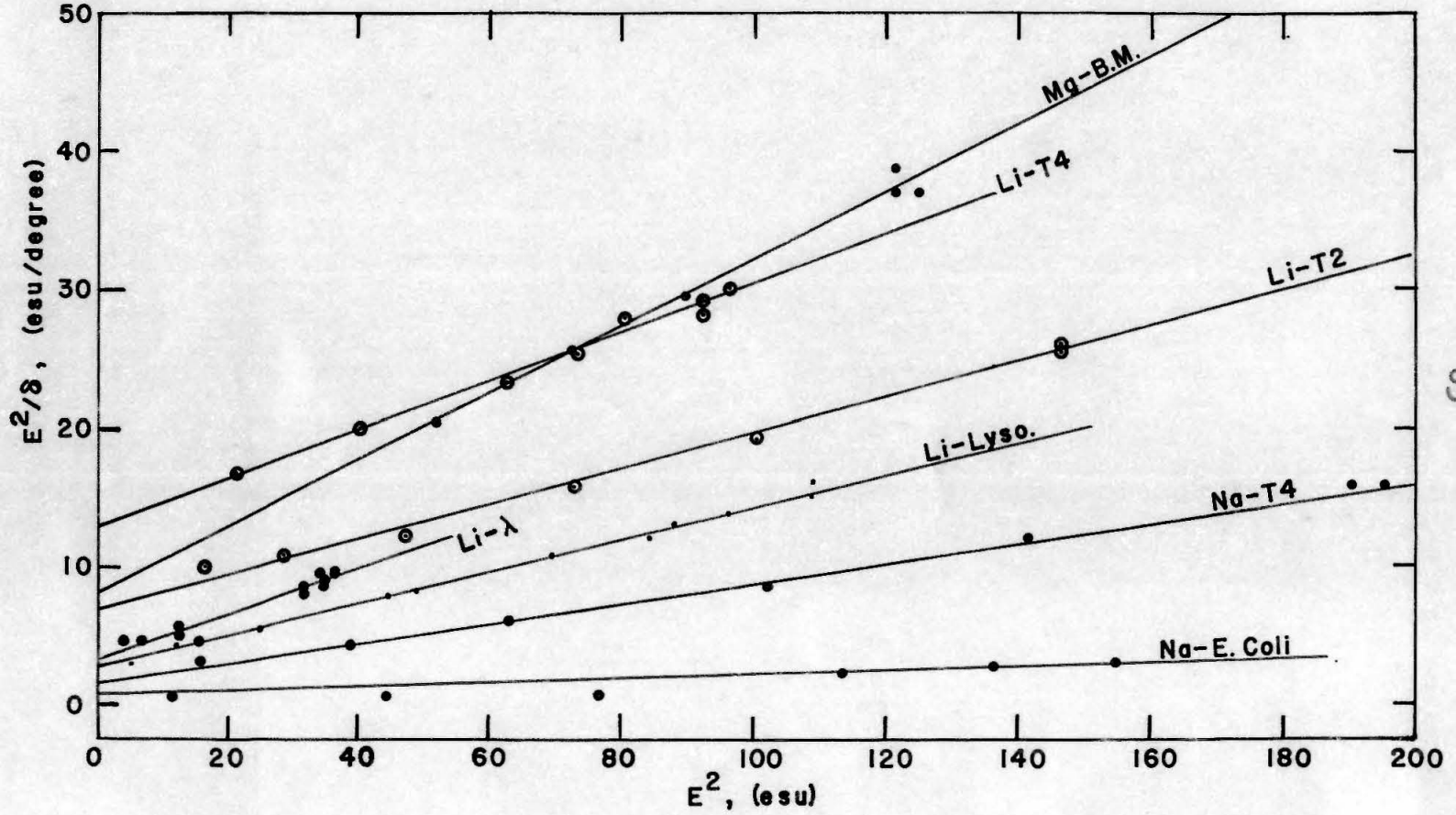
50
40
30
20
10
0
E^2/δ, (esu/degree)
0
20
40
60
80
100
120
140
160
180
200
E^2, (esu)
Mg-B.M.
Li-T4
Li-T2
Li-Lyso.
Li-λ
Na-T4
Na-E. Coli

Figure 16

Table I

Sample Number	Type of DNA	Ionic Str. x 10^4	Conc. mg/l	Slope $\frac{1}{\delta}$ vs. $\frac{1}{E^2}$	$(\frac{E^2}{\delta})_o$	Slope $(\frac{E^2}{\delta})$ vs. E^2	$\frac{1}{\delta_s}$
1	Na-C.T.	1.	93.3	0.752*	0.994*	0.0497	0.0513
4	"	1.30	26.8	0.568*	1.21*	0.119	0.112
5	"	1.35	26.8	1.14	1.15	0.112	0.112
6a	Li-C.T.	2.14	24.2	2.31*	1.49*	0.123	0.112
7	"	2.82	24.2	3.43	3.04	0.124	0.121
8	"	2.85	24.2	3.45	3.47	0.113	0.112
9	Mg-C.T.	1.38	72.2	2.42	2.53	0.0425	0.0431
10a	"	2.19	72.2	4.18	4.21	0.0443	0.0439
11	"	3.73	54.0	6.47	6.26	0.0780	0.0823
13	"	1.26	28.2	2.43*	1.88*	0.0566*	0.0501*
14	"	0.79	24.4	4.91	4.84	0.0997	0.0979
16	"	0.68	15.4	10.03*	11.54*	0.359	0.375
19	Na-T-4	1.82	51.4	1.65	1.53	0.0737	0.0727
20	"	2.43	51.4	5.46	5.44	0.0802	0.0802
21a	"	1.57	19.9	4.44*	5.22*	0.146	0.150
21b	"	4.16	19.9	14.79	14.82	0.214	0.211
21c	"	9.38	19.9	24.48	25.66	0.302	0.313
22a	Li-T-4	3.38	35.4	1.94*	1.72*	0.0662	0.0610
22c	"	3.38	35.4	1.92	1.91	0.0695	0.0694
23	"	9.10	17.0	13.17	12.93	0.177	0.172
24	Mg-T-4	1.18	27.7	10.57	10.36	0.0965	0.0916
25	"	1.26	27.7	2.47*	2.13*	0.0689	0.0687
26	"	0.88	27.6	3.24	3.44	0.0954	0.0977
27	Li-T-2	5.95	21.9	7.94*	7.12*	0.127	0.116
28	Li-λ	11.87	18.5	3.41	3.36	0.163	0.156
29	Na-Coli	1	155.2	0.423*	0.329*	0.0178	0.0164
30	"	1	147.2	1.25	1.25	0.0184	0.0191
33	"	1	118.8	0.483	0.480	0.0165	0.0163
35	"	1	45.6	1.09	1.16	0.213	0.0216
37	Na-Lyso	1.09	72.1	1.08	1.06	0.0246	0.0239
38	Li-Lyso	2.52	23.0	2.85	2.78	0.115	0.114
40	"			3.63	3.54	0.162	0.160
41	Mg-Lyso	1.50	72.9	2.06	2.04	0.0216	0.0215
42	Mg-B.M.		63.6	0.965*	0.834*	0.0118*	0.00886*
43	"	2.88	18.8	8.21	8.33	0.241	0.242

Values marked by * differ by more than 10 %.

Note: cgs and esu were used throughout. δ is in degrees.

Table II

Sample Number	Type of DNA	Ionic Str. x 10^4	Conc. mg/l	R_{230}	Temp. °C	$-\Delta g$ x 10^2	- Ksp x 10^3	$\Sigma\phi a$ x 10^{14}
4	Na-C.T.	1.30	26.8	2.38	4.6	1.88	6.13	5.50
5	Na-C.T.	1.35	26.8	2.38	5.0	1.88	6.44	5.60
6	Li-C.T.	2.14	24.2	2.12	3.4	2.09	5.55	4.31
7	Li-C.T.	2.82	24.2	2.12	3.8	1.93	2.71	2.28
8	Li-C.T.	2.85	24.2	2.12	4.3	2.08	2.37	1.85
9	Mg-C.T.	1.38	72.2	2.07	4.5	1.80_5	1.09	0.98_3
10a	Mg-C.T.	2.19	72.2	2.07	4.9	1.78	0.65_4	0.60
13	Mg-C.T.	1.26	62.1	1.92	3.5	1.81	1.70	1.53
14	Mg-C.T.	0.79	24.4	1.94	4.5	2.36	1.68	1.16
17	Mg-C.T.	0.68	7.0	1.75	5.3	2.15	2.49	1.89
19	Na-T4	1.82	51.4	2.28	3.8	1.51	2.54	2.73
21a	Na-T4	1.57	19.9	2.28	4.0	1.89	1.92	1.65
22a	Li-T4	3.38	35.4	2.04	3.8	2.60	3.26	2.03
23	Li-T4	9.10	17.0	1.78	4.2	1.93	0.90_5	0.76_3
24	Mg-T4	1.18	27.7	2.10	3.3	2.22	0.69_3	0.50_6
25	Mg-T4	1.26	27.7	2.10	4.0	2.97	3.37	1.84
26	Mg-T4	0.88	27.6	1.98	3.8	2.09	2.09	1.63
27	Li-T2	5.95	21.9	1.86	5.6	2.21	1.27	0.94
28	Li-λ	11.9	28.5	1.98	3.7	1.26	2.07	2.66
29	Na-Coli	1	155.2	-	4.0	2.21	3.90	2.87
33	Na-Coli	1	118.8	-	5.2	2.91	3.48	1.95
36	Na-Lyso	1.09	72.1	-	2.9	2.22	4.69	3.42
38	Li-Lyso	2.52	23.0	1.94	4.3	2.15	3.11	2.35
41	Mg-Lyso	1.50	72.9	1.79	4.8	3.60	1.34	0.60_7

Note: cgs and esu were used throughout.

It should be noted, that the optical anisotropy is about minus 0.02 (in cgs units) regardless of the source of the DNA (mammalian, bacterial or viral) and independent of the kind of counterions used (Na^+, Li^+ or Mg^{++}). This result is expected for molecules which align such that their chromophors are oriented perpendicular to the electric field. Furthermore, since Δg is obtained from data extrapolated to infinite field strength, it should be independent of the heterogeneity of the DNA preparations.

The optical anisotropy seems to be somewhat influenced by the ionic strength of the DNA solution (Table III, Fig. 17a), but whether this is due to primary changes in the optical properties of the basepairs or to changes in the overall configuration of the DNA is uncertain.

The reasons for the variations in the Kerr constants, ranging from -0.65×10^{-3} to -6.5×10^{-3} cgs-esu, cannot be explained unambiguously either, but it seems that ionic strength effects are responsible to the largest extent. Table III shows some results with DNA samples in solutions of increasing salt concentrations (as determined from resistance measurements). The experiments on T-4 DNA were run on one sample to which were added increasing amounts of $NaClO_4$ while it was in the bire-

Table III

Sample Number	Type of DNA	Ionic Str. x 10^4	Conc. mg/l	R_{230}	Temp. °C	$-\Delta g$ x 10^2	- Ksp x 10^3	$\Sigma\phi a$ x 10^{14}
21a	Na-T4	1.57	19.9	2.28	4.0	1.89	1.92	1.65
21b	Na-T4	4.16	19.9	2.28	4.6	1.34	0.675	0.820
21c	Na-T4	9.38	19.9	2.28	4.5	0.904	0.390	0.702
17	Mg-C.T.	0.68	7.0	1.89	3.8	2.15	2.49	1.89
14	Mg-C.T.	0.79	24.4	1.94	4.5	2.36	1.68	1.16
13	Mg-C.T.	1.04	35.4	(1.51)	3.8	2.56	1.61	1.02
9	Mg-C.T.	1.38	72.2	2.07	4.5	1.80	1.09	0.983
10a	Mg-C.T.	2.19	72.2	2.07	4.9	1.78	0.654	0.600
15	Mg-C.T.	2.70	21.9	(1.19)	3.7	1.44	0.473	0.535
10b	Mg-C.T.	5.08	72.2	2.07	4.4	1.10	0.224	0.333

Note: cgs and esu were used throughout.

Figure 17

Birefringence data of Na-T4-DNA (full circles) and Mg-calf thymus DNA (open circles) are plotted against the ionic strength of the solutions.
a) Behavior of optical anisotropy.
b) Behavior of specific Kerr constant.
c) Behavior of polarizability calculated from a) and b).
The DNA samples are those listed in table III.

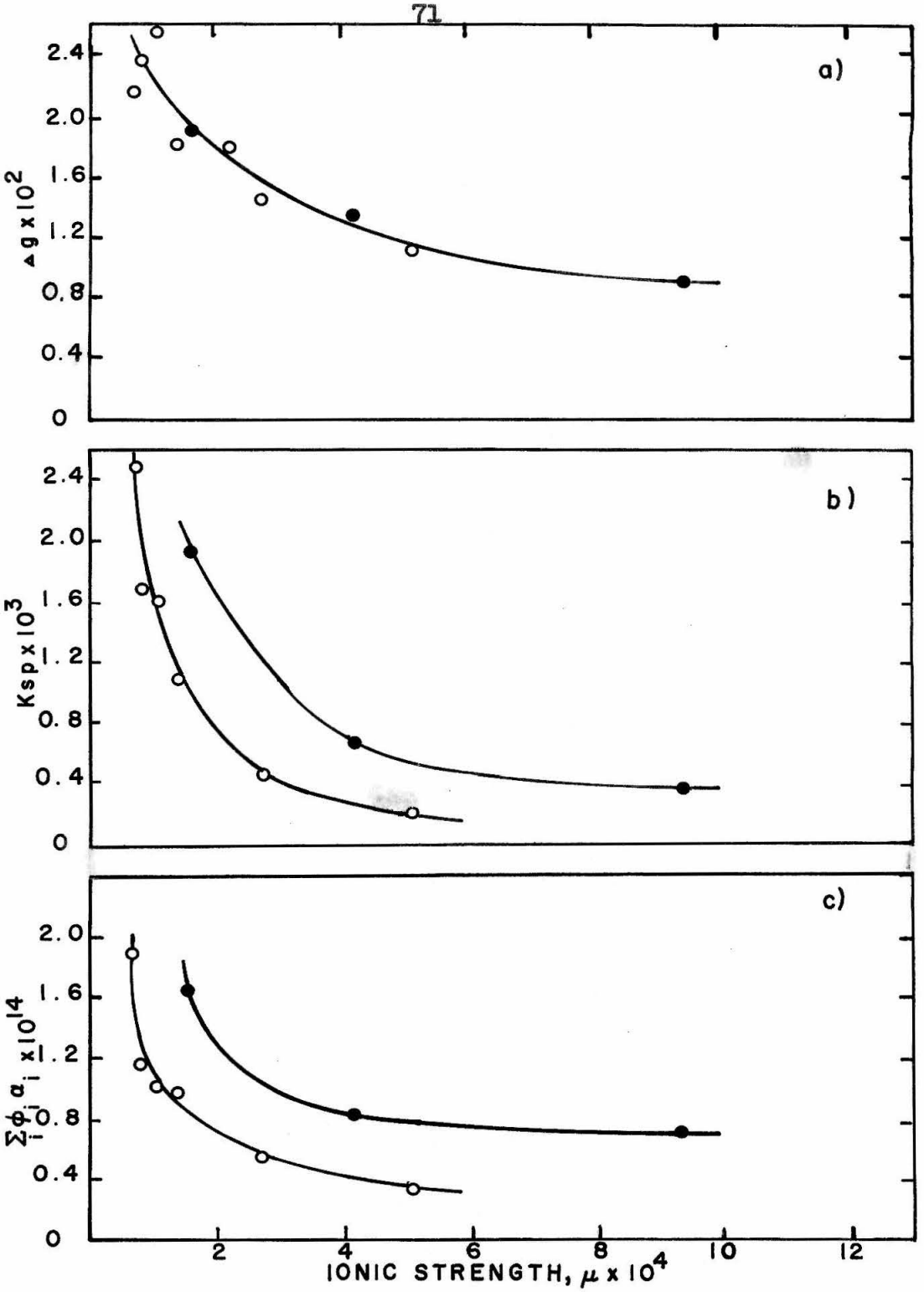
a)
b)
c)
$\Delta g \times 10^2$
$K_{sp} \times 10^3$
$\Sigma \phi_i a_i \times 10^{14}$
IONIC STRENGTH, $\mu \times 10^4$

Figure 17

fringence cell. The experiments with thymus DNA in dilute $Mg(ClO_4)_2$ were carried out on different aliquots of the same preparation, originally designed to show effects of DNA concentration on the birefringence. The results do not indicate that a consistent relation to DNA concentration exists within the range studied. However, a definite trend of the data is observed in relation to changes in the ionic strength of the solutions, with the Kerr constant being affected most (Fig. 17b).

Similar ionic strength effects were observed in measurements of the Kerr constant of bovine serum albumin (27) and agree with predictions for ion atmosphere polarization by O'Konski et al. (28).

Since the electric polarizability is also inversely related to the ionic strength (Fig. 17c), the attempts to interpret the results in terms of changes of the counterion atmosphere of the DNA molecules may seem to be correct, but again changes in the overall structure of the DNA cannot be completely ruled out (see decay behavior p. 82).

The fact that Mg^{++} counterions are as effective as Na^+ or Li^+ in permitting extensive alignment of the DNA, supports the contention that Mg^{++} is bound electrostatically to the negative phosphate groups (29) and not covalently as proposed by Zubay (30).

The generally lower electric polarizability of Mg-DNA's as compared to Na-DNA's may be a result of the tighter electrostatic binding of the Mg^{++}. If that is indeed the case, then the factor $f(\epsilon_{\parallel}, P)$ (Eqn. 10b) may be considerably smaller than unity, as was assumed for the case of completely free movement of charges along the polyion.

Figure 18 shows a graph of equation 10 for f = 1 (Curve a) and f = 0.1 (Curve b) plotted as the log of the polarizability versus the rod length in Ångstrom. The horizontal lines indicate the range of our calculated $\Sigma\phi\alpha$ for Mg^{++}, Na^{+} and Li^{+}.

Since it is known that the Ag^{+} "counterions" are bound at specific sites of the DNA (31), it was of interest to observe the behavior of Ag^{+} calf thymus DNA during a birefringence experiment. Table IV shows the changes in steady state birefringence as a function of the number of high field pulses applied to the sample. The birefringence increases about 70 %, contrary to observations on other DNA preparations. At the same time a profound change in the UV spectrum had taken place. The maximum had shifted by about 40 Å to shorter wavelengths and decreased (Fig. 19). These facts indicated that the internal structure of the Ag-DNA had been changed during application of the

Figure 18

The relation of the electric polarizability as $-\log \alpha_{\parallel}$ to the length, 2a, of rigid, rod-like molecules as given by equation 10.
a) Calculated using $f(\epsilon_{\parallel}, P) = 1$, b = 15 Å, $\epsilon_0^{50} = 86$

b) Calculated using $f(\epsilon_{\parallel}, P) = 0.1$, same b and ϵ_0^{50}.

The horizontal lines indicate the range of observed values for the electric polarizability with Na-, Li- and Mg-calf thymus DNA.

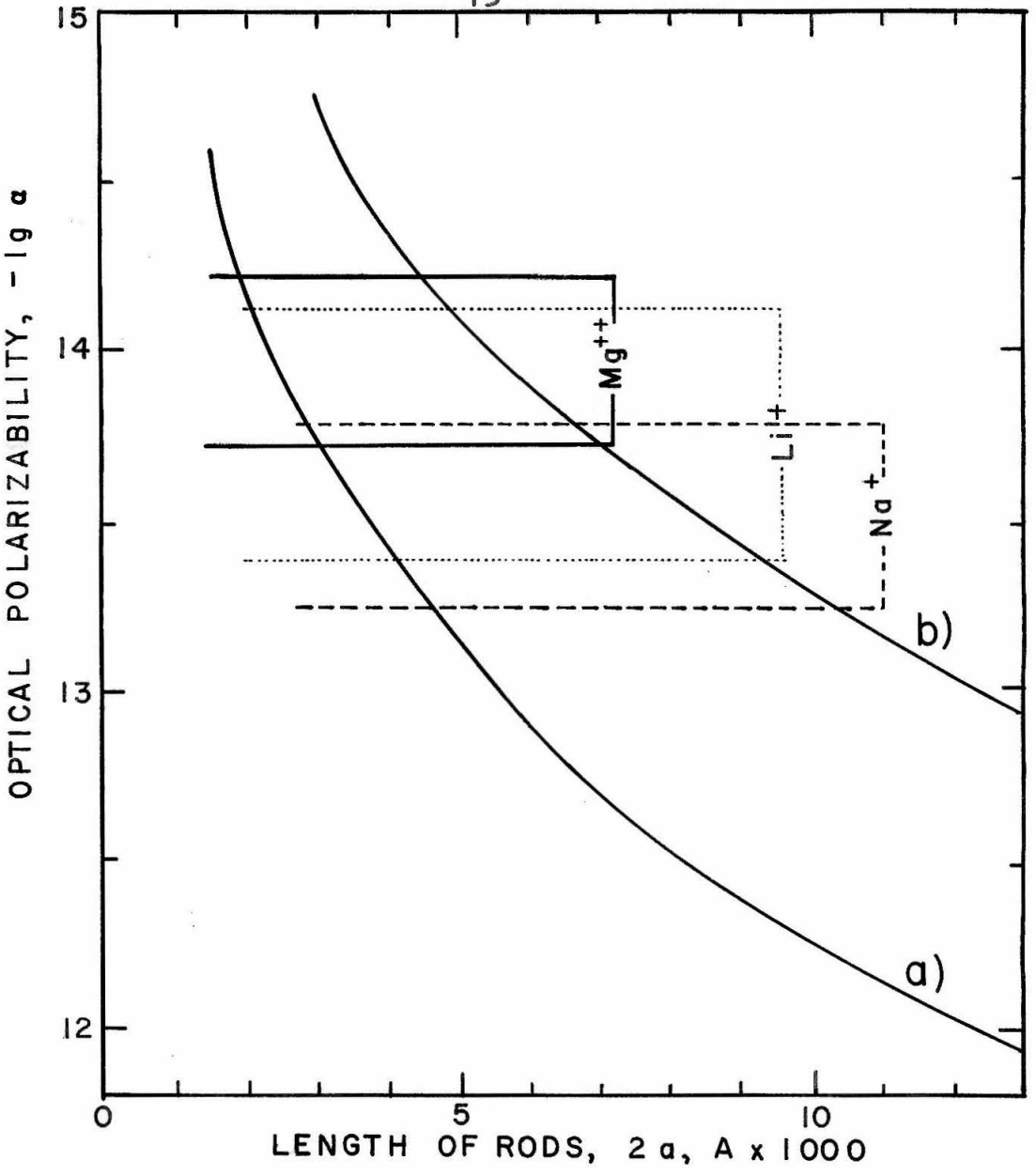
15
14
13
12
0
5
10
OPTICAL POLARIZABILITY, - lg α
LENGTH OF RODS, 2 a, A x 1000
Mg++
Li+
Na+
a)
b)

Figure 18

Table IV

Pulse Number	Field Str. V/cm	Pulse Time msec	Bire-frin-gence	Steady State Pulse Time msec	Steady State Bire-frin-gence
1	4370	3	3.47°	-	-
2	4500	1.5	3.39°	-	-
3	4000	3	3.87°	29.	4.4°
six low field pulses					
10	3750	3	4.56°	50.	6.0°
11	4000	3	5.16°	50.	6.25°
12	4000	3	5.47°	50.	6.65°
13	4040	-	-	50.	7.0°
14	4060	-	-	50.	7.0°

Ag-calf thymus DNA, sample number 18.

fields, giving a more native DNA, probably as a result of the removal of the silver ions from their binding sites between the bases (32). This suggestion would also explain the observed anomalous increase in birefringence signal, for it should be expected, that as the interstitial silver ions are removed, the electrical polarizability is increased.

Figure 19

UV absorption spectrum of a solution of calf thymus DNA in 2.2 x 10^{-4} N Ag^+ (r_b = 2.0) corrected for solvent blank and adjusted to zero absorption at 3600 Å,

a) before birefringence and

b) after birefringence.

Spectrum and birefringence were measured at about 5 °C.
Sample number: 18.

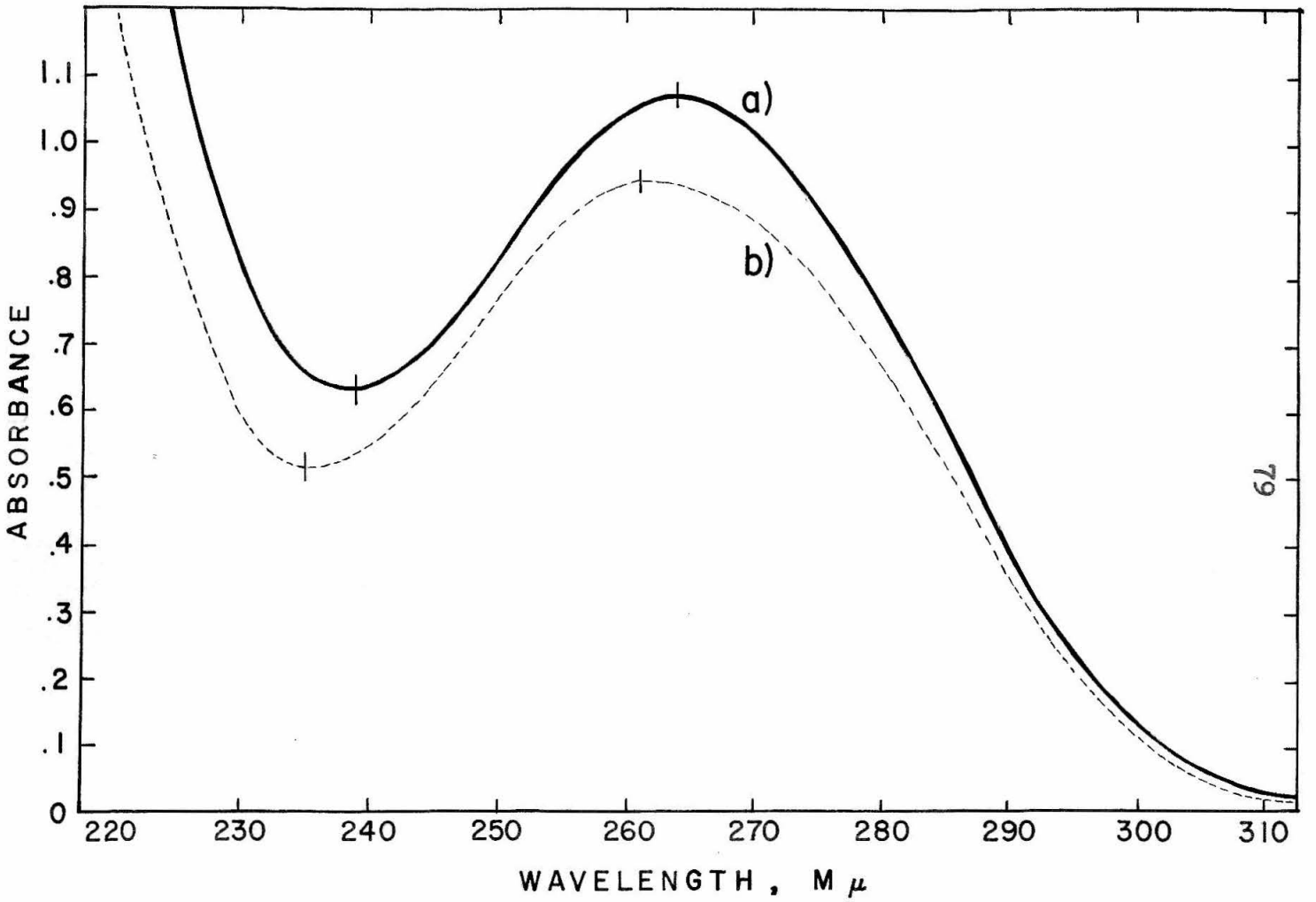
a)
b)
ABSORBANCE
0
.1
.2
.3
.4
.5
.6
.7
.8
.9
1.0
1.1
220
230
240
250
260
270
280
290
300
310
WAVELENGTH, M μ

Figure 19

3. Orientation - Disorientation

Preliminary experiments with sodium calf thymus DNA had shown that the decay behavior of the birefringence signal was that of a very heterogeneous system. It was thought that preparations of bacterial and viral DNA, which are known to be more homogeneous from other measurements (33), would give more homogeneous decay times. That this was not the case can be seen from figure 20, showing a number of representative decay curves from high field steady state birefringence of various DNA samples. Attempts to analyze these decay curves in terms of superimposed decay times of hypothetical rigid rods proved unsuccessful, since the data did not permit unique solutions to the decay equation (Eqn. 20), because neither the volume fractions nor the rotational diffusion constants were known. Depending upon what assumptions were made to fit the decay curves, different answers were obtained.

Furthermore, it must be pointed out that it is at present not possible to distinguish between the birefringence decay of an arbitrary collection of rigid rods and that of more or less flexible molecules without additional information from other sources.

Figures 20a,b

Typical birefringence decay of various DNA samples:

Sample Number	Type of DNA	Ionic Str. x 10^4	Conc. mg/l	R_{230}	Temp. °C	Field Str. V/cm	Pulse Dura. msec	Relax. Time msec
28	Li-λ	11.87	18.5	1.98	3.7	1780	5.0	0.45
27	Li-T2	5.95	21.9	1.86	5.6	3620	50.	0.66
14	Mg-C.T.	0.79	24.4	1.94	4.5	4500	19.	0.86
26	Mg-T4	0.88	27.6	1.98	3.8	4500	51.	2.13
8	Li-C.T.	2.85	24.2	2.12	4.3	4125	51.5	2.7
33	Na-Coli	1	118.8	-	5.2	3500	50.	160.
37	Na-Lyso	1	56.5	1.76	5.2	2940	95.	186.

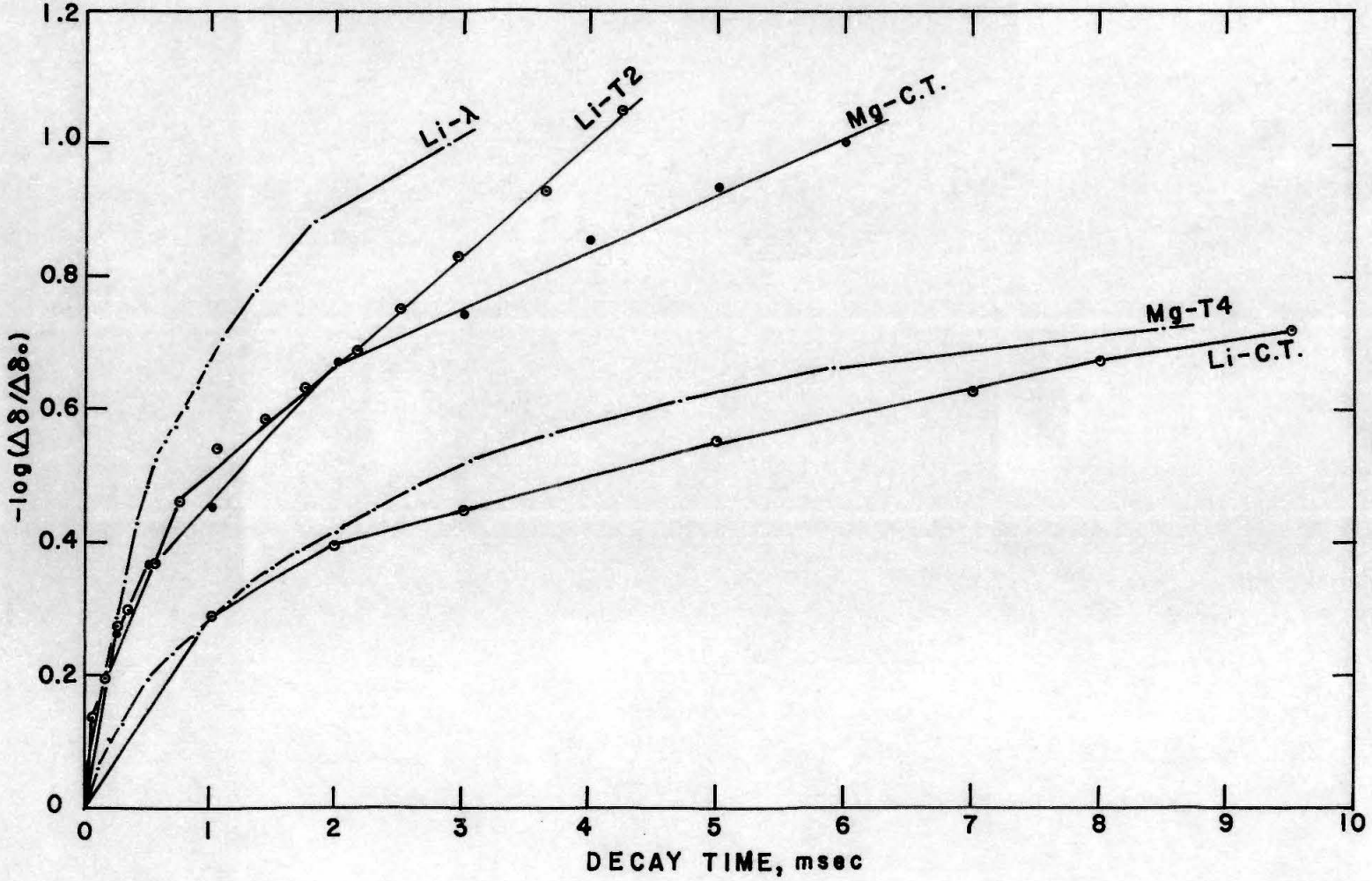
1.2
1.0
0.8
0.6
0.4
0.2
0
-log(Δ8/Δ8∞)
0
1
2
3
4
5
6
7
8
9
10
DECAY TIME, msec
Li-λ
Li-T2
Mg-C.T.
Mg-T4
Li-C.T.

Figure 20a

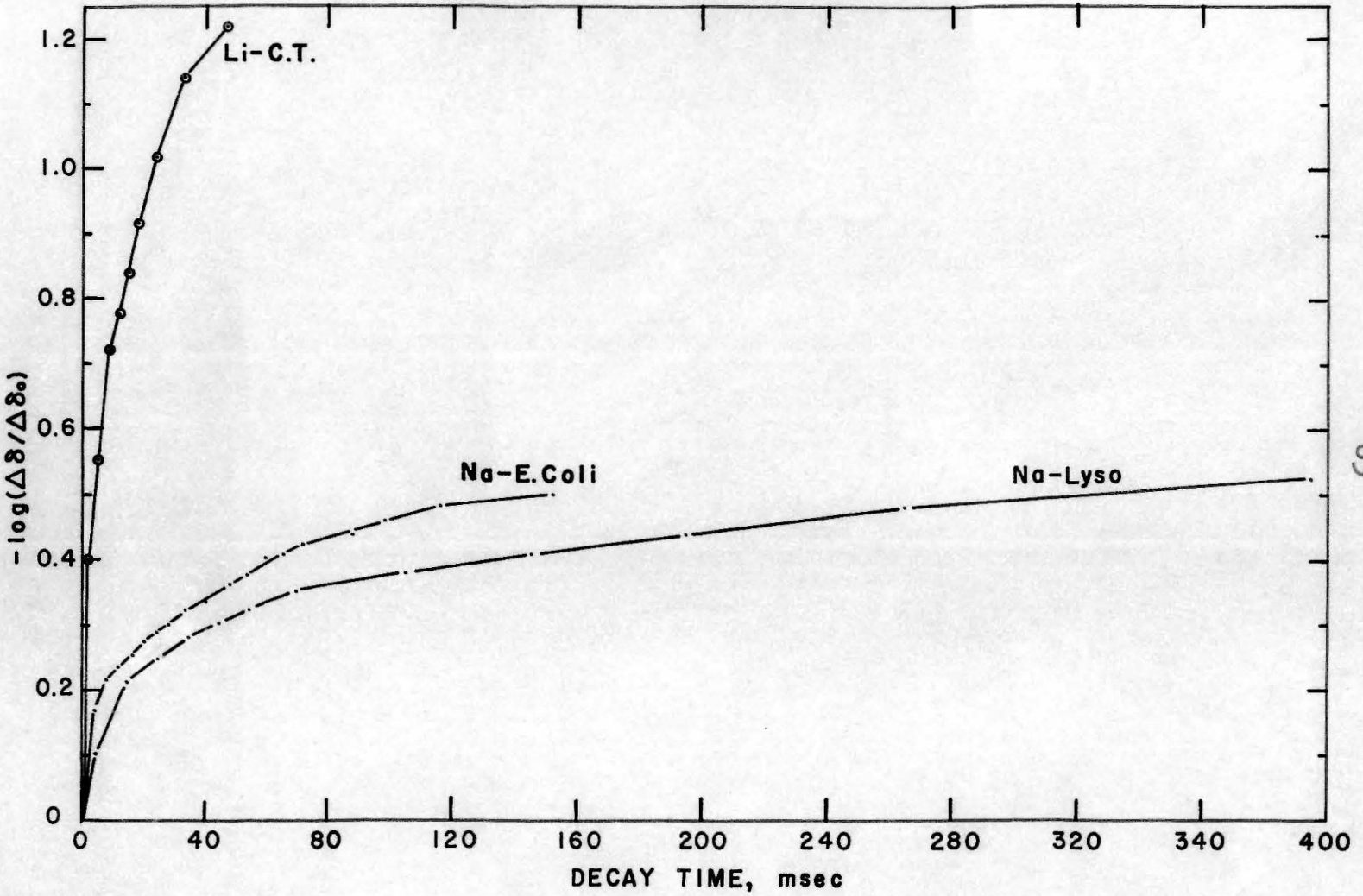
Li-C.T.
Na-E.Coli
Na-Lyso
$-\log(\Delta\delta/\Delta\delta_0)$
DECAY TIME, msec
0
0.2
0.4
0.6
0.8
1.0
1.2
0
40
80
120
160
200
240
280
320
340
400

Figure 20b

Because of these inherent difficulties, we have given up analysis of each individual decay curve with regard to possible size distributions. Rather, we have determined a "characteristic" relaxation time, τ, taken as the time at which the steady state birefringence signal had decreased to 1/e.

In comparing these characteristic relaxation times, it soon became apparent, that a considerable number of parameters were affecting the results:

1) Ionic strength: Increases in the conductivity (salt concentration) of a sample caused a decrease in the decay times (Fig. 21).

2) Field strength: Changes in the amplitude of the applied field had different effects on the relaxation times. In several experiments the data showed a clear trend toward increasing relaxation times with lowered field strengths. This was the case with most Li and Mg-thymus DNA samples, with Li-T-2 and Na-T-4 DNA. In most experiments with Na-E. Coli DNA the effect was reversed. In other experiments no obvious relation was discernable or the data varied too much to permit meaningful conclusions (Fig. 22).

3) Pulse duration: Increasing the duration of the aligning pulse, up to the time when heating became pronounced, gave generally increased relaxation times. However, as in the previous case, there were a few exceptions,

Figure 21

Average "characteristic" relaxation times, τ, for Mg-calf thymus DNA and Na-T4 DNA (dashed lines) are plotted against the ionic strength of the solutions. The vertical lines indicate the average variation of τ. The DNA samples are those listed in table III.

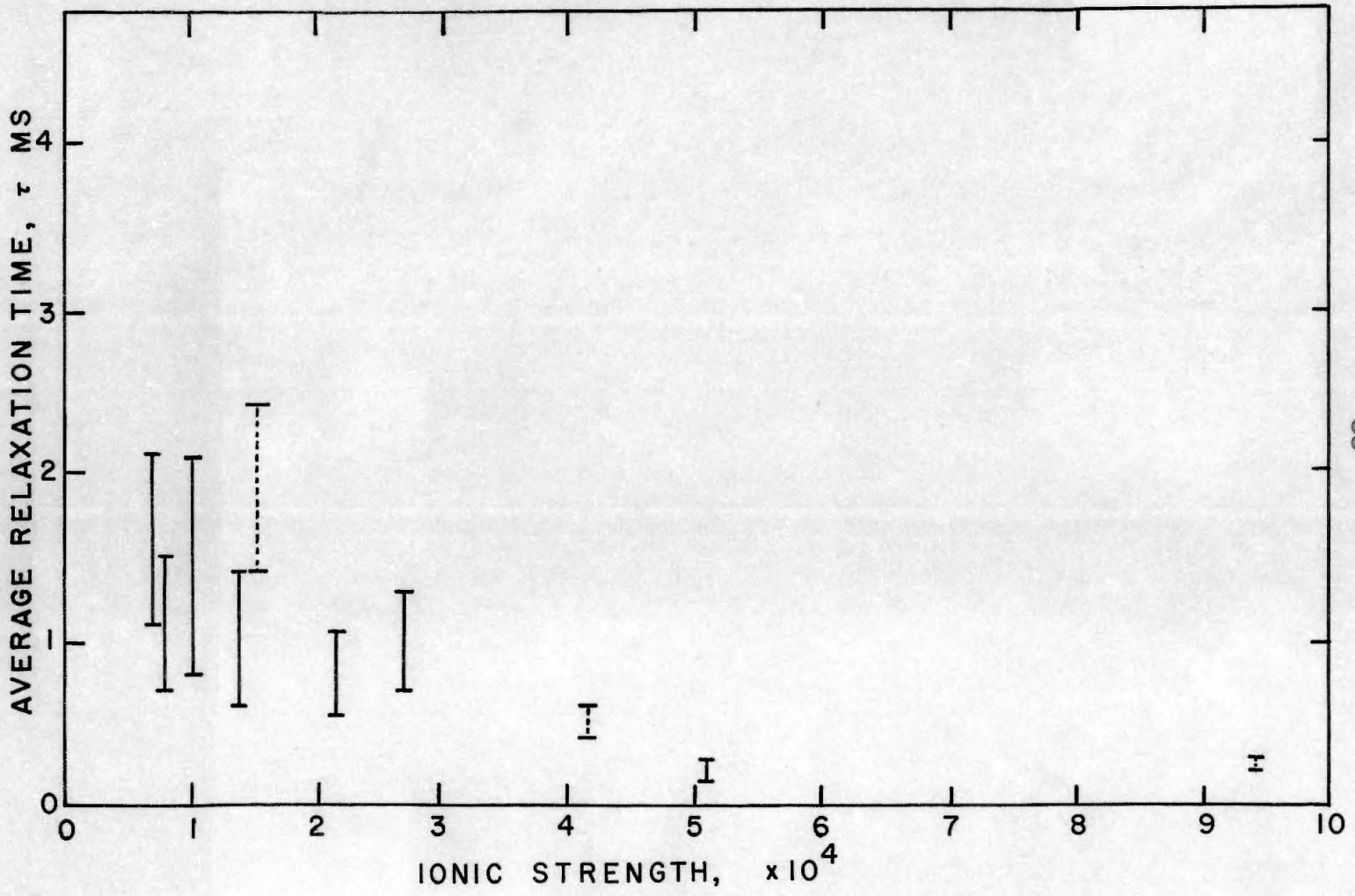
AVERAGE RELAXATION TIME, τ MS
0
1
2
3
4
0
1
2
3
4
5
6
7
8
9
10
IONIC STRENGTH, x10^4

Figure 21

Figure 22

Variation of decay times as a function of field strength for various DNA samples:

Sample Number	Type of DNA	Ionic Strength x 10^4	Concentration mg/l	R_{230}	Temperature °C
14	Mg-C.T.	0.79	24.4	1.94	4.5
8	Li-C.T.	2.85	24.2	2.12	4.3
27	Li-T2	5.95	21.9	1.86	5.6
19	Na-T4	1.82	51.4	2.28	3.8
35	Na-Coli	1	45.6	-	4.9
33	Na-Coli	1	118.8	-	5.2

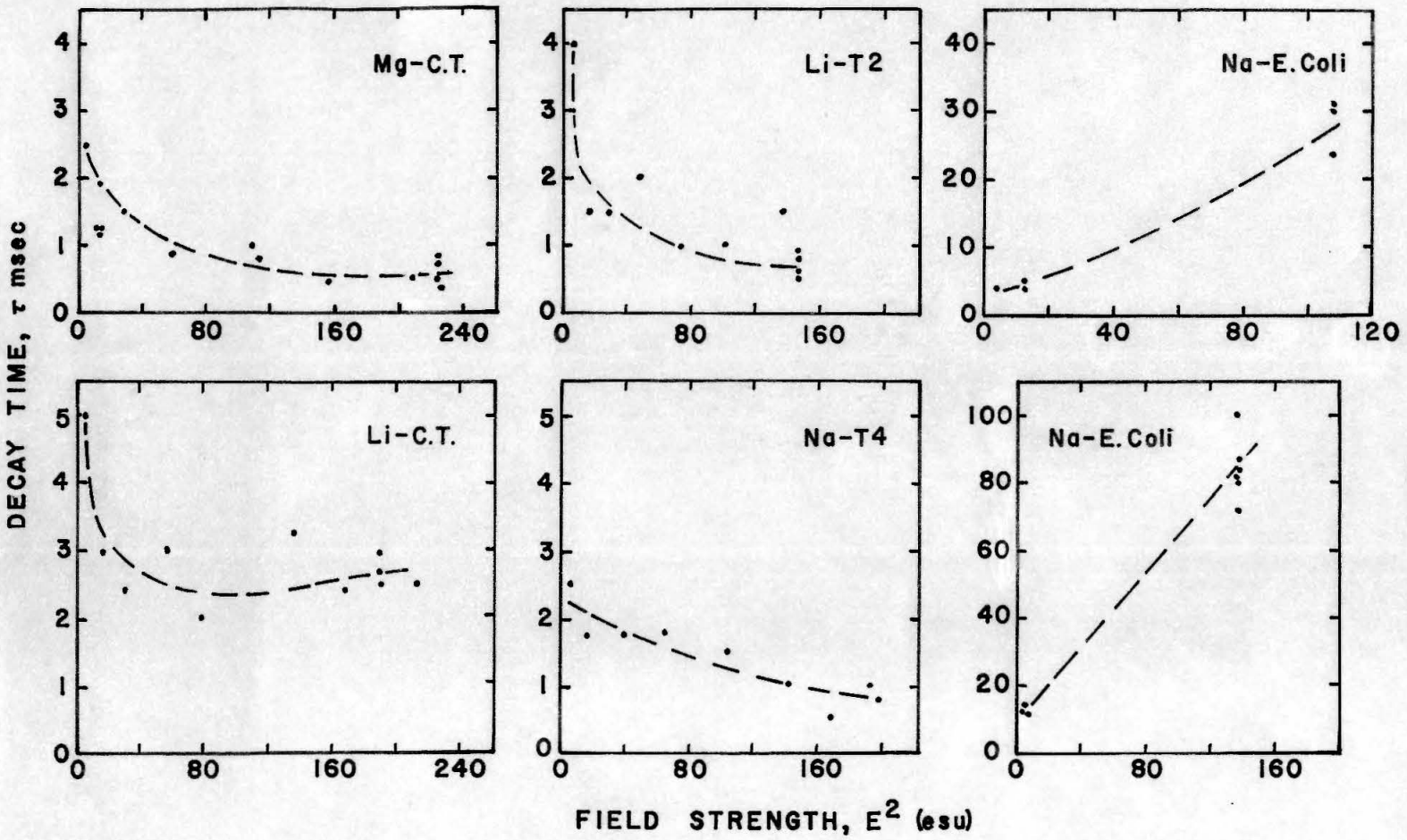
Mg-C.T.
Li-T2
Na-E.Coli
Li-C.T.
Na-T4
Na-E.Coli
DECAY TIME, τ msec
FIELD STRENGTH, E² (esu)

Figure 22

where the reverse effect was observed (Lysodeikticus and Megatherium DNA) or where the effect was negligible or the data too poor (Fig. 23).

4) Temperature: The effects of temperature on the birefringence results will be discussed in more detail later. It suffices here to note that the relaxation times decrease as the temperature increases much above 10° C.

5) Others: Finally, there were the obvious effects of aging, excessive number of pulses and similar things causing degradation of the DNA and therefore a decrease in the characteristic relaxation times.

From the above it should be apparent that interpretation of the relaxation times is rather difficult in view of the many independent parameters affecting the results in varying degrees. In order to obtain meaningful data, it is necessary to understand the effects of each of the variables independently of all the others. This, however, requires an effort, which we considered out of proportion to the information that we wanted to obtain with regard to the structural parameters of the DNA.

Nevertheless, a few interesting conclusions can be drawn from the decay analyses:

1) The decay of DNA solutions is heterogeneous irrespective of the source of the DNA.

Figure 23

Variation of decay times as a function of pulse duration for various DNA samples:

Sample Number	Type of DNA	Ionic Strength x 10^4	Concentration mg/l	R_{230}	Temperature °C
7	Li-C.T.	2.82	24.2	2.12	3.8
25	Mg-T4	1.26	27.7	2.10	4.0
24	Mg-T4	1.18	27.7	2.10	3.3
20	Na-T4	2.43	51.4	2.28	5.9
2	Na-C.T.	1	93.3	-	4
3	Na-C.T.	1	58.4	-	4
12	Mg-C.T.	3.73	58.0	2.0	5.0
29	Na-Coli	1	155.2	-	4.0
36	Na-Lyso	1.09	72.1	-	2.9
42	Mg-B.M.	1	63.6	-	4.1

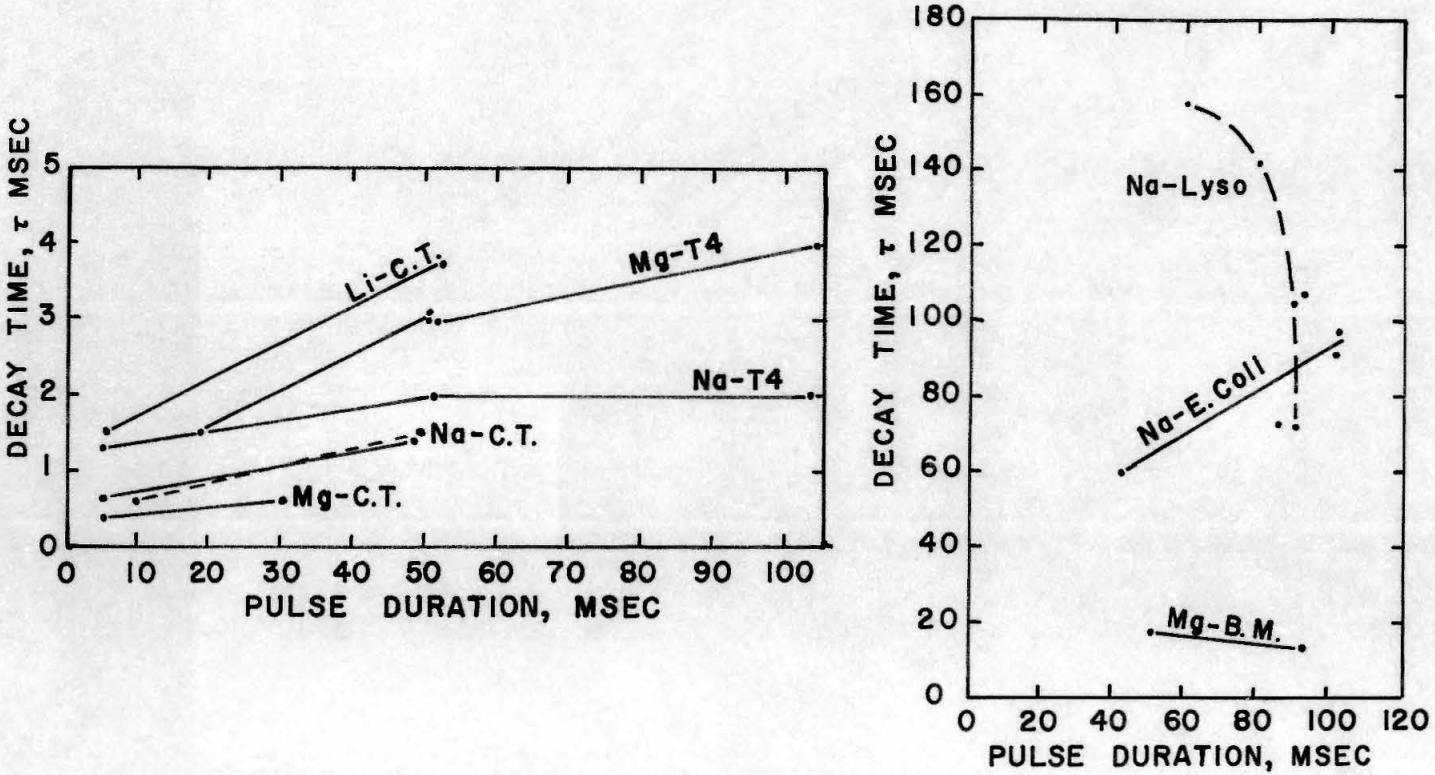
DECAY TIME, τ MSEC
PULSE DURATION, MSEC
Li-C.T.
Mg-T4
Na-T4
Na-C.T.
Mg-C.T.
Na-Lyso
Na-E.Coll
Mg-B.M.

Figure 23

2) Calf thymus and viral DNA's have low characteristic relaxation times ranging from 0.5 to about 15 msec, while bacterial DNA may have decay times which are larger by an order of magnitude.

Table V gives a summary of average characteristic relaxation times measured on a variety of samples. Since the averages of the relaxation times per sample were obtained irrespective of the field strength and pulse duration, the uncertainties are rather large. The data are presented only to indicate the general magnitude of the values that have been observed.

The temperature was about 5° C, and the slight variations have insignificant effects on the decay times. DNA concentrations are given in mg/l. The average ionic strength of each sample is also indicated. The approximate decay times of columns 8 and 9 were estimated from plots of τ versus E^2 and are intended to show the range of variation observed as a function of field strength. Column 10 gives the approximate length of Ångstrom of a rigid rod (estimated from Fig. 3) having a decay time equal to that of the average of the sample (Column 6).

The most striking conclusion that table V suggests is the significantly slower relaxation time of most of the bacterial DNA samples as compared to calf thymus and viral DNA.

Table V

DNA	ion	ion. str. x10^4	DNA mg/l	T°C	av. τ ms	range ms ±	estimated τ ms $E^2 \rightarrow o$	estimated τ ms E^2=100	equiv.rod x 10^{-3} Å	#
C.Th.	Na	1.	93.3	2.	1.6	0.2	1.	1.7	4.5	1
"	"	1.30	26.8	4.6	5.5	0.7	4.	7.	7.	4
"	"	1.35	"	5.0	9.5	1.4	6.	10.	8.5	5
"	Li	2.14	24.2	3.4	3.	0.75	2.	3.5	6.	6
"	"	2.82	"	3.8	3.3	1.4	8.	2.5	6.	7
"	"	2.85	"	4.3	2.9	0.5	5.	2.5	5.5	8
"	Mg	1.38	72.2	4.5	1.	0.4	1.	1.	4.	9
"	"	2.19	"	4.9	0.8	0.25	2.	0.8	3.5	10
"	"	5.08	"	4.4	0.21	0.06	0.25	0.25	3.	10
"	"	1.26	62.1	3.5	1.2	0.3	1.	1.2	4.	13
"	"	3.73	58.0	5.0	0.9	0.3	2.	0.8	4.	11
"	"	0.79	24.4	4.5	1.1	0.4	2.5	0.9	4.	14
"	"	0.68	15.4	3.8	0.6	0.2	1.2	0.6	3.5	16
"	"	0.68	7.0	5.3	1.6	0.5	3.5	1.1	4.5	17
T-4	Na	1.82	51.4	3.8	1.45	0.5	2.5	1.5	4.5	19
"	"	2.43	"	5.9	2.3	0.5	2.5	2.	5.	20
"	"	1.57	19.9	4.0	1.9	0.5	2.5	2.	5.	21
"	"	4.16	"	4.6	0.5	0.1	0.5	0.4	3.5	21
"	"	9.38	"	4.5	0.24	0.02	-	0.25	3.	21
"	Li	3.38	35.4	3.8	12.	5.2	5.	20.	9.	22
"	"		"	4.3	11.1	4.8			9.	22
"	"		"	4.1	9.5	3.0	8.	13.	8.5	22
"	"	9.10	17.0	4.2	0.9	0.1	1.	1.	4.	23
"	Mg	1.18	27.7	3.3	2.	0.8	1.8	1.5	5.	24
"	"	1.26	"	4.0	3.1	0.6	3.5	3.	6.	25
"	"	0.88	27.6	3.8	2.7	0.35	3.	2.5	5.5	26
T-2	Li	5.95	21.9	5.6	1.4	0.6	4.	1.	4.5	27
Lambda	"	11.87	18.5	3.7	0.45	0.01	0.6	-	3.5	28
Coli	Na	1.	155.2	4.0	67.	22.	15.	80.	16.	29
"	"	"	151.8	4.7	106.	3.	-	100.	20.	30
"	"	"	148.5	6.	46.	38.	10.	55.	14.5	31
"	"	"	147.2	5.0	26.6	26.1	5.	40.	12.	32
"	"	"	118.8	5.2	52.	36.	10.	65.	15.	33
"	"	"	45.6	3.4	16.8	16.4	1.	50.	10.5	34
"	"	"	"	4.9	8.2	7.7	3.	27.	7.	35
Lyso	"	1.09	72.1	2.9	96.	37.	10.	120.	19.5	36
"	"		56.5	5.2	142.	81.	10.	180.	24.	37
"	Li	2.52	23.0	4.3	6.7	2.1	4.	8.	7.5	38
"	"			4.0	14.5	3.6	-	17.	10.	39
"	"			4.2	2.6	0.9	3.	3.	5.5	40
"	Mg	1.50	72.9	4.8	76.	65.	10.	180.	18.	41
Mega.	"		63.6	4.1	12.7-	5.1	4.	20.	9.5	42
"	"	2.88	18.8	4.8	1.2	0.2	-	1.3	4.	43
"	"		15.6	3.8	1.5	0.5	-	1.5	4.5	44

4. Temperature Effects

Work by a number of investigators (34) had shown that DNA undergoes drastic structural changes upon heating in dilute salt solutions. These changes involve breakage of the intramolecular hydrogen bonds of the DNA double helix and subsequent unwinding of the individual strands to form highly flexible random coils. It was therefore of interest to examine the changes in birefringence behavior of DNA solutions upon heating to investigate the effects which these structural rearrangements have on the various parameters.

With this in mind, it is important that extraneous temperature effects on the electric and optic behavior of the system, as well as the hydrodynamic behavior of the solution are analyzed and compensated for.

With regard to the optical system, temperature variations should not change the optical properties and equation 6 should still be applicable for the determination of δ. Changes in the refractive index due to the temperature changes should not effect the intensity ratio unless there are inhomogeneous refractive index variations due to convection and localized heating.

As for the electric system, an increase in temperature results in a decrease of the electric field due to the decreasing resistance of the solution. However, since we measure the field simultaneously with the birefringence signal, the field strength can be accurately determined. In fact, we should be able to calculate the temperature changes during a pulse from the change in field strength and a knowledge of the conductivity behavior of the solution as a function of temperature, if we assume that the power input remains constant.

The effect of temperature on the electro-optical properties of the DNA should be due to the sum of the changes of each of the main parameters which determine the birefringence:

1) Variations in the polarizability of the counterion atmosphere.

2) Variations in the hydrodynamic properties of the solution as evidenced by changes in the rotational diffusion constant, which should be proportional to T/η_{H_2O}, irrespective of the molecular shape. This effect should be particularly pronounced in the decay of the birefringence signal, with short relaxation times being affected more than longer ones.

Figure 24

Oscilloscope tracing of changes in the transmitted light (I_A) of a 10^{-4} F $NaClO_4$ solution initially at 4.8 °C in response to a 2.1 sec pulse of a 10 Kc/sec alternating field of initially 3000 V/cm (final field 1625 V/cm). I_{A_o} = 135 mV.

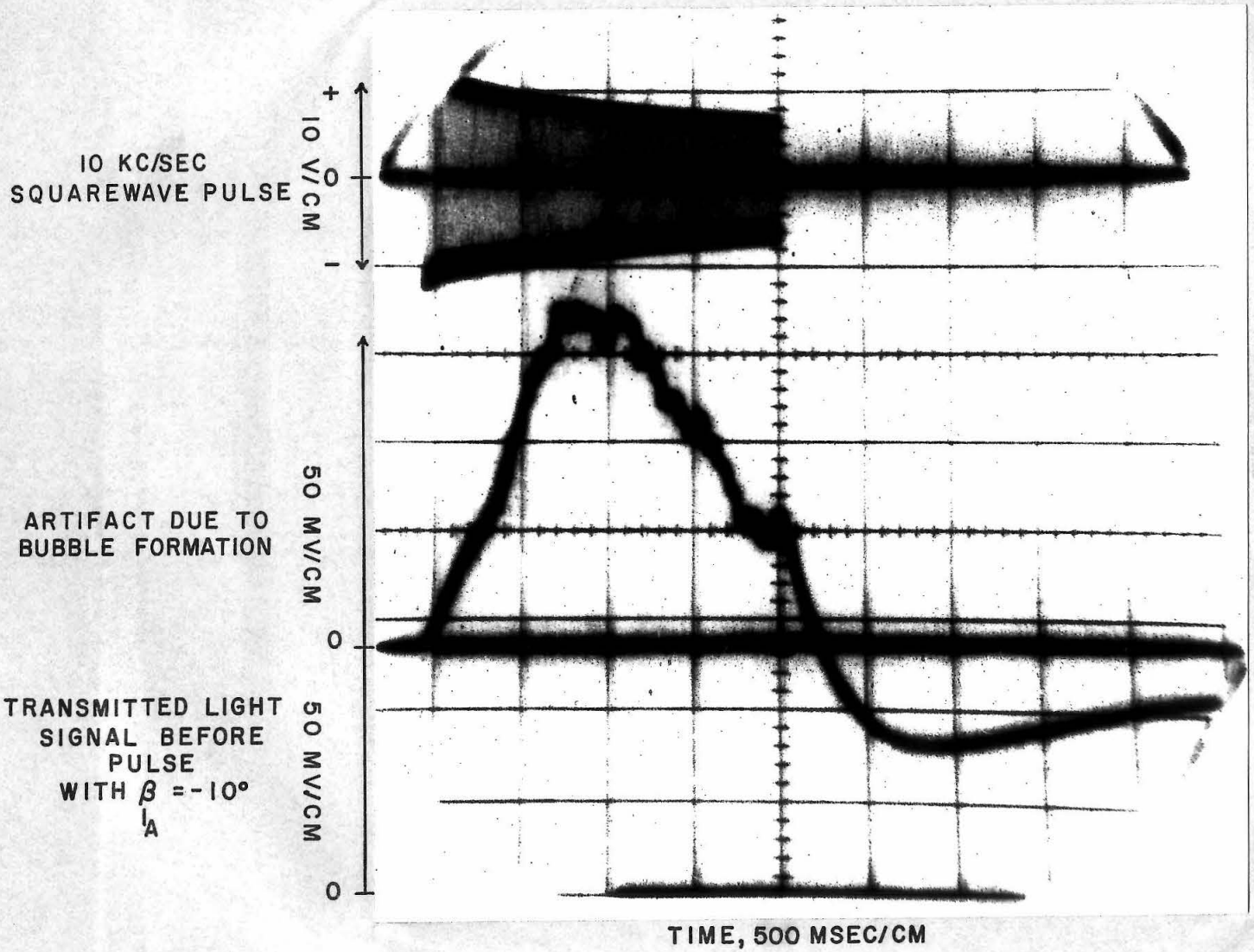
10 KC/SEC
SQUAREWAVE PULSE
+
10 V/CM
0
-
ARTIFACT DUE TO
BUBBLE FORMATION
50 MV/CM
0
TRANSMITTED LIGHT
SIGNAL BEFORE
PULSE
WITH $\beta = -10°$
I_A
50 MV/CM
0
TIME, 500 MSEC/CM

Figure 24

3) Variations in the optical anisotropy should be due mainly to intramolecular changes such as weakening of the hydrogen bonds, permitting bending, or even rotation of the individual bases. Slight displacements of the base pairs from their positions perpendicular to the molecular axis should have pronounced effects on Δg.

Blank experiments with 10^{-4} F $NaClO_4$ at temperatures from 1.8 to 32° C showed that there was danger of erratic changes in transmitted light intensity upon application of long, high field (4000 V/cm) 10 kc/sec square wave pulses, which could be traced to the formation of tiny bubbles (either from boiling or electrolysis). A typical signal is shown in figure 24. Turning the field off resulted generally in a decrease in light intensity, sometimes below that of the initial intensity, due to a sudden release and rise of the bubbles. Thus, it is essential that the solutions are de-gassed before a temperature experiment and that the field strength and pulse duration are kept below that required for bubble formation.

From the above it is evident that heating of the DNA solution should not be carried out by using long aligning pulses, but rather by immersing the solution in a temperature bath prior to application of the fields.

Figure 25 shows the results of two heating experiments with Na-calf thymus DNA. The samples were heated slowly and a series of low to high field pulses was applied at certain temperatures so that the birefringence signal at infinite field could be determined for each of these temperatures. These saturation birefringence signals are according to equation 16, directly proportional to C_v, if the slight changes in the refractive index with temperature are neglected. C_v may be interpreted here in terms of the volume fraction of alignable, i. e. native DNA molecules or molecular regions. Thus, changes in δ_s should indicate the degree of denaturation of the DNA. In comparing the birefringence data with the heat denaturation curve, it was assumed that the saturation birefringence of denatured DNA is zero. If this assumption is accepted, then it must be deduced from the "birefringence melting curve", that there are structural changes which occur about 8 to 10° C below the breakage of hydrogen bonds as measured by heat denaturation.

Further indications as to the nature of these structural changes may be obtained from an analysis of the relaxation times. For this purpose it is useful to multiply the characteristic relaxation times by a temperature dependent factor $(T\eta_o/T_o\eta)$ in order to standardize the structural

Figure 25

Heat denaturation of Na calf thymus DNA (26.8 mg/l, $R_{230} = 2.38$, sample number 4) in Na-cacodylate (1.30×10^{-4} μ_Ω)
Curve 1 measured in the Cary spectrophotometer.
Curve 2 measured by changes in the saturation birefringence, normalized to zero birefringence for denatured DNA. Full and open circles represent two sets of experiments run 8 days apart on different aliquots of the same DNA (samples number 4 and 5).

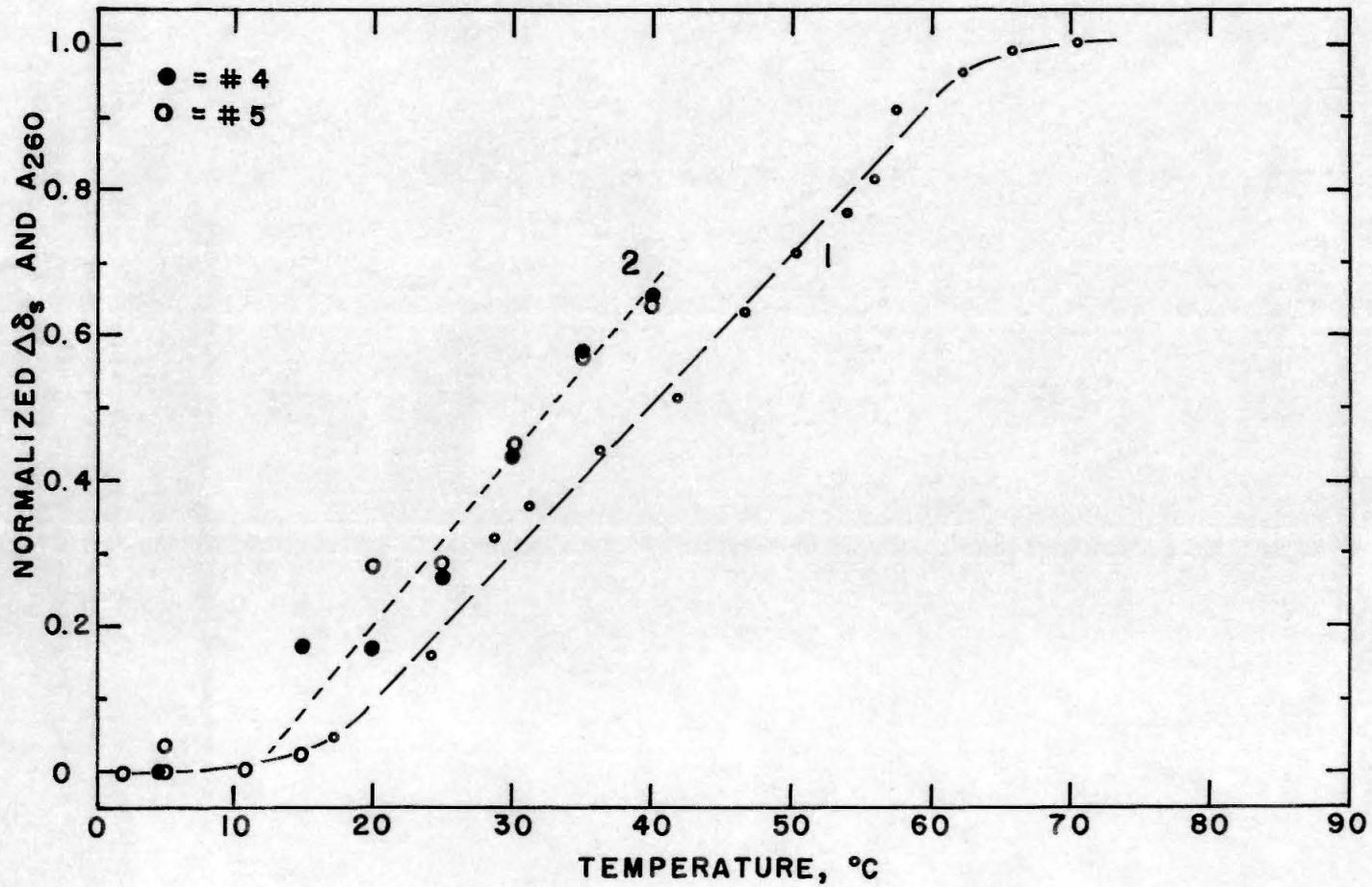
● = #4
o = #5
NORMALIZED $\Delta\delta_s$ AND A_{260}
TEMPERATURE, °C
1.0
0.8
0.6
0.4
0.2
0
0
10
20
30
40
50
60
70
80
90
1
2

Figure 25

parameters and to remove the temperature dependence (η_o = 0.018 for H_2O at 0°C, T_o = 273.16 °K)

$$\tau_o = \tau \frac{T\ \eta_o}{T_o \eta} = \frac{4\pi\eta_o}{9\ kT_o} \frac{a^3}{(\ln(2a/b) - 0.80)} \qquad (24)$$

The data (Fig. 26a) show that the decrease in saturation birefringence is followed or even preceded by a decrease in relaxation times, confirming that structural changes do occur before significant hydrogen bond disruption and suggesting that these changes are either due to breakage (double strand scission) or increased flexibility of the double helix.

For comparison with the above results figure 26b shows the changes in τ_o observed during heating of a sample of Na-E. Coli DNA. This sample, having much higher relaxation times than calf thymus DNA, shows much less fluctuations in the decay times at a given temperature than calf thymus DNA. There is also much less tendency for the early rapid decrease in decay times observed with calf thymus DNA. In fact the behavior is very much like that commonly observed during heat denaturation monitored by optical density changes. There is also considerable recovery of longer decay times when the DNA is slowly cooled after partial and complete denaturation (dashed lines).

Figure 26a

Changes in the characteristic relaxation time, standardized with respect to 0 °C, τ_0, and in the saturation birefringence, δ_s, upon heating a sample of Na-calf thymus DNA (26.8 mg/l, $R_{230} = 2.38$, sample number 4) in Na-cacodylate (1.30×10^{-4} $\mu\Omega$).
Pulse duration: 50 msec at 5 °C and less at higher temperatures.
Field strength: 3750 to 4375 V/cm.

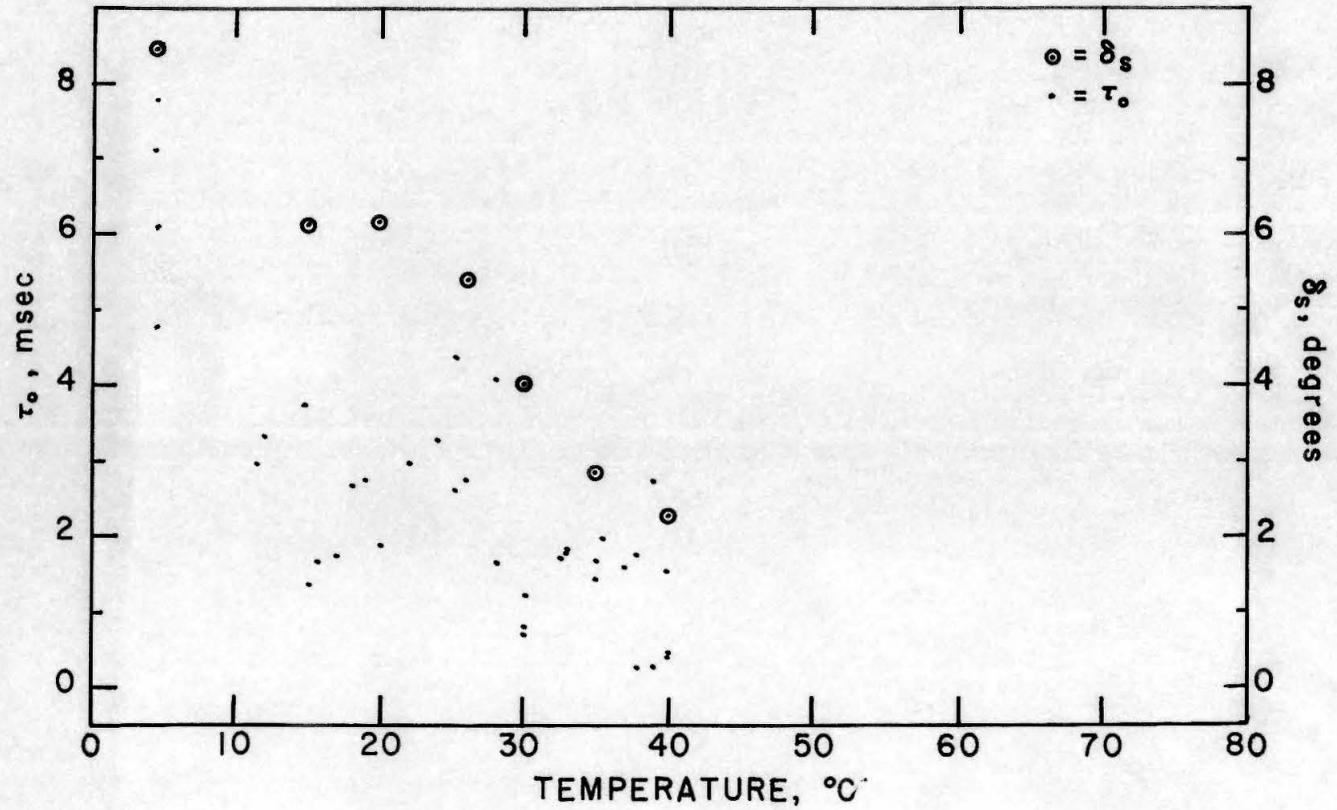
⊙ = δs
• = τo
τo, msec
δs, degrees
TEMPERATURE, °C
0
2
4
6
8
0
10
20
30
40
50
60
70
80

Figure 26a

Figure 26b

Changes in the characteristic relaxation time, standardized with respect to 0 °C, τ_0, upon heating a sample of Na-E. Coli DNA (148.5 mg/l, sample number 31) in 10^{-4} F $NaClO_4$.
Pulse duration: 50 ms at all temperatures.
Field strength: 3280 to 3625 V/cm.

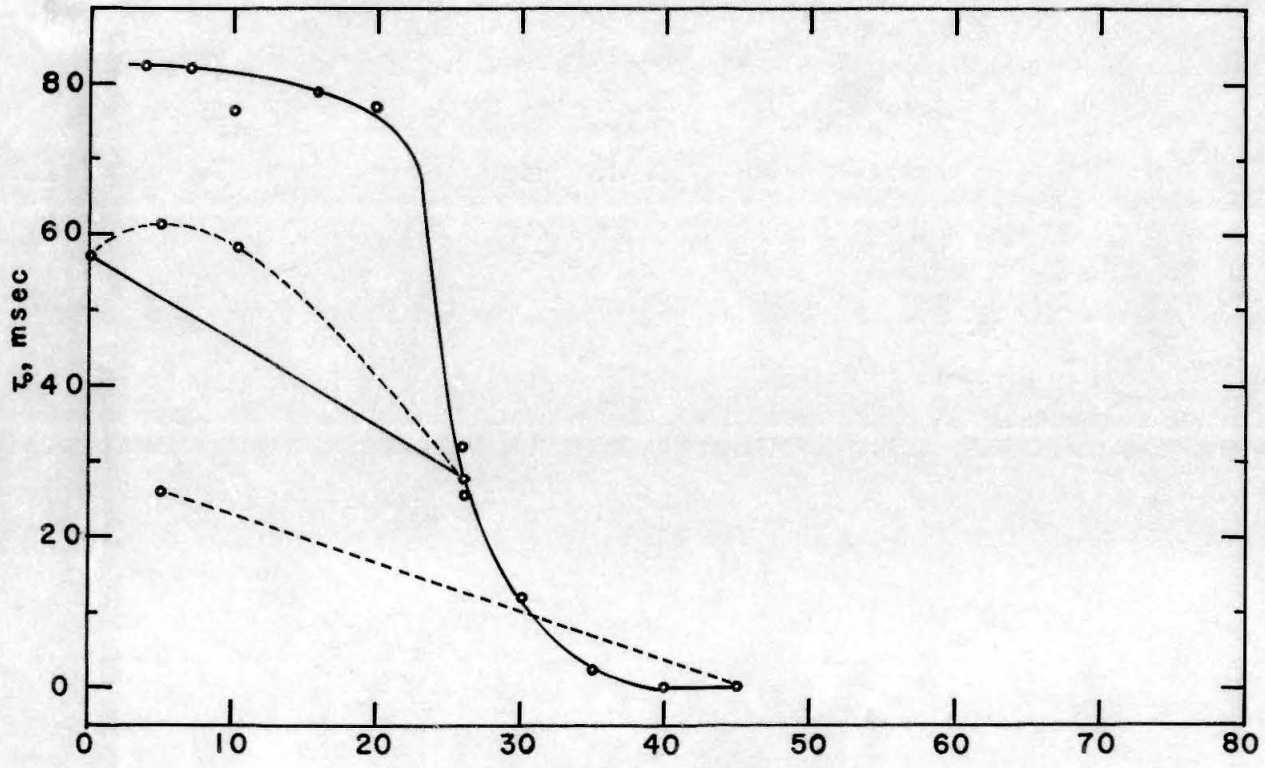

Figure 26b

5. Transient Effects

The possibility of using rapidly repetitive pulses for the analysis of transient structural changes is demonstrated in figure 27a. Here eleven high field (3125 V/cm) 49 msec pulses were applied in rapid succession (within 9 sec) causing almost complete disappearance of the birefringence. Five minutes later recovery of the birefringence signal was complete and another series of 5 pulses was applied (within 3 sec) causing similar effects as in the previous case (Fig. 27b). Figure 28 shows the decay behavior during another series of pulses applied four minutes after the previous ones. This phenomenon and especially its recovery suggests strongly, that it is possible to almost completely distort the axial arrangement of the basepairs (whether this is accompanied by hydrogen bond breakage is uncertain) without causing substantial unwinding at the same time. In order to analyze these kinds of data, however, it is necessary to monitor the temperature changes in the birefringence cell.

Other interesting insights into the processes involved in alignment of the DNA molecules by electric fields may be obtained by a more detailed analysis of the rise (Fig. 29) and steady state signals (Fig. 30). The observable tran-

Figure 27a

Oscilloscope tracings demonstrating the decrease in the birefringence signal of E. Coli DNA (45.6 mg/l, sample number 34) in 10^{-4} F $NaClO_4$ initially at 3.4 °C in response to eleven 49 msec pulses of a 10 Kc/sec alternating electric field of 3125 V/cm applied within 9 sec.
Maximum birefringence: approximately 20°
I_{A_o}: 67.4 mV.

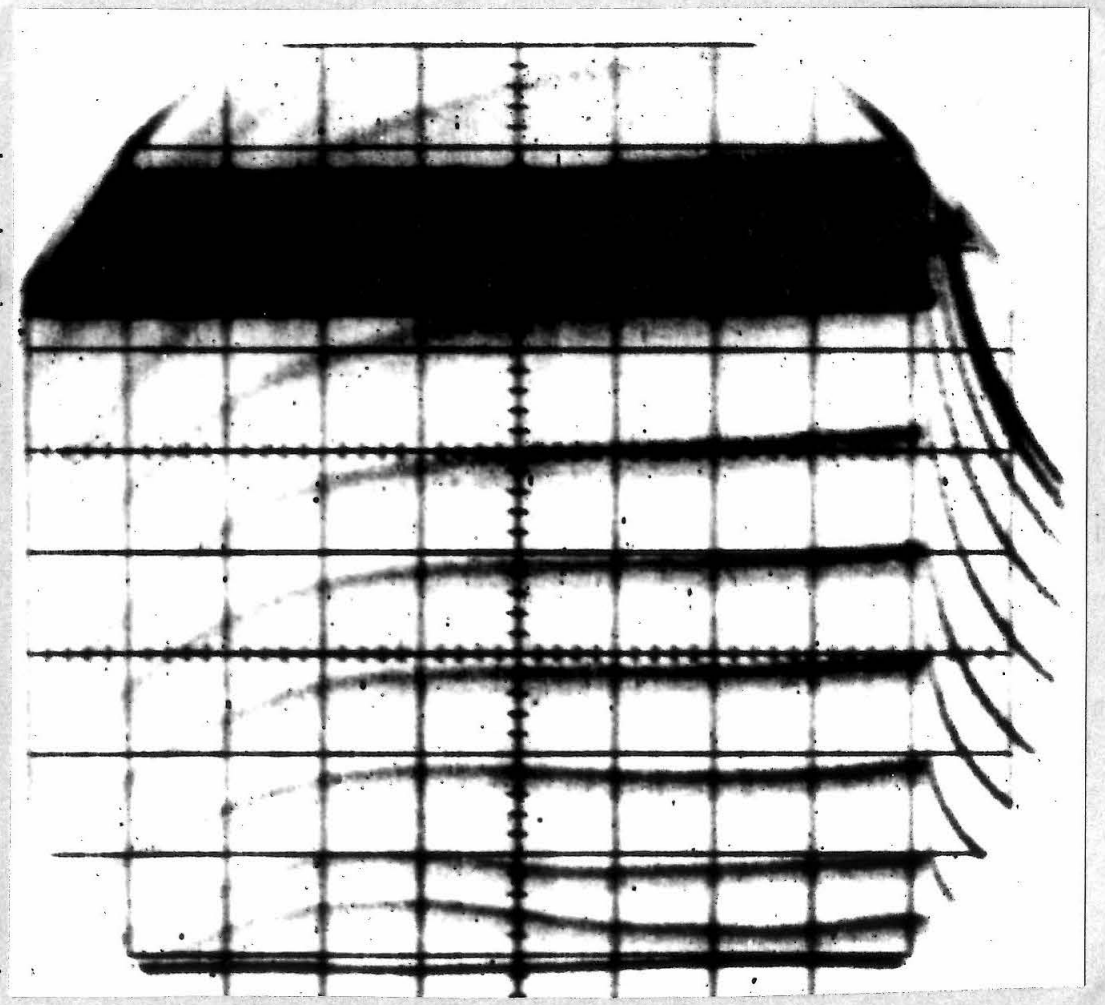
ELEVEN
10 KC/SEC
SQUAREWAVE PULSES
+
20 V/CM
0
-
BIREFRINGENCE
SIGNAL
I_δ
20 MV/CM
0
TIME, 5 MSEC/CM
109

Figure 27a

Figure 27b

Oscilloscope tracings demonstrating the recovery of the birefringence within 5 min. after the treatment shown in figure 27a, and the repeatability of the effect. Five 49 msec pulses of a 10 Kc/sec alternating electric field (not photographed) of 3125 V/om were applied within 3 sec.

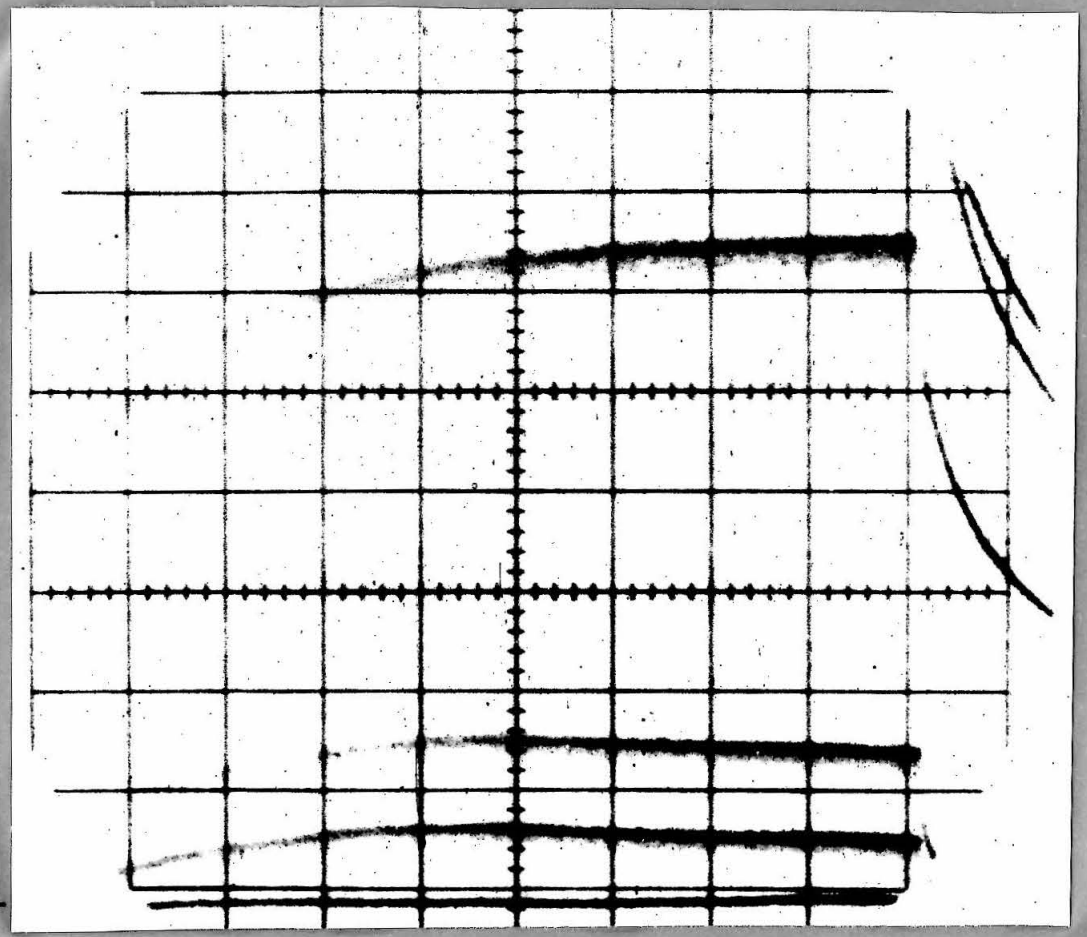

Figure 27b

Figure 28

Oscilloscope tracings of the decay of the birefringence signals of another series of pulses (8 x 49 msec pulses 3125 V/cm applied within 5 sec.) 4 min. after those shown in figure 27b.
Note: The baseline must have shifted downward during application of the pulses, probably as a result of an increase in temperature.

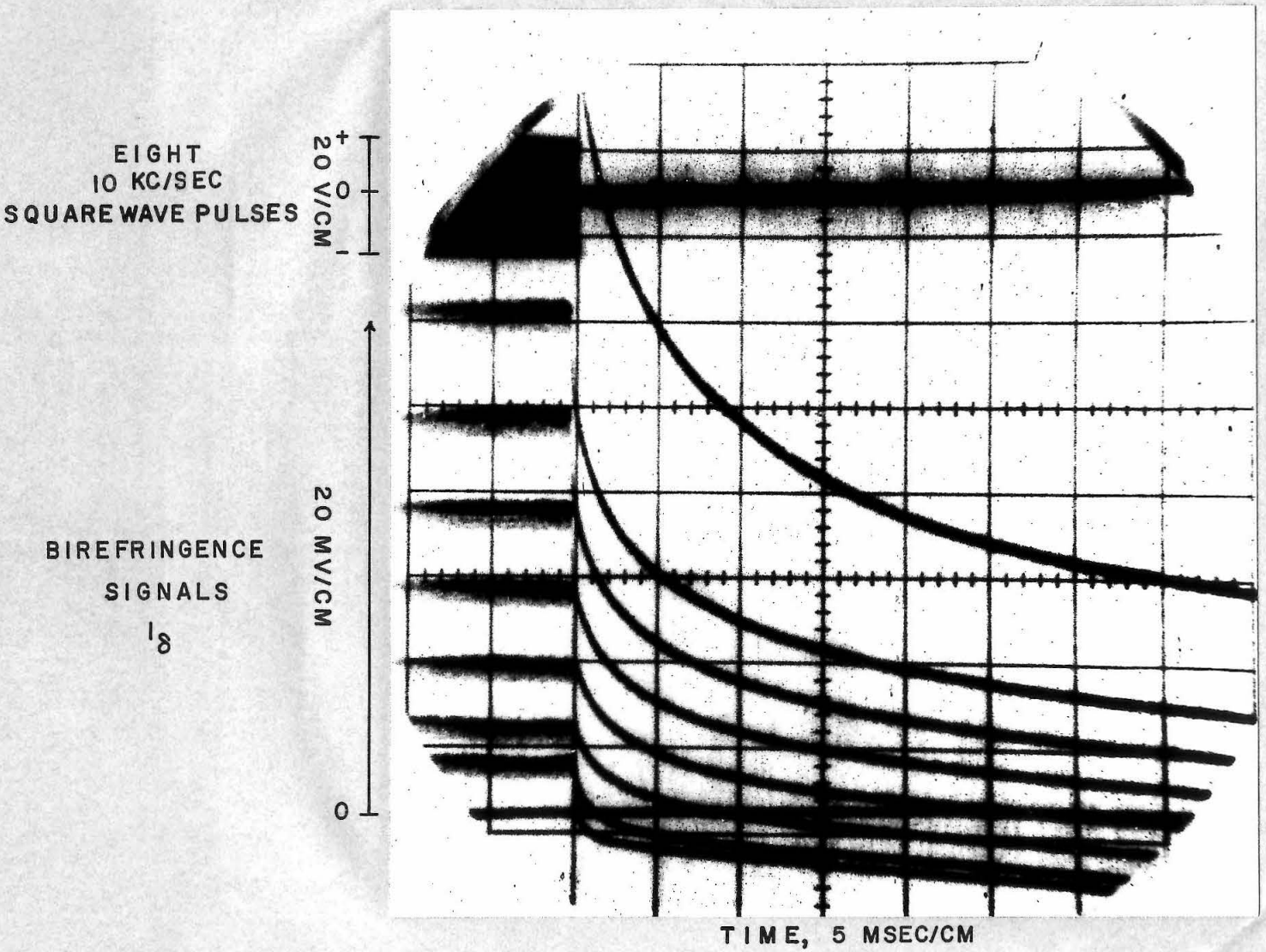
EIGHT
10 KC/SEC
SQUARE WAVE PULSES
+
20 V/CM
0
-
BIREFRINGENCE
SIGNALS
I_δ
20 MV/CM
0
TIME, 5 MSEC/CM

Figure 28

Figure 29

Oscilloscope tracing of the rise of the birefringence signal of E. Coli DNA (155.2 mg/l, R_{230} = --, sample number 29) in 10^{-4} F $NaClO_4$ at 4.0 °C in response to a 10 Kc/sec alternating field of 2250 V/cm.
Pulse duration: 0.98 msec.
Miximum birefringence: 14.55°
I_{A_o} = 124. mV.

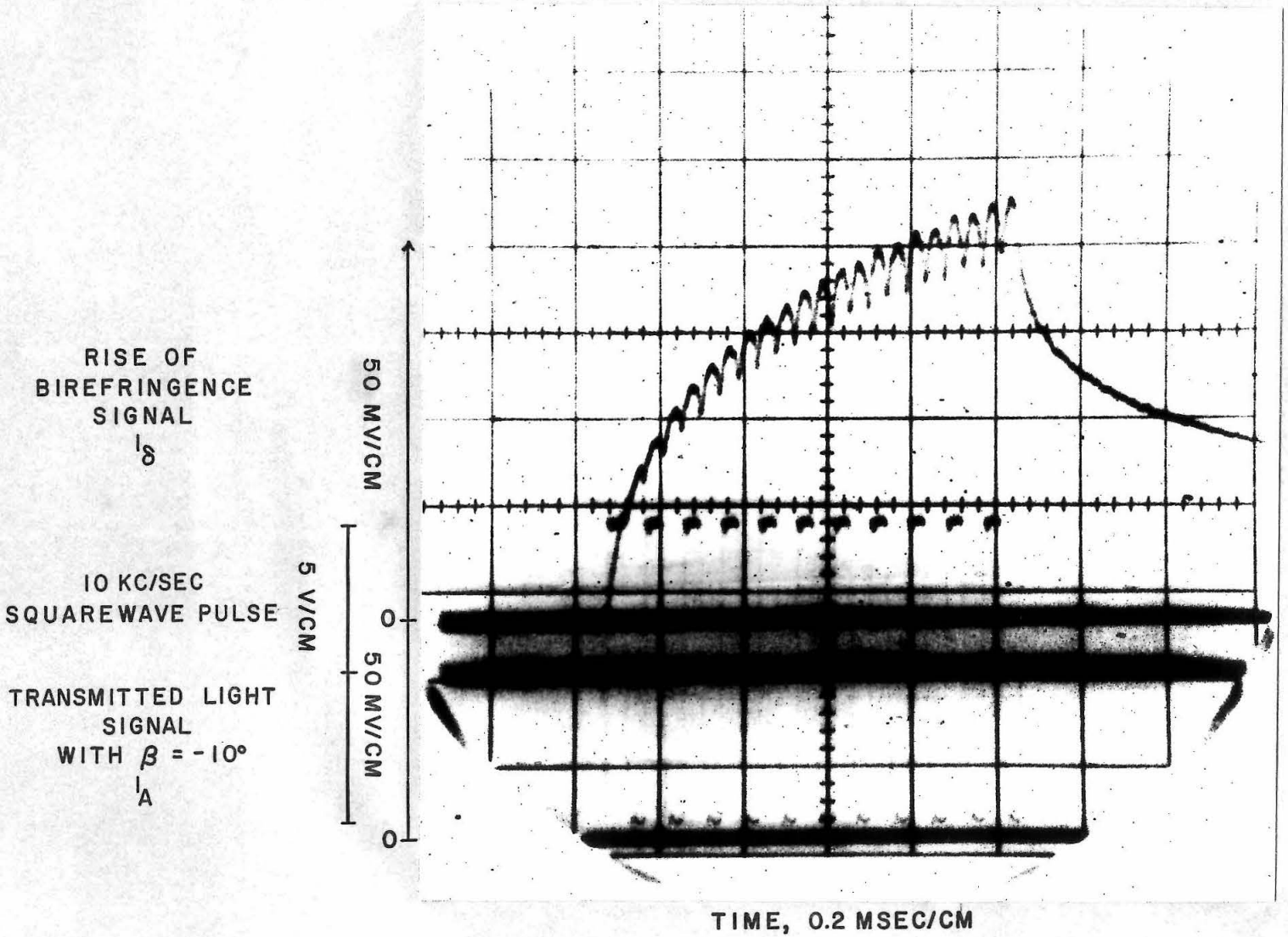
RISE OF
BIREFRINGENCE
SIGNAL
I_δ
10 KC/SEC
SQUAREWAVE PULSE
TRANSMITTED LIGHT
SIGNAL
WITH $\beta = -10°$
I_A
50 MV/CM
5 V/CM
0
50 MV/CM
0
TIME, 0.2 MSEC/CM

Figure 29

Figure 30

Oscilloscope tracing of the steady state birefringence signal of calf thymus DNA (24.2 mg/l, $R_{230} = 2.12$, sample number 8) in Li-cacodylate (2.85×10^{-4} $\mu\Omega$) at 4.3 °C in response of a 1.0 Kc/sec alternating field of 4700 to 3625 V/cm.
Total pulse duration: 9 msec.
Maximum birefringence: 8.05°
$I_{A_o} = 75.5$ mV.

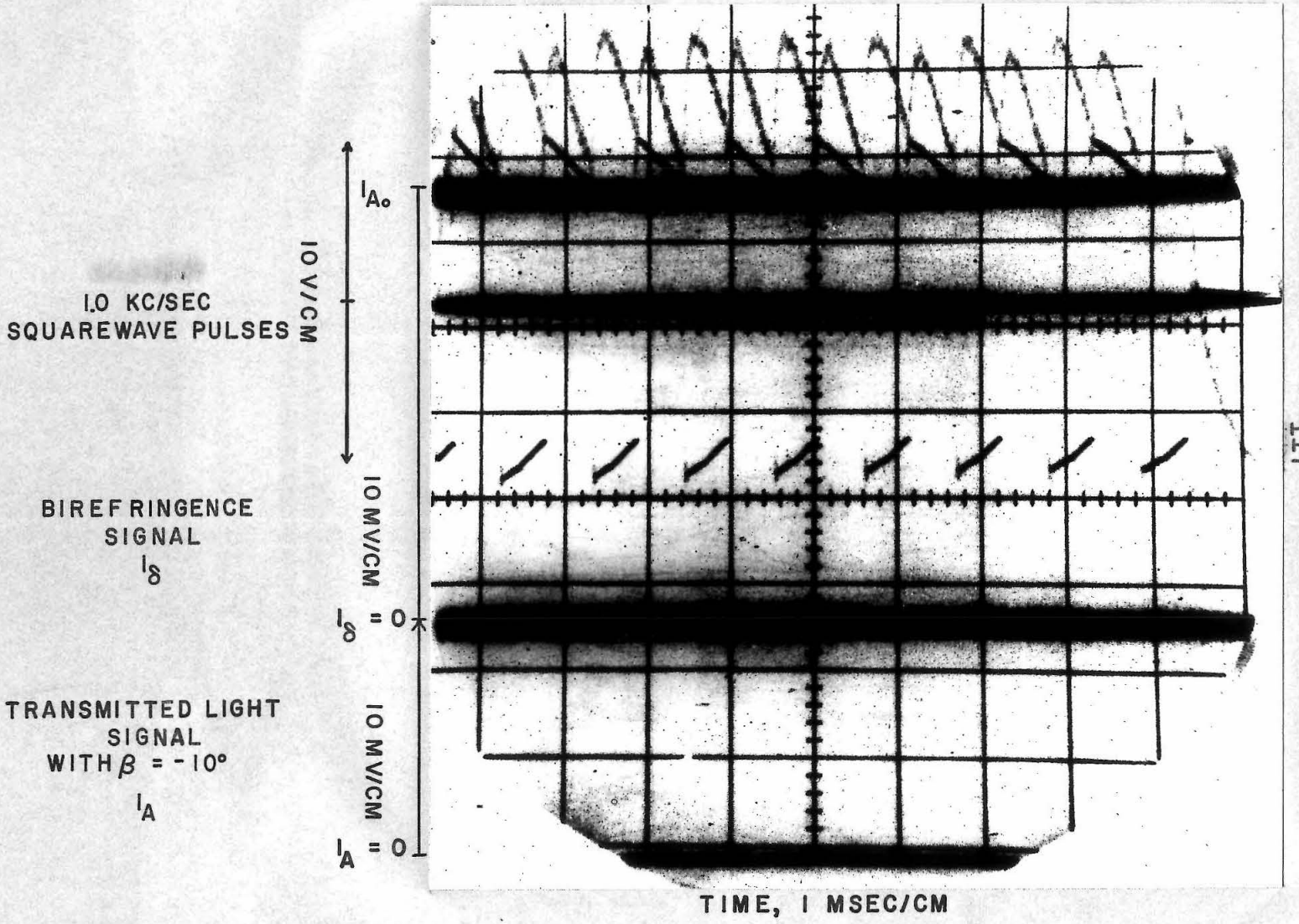
1.0 KC/SEC
SQUAREWAVE PULSES
BIREFRINGENCE
SIGNAL
I_δ
TRANSMITTED LIGHT
SIGNAL
WITH $\beta = -10°$
I_A
10 V/CM
I_{A_o}
10 MV/CM
$I_\delta = 0$
10 MV/CM
$I_A = 0$
TIME, 1 MSEC/CM
117

Figure 30

sient changes can be studied by changing the type of the aligning fields (square wave to sinusoidal)(Fig. 31) as well as the frequency.

With regard to the effect of frequency changes on the birefringence signal, it was found that maximum alignment occurred between 10 and 20 kc/sec. At 5 kc/sec and lower frequencies the decrease in the signals is probably due to electrode reactions, such as polarization or electrolysis, while at above 50 kc/sec the decrease is most likely due to the inability of the counterions to react to the rapidly reversing field, thus causing a decrease in the induced electric polarizability.

Figure 31

Oscilloscope tracings of the birefringence signal of calf thymus DNA (24.2 mg/l, R_{230} = 2.12, sample number 8) in 2.85 x 10^{-4} μ (Li-cacodylate, pH 6.5) at 4.0 °C in response to a 0.5 Kc/sec sinusoidal electric field.
Maximum field strength: 1560 V/cm.
Total pulse duration: 5 msec.
Maximum birefringence: 5.78°.
I_{A_o}: 59.3 mV.

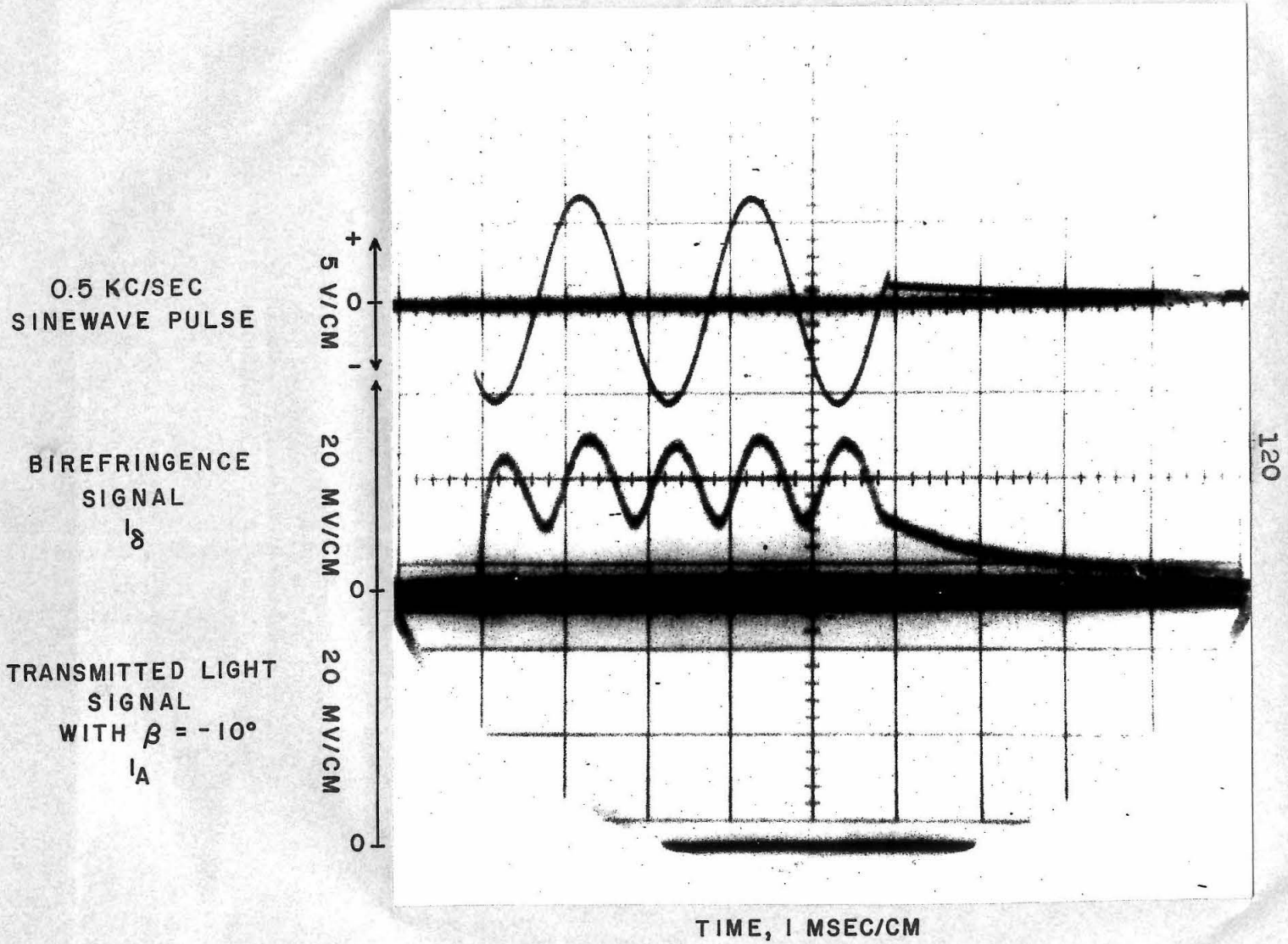
0.5 KC/SEC
SINEWAVE PULSE
BIREFRINGENCE
SIGNAL
I_δ
TRANSMITTED LIGHT
SIGNAL
WITH $\beta = -10°$
I_A
+
0
-
5 V/CM
20 MV/CM
0
20 MV/CM
0
120
TIME, I MSEC/CM

Figure 31

IV. Discussion and Conclusions

It is hoped that the data presented have demonstrated that electric birefringence can be a useful tool in determining a variety of macromolecular parameters, but that it is important to consider the effects of a substantial number of variables before the data can be interpreted unequivocally. This requires considerable, tedious calculations and should perhaps be done by a computer, which could be programmed to read the birefringence signals directly, thus eliminating the often considerable errors in the visual estimation of the signals. Then it would also be possible to obtain results immediately so that the variables can be changed in relation to these results before the sample has degraded by prolonged storage. It is also desirable to know during an experiment whether further changes in field strength, pulse duration etc. are necessary to give enough data for meaningful extrapolations.

Since no satisfactory theory has as yet been developed to explain the birefringence behavior of flexible macromolecules like DNA, much of the data cannot be interpreted and must therefore be correlated by empirical relations like that of equation 21.

Despite the incompleteness of this work, some new insight has been obtained in regard to the electro-optic behavior of DNA:

DNA can be aligned by a rapidly alternating (10 to 20 kc/sec) electric squarewave pulse, indicating that counterion polarization is the important mechanism by which the DNA is aligned. Such a mechanism would also predict, that changes in ionic strength affect the Kerr constant and the electric polarizability as was observed.

The relation of field strengths to birefringence can be represented in a rather simple empirical equation (Eqn. 21). That this equation holds rather than O'Konski's, is probably the result of the flexibility of the DNA molecule.

The optical polarizability is rather independent of the source and heterogeneity of the DNA, as well as of the kind of counterions used, except for ions with specific binding. This must be the result of similarities of the primary structure and counterion binding of DNA from virus, bacterium and mammal.

The birefringence decay behavior of DNA is non-exponential even for viral DNA which is known to be rather homogeneous in terms of molecular weight distribution. Thus, flexibility must play a significant role in determining the mode of alignment and relaxation of DNA.

Bacterial DNA's must be considerably stiffer than other DNA's, for they show relaxation times which can be an order of magnitude larger than those of calf thymus and viral DNA's. This behavior may be a reflection of the less folded structure of bacterial DNA's *in vivo*.

"Birefringence melting curves" show that structural changes in calf thymus DNA occur well before actual denaturation. The E. Coli DNA sample, on the other hand, shows a greater ability to maintain its more rigid structure, which seems to collapse together with the breakage of hydrogen bonds.

APPENDIX I

Optical Anisotropy

Clausius-Mosotti Relation: $\frac{\epsilon - 1}{\epsilon + 2} = \frac{4\pi N\alpha}{3}$. (1)

Eqn. (1) holds for induced dipoles only.

Similarly $$\frac{n^2 - 1}{n^2 + 2} = \frac{4\pi}{3}(N_1\beta_1 + N_2\beta_2) . \quad (2)$$

In terms of refractive indeces parallel and perpendicular to the electric field direction eqn. (2) becomes

$$\frac{n_{//}^2 - 1}{n^2 + 2} = \frac{4\pi}{3}(N_1\beta_1'' + N_2\beta_2) \qquad \frac{n_{\perp}^2 - 1}{n^2 + 2} = \frac{4\pi}{3}(N_1\beta_1^{\perp} + N_2\beta_2) . \quad (3)$$

Subtracting eqns. (3) from each other gives:

$$\frac{n_{//}^2 - n_{\perp}^2}{n^2 + 2} = \frac{4\pi}{3}(N_1\beta_1'' - N_1\beta_1^{\perp}) = \frac{(n_{//} - n_{\perp})(n_{//} + n_{\perp})}{n^2 + 2} = \frac{2n\,\Delta n_s}{n^2 + 2} . \quad (4)$$

Letting $C_{v_1} = N_1\bar{v}_1/(N_1\bar{v}_1 + N_2\bar{v}_2)$ and observing that for dilute solutions $N_1\bar{v}_1 + N_2\bar{v}_2 \simeq N_2\bar{v}_2 \simeq 1$ so that $N_1 \simeq C_{v_1}/\bar{v}_1$

gives $$\Delta n_s = \frac{2\pi C_{v1}}{3\bar{v}_1}(\beta_{//} - \beta_{\perp})\left(\frac{n^2 + 2}{n}\right) . \quad (5)$$

The optical anisotropy is defined as

$$\Delta g \equiv \frac{\Delta\beta}{\bar{v}_1} = \Delta n_s \frac{n}{2\pi C_v}\left(\frac{3}{n^2 + 2}\right) . \quad (6)$$

Note: The Peterlin-Stuart equation assumes $3/(n^2 + 2) \simeq 1$

so that $$\Delta g = \Delta n_s \frac{n}{2\pi C_v} . \quad (7)$$

APPENDIX II

Intensity - Amplitude Relation

Incident light: $E_p = E_o \sin(\omega t - \frac{\omega l}{v})$, (1)

let $n = c/v$ and $k = 2\pi l/\lambda$:

Emergent light: $E_x = E_p \cos\alpha = E_o \cos\alpha \sin(\omega t - kn_x)$, (2)

$E_y = E_p \sin\alpha = E_o \sin\alpha \sin(\omega t - kn_y)$. (3)

If the incident light is polarized at 45° then the emergent light becomes:

$$E_x = \frac{E_o}{\sqrt{2}} \sin(\omega t - kn_x); \quad E_y = \frac{E_o}{\sqrt{2}} \sin(\omega t - kn_y). \tag{4}$$

If the analyzer prism is in the crossed position, the emergent light becomes:

$$E'_A = E_y \cos\alpha - E_x \sin\alpha . \tag{5}$$

Substituting eqns. (4) and letting $\alpha = 45^o$ gives:

$$E'_A = \frac{E_o}{2}\left[\sin(\omega t - kn_y) - \sin(\omega t - kn_x)\right]. \tag{6}$$

Letting $\bar{n} = \frac{n_x + n_y}{2}$ and $\delta = \frac{2\pi l}{\lambda}(n_x - n_y) = \frac{\Delta n\, l}{\lambda}$ gives:

$$E'_A = E_o \cos(\omega t - k\bar{n}) \sin\frac{\delta}{2} . \tag{7}$$

If the analyzer prism is moved β^o off the crossed position:

$$E_A = E_y \cos(\tfrac{\pi}{4} - \beta) - E_x \cos(\tfrac{\pi}{4} + \beta). \tag{8}$$

Substituting eqns. (4) gives:

$$E_A = \frac{E_o}{\sqrt{2}}\left[\sin(\omega t - kn_y)\cos(\tfrac{\pi}{4} - \beta) - \sin(\omega t - kn_x)\cos(\tfrac{\pi}{4} + \beta)\right] \tag{9}$$

Expansion of eqn. (9) and use of trigonometric identities gives with $\alpha = 45^{o}$:

$$E_A = E_o\left[\cos\beta \sin\frac{\delta}{2} \cos(\omega t - k\bar{n}) + \sin\beta \cos\frac{\delta}{2} \sin(\omega t - k\bar{n})\right]. \quad (10)$$

Averaging over time gives for the emerging light intensity:

$$I_A = E_A^2 = I_o \left(\cos^2\beta \sin^2\frac{\delta}{2} + \sin^2\beta \cos^2\frac{\delta}{2}\right) \quad (11)$$

or

$$\underline{\underline{I_A = I_o \left[\sin^2\beta + \sin^2\frac{\delta}{2} (1 - 2\sin^2\beta)\right]}} . \quad (12)$$

Introducing a quarter wave prism before the analyzer retards E_p by $(\frac{\pi}{2} - \phi)$. E_p becomes the slow vector:

$$E_p = E_o \sin(\omega t - k\bar{n} - \frac{\pi}{2} + \phi) \cos\frac{\delta}{2} . \quad (13)$$

Substituting eqns. (7) and (13) in

$$E_A = E_A'\cos\beta + E_p\sin\beta \quad (14)$$

gives: (15)

$$E_A = E_o \left[\cos\beta \cos(\omega t - k\bar{n})\sin\frac{\delta}{2} + \sin\beta \sin(\omega t - k\bar{n} - \frac{\pi}{2} + \phi)\cos\frac{\delta}{2}\right],$$

$$E_A = E_o \left[\cos\beta \cos(\omega t - k\bar{n})\sin\frac{\delta}{2} - \sin\beta\left\{\cos(\omega t - k\bar{n})\cos\phi - \sin(\omega t - k\bar{n})\sin\phi\right\}\cos\frac{\delta}{2}\right], \quad (16)$$

$$E_A = E_o \left[\cos(\omega t - k\bar{n})\left\{\cos\beta \sin\frac{\delta}{2} - \sin\beta \cos\frac{\delta}{2} \cos\phi\right\} + \sin(\omega t - k\bar{n})\sin\beta \cos\frac{\delta}{2} \sin\phi\right]. \quad (17)$$

Averaging over time gives:

$$I_A = E_A^2 = E_o^2\left[\cos^2\beta \sin^2\frac{\delta}{2} - \frac{\sin 2\beta}{2}\cos\phi \sin\delta + \sin^2\beta \cos^2\frac{\delta}{2}\right], \quad (18)$$

$$I_A = I_o \left(\sin^2\frac{\delta}{2} - \frac{\sin 2\beta}{2}\cos\phi \sin\delta + \sin^2\beta - 2\sin^2\beta \sin^2\frac{\delta}{2}\right). \quad (19)$$

Using the trigonometric identity $\sin^2 x = (1 - \cos 2x)/2$ gives

$$\underline{\underline{I_A = \frac{I_o}{2}\left(1 - \sin 2\beta \sin\delta \cos\phi - \cos 2\beta \cos\delta\right).}} \quad (20)$$

For a perfect quarter wave prism $\phi = 0$. Therefore:

$$\underline{\underline{I_A = \frac{I_o}{2}\left[1 - \cos(2\beta - \delta)\right] = I_o \sin^2(\beta - \frac{\delta}{2}).}} \quad (21)$$

If the analyzer is at the crossed position $\beta = 0$. Therefore:

$$\underline{\underline{I_A = I_o \sin^2\frac{\delta}{2}}}. \quad (22)$$

In practice: $I_A = I_\beta + I_\delta - I_s \equiv I_{A_0} + I_\delta$; $I_{A_0} = I_o \sin^2\beta$ if $\delta = 0$.

$$\frac{I_A}{I_{A_0}} = \frac{I_{A_0} + I_\delta}{I_{A_0}} = \frac{1 - \sin 2\beta \sin\delta \cos\phi - \cos 2\beta \cos\delta}{2 \sin^2\beta}, \quad (23)$$

$$\frac{I_\delta}{I_{A_0}} = \frac{1 - \sin 2\beta \sin\delta \cos\phi - \cos 2\beta \cos\delta - 2\sin^2\beta}{2\sin^2\beta}. \quad (24)$$

Since $\cos 2\beta = 1 - 2\sin^2\beta$:

$$\underline{\underline{\frac{I_\delta}{I_{A_0}} = \frac{\cos 2\beta\,(1 - \cos\delta) - \sin 2\beta \sin\delta \cos\phi}{2 \sin^2\beta}}}. \quad (25)$$

APPENDIX III

Quarter Wave Retardation Prism

The following instructions for the construction of a quarter wave retardation prism are those of C. T. O'Konski, who has kindly sent us a preprint and drawing describing its construction and optical properties.

"Light enters an ordinary retardation prism, or Fresnel rhomb, perpendicular to one face, is totally reflected twice within the rhomb, and emerges perpendicular to the other face. At each total reflection, light polarized perpendicularly to the plane of reflection is retarded 45° with respect to light polarized in the plane of reflection. The total relative retardation of 90° produced by the rhomb is analogous to that produced by a quarter wave plate. A Fresnel rhomb is superior to a quarter wave plate since the retardation is not as dependent on the wavelength.

The angle of reflection necessary for any relative retardation can be calculated from equation 30:

$$\tan\frac{\Delta}{2} = \frac{\cos\Phi\sqrt{\sin^2\Phi - 1/m^2}}{\sin^2\Phi} \qquad (30)$$

where Δ is the relative retardation desired, Φ is the necessary angle of reflection, and m is the index of refraction of the rhomb divided by the index of refraction of the air.

If this equation is solved for Φ, it can be seen that a retardation of 90° on two reflections is not possible unless the index of refraction of the rhomb material exceeds 1.4974. The index of refraction of fused quartz ranges from 1.486 to 1.455 in the 3000 to 7000 Ångstrom region.

Theoretically, the desired 90° total retardation could be achieved in fused quartz by three reflections of 30° retardation each. However, a system of two prisms involving two reflections of relative retardation 22.5° in each has the great advantage that the optic axis emerges from the second prism along the same line along which it enters the first prism as shown in Figure 1. Thus, the optic system can be used either with or without the prisms; any other type of retardation prism causes either a lateral displacement or an angular shift of the optic axis that makes the optical system useless when the prism is removed.

Design calculations were made using equation 30. The angle of reflection chosen for each reflection in the prisms was 74° 18' ± 5'. This gave a total relative retardation for the two prisms of 90° ± 1.5° for all wavelengths between 3000 and 7000 Ångstroms. Each prism was 1 x 1 cm in cross section and 7.1 cm long... The index of refraction of fused quartz is 1.4163 at 7060 Ångstroms and 1.3975 at 3030 Ångstroms.

Φ ANGLE OF REFLECTION FOR A 22.5° RELATIVE RETARDATION BETWEEN LIGHT POLARIZED IN THE PLANE OF REFLECTION AND LIGHT POLARIZED PERPENDICULAR TO THIS PLANE.

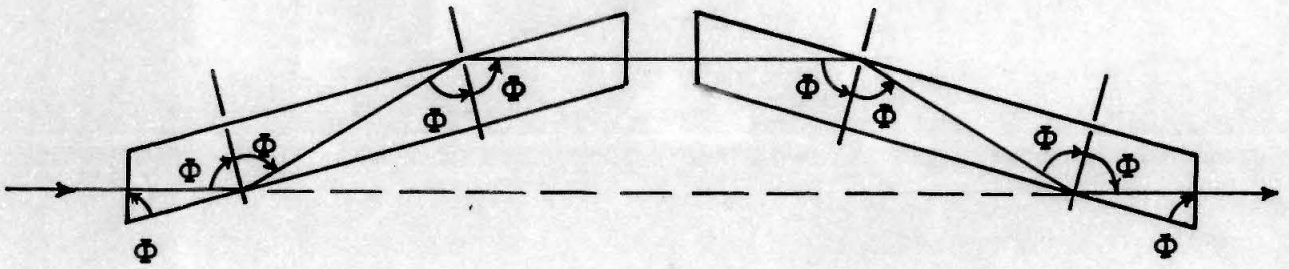

NOTE: THE PRISMS ARE SHOWN FULL SCALE

Figure 1

Light path through retardation prisms

REFERENCES

References

1) J. D. Watson and F. H. Crick, Nature, 171, 737 (1953).

2) a) D. O. Jordan, Progr. Biophys., 2, 51 (1952).

b) C. A. Dekker and H. K. Schachman, Proc. Natl. Acad. Sci. U. S., 40, 894 (1954).

c) D. O. Jordan, The Chemistry of Nucleic Acids, Butterworths, Washington, 1960, p. 175.

3) Electric Birefringence of Polyions.

a) H. Benoit, Ann. Phys., 6, 561 (1951).

b) C. Sadron, J. Applied Chem., 1, 290 (1951).

c) H. Benoit, J. Chim. Phys., 49, 517 (1952).

d) I. Tinoco, Jr., J. Am. Chem. Soc., 77, 3476 (1955).

e) I. H. Billich and J. D. Ferry, ibid., 78, 933 (1956).

f) P. Doty, J. H. Bradbury and A. M. Holtzer, ibid., 78, 947 (1956).

g) I. Tinoco, Jr., ibid., 79, 4336 (1957).

h) C. T. O'Konski, K. Yoshioka and W. H. Orttung, J. Phys. Chem., 63, 1558 (1959).

i) P. Ingram and H. G. Jerrard, Nature, 196, 57 (1962).

j) P. Moser, P. Squire and C. T. O'Konski, Biophysics Society Abstracts, Feb. 24 - 26, 1965, p. 141.

k) P. Squire, P. Moser and C. T. O'Konski, ibid., p. 141.

See also references 4 and 5.

4) Electric Birefringence of TMV.

a) M. A. Lauffer, J. Am. Chem. Soc., 61, 2412 (1939).

b) C. T. O'Konski and B. H. Zimm, Science, 111, 113 (1950).

c) C. T. O'Konski, Nature, 178, 1464 (1956).

d) C. T. O'Konski and A. J. Haltner, J. Am. Chem. Soc., 78, 3604 (1956).

e) A. Norman, Arch. Biochem. Biophys., 70, 257 (1957).

f) C. T. O'Konski and A. J. Haltner, J. Am. Chem. Soc., 79, 5634 (1957).

g) C. T. O'Konski and R. M. Pytkowicz, ibid., 79, 4815 (1957).

h to j) Loc. cit. refs. 3a, 3c, 3h)

5) Electric Birefringence of DNA.

a) H. Benoit, J. Chim. Phys., 47, 719 (1950).

b) H. Benoit, ibid., 48, 612 (1951).

c) A. Norman and J. A. Field, Jr., Arch. Biochem. Biophys., 71, 170 (1957).

d) R. F. Itzhaki, Nature, 194, 1241 (1962).

e) R. F. Itzhaki, ibid., 194, 4835 (1962).

f) G. A. Dvorkin and Ye. I. Golub, Biofizika, 8, No. 3, 301 (1963).

g) E. I. Golub and G. A. Dvorkin, Doklady, Biol. Chem. Sect., 151, 224 (1963)

h) E. I. Golub, G. A. Dvorkin and V. G. Nasarenko, Biokhimiya, 28, 1041 (1963).

i) E. I. Golub, Biopolymers, 2, 113 (1964).

j) C. T. O'Konski and N. C. Stellwagen, private communication, June 1964.

k) N. C. Stellwagen, M. Shirai and C. T. O'Konski, J. Polymer Sci., in print (1965).

l and m) Loc. cit. refs. 3i, 4d).

6) P. Langevin, Compt. Rend., 151, 475 (1910); Le Radium, 7, 249 (1910).

7) M. Born, Ann. Phys., 55, 177 (1918).

8) R. Gans, ibid., 64, 481 (1921).

9) A. Peterlin and H. A. Stuart, Z. Phys., 112, 129 (1939); Hand- und Jahrbuch der chemischen Physik, Bd. VIII, Abt. IB, Becker und Erler Verlag, Leipzig, 1943.

10) Birefringence of DNA Fibers.

a) M. H. F. Wilkins, R. G. Gosling and W. E. Seeds, Nature, 167, 759 (1951).

b) J. C. White and P. C. Elmes, ibid., 169, 151 (1952).

c) G. Romhányi, Acta Histochemica, 3, 308 (1957).

11) a) W. J. Schmidt, Die Doppelbrechung von Karyoplasma, Zytoplasma und Metaplasma, Verlag Gebr. Borntraeger, Berlin, 1937, p. 92.

b) M. J. Fraser and R. D. B. Fraser, Nature, 167, 761 (1951).

c) E. J. Ambrose and J. A. V. Butler, Disc. Faraday Soc., 13, 261 (1953).

12) Flow Birefringence of DNA.

a) Ch. Sadron, J. Phys. Radium, 9, 384 (1938).

b) G. Boehm, Abderhalden's Handbuch der biologischen Arbeitsmethoden, Abt. II, Teil 3, 1939, p. 3939.

c) J. P. Greenstein and W. V. Jenrette, J. Natl. Cancer Inst., 1, 77 (1940).

d) J. T. Edsall, Advan. Colloid Sci., 1, 269 (1942).

e) K. Kanamaru and T. Tanaka, J. Soc. Chem. Ind. Japan, 45, Suppl., 190 (1942).

f) A. E. Mirsky and A. W. Pollister, Proc. Natl. Acad. Sci., 28, 344 (1942).

g) J. P. Greenstein, Advan. Protein Chem., 1, 209 (1944).

h) O. Snellman and S. Widstrom, Ark. Kemi, 19A, No. 31 (1945).

i) R. Jeener, Compt. Rend. Soc. Biol., 140, 1138 (1946).

j) J. M. Creeth, J. M. Gulland and D. O. Jordan, J. Chem. Soc., 1947, 1141.

k) W. Kuhn and H. Kuhn, J. Colloid Sci., 3, 11 (1948).

l) H. Schwander and R. Cerf, Helv. Chim. Acta, 32, 2356 (1949).

m) J. T. Edsall, H. A. Scheraga and A. Rich, Abstracts of the 119th Meeting of the American Chemical Society, Apr. 1951, p. 5J.

n) H. Schwander and R. Cerf, Experiencia, 7, 95 (1951).

o) H. Schwander and R. Signer, Helv. Chim. Acta, 34, 1344 (1951).

p) R. Cerf and H. A. Scheraga, Chem. Rev., 51, 185 (1952).

q) J. T. Edsall, A. Rich and M. Goldstein, Rev. Sci. Instr., 23, 695 (1952).

r) P. Horn, J. Leray, J. Pouyet and Ch. Sadron, J. Polymer Sci., 9, 531 (1952).

s) P. Horn and H. Benoit, ibid., 10, 29 (1953) p. 35.

t) J. W. Rowen, Biochim. Biophys. Acta, 10, 391 (1953).

u) M. Goldstein, J. Am. Chem. Soc., 76, 3337 (1954).

v) A. R. Mathieson and M. R. Porter, Biochim. Biophys. Acta, 14, 288 (1954).

w) A. R. Mathieson and M. R. Porter, Nature, 173, 1190 (1954).

x) M. E. Reichmann, S. A. Rice, C. A. Thomas and P. Doty, J. Am. Chem. Soc., 76, 3047 (1954) p. 3052.

y) L. R. Rey, J. Chim. Phys., 51, 85 (1954) p. 97.

z) J. W. Rowen and A. Norman, Arch. Biochem. Biophys., 51, 524 (1954).

A) A. R. Mathieson and S. Matty, Biochim. Biophys. Acta, 17, 448 (1955).

B) W. J. Frajola, J. G. Rabatin and H. C. Smith, ibid., 19, 540 (1956).

C) A. Norman and J. W. Rowen, ibid., 22, 203 (1956).

D) R. Cerf, J. Polymer Sci., 23, 125 (1957) p. 142.

E) J. Leray, ibid., 23, 167 (1957) p. 173.

F) R. Wahl, M. Joly and E. Barbu, Trans. Faraday Soc., 53, 249 (1957).

G) M. Joly, J. Polymer Sci., 29, 77 (1958).

H) J. Leray, J. Chim. Phys., 57, 323 (1960), p. 346.

13) J. C. Maxwell, Treatise on Electricity and Magnetism, 1892.

14) C. T. O'Konski, K. Yoshioka and W. H. Orttung, J. Phys. Chem., 63, 1558 (1959).

15) M. Eigen and G. Schwarz, Z. Phys. Chem., 4, 380 (1955); Electrolytes, Pergamon Press, Oxford, London, New York, Paris, 1962, p. 309.

16) Rotational Diffusion Constant as a Function of The Particle Dimensions for Various Models.

a) R. Gans, Ann. Phys., 86, 628 (1928).

b) F. Perrin, J. Phys. Radium, 5, 497 (1934).

c) J. M. Burgers, Verh. Koninkl. Ned. Akat. Wetenschap. Afdeel. Natuurk., Sec. 1, Dell XVI, No. 4, 113 (1938). Ref. given by C. T. O'Konski et al., ref. 4d.

d) A. E. Alexander and P. Johnson, Colloid Science, Vol. I, Oxford At The Clarendon Press, 1949, p. 380.
e and f) Loc. cit. refs. 8, 12u).

17) Loc. cit. refs. 6, 7).

18) Loc. cit. ref. 9).

19) S. Krause and C. T. O'Konski, J. Am. Chem. Soc., 81, 5082 (1959).

20) H. Benoit, Compt. Rend., 228, 1716 (1949).

21) A. R. Jones, Research Report, California Institute of Technology, 1961.

22) W. F. Dove, Ph. D. Thesis, California Institute of Technology, 1962, p. 27.

23) B. H. Zimm and D. M. Crothers, Proc. Natl. Acad. Sci., 48, 905 (1962).

24) J. Marmur, J. Mol. Biol., 3, 208 (1961).

25) Phenol Extraction of DNA.
a) K. S. Kirby, Biochem. J., 66, 495 (1957).
b) K. S. Kirby, ibid., 70, 260 (1958).
c) J. D. Mandell and A. D. Hershey, Anal. Biochem., 1, 66 (1960).

26) Degradation of DNA at Low Ionic Strength.
a) R. Thomas, Bull. Soc. Chim. Biol., 35, 609 (1953).
b) R. Thomas, Biochim. Biophys. Acta, 14, 231 (1954).
c) R. Thomas, Trans. Faraday Soc., 50, 304 (1954).

d) L. F. Cavalieri, M. Rosoff and B. H. Rosenberg, J. Am. Chem. Soc., 78, 5239 (1956).

27) Loc. cit. ref. 19).

28) Ion Atmospere Polarization.

a) C. J. F. Böttcher, Theory of Electric Polarization, Elsevier Publishing Co., Amsterdam, 1952, Ch. 10.

b) J. Th. G. Overbeek in Colloid Science, edited by H. R. Kruyt, Elsevier Publishing Co., Amsterdam, 1952, Vol. I, Ch. 5.

c) C. T. O'Konski, J. Chem. Phys., 23, 1559 (1955).

d) M. Eigen and G. Schwarz, J. Colloid Sci., 12, 181 (1957).

e) C. T. O'Konski, J. Phys. Chem., 64, 605 (1960).

f and g) Loc. cit. refs. 4f, 15).

29) W. F. Dove and N. Davidson, J. Mol. Biol., 5, 467 (1962) p. 476.

30) G. Zubay, Biochim. Biophys. Acta, 32, 233 (1959).

31) R. H. Jensen and N. Davidson, Biopolymers (1965) in press.

32) R. H. Jensen, Ph. D. Thesis, California Institute of Technology, 1965.

33) I. Leslie in The Nucleic Acids, edited by E. Chargaff and J. N. Davidson, Academic Press Inc., New York, London, 1955, Vol. II, Ch. 16, p. 1.

R. L. Sinsheimer, ibid., Vol. III, Ch. 33, p. 193.

34) Heat Denaturation of DNA.

a) G. Goldstein and K. G. Stern, J. Polymer Sci., 5, 687 (1950).

b) T. Miyaji and V. E. Price, Proc. Soc. Exptl. Biol. Med., 75, 311 (1950).

c) S. Zamenhof and E. Chargaff, J. Biol. Chem., 186, 207 (1950).

d) S. G. Laland, W. A. Lee, W. G. Overend and A. R. Peacocke, Biochim. Biophys. Acta, 14, 356 (1954).

e) S. Zamenhof, H. E. Alexander and G. Leidy, J. Exptl. Med., 98, 373 (1954) p. 379.

f) S. Zamenhof, G. Griboff and N. Marullo, Biochim. Biophys. Acta, 13, 459 (1954).

g) G. H. Beaven, E. R. Holiday and E. A. Johnson, The Nucleic Acids, edited by E. Chargaff and J. N. Davidson, Academic Press Inc., New York, London, 1955, Vol. I, Ch. 14, p. 514.

h) P. Doty and S. A. Rice, Biochim. Biophys. Acta, 16, 446 (1955).

i) R. A. Cox and A. R. Peacocke, J. Chem. Soc., 1956, 2646.

j) P. D. Lawley, Biochim. Biophys. Acta, 21, 481 (1956).

k) K. V. Shooter, R. H. Pain and J. A. V. Butler, ibid., 20, 497 (1956).

l) R. A. Cox and A. R. Peacocke, J. Chem. Soc., 1957, 4724.

m) S. A. Rice and P. Doty, J. Am. Chem. Soc., 79, 3937, (1957).

n) P. Doty, H. Boedtker, J. R. Fresco, R. Haselkorn and M. Litt, Proc. Natl. Acad. Sci. U. S., 45, 482 (1959).

o) H. G. Jerrard and B. A. W. Simmons, Nature, 184, 1715 (1959).

p) J. Marmur and P. Doty, Nature, 183, 1427 (1959).

q) J. Marmur and P. Doty, J. Mol. Biol., 5, 109 (1962).

r and s) Loc. cit. refs. 2b, 26b).

PART II

SELECTIVE DISSOCIATION OF NUCLEOHISTONE COMPLEXES

I. Introduction

The second part of this dissertation describes an investigation of the dissociation behavior of deoxyribonucleohistones (DNH), the complexes found in quantity only in the cell nuclei of higher plants and organisms. The nucleohistones consist mainly of basic proteins (histones) and deoxyribonucleic acids (DNA). Together with appreciable amounts of non-histone proteins they are organized into the chromosome superstructure (1); they may also be involved in the regulation of genetic activity as first suggested by Stedman and Stedman (2) in 1950. In 1962 the Stedman proposal was supported by Huang and Bonner (3), who found that DNA molecules, which were fully complexed with histones are inactive in supporting DNA-dependent RNA synthesis in vitro.

If histones are in fact the biological substances which serve in exerting genetic control, then it would be expected, that their interactions with DNA should be highly specific. This specificity could be due to either chemical differences among the histones themselves or to a specific mode of assembly.

To study the degree of specificity and the mode of interaction of histones with DNA was the objective of this work. Since DNA is characterized as a negative polyion and histones as positive polyions, and since ionic interactions

are least specific and thus easier to examine than the more specific structural interactions, it seemed logical to start investigating the DNA-histone complexes by looking at the extent of the competition between monovalent cations and histones for the DNA polyanion.

Equilibrium dialysis studies at various salt concentrations have been carried out by Akinrimisi et al. (4), but in these studies acid extracted histones and very low histone to DNA weight ratios (about 1 to 10) were used mainly because it was not possible to keep the nucleohistone complexes in solution. Furthermore, a number of studies was undertaken to determine the chemical and physical properties of nucleohistones at various salt concentrations (5), but because of the low solubility of these materials in the range of 0.02 to 0.5 M NaCl (6), most of the data relate to very low (less than 10^{-2} M NaCl) or rather high ionic strengths (above 0.5 M NaCl). In addition, most of the nucleoprotein preparations studied up to 1959 were either degraded preparations (7) or crosslinked gels (8) or reconstituted aggregates (9), because they were precipitated from dissociated material in solutions at high salt concentrations by means of dilution to low salt concentrations (10).

Treatment of DNH with high salt concentrations has been employed previously for the preparative extractions

of histones (11). It has been observed that lysine rich histones are removed first (12) by salt extraction of DNH. However, none of these investigations was very successful in determining the specificity and quantitativeness of the interactions of histones and DNA in native nucleohistones and very little is known about the nature of the residual, partially salt extracted, native nucleohistones.

In our studies we have used zone ultracentrifugation of DNH through preformed salt gradients, superimposed on a stabilizing D_2O or sucrose gradient, a procedure which will be described in detail. It facilitates the determination of the range of salt concentrations necessary to induce dissociation of complexes without having to make a large number of experiments at different salt concentrations. At the same time approximate sedimentation coefficients can be obtained to aid in the characterization of the dissociation products. The procedure is also potentially useful in estimating quantitatively the amounts and distribution of the dissociating products.

The results of the procedure mentioned above have been verified by the conventional preparative sedimentation technique. Here, nucleohistone solutions at various salt concentrations were centrifuged and the salt extracted histones remaining in the supernatant as well as those sedimenting

together with the DNA were analyzed by Amberlite cation exchange chromatography.

Because histones and nucleohistones tend to aggregate easily and especially at concentrations exceeding about 0.1 mg/ml at high salt concentrations (above 0.2 F) and since quantitative results concerning nucleohistone dissociation can only be obtained if aggregation is essentially avoided, many of the experimental problems discussed are due to the requirement of having to work with rather low nucleohistone concentrations. Thus, various methods of detecting small amounts of histones by UV, ninhydrin and the Lowry procedure are discussed in addition to experimental difficulties like those encountered in desalting small quantities of histones. Readers who are not particularly concerned with performing similar experiments and who are disinterested in the details of the experimental effectiveness of the procedures used, are advised to skip the experimental parts and to look instead at the short summaries at the beginning of each of the various sections. Of the large number of figures presented, figures 11, 28, 37 and 57ff. should be of greatest interest.

The results of the salt extraction experiments suggest that the different major histone fractions are selectively dissociated from native DNH by increasing salt con-

centrations. It was possible to prepare partially dissociated, native nucleohistones from which histone I, histones I and II etc. were extracted. Some of the interesting properties of these partially extracted nucleohistones have been investigated. Mobilities have been measured by zone electrophoresis and the single bandedness of the material indicated that equal, proportional amounts of histones are dissociated from each nucleohistone molecule.

The two-step melting behavior of partially extracted nucleohistone at low salt concentration showed that the histones are non-randomly distributed along the DNA chain. However, the indications are that the uncovered regions are not of gene-size length. Nevertheless, the RNA-priming activity of these preparations does increase as more and more histones are extracted.

II. Preparation and Properties of Materials

1. Histones

Histones are basic, nuclear proteins because of their large percentage of arginine and lysine (20 to 30 mole %). They can be separated from other proteins by their solubility in mineral acids (13). It has also been possible to fractionate the histones themselves by a variety of procedures such as column chromatography on Amberlite (14), Sephadex (15), carboxymethylcellulose (16) and others (17), by electrophoreses of various kinds including zone or band (18), boundary (19), starch gel (20), acrylamide gel (21) and other electrophoreses (22). It is presently known that up to twenty and possibly many more types of histones exist. These types may be tentatively grouped according to their arginine to lysine ratios as suggested by Murray(23). Their molecular weights range from approximately 8 000 to perhaps 50 000 depending somewhat on the procedures used (24).

Recent evidence shows that there exists cell, organ, and species specificity of the histones present in the cell nuclei (25), but until now no biologically significant specificity has been found.

Since the histone fractions used in this investigation were characterized and prepared by Amberlite chromatography

with guanidinium chloride (GuCl) according to the method of Luck et al. (26), we adopted their histone nomenclature which is based on the elution pattern of acid extracted calf thymus histones. The four major fractions are numbered I through IV, while any subfractions obtained are lettered alphabetically.

Figure 1 shows an elution pattern of acid (H_2SO_4, pH 0.7) extracted calf thymus histones obtained by small scale Amberlite chromatography. A certain amount of material (here 5.4 % of the total TCA precipitable material in the effluent) elutes with the initial eluent and is referred to as the run-off peak. It consists presumably of non-histone proteins (27). Histones Ia and Ib follow as barely resolved peaks (HIa = 16.3 % and HIb = 10.1 %). The next and largest peak (51.1 %) consists of unresolved histone IIa and IIb (HII) and the last peak (17.1 %) is due to unresolved histones III and IV (HIII(IV)).

The amino acid compositions of the individual fractions were determined by Murray (28) and are shown in table I. Table II gives the tentative results for corresponding fractions of histones from pea bud DNH as measured by Fambrough (27).

The interesting features of these analyses with regard to our work are:

Figure 1

Amberlite IRC-50 cation exchange chromatography.

Elution pattern of H_2SO_4 (pH 0.7) extracted, whole calf thymus histones using a gradient concentration of guanidinium chloride (GuCl). 4.0 mg of histones were dissolved in 0.2 ml 8 % GuCl and applied to the column (57 x 0.65 cm diameter). Protein concentration of the effluent was determined by optical density at 4000 Å of the turbid solution resulting 15 minutes after 0.2 ml of the effluent were mixed with 0.6 ml water and 0.4 ml 3.3 M trichloroacetic acid.
Arabic numbers give the percentages of material in the peaks; roman numbers indicate the histone fractions.

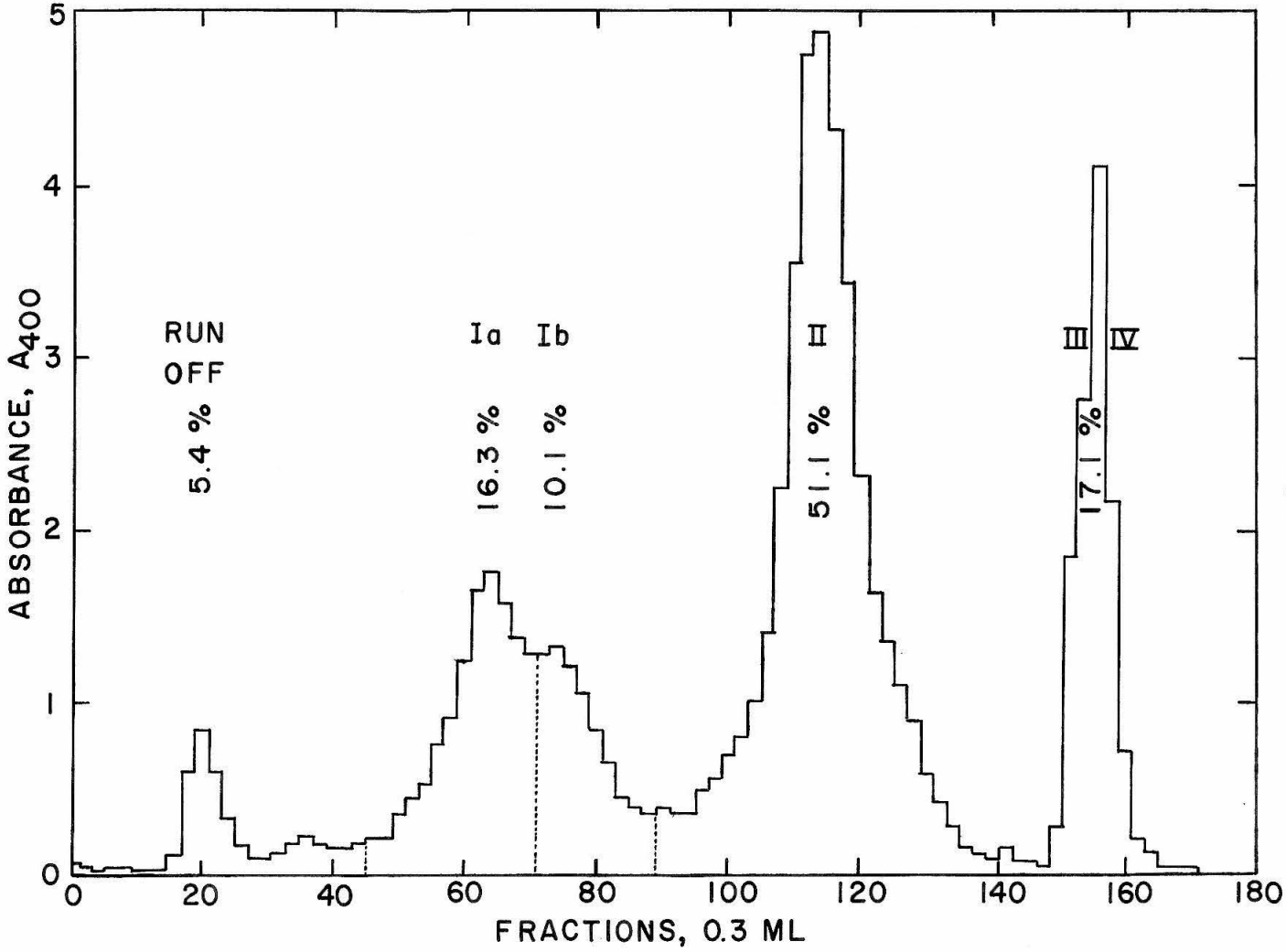
ABSORBANCE, A_{400}
FRACTIONS, 0.3 ML
RUN OFF
5.4 %
Ia
16.3 %
Ib
10.1 %
II
51.1 %
III
IV
17.1 %
0
1
2
3
4
5
0
20
40
60
80
100
120
140
160
180

Figure 1

Amino Acid Composition of Histone Fractions From Calf Thymus in Mole %

Kenneth Murray (28)

Amino Acids	Calf Thymus Histone Fraction No.							
	Iaa	Ia	Ib	IIaa	IIa	IIb	III	IV
ε-N-MeLys	0	0	0	0.5	0.3	0	0.7	0.8
Lys	13.8	25.3	26.2	10.2	9.6	13.5	9.3	8.9
His	2.2	0.4	0.2	1.9	1.9	2.8	1.6	1.6
Arg	8.2	3.0	2.6	11.2	11.6	7.9	12.8	12.7
Asp	4.5	2.5	2.5	4.9	4.8	5.6	4.4	4.5
Glu	8.9	4.5	4.3	9.1	9.6	8.7	9.8	10.5
Pro	5.5	8.6	9.1	3.4	3.7	4.7	3.8	4.2
Thr	6.2	5.8	5.4	7.1	6.8	5.2	7.3	7.3
Ser	6.6	6.4	6.5	5.0	4.6	7.8	4.1	4.1
Gly	8.8	6.7	7.3	10.0	9.8	8.2	8.7	7.8
Ala	14.7	24.0	24.2	10.2	11.2	11.5	11.7	12.2
Val	5.0	4.9	4.0	6.8	6.5	6.7	5.8	5.6
Met	0.6	0.1	0.1	1.2	1.2	0.8	1.2	1.2
Ileu	3.8	1.3	1.2	5.4	5.4	4.5	5.4	5.4
Leu	8.2	5.3	5.0	8.0	8.7	8.6	8.6	8.9
Try	1.6	0.7	0.7	2.9	2.8	3.0	2.4	2.3
Phe	1.6	0.6	0.6	2.2	2.3	1.3	2.5	2.7
Cys	0	0	0	0	0	0	0	0
$\frac{Arg}{Lys}$	0.59	0.12	0.10	1.11	1.21	0.59	1.37	1.42
Σ+ AA	24.2	28.7	29.0	23.8	23.4	24.2	24.4	24.0
Σ- AA	13.4	7.0	6.8	14.0	14.4	14.3	14.2	15.0
net + AA	10.8	21.7	22.2	9.8	9.0	9.9	10.2	9.0
$x10^{-3}$ MWT	~8	~8	~8	12	15	18	25	30

Table I

Amino Acid Composition of Histone Fractions

From Pea Buds in Mole %

Douglas Fambrough (27)

Amino Acids	Pea Bud Histone Fraction No.			
	Run-Off	I	II	III(IV)
Lys	8.0	23.0	17.0	9.5
His	1.5	1.0	1.5	2.0
Arg	3.0	3.0	7.0	11.0
Asp	7.0	3.0	6.5	6.0
Glu	9.5	8.0	8.5	9.0
Pro	7.0	10.0	7.0	4.0
Thr	5.0	4.5	4.5	6.0
Ser	8.0	5.5	7.5	4.5
Gly	12.0	3.5	10.5	10.0
Ala	13.0	23.0	8.0	9.5
Val	7.5	6.0	4.5	6.5
Met	1.0	trace	0.7	trace
Ileu	5.0	3.0	4.0	6.0
Leu	8.5	4.5	8.0	10.5
Try	2.0	1.0	2.0	2.5
Phe	2.0	1.0	3.0	3.0
$\frac{Arg}{Lys}$	0.38	0.12	0.43	1.12
$\Sigma+$ AA	12.5	27.0	25.5	22.5
$\Sigma-$ AA	16.5	11.0	15.0	15.0
net + AA	- 4.0	16.0	10.5	7.5

Table II

1) The increasing amounts of arginine and the decreasing amounts of lysine, so that the arg/lys ratio increases from fraction I to fraction IV.

2) The relative constancy of total basic amino acids of about 25 mole % for all histone classes.

3) The relatively high over-all net positive charge of histone I in comparison with those of the other three fractions.

4) The higher proline content of histone I as compared with the other three fractions, suggesting less alpha-helical structure for histone I (29).

5) The increase in molecular weight from approximately 10 000 to about 50 000 or more for fractions I through IV respectively. The molecular weight data vary depending upon the methods used for their determination as well as the procedures used for the fractionation of the histones. Probably the most reliable values available at present are those based on chemical methods like end group determinations (30).

2. Reconstituted Nucleohistones

We began our study of the interactions of histones with DNA with reconstituted nucleohistones, because we felt that they were better defined systems than the whole, native DNH. The totally covered, reconstituted complexes were prepared by Dr. R. C. Huang (31) by dialyzing a solution containing a mixture of DNA and a certain histone fraction at high salt concentration (2 F NaCl) gradually into low salt concentration (0.015 F NaCl and 0.0015 F Na citrate, pH 7). The dialyzates were sedimented shortly to remove any large aggregates and dust. The clear supernatants containing the DNH were either used as such in our studies or lyophilized to give white fibers of DNH. These fibers could be stored at 4° C for extended periods of time. They were easily soluble in 10^{-3} F salt at 4° C, but before using these solutions, they were sedimented for 30 minutes at 5000 rpm (SW 39 rotor) to remove any dust and possible aggregates.

The following served as evidence that real complexes had formed:

1) In reconstituted DNH I through IV dissolved in low salt solutions, DNA and histones sediment together at a reproducible rate. Fully complexed calf thymus DNH has a sedimentation coefficient of 25 to 30 S (Svedberg), while that of the DNA alone lies around 15 S (32).

2) They move together in zone electrophoresis (33) at a constant and reproducible mobility, which is lower than that of DNA.

3) Reconstituted DNH I and II melt at a substantially higher temperature than DNA alone (34).

4) Reconstituted DNH I and II show a marked decrease in their ability to prime DNA-dependent RNA synthesis (35) as compared to that of uncomplexed DNA.

3. Native Nucleohistones

The preparation of native nucleohistones used in our investigations involves as its first step the preparation of crude chromatin from fresh, homogenized tissue. Removal of the non-chromosomal proteins by sucrose density gradient sedimentation gives "purified" chromatin (36). Following the general method of Zubay and Doty (37) the nucleohistone was prepared from this purified chromatin (38).

The essential point of these procedures is that low salt concentrations are used. Thus, the sodium ion concentration for the preparation of purified chromatin is never greater than 0.125 N and that for the subsequent manipulation involved in the preparation of DNH not greater than 0.02 N.

A good calf thymus DNH preparation had a sedimentation coefficient in low salt of around 30 S (DNA ~ 21 S) (39) and a melting point considerably above that of DNA (40). It has a histone to DNA mass ratio of about 1.4 (41) and contains little or no non-histone protein. There are indications that it is extremely difficult, if not impossible, to remove approximately 5 % residual RNA (42) without removing the histones as well.

III. Analytical Methods and Experimental Techniques

1. General Considerations

In studying the literature about histone and nucleohistone investigations, one cannot fail to notice the lack of quantitative data. This is most likely due to the great difficulties encountered in handling preparations of histones and nucleohistones. In this regard their tendency to aggregate (43) is by far more serious than their degradability on standing (44), which can be effectively decreased by versine (37), or the presence of small amounts of non-removable "impurities" (45).

Phillips (46) and others (47) have investigated the formation of aggregates of a number of histone fractions. Their findings were that fractions containing little arginine aggregate less extensively than fractions containing much arginine (48). Precipitation is enhanced by pH values above 10, higher ionic strength, and higher histone concentrations, to name only the most important parameters.

We observed similar effects with nucleohistones as well. They seem to be most easily aggregated in solutions of monovalent salt concentrations ranging from 0.2 to 0.4 F. This range turned out to be the one which was of main interest in our study. Immediate precipitation and cloudiness results,

if concentrated nucleohistone solutions are mixed with salt solutions in the above range. Thus, we could not use nucleohistone concentrations which were much above about 100 mg DNA per liter (A_{260} = 2), if we wanted to get quantitative results. Also, considerable difficulty was encountered in trying to redissolve the pellets obtained by centrifugation from more concentrated DNH solutions, especially those precipitated by about 0.25 F $NaClO_4$. Thus, techniques had to be found with which we could handle and detect rather small amounts of material.

For instance, in a typical salt gradient sedimentation experiment, only 0.25 ml of a DNH solution of about A_{260} = 2 was used, which is approximately 25 x 10^{-6} g DNA and about the same amount of histone. After the experiment this material may be distributed over ten to fifteen 0.25 ml fractions. This calls for the analysis of <u>circa</u> 2 micrograms of material per sample.

While the quantitative detection of DNA at these concentrations is rather easy because of its high extinction coefficient at 2600 Å (ϵ(P) = 6600 to 6700; 2 micrograms per 0.25 ml give an A_{260} = 0.16 (49)), the problem of detecting histones is more difficult.

Although we were able to develop a micro ninhydrin procedure which was capable of detecting less than 1 microgram of amino acid per ml, we were not able to detect unhydrolyzed

histones at these low concentrations. A micro Lowry procedure which could detect concentrations of histones down to about 20 micrograms per ml was also only as sensitive as the detection of histones by their absorption at 2200 Å. Since the UV measurements were the most simple to perform, it was the method of choice. When it was necessary to establish unambiguously that the UV measurements were those of histones, the micro ninhydrin procedure was used.

2. UV Analysis

The following describes the procedures and precautions required to obtain more reliable UV measurements at lower wavelengths. A number of uncertainties in the quantitative estimation of histone concentrations by UV are discussed.

All UV measurements were made in the Cary Model 14 Recording Spectrophotometer using quartz microcells (0.5 ml capacity, 1 cm light path, 3 mm width) from the Pyrocell Manufacturing Co.

Since we intended to use the absorption of 2200 Å for the determination of the histone concentrations, it was important to keep UV absorbing impurities to a minimum. It was for this reason, that we used redistilled D_2O rather than sucrose for the density gradients, and $NaClO_4$ (prepared by neutralizing $HClO_4$ with NaOH) rather than NaCl, for our salt gradients.

All absorbances and calculations involving DNA concentrations are based on the absorption at 2600 Å (A^{D}_{260}), Those involving histone concentrations are based on the absorption at 2200 Å (A^{NH}_{220}) corrected for the DNA absorption giving A^{H}_{220}. All measurements were corrected for solvent or H_2O blanks and normalized to zero absorption at 4000 Å.

The normalization assumes that any difference in absorption between solvent and sample is due to a baseline shift. It ignores the fact that scattering of the sample is sometimes appreciable and contributes to A_{400}. However, since the sizes of the scattering particles are generally unknown, adequate corrections cannot be made. It was therefore decided to use the simplest form of normalization, i. e. normalizing to A_{400} = zero, and to report the observed A_{400} when it exceeded 5 % of the A_{260}.

Using an extinction coefficient for DNA of 6600 at 2600 Å (49) and an average molecular weight per base of 324, an absorbance of 1 corresponds to 49 x 10^{-6} g DNA/ml. The ratio of the absorbance of 2600 Å to that of 2200 Å (R_{220}) was used as another indication of the kind of material present in the various regions. Pure DNA has an $R_{220} \geq 1.5$. The ratio decreases as the histone concentration increases.

Since good extinction coefficients for histones are not yet available, all our UV data are reported in relation to the original absorbance present in the sample. However, in order to indicate the approximate sensitivity of the UV measurements of histones at 2200 Å it is worthwhile to consider data obtained by Goldfarb et al. (50). From a survey of UV absorbance spectra of a number of different proteins, they suggested that the extinction coefficients of peptides at low wavelengths are rather independent of the kind of

proteins investigated (ϵ = 21.5 ± 1.1 l/g protein at 2100 Å).

If we assume that the extinction coefficient of histones at 2100 Å is similar to that of other proteins, and if we assume further that the absorption at 2200 Å is half and that at 2300 Å is a quarter of that at 2100 Å, as indicated by our data (Fig. 2), then we find that 0.1 mg of histones per ml have A_{230} = 0.54 ± 0.03, A_{220} = 1.08 ± 0.06, and A_{210} = 2.15 ± 0.11.

Recent data by Dr. R. H. Jensen (51) and Miss D. Tuan (52) indicate that A_{230} = 0.42 for 0.1 mg of whole calf thymus histones.

Since absolute, quantitative relations between DNA and histones in the DNH complexes are important only in electrophoresis, we shall defer any further discussion to that section. Because of the uncertainty in obtaining accurate histone concentrations, we preferred to characterize DNH complexes by their R_{220} rather than by their histone to DNA weight ratios (H/D). In those instances where the H/D is given, we assumed an R_{220} of 1.50 for DNA correction and an A^{H}_{220} of 1.00 for 0.1 mg histone/ml. Figure 3 shows a plot of R_{220} versus H/D.

The main conclusion to be drawn from the above is that histones can be detected down to about 20 or less micrograms/ml by their absorbance at 2200 Å, if UV impurities can be effectively eliminated.

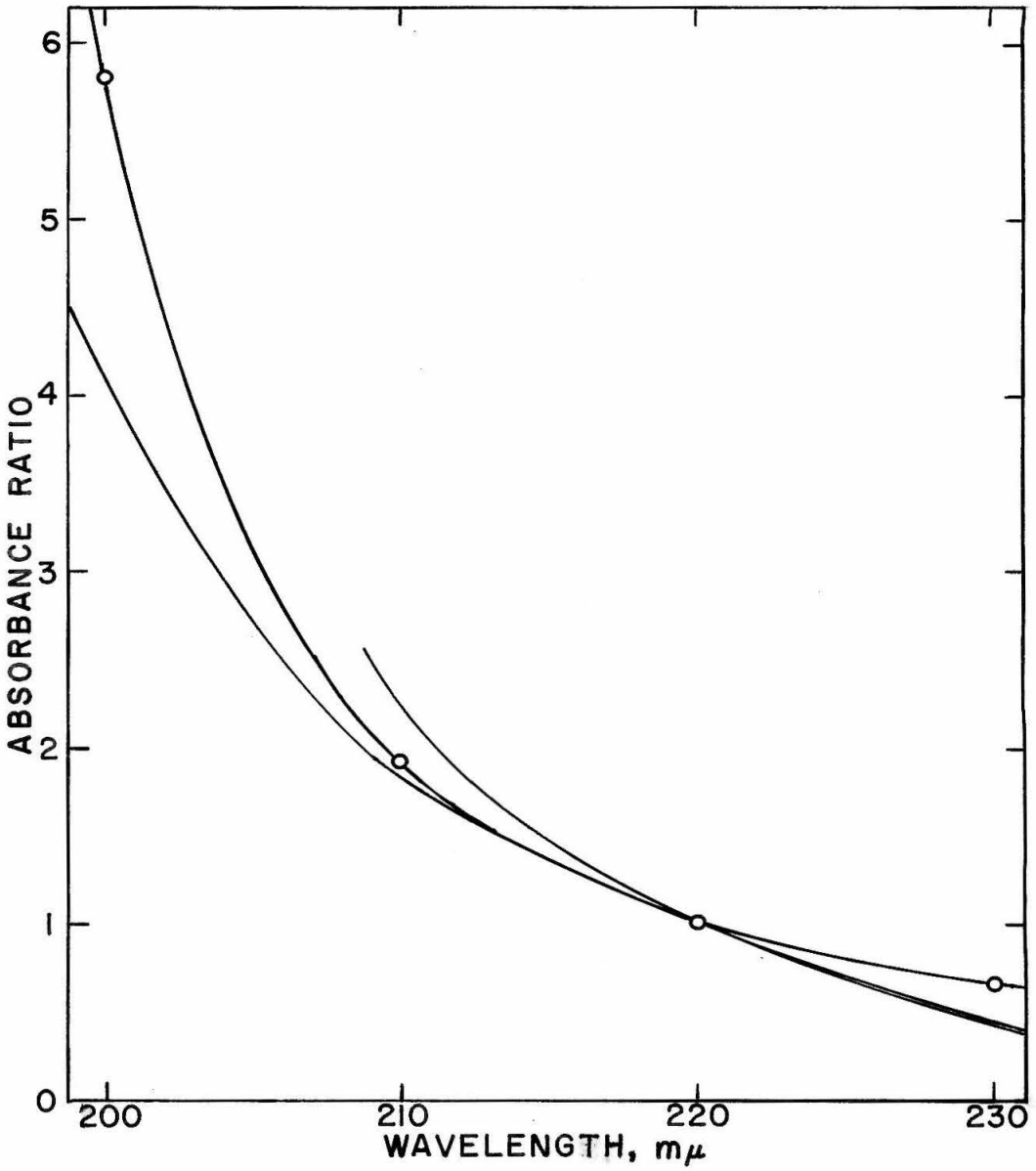

Figure 2

UV absorption of histones relative to an absorbance at 2200 Å of 1. Data for histones Ib, IIb, and III indicate that A_{230} is about (1/2) x A_{220}, and A_{210} is about 2 x A_{220}.

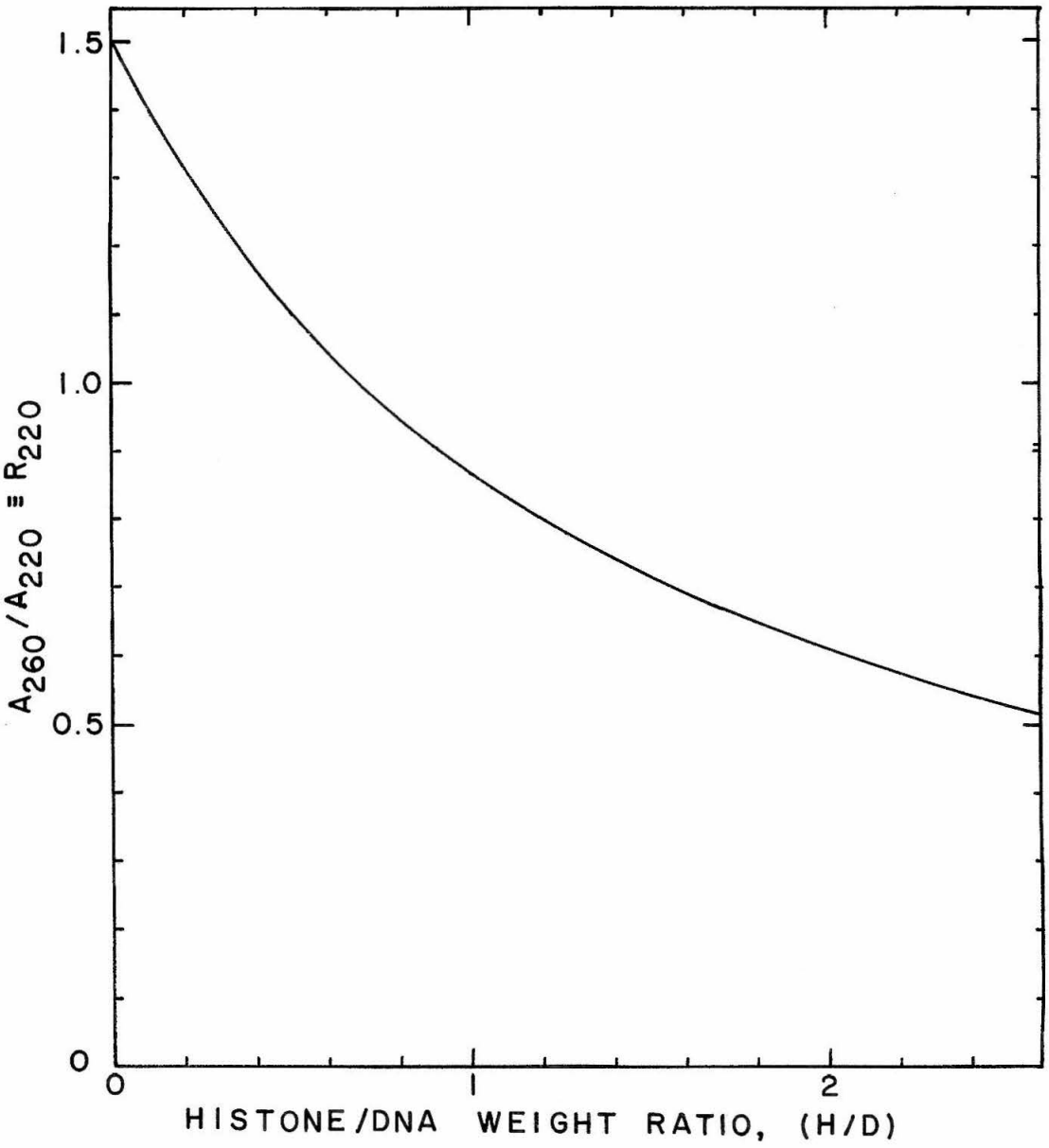

Figure 3

Plot of absorbance ratio $A_{260}/A_{220} \equiv R_{220}$ versus histone to DNA weight ratio (H/D).

3. Dialysis

In order to keep UV absorbing impurities to a minimum, is was necessary to pretreat the Visking dialysis tubing, which was known to release these impurities into the DNA solution. To this end the tubing was boiled in a concentrated $NaHCO_3$ solution for 15 minutes, rinsed with redistilled water, especially on the inside, boiled in two changes of redistilled water for 15 minutes each, rinsing on the inside after each boiling, and then stored at 4° C in redistilled water (53). The tubing was handled only with plastic gloves. The dialyses were carried out in a cold room at about 4° C.

When necessary, dilute versene (EDTA) solutions were used instead of redistilled water to eliminate any divalent ions.

4. Measurements of Heating Curves

Our heat denaturation studies with DNA and DNH were carried out either manually in the Cary Model 14 using a special heating compartment designed by Dr. Wm. Dove (54) or automatically in the Gilford Multiple Sample Absorbance Recorder using a Beckman spectrophotometer for the UV measurements.

In the Cary the complete UV spectra of the samples were recorded and the temperatures were measured on the fly using a copper-constantin thermocouple. One of the junctions was placed in close thermal contact to the glass stoppered Pyrocell microcell containing the sample, and the other junction was immersed in a water-ice bath. The potential was read on a Leeds and Northrop Model K-2 potentiometer. The temperature was determined from a calibration curve made against a thermometer, which had been standardized by the National Bureau of Standards.

The heating curves made with the Gilford, which had been standardized by Dr. R. H. Jensen, were found to agree with those determined with the Cary to within 0.5 °C.

The microcells were carefully cleaned with boiling, doubly distilled water, and all samples were evacuated to remove any dissolved air prior to heating. The rate of heating was about 0.5 deg/min up to about 100° C. The

weight of the sample cells was determined before and after heating to assure that no evaporation had taken place. Weight losses were generally less than 5 %.

The percent hyperchromicity (% H) was calculated on the basis of the initial A_{260} (A^i_{260}) corrected for solvent blank and initial A_{400} (A^i_{400}). Thus,

$$\% H = \frac{[(A^T_{260} - A^T_{400}) - (A^i_{260} - A^i_{400})] \times 100}{(A^i_{260} - A^i_{400})} \qquad (1)$$

In the experiments performed on the Gilford, only A^T_{260}, the absorbance at 2600 Å at T° C, is measured, so that variations in the baseline during heating due to changes in scattering etc. cannot be corrected for by subtracting A^T_{400}, and the % H may be somewhat in error in that case.

The temperature of the midpoint of the melting profile (Tm) was determined and also the width of the curve, which we defined as the difference in temperature at which 10 and 90 % of the transition had been reached. For a few cases which showed distinct two-step melting behavior, the Tm's for the separately melting regions are also reported.

In order to give an indication of the steepness of the transition at Tm, we calculated a normalized slope

$$S_{Tm} = \left(\frac{\Delta H}{^oC}\right) \frac{100}{H_{total}} \qquad (2)$$

where $\Delta H/^{o}C$ = change in % H per degree at Tm and H_{total} = total % H for the transition with its midpoint at T_m.

5. Measurements of Electrophoretic Mobilities

The apparatus used to measure the mobilities of our DNA and DNH preparations has been described in detail by Olivera, Baine and Davidson (55). The apparatus consists basically of a vacuum jacketed, ice-water cooled (1 to 2° C), vertical quartz tube which can be scanned by a UV scanning device. The transmitted light is detected by a photocell and the signal amplified and recorded on a paper recorder.

The tube is connected to the electrode compartments by means of two sidearms, containing solutions with different electrolyte and sucrose concentrations. It is filled with a sucrose density gradient (5 to 20 %) containing 0.01 F NaCl and 0.001 F tris buffer (pH 7.5). The sample (0.2 ml, A_{260} about 1 to 2) containing approximately 2.5 % sucrose is layered as a zone onto the sucrose gradient. Finally, solvent is carefully layered onto the sample to establish electrical contact with the upper sidearm. Turning a stopper at the bottom of the tube establishes electrical contact with the lower sidearm.

An electric field of about 360 volts is applied across the central tube and the movement of the zone is recorded in intervals together with the amount of current that has passed through the tube. The mobility is calculated from the slope of a plot of distance traveled by the zone (d)

versus coulombs (q) using the following relationship:

$$u = d/qR \qquad (3)$$

where R is the average resistance per unit tube length. It is 2850 ohms/cm in the central tube (area = 0.80 cm^2).

6. Salt Gradient Sedimentation

A. Experimental Procedure

The following describes the experimental techniques and the accessory apparatus required for salt gradient sedimentation.

In order to avoid having to run a large number of sedimentation experiments at differing salt concentrations to monitor the extent of dissociation of DNH, we decided to explore the possibility of sedimenting a thin layer of DNH through a preformed salt gradient superimposed on a stabilizing density gradient. Because of the difference in molecular weight of DNA and histones, we expected to find a non-sedimenting zone of histones at the position where dissociation occurs.

a) Use of Quartz Tubes

To facilitate a more efficient and accurate determination of this zone position, we used flat-bottom, cylindrical quartz tubes instead of the commonly employed plastic sedimentation tubes. The quartz tubes could be scanned before and after a run at various wavelengths in the Cary spectro-

photometer, thus eliminating the tedious dripping technique necessary for analyzing the results in plastic tubes.

The quartz tubes (4.34 cm high, 1.07 cm inner diameter) were supplied by the Spinco Division of the Beckman Corp. and were designed to fit into the buckets of the SW 39L rotors, the round bottom of the buckets being filled by a 0.67 cm high aluminum half sphere. Because of the fragility of the quartz tubes, the inner liquid head had to be counterbalanced on the outside by a liquid head having the average density of that inside the tube (56). Furthermore, it is important in handling the tubes, that the surface is touched only with gloves or plastic covered tweezers to prevent scratching or dirtying of the soft quartz surface.

b) Layering Technique

The linear gradient layering apparatus (Fig. 4) had been designed by Mr. J. Kaspar (57) and is described in more detail by Dr. J. Vasilevskis (58). It consists of two cams which were driven by a common driveshaft. Each cam in turn pushes a plunger of a syringe, one containing the heavy, the other the light D_2O or sucrose salt solutions. The radii of the cams varied in such a way that when the solutions from the two syringes were mixed, a linear gradient resulted (Fig. 7). Mixing was accomplished by letting the solution flow through a spiral of plastic tubing. For our purposes the thin capillary outlet was replaced by a carefully

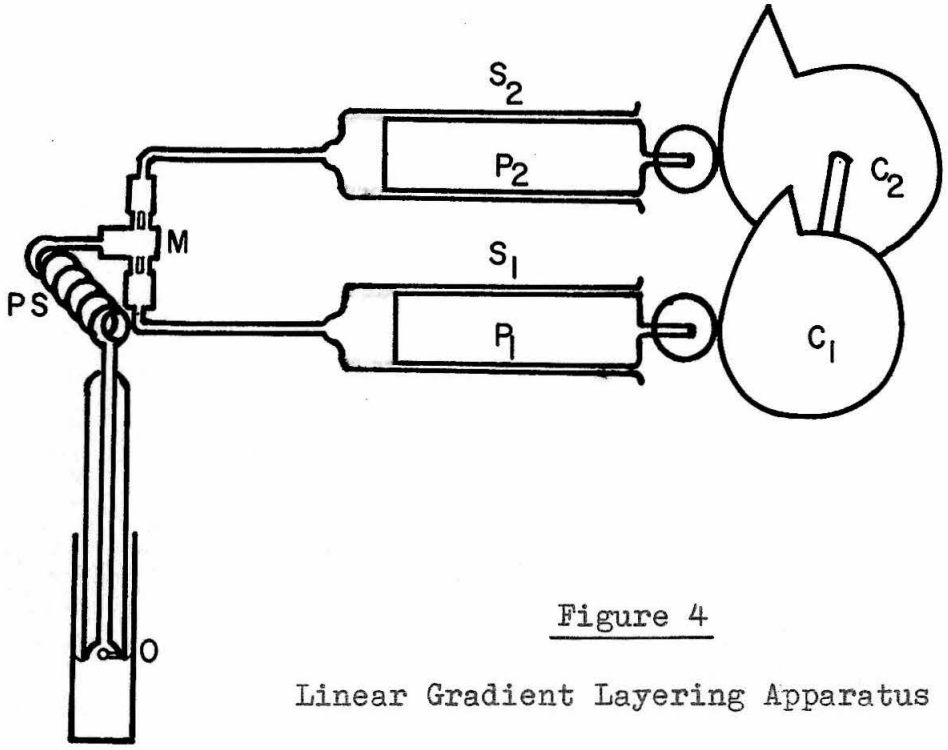

Figure 4

Linear Gradient Layering Apparatus

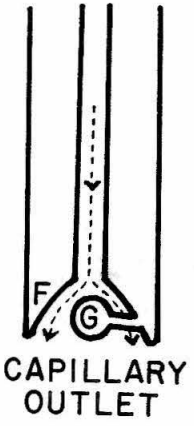

Two metal cams (C_1 and C_2) push the plungers (P_1 and P_2 of two syringes (S_1 and S_2) so that the heavy and light liquids are forced into the mixing chamber (M) and through the plastic spiral (PS) past the glass capillary outlet (O). A small glass ball (G) is fused to the flange (F) at the outlet in order to divert the liquid stream evenly to the walls of the flange.

flanged, widemouth capillary (see Fig. 4). A small glass-ball was fused to its exit so that it diverted the outflowing liquid stream evenly to the walls of the flange. Using this outlet it was possible to fill the quartz tubes so that the dense solution (high salt in 100 % D_2O or 25 % sucrose) was layered onto the tube bottom first and then the less dense solution (low salt in 25 % D_2O or 5 % sucrose) onto the heavier solution, while the tube was lowered by a machine at the rate of filling. Filling of a tube with 3.5 ml gradient took about 5 minutes.

This procedure prevented unnecessary disturbances of the gradient after it was layered. It was fortuitous, that the same machine which was designed for the scanning of the quartz tubes in the Cary spectrophotometer was usable for the lowering of the tubes during filling.

After the three quartz tubes were filled with gradients, 0.25 ml of the DNH sample was carefully layered on top followed by a layer of solvent or H_2O. By using a micropipette which is touching the tube wall at the meniscus, very sharp layers were obtained. Figure 5 shows the 2600 Å scan of a layer of DNH IIb in 10^{-3} F $NaClO_4$ above a D_2O density gradient (25 to 100 %). The final layer of solvent or water was added at the top to move the meniscus, which looks like another zone at the top of the solution, away from the sample position. It is clear that the meniscus would otherwise obscure the zone position. As can be seen from the figure,

Figure 5

Quartz tube scan at 2600 Å of a layer of DNH IIb in 10^{-3} F $NaClO_4$ above a D_2O density gradient. The meniscus was moved up by layering solvent on top of the DNH zone. The absorbance cutoffs at top and bottom are due to the metal holder and serve as reference points. The tube bottom is the interphase between the quartz disk at the bottom and the solution. Sedimentation is from left to right.

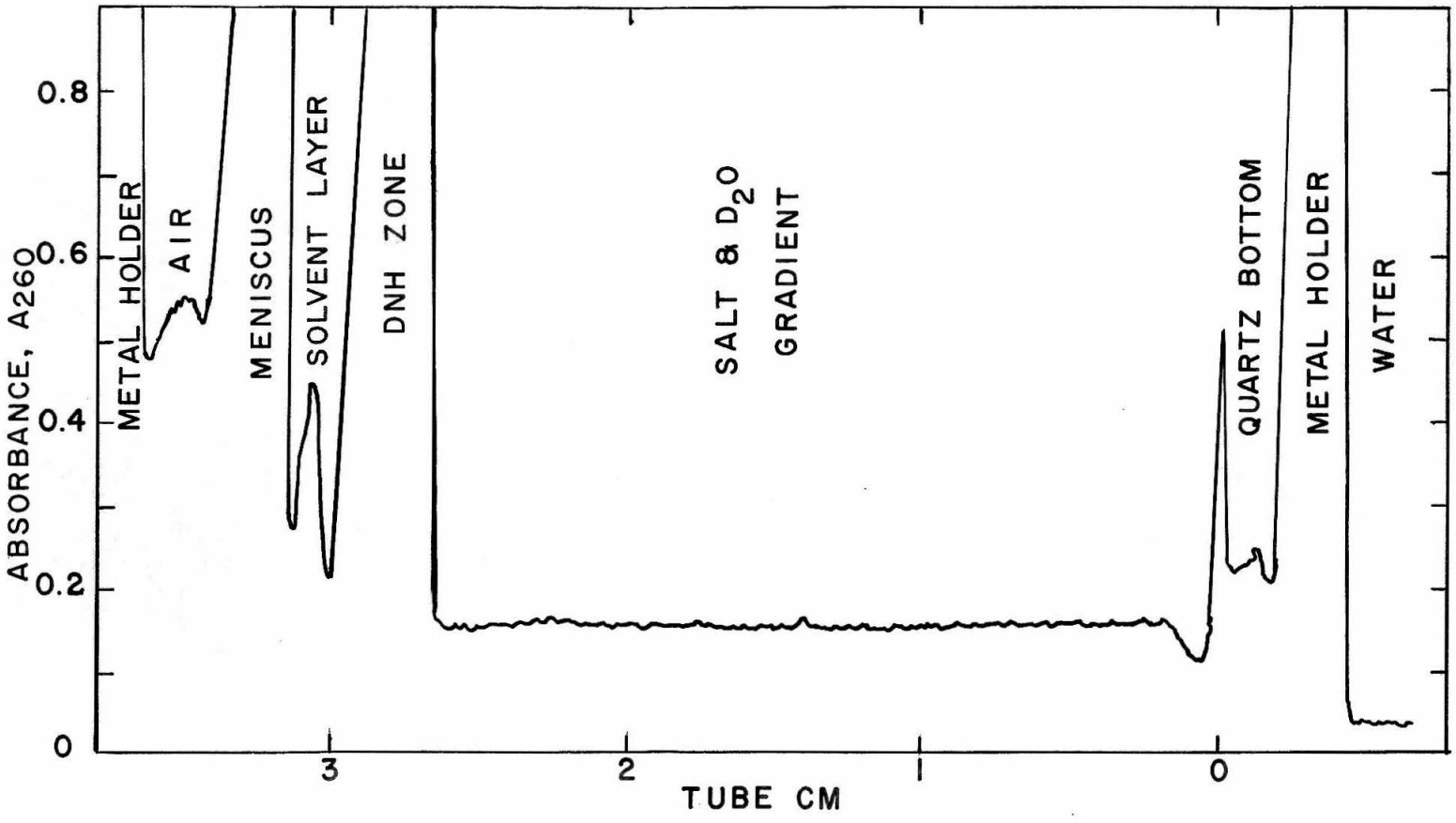
ABSORBANCE, A260
0
0.2
0.4
0.6
0.8
METAL HOLDER
AIR
MENISCUS
SOLVENT LAYER
DNH ZONE
SALT & D2O
GRADIENT
QUARTZ BOTTOM
METAL HOLDER
WATER
3
2
1
0
TUBE CM

Figure 5

mixing of the top layer and the DNH layer was negligible, making it unnecessary to increase the density of the sample layer by D_2O or sucrose. The peak in the solvent layer is due to schlieren effects.

c) Scanning Technique

The tube scanning device for the Cary spectrophotometer was designed by Dr. J. Vasilevskis (59). The quartz sedimentation tubes were secured watertightly in a plunger, which could be lowered or raised by the machine into a water bath and past a 0.5 mm slit. The water bath was necessary to diminish reflection and refraction of the light beam on the round quartz surface of the sedimentation tubes. The bath, containing two quartz windows, the plunger, and the slit were positioned in the path of the Cary light beam. To avoid artifacts due to divergence or convergence of the light beam, a diffusion plate had to be inserted before the slit. However, the amount of light lost in this way required that a 1.5 to 2.0 optical density filter be inserted into the reference compartment of the Cary. Some of the uncertainties of the absorbance measurements observed are due to the fact that rather small amounts of light are actually measured in scanning the tubes. Scans were generally made at 4000, 2600 and 2200 Å.

d) Acceleration, Deceleration

In our first experiment is was not possible to preserve the sample zone even during short sedimentations, but it was soon discovered that the rate of acceleration and deceleration of the rotor was responsible. That fast acceleration was the prime factor for zone destruction was shown by a series of experiments under varying conditions of acceleration. Figure 6, for example, shows the effect of fast acceleration on an initially sharp zone (Curve 1) of Escherichia Coli DNA in 2.5 % sucrose and 0.1 F NaCl and covered by H_2O. The SW 39L rotor of a Spinco Model L ultracentrifuge was accelerated to 10 000 rpm within 1.5 minutes, kept at this speed for 1 minute and then decelerated during 4.5 minutes without the brakes. The tube was scanned immediately after the sedimentation run (Curve 3). The time was 77 minutes after that of curve 1. Curve 2 shows the effect of diffusion on standing of a similar zone during the same time interval (72 minutes). It is clear from curve 3, showing the broad and irregular remnant of the original layer, that zone destruction by fast acceleration poses a serious problem to successful velocity sedimentation runs.

An experiment with the new wobblefree Spinco L-2 model, kindly made available to us by Prof. W. J. Dreyer, resulted in complete destruction of the layer, because of

Figure 6

Effect of fast acceleration of the SW 39L rotor of a Spinco Model L ultracentrifuge on a zone of Escherichia Coli DNA (Curve 1), A_{260} = 0.55 in 2.5 % sucrose and 0.1 F NaCl, layered on top of a 5 % sucrose solution in 0.1 F NaCl and covered by H_2O. The rotor was accelerated in 1.5 minutes to 10 000 rpm, was kept at this speed for 1 minute and then decelerated without brakes in 4.5 minutes. Curve 3 was traced 77 minutes after curve 1. Curve 2 shows the effects of diffusion on a non-accelerated zone after 72 minutes at room temperature.

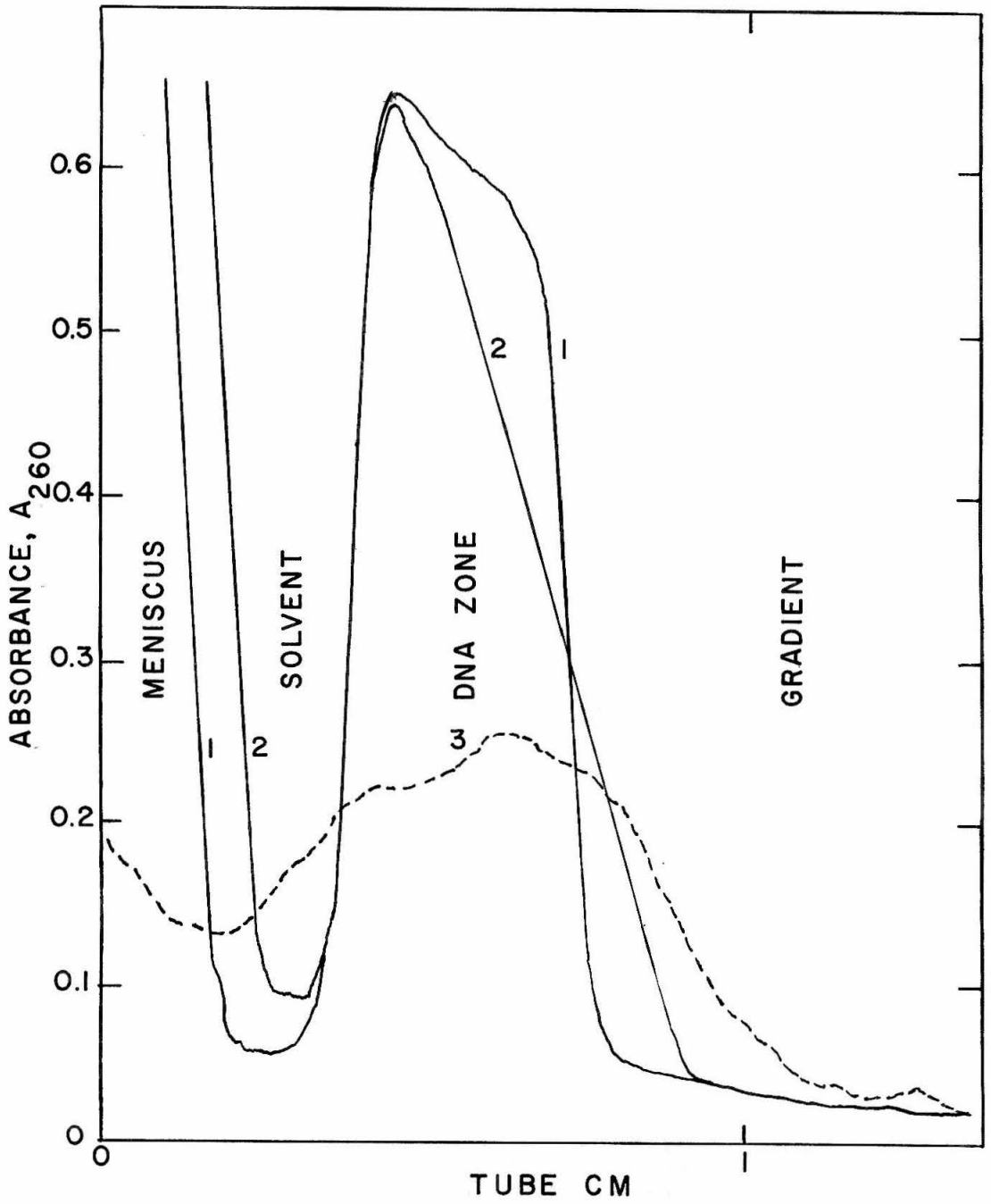
ABSORBANCE, A_{260}
0.6
0.5
0.4
0.3
0.2
0.1
0
0
TUBE CM
MENISCUS
SOLVENT
DNA ZONE
GRADIENT
1
2
2
1
3

Figure 6

fast acceleration and deceleration. Since it was difficult to accelerate the SW 39L rotor slowly enough, we used the larger SW 25 rotor, employing a teflon adaptor for the buckets. This adaptor was designed by Dr. R. Lief (60) to accommodate the SW 39 sedimentation tubes. The larger rotor was accelerated manually to 20 000 rpm (close to the maximum permissible rpm for the quartz tubes) at a rate of not more than 1000 rpm per minute. The deceleration was that due to the friction of the rotor itself (brakes were off) and took 45 minutes. All runs lasted from 15 to more than 20 hours each.

B. Analysis of Data

In all those cases in which the histones had dissociated in fairly narrow bands, forming easily distinguishable peaks in the 2200 Å scans from those of the DNA further down the tube (e. g. Fig. 11), the sedimentation procedure described lends itself, in principle at least, to the determination of

a) the salt concentration range at which dissociation takes place,

b) the sedimentation coefficient of DNA and DNH,

c) the amounts of dissociated material and their distribution, if certain parameters can be measured accurately.

Should the histone dissociation be gradual, it can be easily observed by comparing the scan at 2600 Å with that at 2200 Å. However in this case, the quantitative analysis of the data is often inaccurate due to uncertainties in the baseline positions.

a) Salt Concentration Range

The ease of determining the range of salt concentration required for the DNH complex dissociation is probably the most valuable feature of the sedimentation procedure. Only a few experiments are required to get a good idea

about the dissociation charateristics, and the results can then be verified and the products more thoroughly characterized by using larger scale preparative experiments.

The reliability of the results is a function of the linearity of the salt gradient and the exactness with which the tube position can be measured. That the salt gradient remains indeed quite linear throughout the time and operations required for sedimentation and analysis of the results (more than 10 hrs), can be seen from refractive index measurements of fractions from the experiments with sucrose density gradients (Fig. 7). Experiments with D_2O gradients do not lend themselves to this kind of analysis, since the refractive index decrease due to the increasing concentration of D_2O counterbalances almost completely the increase due to the increasing salt concentration.

With respect to the accuracy of the determination of the position along the quartz tubes from the scans, it was found that the error was within $\pm$ 2.5 x 10^{-3} cm, if reliable reference points are chosen (e.g. absorbance cut-off due to the metal holder at the top and bottom of the quartz tubes, see Fig. 5). This shows that the Cary chart speed and the motor scanning speed were highly reproducible.

Figure 7

Linearity of density gradients. The refractive indices of the fractions from salt gradients superimposed on sucrose density gradients (5 to 20 %) are plotted versus fraction number.
Curve 1: Uniform 0.4 F NaCl concentration.
Curve 2: 0.4 to 0.8 F NaCl gradient.
Curve 3: Uniform 0.6 F NaCl concentration.
Curve 4: 0.4 to 0.6 F NaCl gradient.

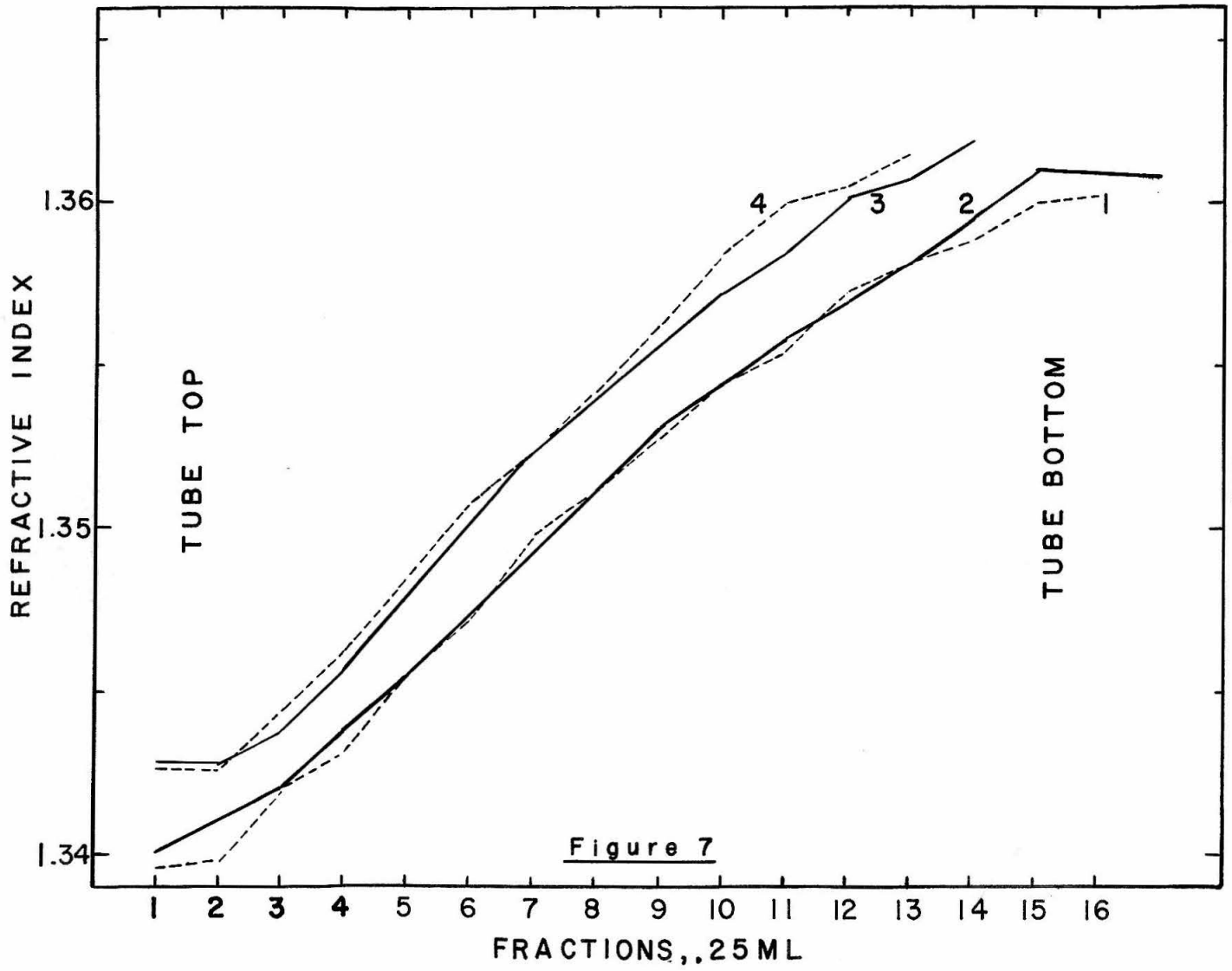
REFRACTIVE INDEX
1.36
1.35
1.34
TUBE TOP
TUBE BOTTOM
4
3
2
1
1 2 3 4 5 6 7 8 9 10 11 12 13 14 15 16
FRACTIONS,,25ML

Figure 7

b) Sedimentation Coefficients

For the determination of reasonably reliable sedimentation coefficients, we measured the distance traveled from the midpoint of the initial layer to the peak maxima. Using a uniform low salt concentration in one of the tubes, a sedimentation coefficient for the DNH was obtained. Sedimenting the DNH through a uniform high salt concentration, a sedimentation coefficient for the corresponding DNA can be determined, since the histones are left behind at the initial zone position. A combination of these two sedimentation coefficients is required to account for the distances traveled in a third tube having a salt gradient which causes dissociation of the DNH in the middle of the gradient: DNH from the initial zone position to the histone peak, and DNA from there on to the final DNA peak. This, of course, assumes that the dissociation is quantitative and fast with respect to the sedimentation speed.

The sedimentation coefficient is computed according to the following relationship (61):

$$s = \frac{\ln (r_b/r_z)}{\omega^2 t} \qquad (4)$$

where r_b = the distance from the center of rotation to the midpoint of the band after sedimentation, r_z = the distance from the center of rotation to the midpoint of the initial

zone position, ω = the angular speed of rotation in radians per second, and t = the corrected sedimentation time in seconds. Since acceleration and deceleration were rather slow, average rpm values were computed for each 5000 rpm interval of change in the speed of rotation, and the time for each interval was converted to an equivalent time at 20 000 rpm using the relation (62)

$$\begin{pmatrix}\text{equivalent time}\\ \text{at 20 000 rpm}\end{pmatrix} = \left(\frac{\text{average rpm of interval}}{20\ 000}\right)^2 \times \begin{pmatrix}\text{min. of}\\ \text{interval}\end{pmatrix} \tag{5}$$

The sedimentation coefficients were not corrected for the density of the solution or standardized with regard to temperature or concentration, since we did not feel the accuracy of the present data warranted these more elaborate calculations and calibrations. For the case of mixed sedimentation of DNH followed by DNA in a salt gradient, the midpoint of the histone band was chosen as the point at which DNH was quantitatively converted to DNA. The time for which the DNA sedimented was found by

$$t_{DNA} = t_{total} - \frac{\ln (r_b^{DNA}/r_b^H)}{\omega^2 s_{DNA}} \tag{6}$$

and therefore,

$$s_{DNH} = \frac{\ln (r_b^H/r_z)}{\omega^2 (t_{total} - t_{DNA})} . \tag{7}$$

A number of s_{DNH} values obtained in this manner is listed in table III together with the corresponding sedimentation coefficients for the DNA, which were found by using a high salt concentration throughout the tube so that only the DNA sedimented.

c) Material Balance

The following sections are intended for those readers who are planning to use the preparative ultracentrifuge for quantitative measurements. It describes in detail the problems that are encountered in determining the amounts of material present in the tubes after sedimentation by either the scanning techniques or by various fractionation procedures. The results are presented in terms of UV absorption and show that DNA "recovery" presents in general no difficulties, while the "recovery" of histones is obscured by UV impurities.

Before discussing the various methods used to determine the amount and quantitativeness of the histone dissociation, certain intrinsic complications of the sedimentation method should be mentioned. In determining the distribution of DNA and histones in the sedimentation tubes it must be remembered that the material may be found at any of five distinct places:

1. In the histone band.

Table III

Ionic Strength	S_{DNA} in Svedbergs	S_{DNH} in Svedbergs
0.6	14.65 ± 0.3	
0.4 - 0.6	"	23.2
0.6	15.0	
0.4 - 0.6	"	22.7 ± 1.0
0.4 - 0.6	"	26.7 ± 1.3
0.6	14.1	
0.4 - 0.6	"	22.2 ± 0.5

Sedimentation Coefficients of Reconstituted DNH II

2. In the DNA band.

3. Pelletted at the tube bottom.

4. At the initial zone position, i. e. non-sedimenting material, like fragments (degradation products) and non-complexed histones in the original solution.

5. Sedimented to the tube wall due to the non-sector shape of the tube and from there

a) easily removable

b) removable by the meniscus during fractionation,

c) non-removable except by thorough washing.

The amount of material sedimented to the tube wall can be estimated from the following equation, which is easily derivable from geometric considerations:

$$\% \text{ loss} = \frac{100\ (r_b - r_z)}{r_b} . \qquad (8)$$

Using r_b = 8.83 cm and 11.38 cm for the SW 39 and SW 25 rotors respectively and a distance of sedimentation of 3.0 cm for $(r_b - r_z)$ we find that as much as 34.0 % and 26.4 % of the initial material may sediment to the tube wall.

Because it is often difficult to distinguish between the various regions, all attempts to determine the recovery of material are quite approximate. Thus, the histone band is always "contaminated" with DNA which has sedimented to the tube wall. Material which has pelletted, decreases the amount recovered, for it cannot be seen in the scans and may be difficult to remove during fractionation. Bands of

histones which have dissociated at the top of a high salt gradient may be indistinguishable from material that did not sediment at all due to degradation and remained at the initial zone position. Therefore, blank runs with low salt gradients are often required.

These difficulties, however, are minor compared to those due to the errors in UV measurements, which are accumulative in nature.

I) Data From the Scans

1) Uncertainty in Absorbance Measurements

Quantitative estimates of the amounts of material from measurements of the areas under the various peaks depended greatly on the accuracy of the absorbance measurements and the reproducibility of the baseline. The large contributions of only small errors and changes in the background absorption and the baseline to the measurements of the areas made it quite unreliable to use the baselines taken before the sedimentation experiment to correct for the absorption of the salt plus density gradients.

Even the more dependable procedure of selecting a few strategic positions along the tube and scanning these positions from 4000 to 2000 Å and correcting the relative absorbancies thus obtained by those determined in a similar manner for the gradients before sedimentation, gave results which were not very reliable. An inherent uncertainty for each individual absorbance measurement of ± 0.005 gives rise to an error in the sample absorbance of ± 0.02 absorbance units. The effects of such an error is naturally much greater on broad, dilute bands of material and figure 8 illustrates their distortion of the results on a rather "good" band of histones. Here, the area under the peak represents 23 % of the total histone present in the initial

Figure 8

The effect of a baseline shift of 0.02 absorbance units on the area under a histone peak. Histones in the peak are those extracted by 0.6 F $NaClO_4$ from native calf thymus DNH (R_{220} = 0.707, 7 days old) on top of a 0.6 to 2.0 F $NaClO_4$ gradient in D_2O (see Fig. 29).
The area down to the dashed line represents 23.0 % of the total histones in the initial zone. The error due to the baseline shift is ± 3.8 % or ± 16.5 % of the peak.

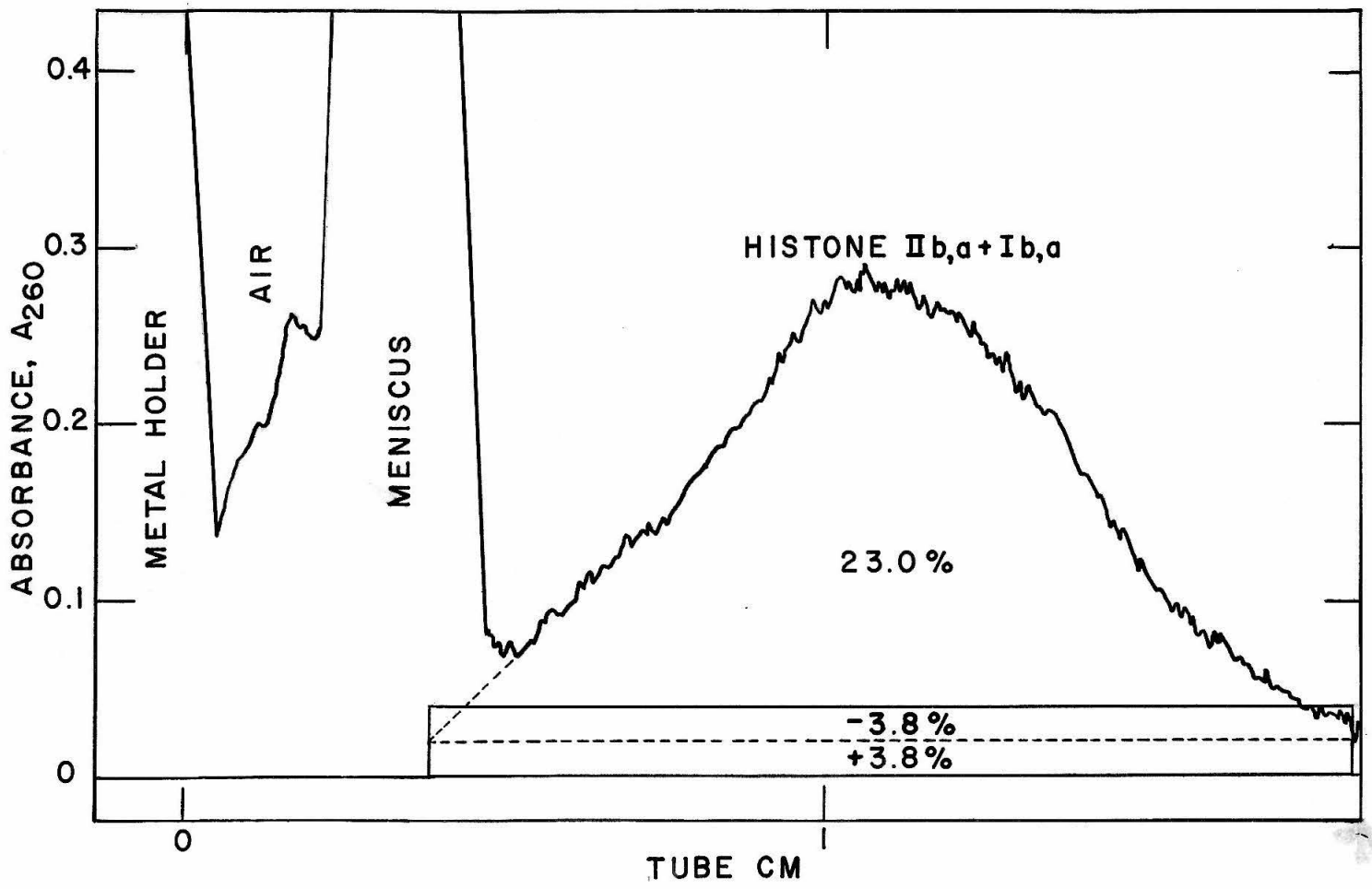
0.4
0.3
0.2
0.1
0
ABSORBANCE, A_{260}
METAL HOLDER
AIR
MENISCUS
HISTONE IIb,a+Ib,a
23.0%
-3.8%
+3.8%
0
TUBE CM

Figure 8

DNH used. The ± 0.02 absorbance error amounts to ± 3.8 % of total histones and to ± 16.5 % of those in the band.

The fact that "recovery" of DNA in terms of its absorbance at 2600 Å is generally much better than that of histones, which is often much too high, suggests that UV impurities cannot be adequately eliminated in spite of the precautions taken. Ideally, a second quartz tube filled with the same gradient should be scanned in the Cary reference compartment simultaneously with the tube containing the sample, but this required a much more elaborate scanning device than was available to us.

2) Scan Material Balance

A few of the better results of material analyses from the scans are given in table IV. They are from runs in which extensive pelletting of the DNA was avoided. The data listed are in terms of

a) % of total initial DNA detectable (% A^{D}_{260}) in the various regions of the tube as measured from the A_{260} scan.

b) % of total initial histone detectable (% A^{H}_{220}) in the same regions as measured from the A_{220} scan and corrected for the DNA absorbance at this wavelength using a ratio of A_{260} to A_{220} (R^{D}_{220}) of 1.5.

Table IV

Scan Material Balance

Reconstituted Calf Thymus Nucleohistones

Sample	DNH Ib	DNH Ib	DNH IIb	DNH IIb	DNH IIb
F $NaClO_4$	0.0-0.25	0.2 - 0.6	0.4-0.6	0.4 - 0.6	0.6
days old	1	0	16	0	27
A_{260} init	3.31	3.31	1.86	3.40	2.965
A_{220} init	2.81	2.81	2.27	3.425	3.02
R_{220}	1.18	1.18	0.817	0.993	0.982
A_{400} init	0.102	0.102	-	-	-
% A_{260}rec	93.3	90.95	98.9	81.85	87.75
% not sed	9.25	5.45	8.2	-	-
% banded	68.5	72.7	48.2	61.9	74.6
% in H bd	-	-	27.7	6.35	5.7
% in pel	15.55	12.8	14.8	13.6	7.45
% A_{220}^{NH}	109.3	106.0	77.5	94.3	95.16
% A_{220}^{H}	163.5	156.5	56.1	118.	109.45
% not sed	112.5	118.7	17.6	-	-
% banded	-	-	37.8	110.5	98.25
% in DNA	43.0	33.4	0.7	5.4	8.25
% in pel	7.95	4.4	-	1.7	2.95
R_{220}^{A}	1.28	1.33	1.49	1.445	1.43

c) The actual R^{A}_{220} of the DNA band as calculated by the ratio of the area under the A_{260} peak to the area under the corresponding A_{220} peak.

The data show that the scan analysis does lend itself to the quantitative estimation of material in the tubes. The computed recovery of the histones is not so accurate and tends to be high. The reason that the histone data are not as reliable is not due to the procedure used as such, but rather to the difficulty of correcting adequately for UV impurities, and baseline fluctuations. The significance of the variations in the amounts of material at the various tube positions will be discussed as part of the results section.

II) Analysis of Fractions

1) Fractionation Procedures

Because of the unpredictable nature of the sources of errors mentioned above, it was necessary to verify the data obtained from the scans by fractionating the solutions in the quartz tubes after the sedimention and analyzing the individual fractions.

Various fractionation procedures were tried. Their differences are described in detail to point out the artifacts that may affect the results.

1. Fractionation from the top of the solution, either by using a micro pipette or a Sigma motor pump.

2. Fractionation by pumping heavy fluorocarbon oil to the tube bottom and collecting the solution by pushing it upward through a capillary opening as suggested by Dr. R. C. Lief and illustrated in figure 9.

3. Fractionation from the tube bottom by means of a thin capillary and the Sigma pump; a method comparable to the usual dripping technique.

Using procedure 3, the material which had sedimented toward the tube wall is being desorbed by the meniscus of the solution. Similar to procedure 1, in which the material at the wall is desorbed in each successive fraction, pro-

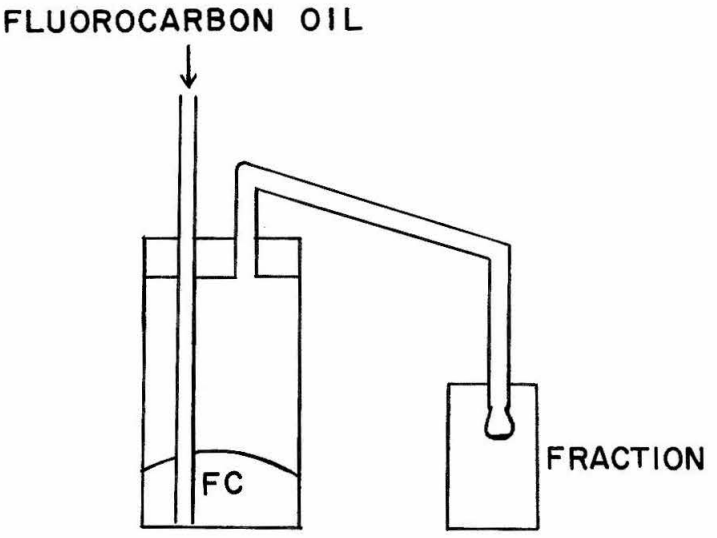

Figure 9

Fractionation procedure using fluorocarbon oil pumped to the tube bottom. The solution is pushed through a capillary at the top and collected. Material at the tube wall is not desorbed by the fluorocarbon - solution interphase.

cedure 3 gives close to 100 % recovery of the initial DNA if extensive pelletting is avoided. (See case 5b, p.194). Procedure 2 on the other hand gives only 70 to 80 % recovery, due to the fact, that the material at the tube wall is not removed by the fluorocarbon - solution interphase. (See case 5c, p.194).

The fractions, 0.25 ml each, were analyzed for DNA by UV absorption at 2600 Å and for histones by UV at 2200 Å and a micro ninhydrin procedure.

Figure 10 illustrates the differences in the fractionation procedures in terms of the DNA absorbance of the fractions. The direction of sedimentation is from left to right. Graph (a) shows the distribution of absorbance if the solution is fractionated from the top of the solution. The DNA has banded near the tube bottom and the recovery of A_{260} is 96.1 % of the charge.

Graph (b) shows a similar distribution after fractionation by using fluorocarbon oil, but the total A_{260} recovery is only 72.0 % of the charge. Fractionation from the tube bottom is illustrated in graph (c). A considerable amount of DNA is desorbed by the meniscus and the distribution is quite distorted. Total recovery of A_{260} is 106 %, i. e. quantitative. 29.4 % are present in the top five fractions. The % lost by sedimentation to the wall, calculated by equation (8) was 25.3 %.

Figure 10

Comparison of fractionation procedures.
The sedimented zones were reconstituted calf thymus DNH IIb.
For clarity's sake only A^{D}_{260} is shown. The direction of sedimentation is from left to right.

a) Fractionation from the top of the solution using a micro pipette. Material is desorbed from the quartz wall by the meniscus.
b) Fractionation from the top using fluorocarbon oil to push the solution upward. Material at the quartz wall is not desorbed.
c) Fractionation from the tube bottom by means of a thin capillary and a Sigma pump (this procedure is comparable to dripping). Material at the quartz wall is desorbed by the descending meniscus and is "recovered" in the top fractions.

The percentages of recovered material are based on the A^{D}_{260} in the initial zone.

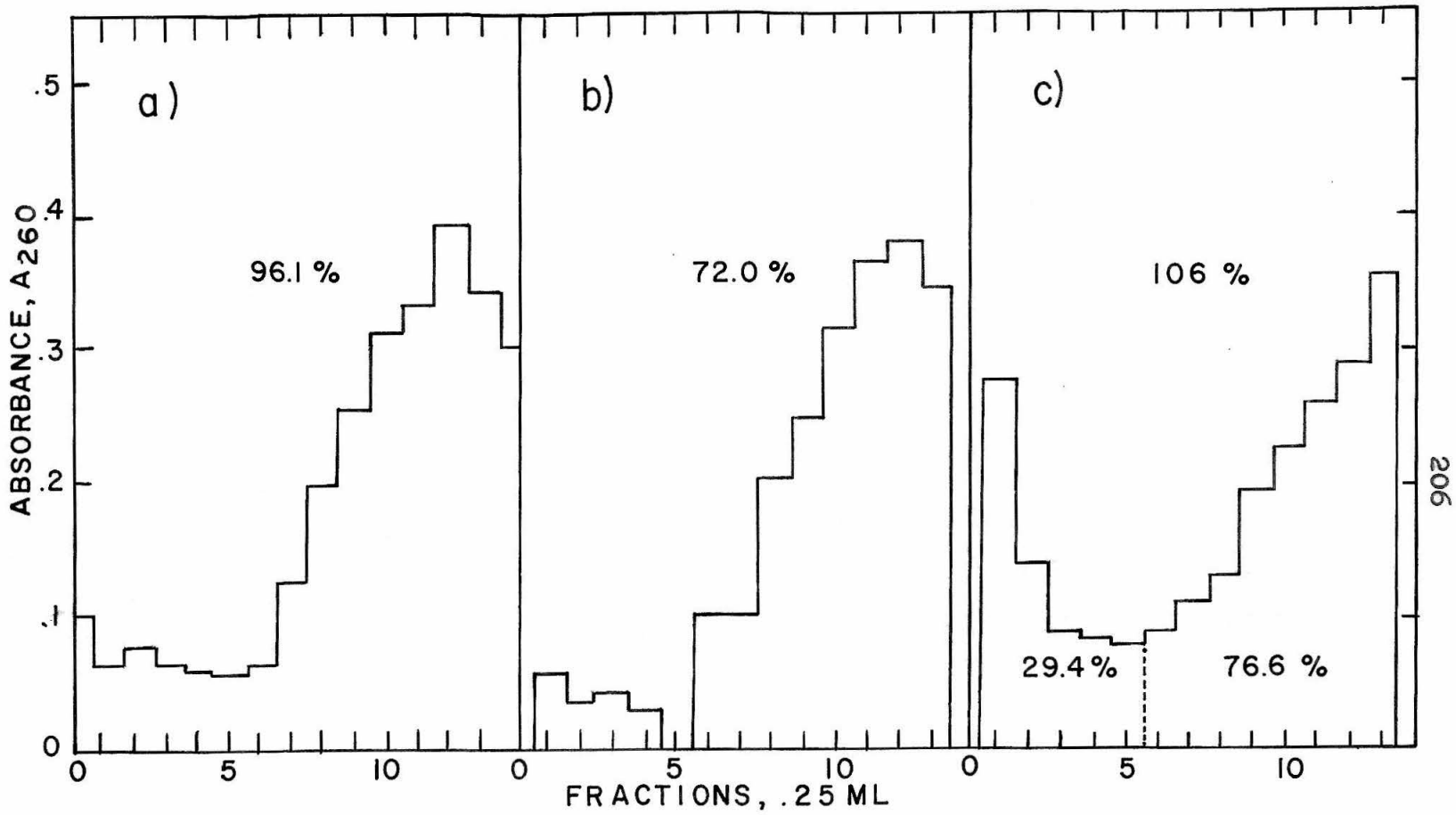
a)
b)
c)
96.1 %
72.0 %
106 %
29.4 %
76.6 %
ABSORBANCE, A260
FRACTIONS, .25 ML
0
.1
.2
.3
.4
.5
0
5
10
206

Figure 10

It is important that the differences in the fractionation procedures be considered in relation to the purpose of the experiments. From an analytical standpoint the fluorocarbon technique is probably the best, since the effect of sedimentation to the wall is eliminated. If total recovery is the important aim, fractionation from the top is to be preferred over that from the bottom.

Figure 11 shows in semi-quantitative terms the agreement of scan absorbance measurements, UV absorption and ninhydrin tests of individual fractions taken from the top of the solution. The initial layer contained reconstituted DNH IIb (R_{220} = 1.0). It was sedimented through $NaClO_4$ varying from 0.4 to 0.6 F and superimposed on a D_2O density gradient varying from 25 to 100 %. The band of dissociated histones can be clearly identified by its A_{220} centered around a $NaClO_4$ concentration of 0.452 F. This position is confirmed by the A_{220} of the fractions and the ninhydrin tests. Only small amounts of DNA are present at this position. The band further down the tube is due to the extracted DNA. It is beginning to pellet at the tube bottom. Again agreement with the absorbance measurements of the fractions is quite good although it should be noted that the absorbance at 2200 Å of the fractions is significantly higher than that of the scan. Also the ninhydrin tests show considerable background color in the DNA.

Figure 11

Quartz tube scans before and after sedimentation of a zone of reconstituted calf thymus DNH IIb (R_{220} = 1.0; 0 days old) through a 0.4 to 0.6 F $NaClO_4$ gradient in D_2O. The scans are superimposed on absorbance and ninhydrin measurements of the fractions taken from the top of the tube. The histone peak is centered around 0.452 F $NaClO_4$ and its minimum and maximum area correspond to 71.6 % and 118 % of the initial A^H_{220} in the zone.

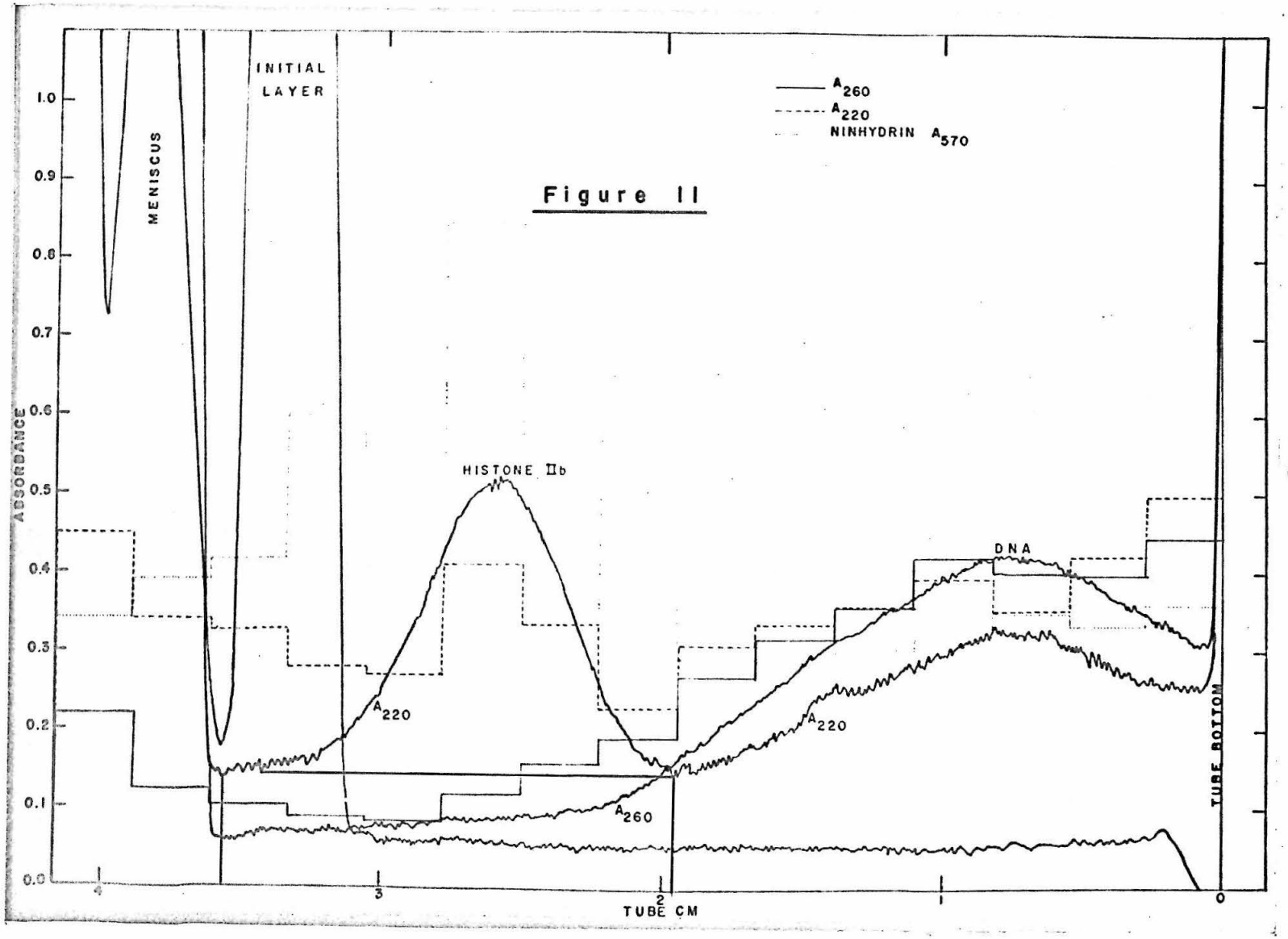
Figure II
A260
A220
NINHYDRIN A570
INITIAL LAYER
MENISCUS
HISTONE IIb
DNA
A220
A220
A260
ABSORBANCE
1.0
0.9
0.8
0.7
0.6
0.5
0.4
0.3
0.2
0.1
0.0
4
3
2
1
0
TUBE CM
TUBE BOTTOM

The minimum area under the histone peak corresponds to 71.6 %, the maximum area to 118 % of the original histone present in the initial layer as measured by A^{H}_{220}. Thus, the dissociation here was essentially complete.

Although the quantitative results are far from satisfactory (see Table IV), qualitatively the agreement is quite good, indicating that the bands detected by the Cary are real and at the correct position and that any distortions due to light reflections etc. are negligible.

2. Analysis of the Protein Content of the Fractions

Because of the difficulties encountered in obtaining a satisfactory material balance for histones from the UV measurements, we investigated the possibility of using more specific tests for proteins to perhaps get better agreement. This section describes our results with a micro Lowry and a micro ninhydrin method. They indicate that this micro Lowry method is only about as sensitive as the UV determinations, while the micro ninhydrin procedure, although much more sensitive, requires that the proteins are hydrolyzed for best results. Since we tried to avoid this hydrolysis step for the time being, we did not yet utilize the sensitivity of this ninhydrin procedure to its full capability.

a) Lowry Procedure

In our search for an easy and accurate procedure for the determination of proteins in our fractions, we tried the Lowry procedure first, because it is one of the simplest methods. The standard procedure (63) was only sensitive to about 50 micrograms of proteins per ml (10 μg/0.2 ml sample give an A_{750} of about 0.1, as can be seen from figure 12). Figure 12 shows the absorbance at 7500 Å due to the Lowry color reaction using bovine serum protein as the standardi-

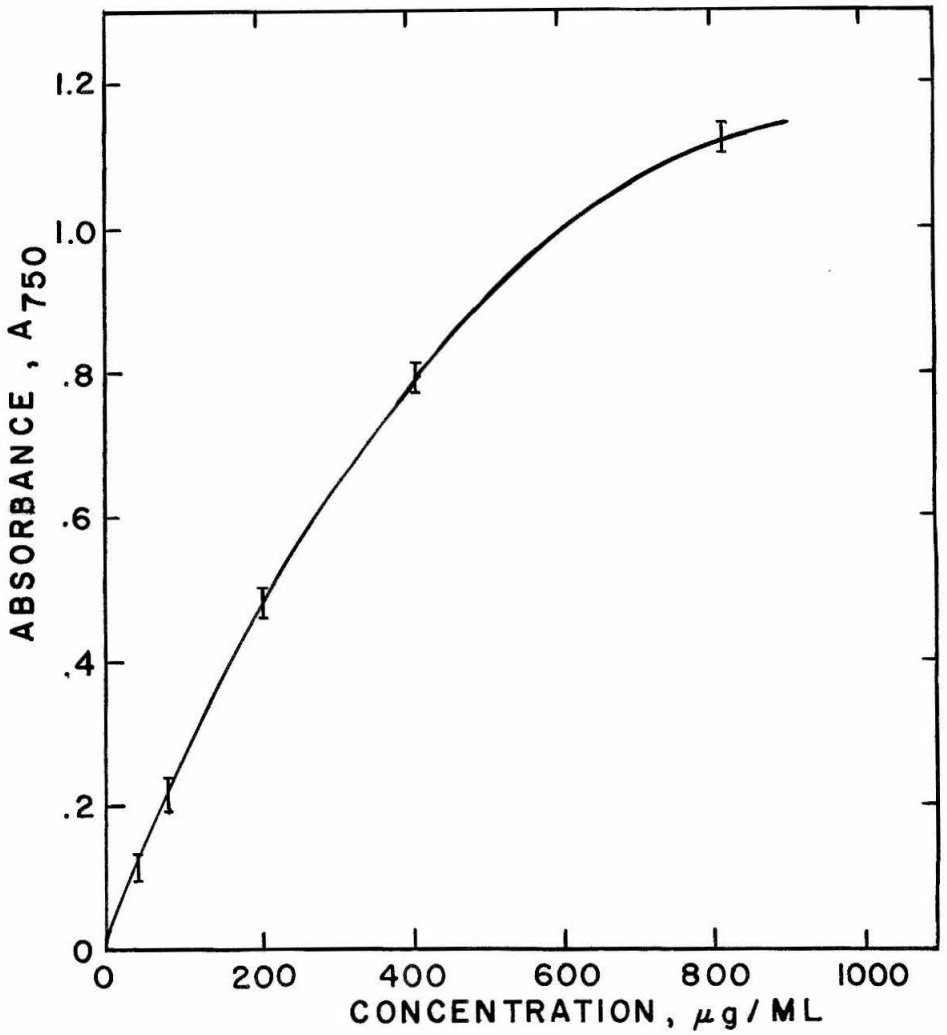

Figure 12

Measurement of bovine serum protein concentration by the standard Lowry procedure (see text). Vertical bars indicate the range of absorbance measurements at 7500 Å taken at 30 to 1300 minutes after addition of Folin reagent (no dependence on time was observed).

zation protein, whose concentration is plotted as micrograms per ml on the abscissa. Fluctuations in the measurements are indicated by the vertical lines.

A micro method is described by Lowry (63), but it involves too many steps, including one of sedimentation, to be of practical value for large numbers of samples.

We succeeded in increasing the sensitivity of the standard procedure simply by lowering the volume of the reagents, increasing the concentrations proportionately. A summary of the procedures follows:

Standard Lowry Method	Micro Procedure
0.2 ml protein solution	0.2 ml protein solution
1.0 ml solution C	0.2 ml solution C"
wait 10 minutes	wait 10 minutes
0.1 ml Folin reagent	0.1 ml Folin reagent
1.3 ml wait 60 minutes	0.5 ml wait 60 minutes
measure A_{750}	measure A_{750}.
Solution C = 50 ml 2 %	Solution C" = 2.0 ml 10 %
Na_2CO_3 in 0.10 N NaOH	Na_2CO_3 in 0.50 N NaOH
1 ml 0.5 % $CuSO_4$ and	0.1 ml 2 % $CuSO_4$ and
1.0 % Na-K-tartrate.	4 % Na-K-tartrate.

This modified procedure gave fairly reliable results down to about 20 micrograms of protein per ml, as seen from

Figure 13

Measurements of the concentration of bovine serum protein (BSP) and histone fraction III (H III) by the micro Lowry procedure (see text). Absorbance at 7500 Å was measured at 70 to 1050 minutes after addition of the Folin reagent.

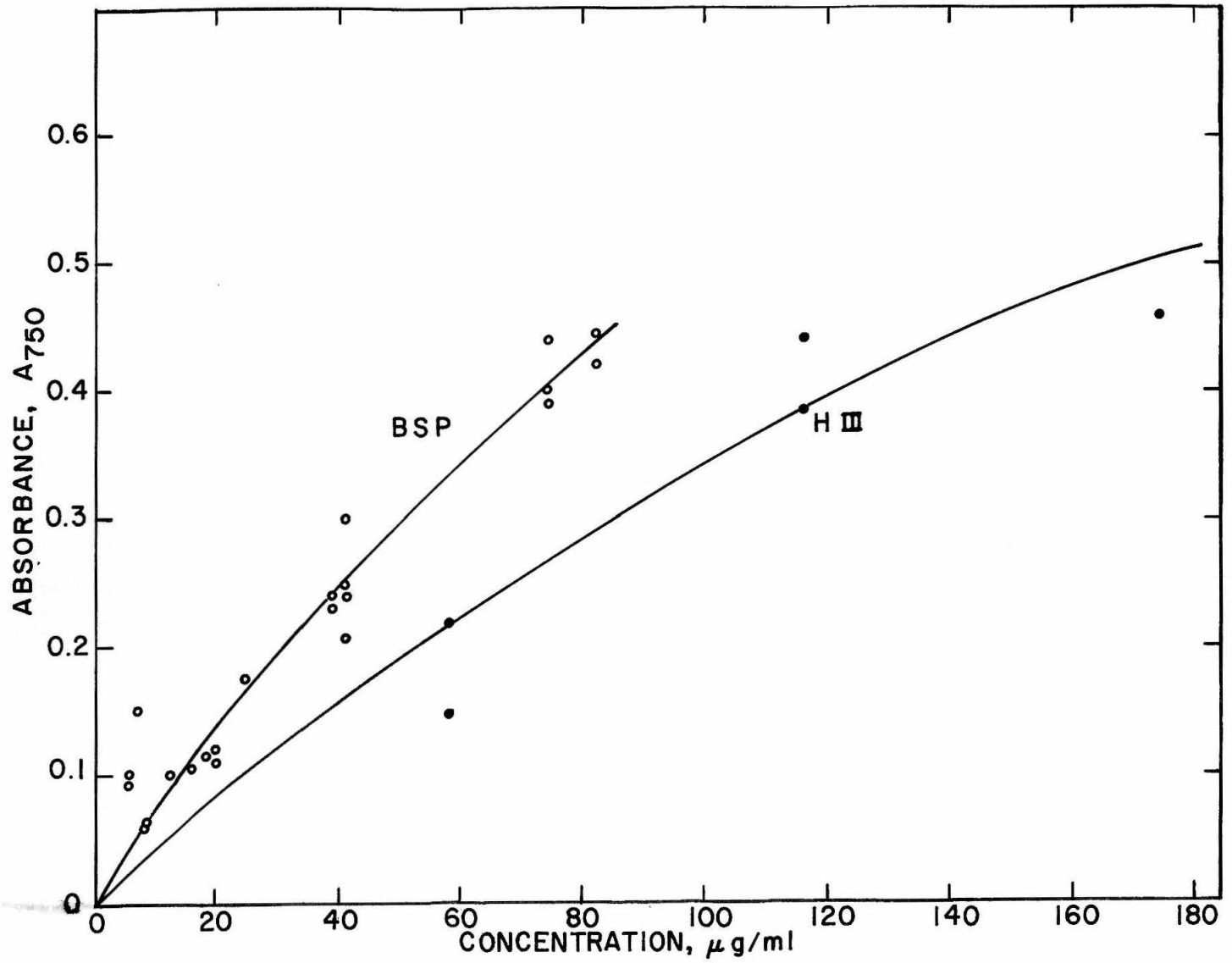
ABSORBANCE, A_{750}
0.6
0.5
0.4
0.3
0.2
0.1
0
BSP
H III
0
20
40
60
80
100
120
140
160
180
CONCENTRATION, μg/ml

Figure 13

figure 13. Here, the results of our analyses for bovine serum protein and histone III are presented in terms of the absorbance at 7500 Å corrected for H_2O due to the Lowry color reaction. The concentrations are based on the weight of vacuum dried protein. As can be seen, the sensitivity is only about the same as that of the UV analysis at 2200 Å (i. e. about 20 micrograms per ml), which is much easier to perform, so that this procedure had only limited value for our work.

b) Ninhydrin Procedure

The ninhydrin procedure of Moore and Stein (64) detects concentrations of amino acids down to 2 mM (about 240 micrograms per ml). However, we were able to develop a micro procedure, which could detect concentrations down to about 0.02 mM (2 micrograms per ml) as follows:

Moore and Stein Method	Micro Procedure
0.1 ml amino acid sample	0.1 ml amino acid sample
1.0 ml ninhydrin reagent	1 drop fresh $SnCl_2$ solution
	0.1 ml ninhydrin reagent
heat for 20 minutes	heat for 20 minutes
at 100° C.	at 100° C.
5.0 ml diluent	read A_{570} after ¼ hr.
read A_{570} after ¼ hr.	make sure sample is 0.2 ml.

Exact timing is desirable.

Ninhydrin reagent = 4.0 g ninhydrin per 100 ml methyl cellosolve plus 100 ml citrate buffer prepared by diluting 10.5 g citric acid, neutralized to pH 5.0 with NaOH, and 0.4 g $SnCl_2.2\ H_2O$ to 250 ml. The ninhydrin solution is flushed for 30 minutes with nitrogen and stored in the dark in a brown bottle.

Diluent = n-propanol diluted 1:1 with water.

Moore and Stein recommend that fresh ninhydrin solutions be used for the analysis. However, it was found that addition of a small drop of freshly prepared $SnCl_2$ solution (0.2 g/100 ml H_2O) to the sample in order to reduce any dissolved oxygen just before addition of the ninhydrin reagent, gave reproducible results even with 6 months old reagent.

In order to get reproducible results it is of utmost importance that the glass ware containing the samples is free of dust and other impurities and that contaminants are kept out during the heating period. The color reaction is indeed quite sensitive! Figure 14 shows the results of our analyses using arginine.HCl as the calibration substance. The absorbance maximum at 5700 Å of the colored dye, normalized to zero absorbance at 7000 Å and corrected for the absorbance of water is plotted against the millimolar concentration of arginine.HCl. Concentrations of 0.005 mM

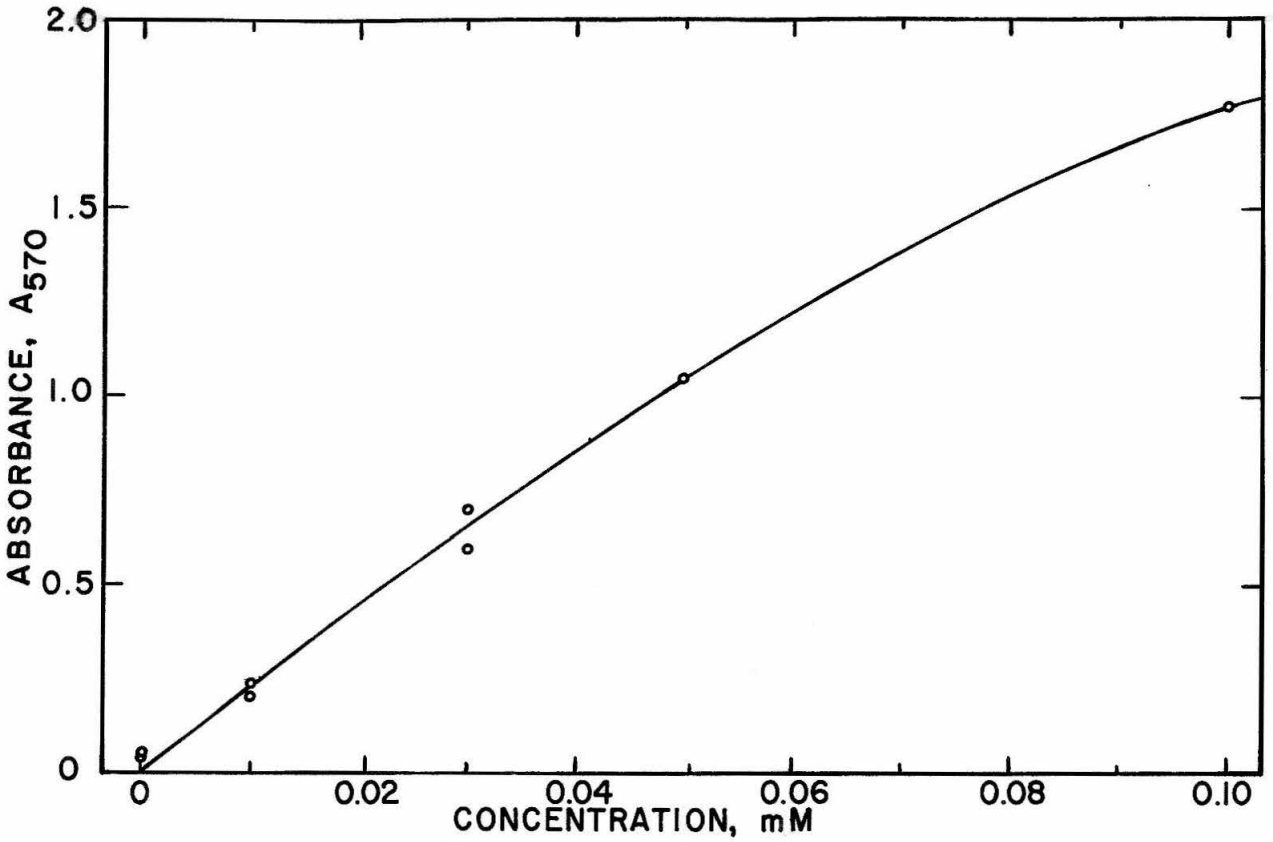

Figure 14

Detection of arginine by the micro ninhydrin procedure (see text). The absorbance maximum of the dye at 5700 Å was normalized to zero absorbance at 7000 Å and corrected for H_2O absorbance.

should still be detectable.

The most serious drawback of the procedure is that it requires that the proteins are hydrolyzed to amino acids for best results. In order to avoid the digestion of histones with concentrated HCl, we tested various undigested histone fractions for their sensitivity in the micro procedure. The results (Fig. 15 and 16) show considerable variation in the sensitivity of the reaction for the samples tested. The data are plotted as A_{570} versus concentration in micrograms per ml. Thus, an absorbance of 0.1 at 5700 Å would equal

26.6	micrograms	of	H Ib/ml
36.4	"	"	H IIb/ml
3.47	"	"	H III/ml
0.785	"	"	arg/ml

The sensitivity of the reaction for histones tended to increase with storage time of the solution, suggesting that enzymatic degradation may have been at work.

Although it is clear that the procedure is highly sensitive for the detection of amino acids like arginine, we have used it only for the qualitative determination of histones to verify the UV data and scans (see Fig. 11).

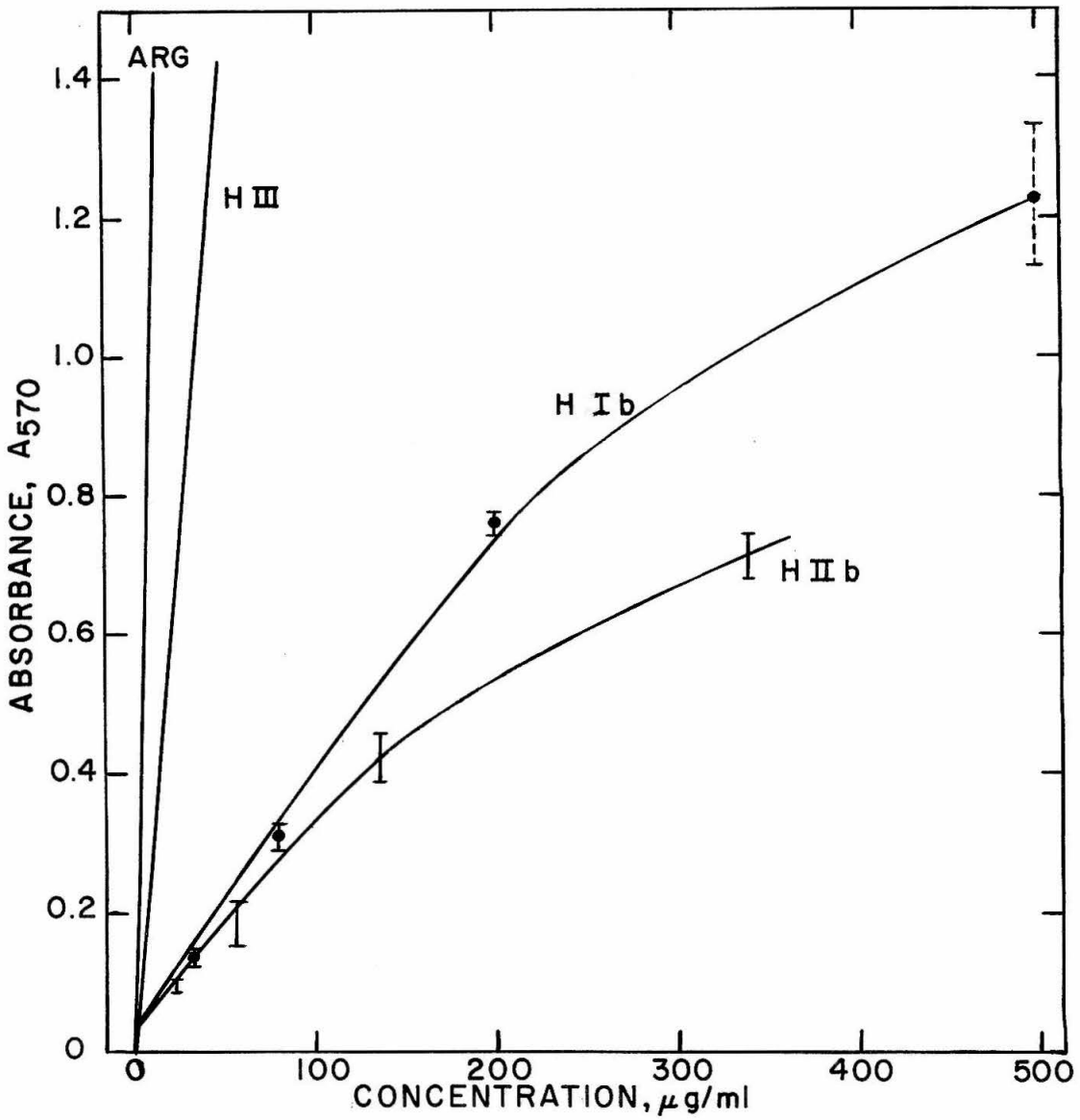

Figure 15

Detection of arginine and non-hydrolyzed histone fractions Ia, IIb, and III by the micro ninhydrin procedure (see text). The absorbance maximum of the dye at 5700 Å was normalized to zero absorbance at 7000 Å and corrected for H_2O absorbance. The vertical bars for H Ib and H IIb indicate the range of the measurements.

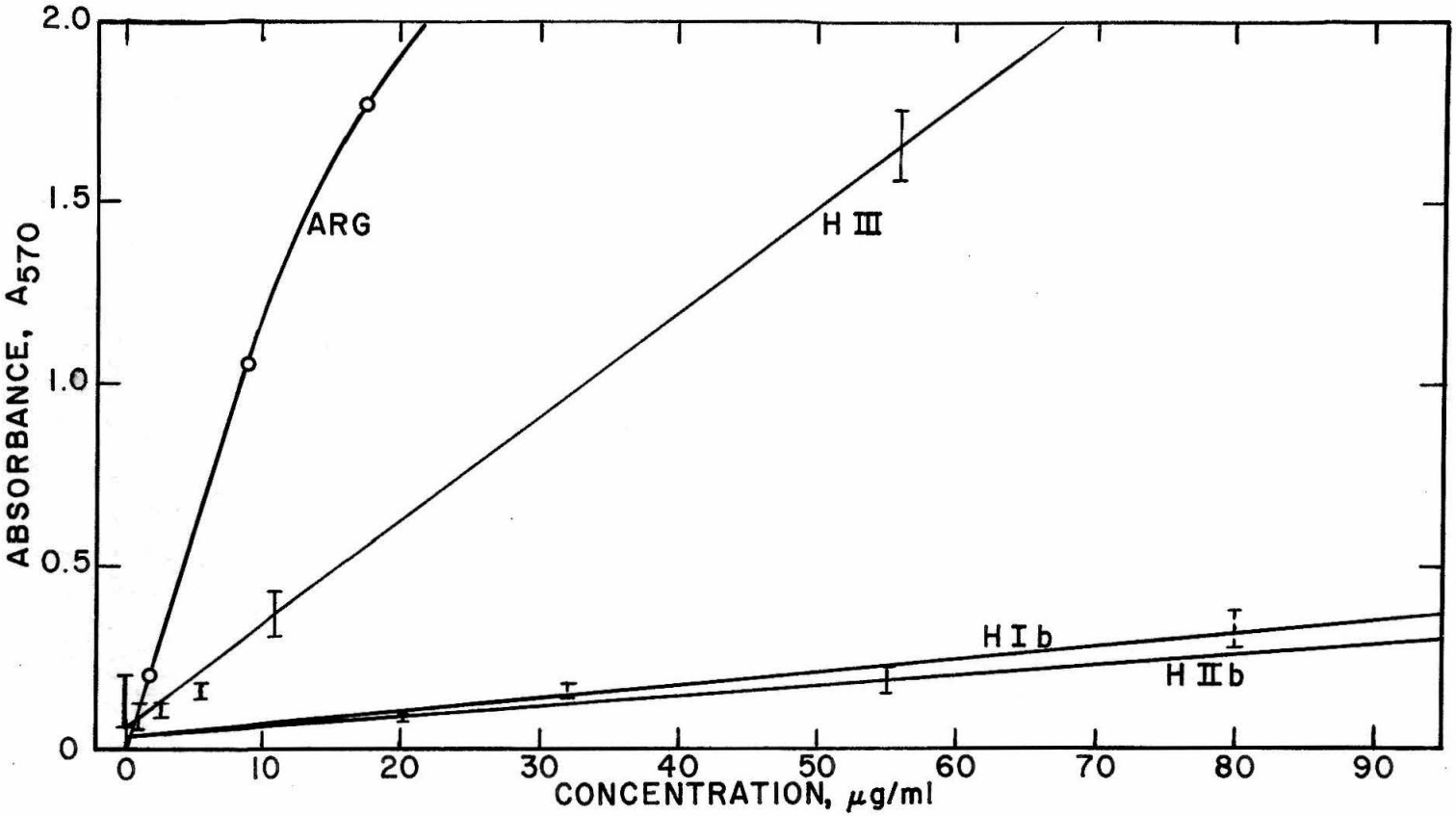

Figure 16

Same as figure 15 with an expanded concentration scale. Arginine data were replotted for comparison. Vertical bars for H III indicate the standard deviation of the measurements, those for H Ib and H IIb the range of the measurements.

7. Preparative Sedimentation

In order to obtain larger amounts of extracted histones we used zone sedimentation through layers of increasing concentrations of salt (salt layer sedimentation) and sedimentation of batches of uniform DNH - salt solutions (batch sedimentation) for preparative purposes. The advantage of the first procedure was that successive fractions of histones were extracted as the DNH sedimented from layer to layer. Its main disadvantage was that the amount of extractable material per experiment was limited, since the DNH concentration of the initial zone could not be too high in order to avoid excessive aggregation.

In the batch sedimentation procedure much larger quantities of DNH could be extracted, but the extracted material was not obtained as separate fractions. Successive extraction of the pellets by increasing salt concentrations was difficult because it was difficult to redissolve the pellets, especially after treatment with 0.2 to 0.3 F salt.

A. Salt Layer Sedimentation

In order to verify the scanning data and to determine the nature of the material extracted by $NaClO_4$ from native DNH, preparative experiments in 35 ml plastic sedimentation tubes were carried out. Solutions of decreasing density (D_2O or sucrose) and salt concentration were layered on top of one another in the following manner:

$NaClO_4$	0.001	DNH	0.2	0.3	0.4	0.5	0.6	2.0
% D_2O	0	0	25	40	60	80	90	100
ml	2.5	2.5	5.0	5.0	5.0	5.0	5.0	2.5

The sample layer (2.5 ml) containing not more than about 600 micrograms of DNA (A_{260} about 5) was carefully layered onto the D_2O-salt solutions and topped by a layer of solvent (generally 10^{-3} F $NaClO_4$).

After 18 to 25 hrs of sedimentation at 20 000 rpm in the SW 25 rotor, 1 ml fractions were pipetted off the top. Absorbancies were measured and attempts were made to determine the amino acid composition of the extracted histones using a micro amino acid technique developed by Prof. W. J. Dreyer (65) in which as little as 25 micrograms/ml of protein is sufficient for each analysis.

This salt layer sedimentation procedure gave results

which confirm those of the salt gradient sedimentation technique, but it is less elegant and can lead to errors in the estimation of the salt concentrations at which the DNH dissociates. The reason for these errors lies in the fact that the individual layers are not stabilized by density gradients and convection occurs throughout each layer. Thus, it is possible that material, which actually dissociated at the interphase of two layers does not remain there but distributes throughout the lower layer containing the higher salt concentration. The erroneous conclusion would be that the dissociation occurred in this higher salt concentration rather than in the intermediate, lower range.

However, judicious choice of the salt concentration of each layer will make this method useful for larger scale, selective dissociation of individual histone fractions.

B. Batch Sedimentation Experiments

The following procedure was used in order to prepare milligram quantities of extracted histones for characterization by Amberlite chromatography. Since we used fairly concentrated solutions throughout, we did not expect to recover the theoretical amounts of extracted histones and hoped only to recover enough material for a successful histone analysis.

For the sedimentation experiments we used 2.5 ml of fairly concentrated DNH solutions (A_{260} about 50 or somewhat more) which were diluted to 25 ml with the appropriate salt solutions. Since the salt concentration of the final solutions was 10 % lower than that added to the DNH, the results are listed in terms of these final salt concentrations.

The DNH-salt solutions at these concentrations were almost always cloudy before sedimentation indicating considerable aggregation of histones and/or DNH. No cloudiness remained after sedimentation in the SW 25 rotor for about 20 to 30 hrs at 20 000 rpm. The clear supernatants were fractionated (3 to 4 ml fractions) from the top and their UV spectra were taken. Those fractions containing little or no A_{260} were combined and exhaustively dialysed versus 1 F acetic acid to remove the salt. The dialysates were freeze dried and as much of the flaky, white residue as possible

was dissolved in 0.2 ml 8 % guanidinium chloride, buffered at pH 6.8 with 0.1 F phosphate buffer. Any undissolved material was centrifuged down in a clinical centrifuge and the clear supernatant applied to the Amberlite IRC-50 cation exchange column for identification.

For comparison, the salt extracted DNH pellets were treated with sulfuric acid (pH 0.7) to extract the remaining histones. They were precipitated from the sulfuric acid solution by the addition of excess ethanol in the cold. The white precipitate was washed with cold ethanol and dissolved in 0.2 ml 8 % guanidinium chloride (pH 6.8) and applied to the Amberlite column. Undissolved material was sedimented as before.

If it was desired to recover the partially dissociated nucleohistones from the pellets in their native state, it was advantageous to use a concentrated sucrose solution as the lowest layer during sedimentation. This layer prevented the extracted DNH from packing too tightly, making it easier to remove the material from the pellets by dissolving them in water or very low salt solutions.

8. Desalting of Histone Samples

Since we have encountered considerable difficulties in desalting our rather dilute histone solutions and had initially lost substantial quantities of material because of its easy adsorbability, it is worth-while to pass along some of the experience gained.

In exploring better desalting methods for histones, we were initially trying to find a procedure which did not involve the use of acidic solutions, for we hoped to compare non-acid treated, salt extracted histones with those extracted with mineral acids, using either zone electrophoresis or Amberlite chromatography. However, we were not able to desalt histones successfully without using acidic solutions.

a) Dialysis

Dialysis of a small histone sample versus water, which is the method of general choice for desalting of macromolecules, resulted in almost complete loss of material. For instance, in dialysing a one ml sample containing 12 to 37 micrograms of histones, more than 97 % of the material was lost. Only about 5 % was recovered from solutions containing 90 to 190 micrograms of histones per ml.

This loss was mainly due to the fact that most of the histones were adsorbed to the inside wall of the dialysis bags. They could be partially desorbed by HCl, indicating that they had not degraded or dialysed through the bag.

Finally, we dialysed the histone solutions against 1 F acetic acid which prevented extensive adsorption of the histones to the tube wall. The acetic acid and water could then be removed by freeze drying and the desalted histone residues used in Amberlite chromatography. Highest recovery, as measured after Amberlite fractionation, was about 67 %.

b) Acetone Precipitation

Our attempts to use acetone precipitation were also not very successful since appreciable amounts of salt co-precipitated, especially at higher salt concentrations. The procedure may eventually lend itself to quantitative separation of salt and histones, but more work must be done to determine the best conditions for quantitative precipitation of saltfree histones.

c) Sephadex Chromatography

Extensive work with a Sephadex column desalting procedure showed that small quantities of histones could not

be separated from salt by using water as the eluent. Figure 17 shows the elution diagrams in terms of A_{220} of histone IIb in 1 F NaCl from a 38 cm high Sephadex G-25 (66) column with 6.45 ml bed volume. Graph (a) illustrates that elution with distilled water of 75 micrograms of H IIb in 0.5 ml solvent does not result in desalting of the histone. Graph (b) shows partial desalting of an equal amount of H IIb if 10^{-3} F $HClO_4$ is used as the eluent. The complete desalting shown in graph (c) was accomplished by using 10^{-2} F $HClO_4$. Here the column was charged with 37.5 micrograms of H IIb in 0.25 ml 1 F NaCl solution. Further experiments with 0.1 F $HClO_4$ as the eluent indicated that the yield of salt free histones decreased with increasing initial amounts of H IIb. Thus, the recovery was 75 to 90 % for 37.5 micrograms of H IIb charge, but only about 5 % for 300 micrograms charge.

These results indicate once again that histones are rather difficult to work with and that extreme care must be exercised to avoid substantial losses in preparative experiments.

Figure 17

Desalting of histone IIb by Sephadex G-25 (coarse) chromatography. 1.355 g dry gel gave 6.45 ml bed volume; the column height was 38 cm.
a) 75 micrograms of H IIb in 0.5 ml 1.0 F NaCl eluted with distilled water gave no separation of histones from salt.

b) 75 micrograms of H IIb in 0.5 ml 1.0 F NaCl eluted with 0.001 F $HClO_4$ gave partial separation of histones and salt.

c) 37.5 micrograms of H IIb in 0.25 ml 1.0 F NaCl eluted with 0.01 F $HClO_4$ gave complete separation of histones and salt. The histone peak is at the position at which material not entering the gel pores should be. NaCl is at the position expected for material entering the pore volume.

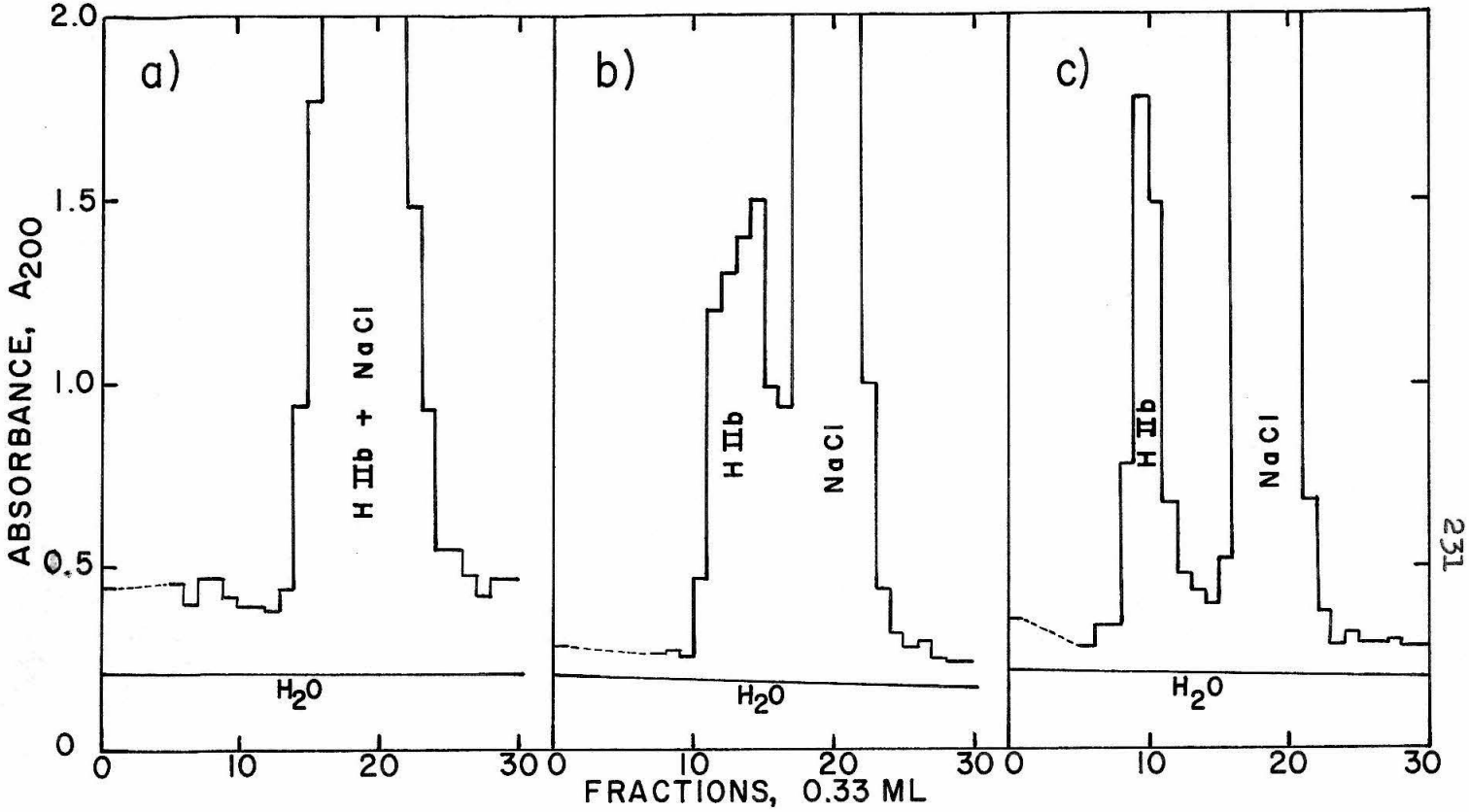
a)
b)
c)
ABSORBANCE, A_{200}
2.0
1.5
1.0
0.5
0
H IIb + NaCl
H IIb
NaCl
H_2O
0
10
20
30
FRACTIONS, 0.33 ML

Figure 17

9. Amberlite IRC-50 Cation Exchange Chromatography

The Amberlite chromatography fractionation procedure for histones is described in detail by Murray (26). The development of a microprocedure requiring as little as 1 mg of histones per experiment is the result of work done by Mr. D. Fambrough, Jr., in Prof. J. Bonner's laboratory. A brief description of the procedure follows:

The column (57 x 0.67 cm diameter) was carefully packed with thoroughly cleaned Amberlite IRC-50 resin. The histone sample was dissolved in 0.2 ml 8 % guanidinium chloride (GuCl) (all GuCl solutions were buffered at pH 6.8 with 0.1 F phosphate buffer) and applied to the column using 0.3 ml 8 % GuCl as wash. The column was then connected to a reservoir containing 15 ml of the 8 % GuCl and a magnetic stirrer. This reservoir was in turn connected to a second vessel containing 19 ml 10.5 % GuCl. All connections were airtight so that the solutions syphoned into the column as the eluent was collected in 0.3 ml fractions by an automatic fraction collector.

After the 19 ml of reservoir 2 were used up, 25 ml 13 % GuCl were added to it. After these had syphoned into flask 1, all flasks were disconnected and replaced by a flask containing 10 ml of 40 % GuCl. Finally, the column was regenerated for the next experiment by flushing it with

15 to 20 ml 8 % GuCl. Each experiment, requiring about 220 fractions, took about 20 hours.

The histone concentration of the effluent was determined by measuring the optical density at 4000 Å (A_{400}^{TCA}) of the turbid solution resulting when effluent, distilled water, and 3.3 F trichloroacetic acid (TCA) were mixed in the ratio of 1:3:2. The calibration for estimating the amount of histones in the effluent (0.765 mg H/ml for A_{400} = 1) was performed by Mr. D. Fambrough.

10. DNA-Dependent RNA Synthesis

The following describes the procedure used by Dr. R. C. Huang for the determination of the RNA-priming activity of a number of partially salt extracted calf thymus nucleohistone samples (67).

The assay and incubation mixture consisted of the following ingredients:

0.02 ml 1.0 M tris buffer (pH 8)

0.04 ml 0.0125 M $MnCl_2$

0.04 ml 0.05 M $MgCl_2$

0.04 ml 5 micromoles each of three NTP's per ml

0.02 ml ATP.C^{14}, 10 microcurie/ml; 1 microcurie/micromole

0.06 ml 0.1 M beta-mercaptoethanol

0.02 ml (or 0.01 ml) RNA polymerase, $A_{280}/A_{260} = 1.5$

0.25 ml primer DNA or DNH in 0.016 M saline citrate.

0.49 ml

The solution is kept for 10 minutes at 35° C. The reaction is stopped by adding TCA and the resulting precipitate is washed on a millipore filter with 6 times 5 ml cold 10 % TCA. The radioactivity in counts per minute (cpm) incorporated into the precipitate as macromolecular RNA is a measure of the RNA-priming activity of the DNH.

IV. Discussion of the Results From Salt Gradient Sedimentation

1. General Considerations

Most of the conclusive evidence for selective dissociation of histones from nucleohistones comes from the preparative experiments (Section V). However, the results of the salt gradient sedimentations have been useful in determining the salt concentrations and ranges at which the individual histone fractions dissociate.

In the following the results of the salt gradient sedimentations of the individual samples of reconstituted and of native DNH are described in detail. They show that DNH I dissociated at less than 0.2 F $NaClO_4$, DNH IIb at 0.45 F $NaClO_4$ and DNH III and IV at concentrations above 0.5 F. In native DNH the dissociation is a combination of that of the individual histone fractions.

The results using salt gradient sedimentation are at present mainly of qualitative interest; however, the method is promising for the quantitative analysis of the dissociation. We have presented the quantitative results in detail to show the feasibility as well as the difficulty of obtaining meaningful data.

The mass balance from the scans for DNA is generally quite satisfactory if pelletting is avoided, but the mass balance for histones is more often than not too high. This is particularly the case, if the dissociation is gradual, so that no distinct histone bands are formed in the salt gradients.

2. Reconstituted Calf Thymus Nucleohistone I

Two freshly prepared DNH I samples, which varied in their R_{220} ratios were investigated. Quartz tube scans after sedimentation of DNH I zones are shown in figures 18 to 20. The direction of sedimentation is from left to right in all of these tracings. The position of the initial layer is indicated below the meniscus from which it is separated by a layer of solvent. The density gradients were 25 to 100 % D_2O.

The DNH sample sedimented in the tube whose scans are shown in figure 18 had an R_{220} of 1.18. Sedimentation through the salt gradient, which varied from 0 to 0.25 F $NaClO_4$, resulted in the gradual removal of the histone; no histone band is observed. The band near the bottom of the tube is due to the extracted DNA and its maximum has a sedimentation coefficient of 16.2 S.

Figure 19 shows the same material after sedimentation through a 0.2 to 0.6 F $NaClO_4$ gradient. Here the histone has come off at the initial zone position in a broad band. The maximum of the DNA band near the tube bottom has a sedimentation coefficient of 14.7 to 15.0 S.

Figure 20 shows the results of sedimenting a DNH I sample having an R_{220} of 0.69 through a salt gradient varying from 0 to 0.2 F $NaClO_4$. The dissociation is gradual,

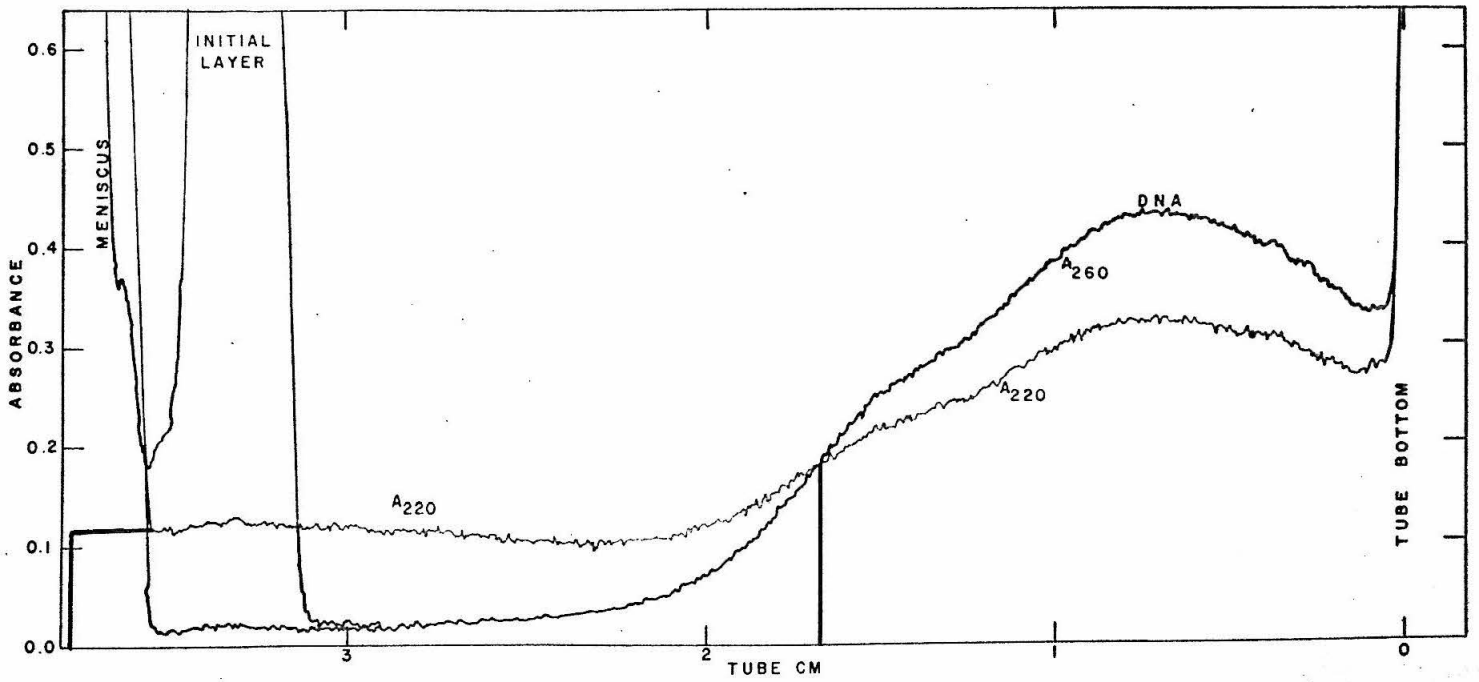

Figure 18

Quartz tube scans before and after sedimentation of a zone of reconstituted calf thymus DNH I (R_{220} = 1.18, 1 day old) through a 0 to 0.25 F $NaClO_4$ gradient in D_2O. The histone is gradually removed in the top half of the tube (area as outlined, corrected for DNA absorbance, corresponds to 112.5 % of the initial A^H_{220}). The band near the tube bottom is extracted DNA; its maximum has a sedimentation coefficient of 16.2 S.

Figure 19

Quartz tube scans before and after sedimentation of a zone of reconstituted calf thymus DNH I ($R_{220} = 1.18$, 0 days old) through a 0.2 to 0.6 F $NaClO_4$ gradient in D_2O. The histone has come off at the initial zone position (area as outlined, corrected for DNA absorbance, corresponds to 118.7 % of the initial A^H_{220}). The band near the tube bottom is extracted DNA; its maximum has a sedimentation coefficient of 14.7 to 15.0 S.

Figure 19

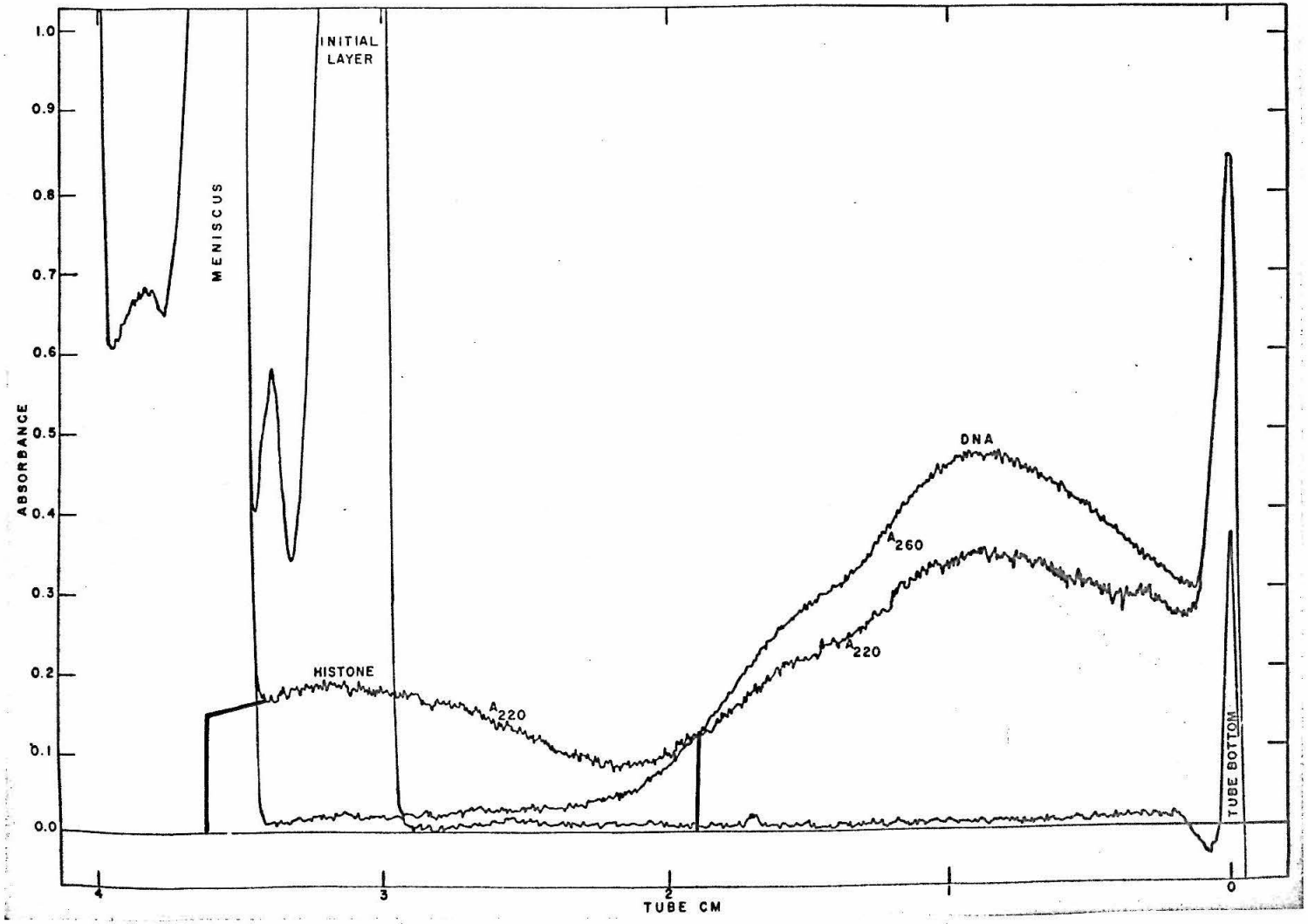
INITIAL LAYER
MENISCUS
ABSORBANCE
1.0
0.9
0.8
0.7
0.6
0.5
0.4
0.3
0.2
0.1
0.0
DNA
A_{260}
A_{220}
HISTONE
A_{220}
TUBE BOTTOM
4
3
2
0
TUBE CM

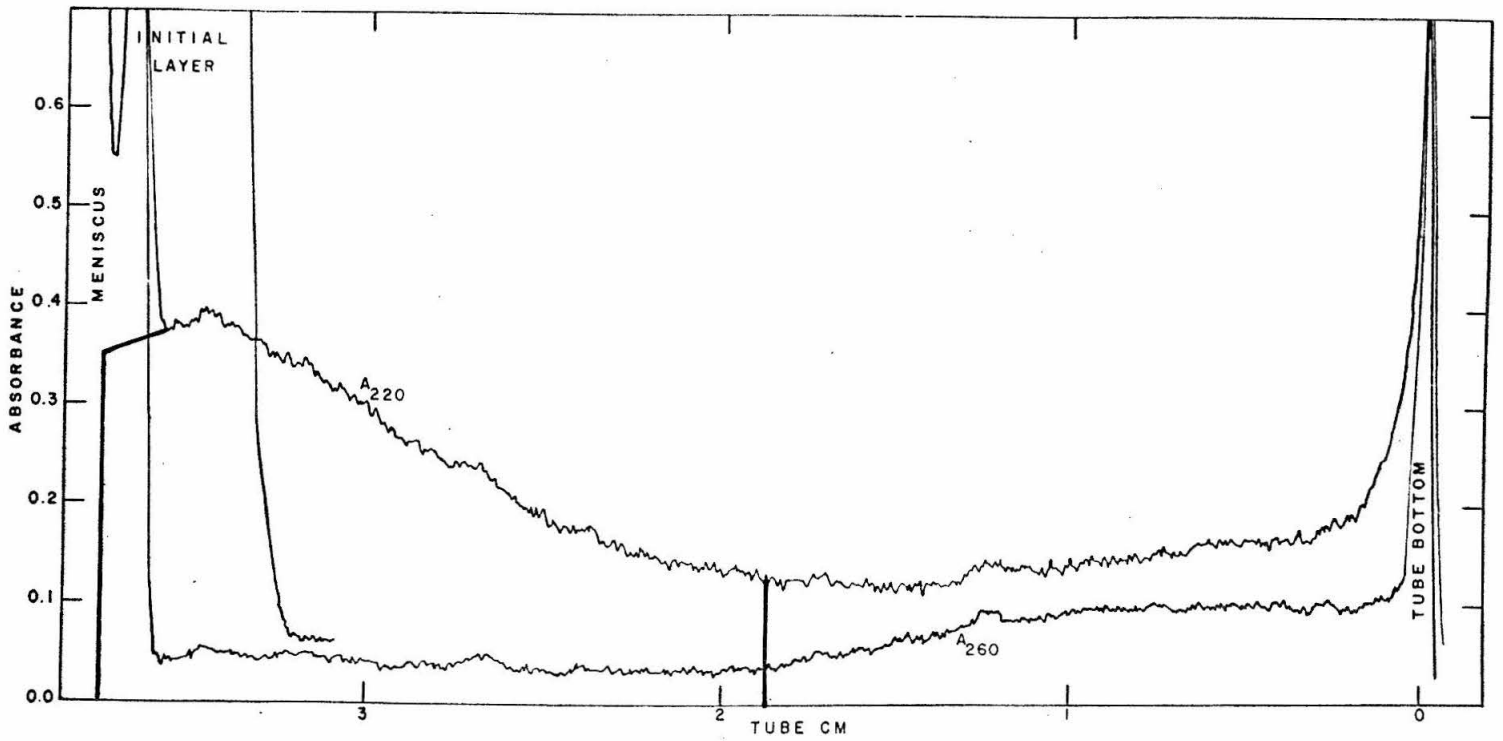

Figure 20

Quartz tube scans before and after sedimentation of a zone of reconstituted calf thymus DNH I (R_{220} = 0.69; 2 days old) through a 0 to 0.2 F $NaClO_4$ gradient in D_2O. A considerable amount of histone I (area as outlined, corrected for DNA absorbance, corresponds to 86.5 % of the initial A^H_{220}) remained at the initial zone position, probably because of the excessive histone coverage. Most of the DNA is pelletted at the tube bottom.

but a considerable amount of histone I had remained at the initial position indicating that the complex was not very tightly bound, probably because of the excessive histone coverage. Most of the DNA had pelletted during this run.

The quantitative analysis of the scans is summarized in table Va. The symbols are explained on the opposite page. Line k gives the "recovery" of the DNA in terms of its A_{260} and shows that it is essentially complete in those cases where extensive pelletting was avoided. The histone recovery (Line q) is always too high, which is probably due to the presence of UV impurities. The data suggest nevertheless, that the bulk of the histones are present as the dissociated, non-sedimenting material at the top of the tube (Line r).

The significant result of these scans is that the amount of histones which dissociated as a band at the top of the high salt gradients is approximately equal to the amount of histones which were more gradually removed in the upper portion of the tubes containing the low salt gradients. Thus, histone I dissociated below 0.2 F $NaClO_4$ from reconstituted DNH I.

The UV analyses of the solutions after fractionation from the top and the redissolved pellets confirm the results: The DNA recovery is nearly quantitative (Table Vb, Line k), but the amount of histones recovered from the upper part of the tubes is again too high (Line r) due to UV impurities.

Explanation of Symbols

Sample: Sample number

F $NaClO_4$: initial and final formal concentration of the $NaClO_4$ gradient superimposed on the D_2O gradient

days old: number of days after preparation of the DNH

S: sedimentation coefficient in Svedberg units

F of pk: formality of $NaClO_4$ at the center of the H peak

A_{260} init: absorption at 2600 Å of the sample in the initial zone corrected for blank and A_{400}

A_{220} init: ditto for 2200 Å

R_{220}: ratio of A_{260} to A_{220} of the initial sample

A_{400} init: Absorption at 4000 Å if more than 5 % of A_{260}

H/D: see figure 3

% A_{260}rec: % of the initial A_{260} recovered after experiment

% not sed: % of the initial material not sedimented

% banded: % of the initial material found in a band

% in H bd: % of the initial A_{260} found in a histone band

% in pel: % of the initial material found in the pellet

% A^{NH}_{220}rec: % of the initial A_{220} recovered after experiment

% A^{H}_{220}rec: % of the initial absorption at 2200 Å due to histones only (A^{H}_{220} is corrected for H_2O blank and A_{400} and for the DNA by using R_{220} = 1.50), recovered after sedimentation

% in DNA: % of initial histone found in the DNA band

R^{A}_{220}: ratio of the area under the A_{260} peak to the area under the corresponding A_{220} peak

Table Va

Reconstituted Calf Thymus Nucleohistone I

a) Sample	2	1	1	2
b) F $NaClO_4$	0.0-0.2	0.0-0.25	0.2-0.6	0.2-0.8
c) days old	2	1	0	0
d) S	-	16.2	14.7-15.0	-
e) F of pk	-	-	-	-
f) A_{260} init	2.253	3.31	3.31	2.253
g) A_{220} init	3.268	2.81	2.81	3.268
h) R_{220}	0.689	1.18	1.18	0.689
i) H/D	1.60	0.37	0.37	1.60
j) A_{400} init	0.465	0.102	0.102	0.465
k) % A_{260}rec	38.3	93.3	90.95	67.9
l) % not sed	10.3	9.25	5.45	21.55
m) % banded	-	68.5	72.7	-
n) % in H bd	-	-	-	-
o) % in pel	?	15.55	12.8	?
p) % A^{NH}_{220}rec	83.5	109.3	106.0	88.2
q) % A^{H}_{220}rec	121.3	163.5	156.5	105.2
r) % not sed	86.5	112.5	118.7	78.4
s) % banded	-	-	-	-
t) % in DNA	-	43.0	33.4	-
u) % in pel	?	7.95	4.4	?
v) R^{A}_{220}	-	1.28	1.33	-

Table Vb

UV of Fractions of Reconstituted Calf Thymus Nucleohistone

a) Sample	2	2
b) F $NaClO_4$	0.0-0.2	0.2-0.8
c) days old	2	0
d) S	-	-
e) F of pk	-	-
f) A_{260} init	2.253	2.253
g) A_{220} init	3.268	3.268
h) R_{220}	0.689	0.689
i) H/D	1.60	1.60
j) A_{400}	0.465	0.465
k) % A_{260}rec	89.35	93.5
l) % not sed	31.85	31.5
m) % banded	?	?
n) % in H bd	-	-
o) % in pel	57.5	62.0
p) % A^{NH}_{220}	116.0	126.9
q) % A^{H}_{220}	138.15	154.7
r) % not sed	117.2	132.5
s) % banded	-	-
t) % in DNA	-	-
u) % in pel	20.95	22.2
v) R^{max}_{220}	1.04	1.06

3. Reconstituted Calf Thymus Nucleohistone IIb

The dissociation behavior of reconstituted DNH IIb (R_{220} = 1.0) was esthetically the most pleasing in that a rather sharp band of histones was observed in salt gradients from 0.4 to 0.6 F $NaClO_4$ (Fig. 11). The histone band was reproducibly centered around 0.450 ± 0.005 F $NaClO_4$ if the density gradient was D_2O. The width of the band at its base was about 0.12 F $NaClO_4$.

In a sucrose density gradient (5 to 20 %) the dissociation of freshly prepared DNH IIb occurred at a higher salt concentration (0.535 F $NaClO_4$). This result may be due to the effect of the change in dielectric constant of the medium on the free energy of association, but more extensive studies are required to establish this point.

Below 0.4 F $NaClO_4$ we did not observe any histone bands. Figures 21 and 22 illustrate the behavior of DNH IIb in D_2O density gradients containing uniform $NaClO_4$ concentrations of 0.2 F. Figure 21 shows A_{260} and A_{220} scans after most of the A_{260} material had sedimented to the tube bottom. The total area under the curves as shown presents 18.3 % of the initial A_{260} and 120 % of the initial A^{H}_{220} in the zone. Because of the flatness of the curves these results would be considerably influenced by small changes in

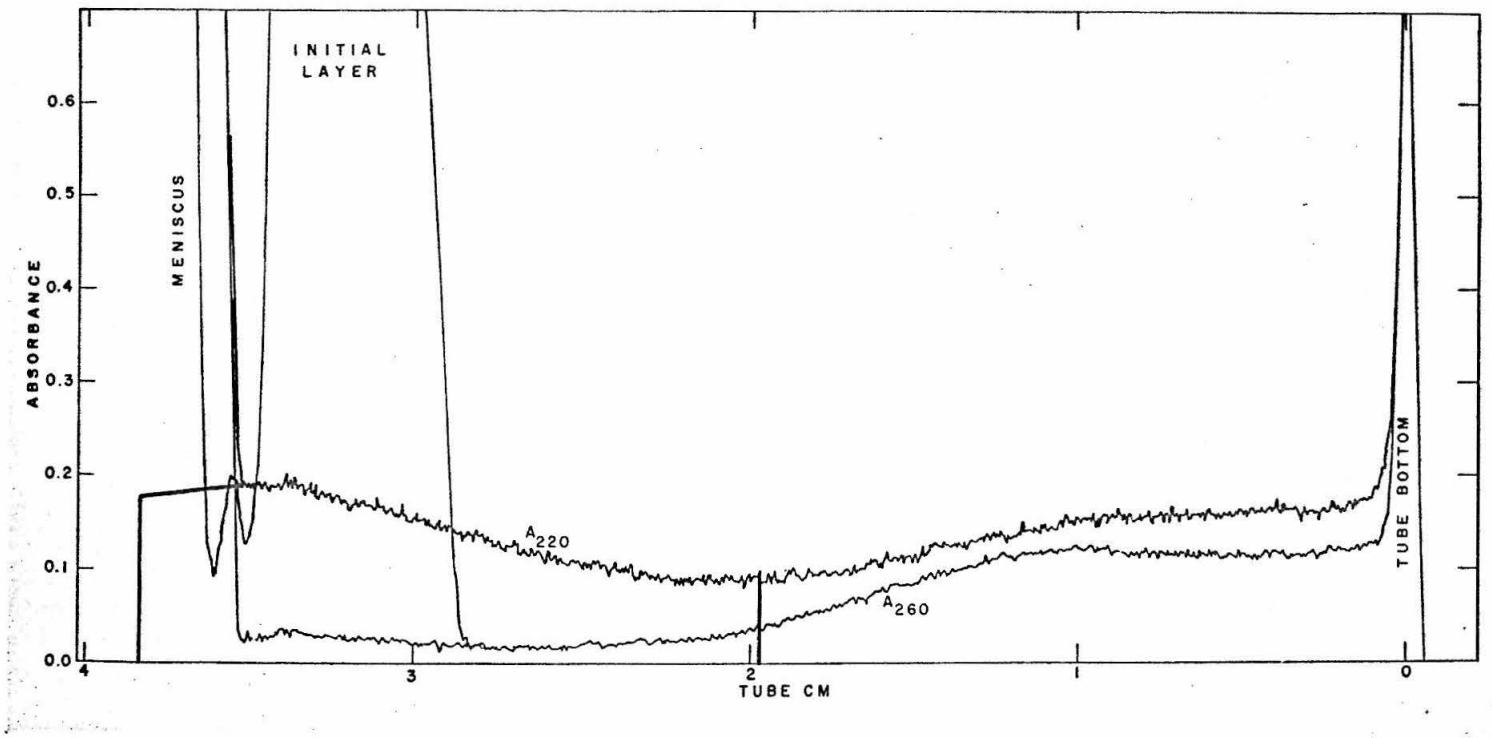

Figure 21

Quartz tube scans before and after sedimentation of a zone of reconstituted calf thymus DNH IIb (R_{220} = 1.0) through a uniform 0.2 F $NaClO_4$ concentration in D_2O. No histone peak is formed. The amount of H IIb in the upper part of the tube (area as outlined, corrected for DNA absorbance, corresponds to 67.6 % of the initial A^H_{220}) is probably exaggerated due to an uncertain baseline. It represents dissociated H IIb due to storage of the solution for 27 days at 4 °C. Most of the DNA is pelletted at the tube bottom.

the baseline. It should be pointed out that no distinct band of A^{H}_{220} material remained behind at the initial position even though the DNH preparation had been stored for 27 days at 4° C. This is in striking contrast to the changes observed on storage of DNH III solutions.

Figure 22 depicts the same DNH IIb preparation after 47 days of standing and this time 21.4 % A^{H}_{220} remained at the initial position. In order to illustrate the band of DNH IIb, this run was terminated after only 6 hours including 23 minutes of acceleration to, and 44 minutes deceleration from 20 000 rpm. Only one band is observed in both the A_{260} and the A_{220} scans and its maximum has a sedimentation coefficient of about 19 S. This is rather low for a completely complexed DNH sample and confirms partial degradation. Also the R^{A}_{220} calculated from the area under the peaks is 1.37 rather than 1.0 as measured for the initial material.

The same figure illustrates further the amount of spreading which occurs during the sedimentation of DNH alone. Since the diffusion coefficient for DNH is rather small (approximately 10^{-8} cm^2/sec (68)), the spreading of the band must be due to molecular weight heterogeneity and s on c effects (69).

Figure 22

Same DNH IIb preparation as figure 21 after 47 days of storage at 4° C. The amount of H IIb in the upper part of the tube is due to degradation (area as outlined, corrected for DNA absorbance, corresponds to 21.4 % of the initial A^{H}_{220}, but the baseline is probably too high). The broad band at the tube center is undissociated DNH IIb; its maximum has a sedimentation coefficient of 19 S. The R^{A}_{220} of the areas under the peak is 1.37. Both, the low S and the high R^{A}_{220} indicate that degradation of the DNH IIb has occurred during storage (compare with Fig. 25).

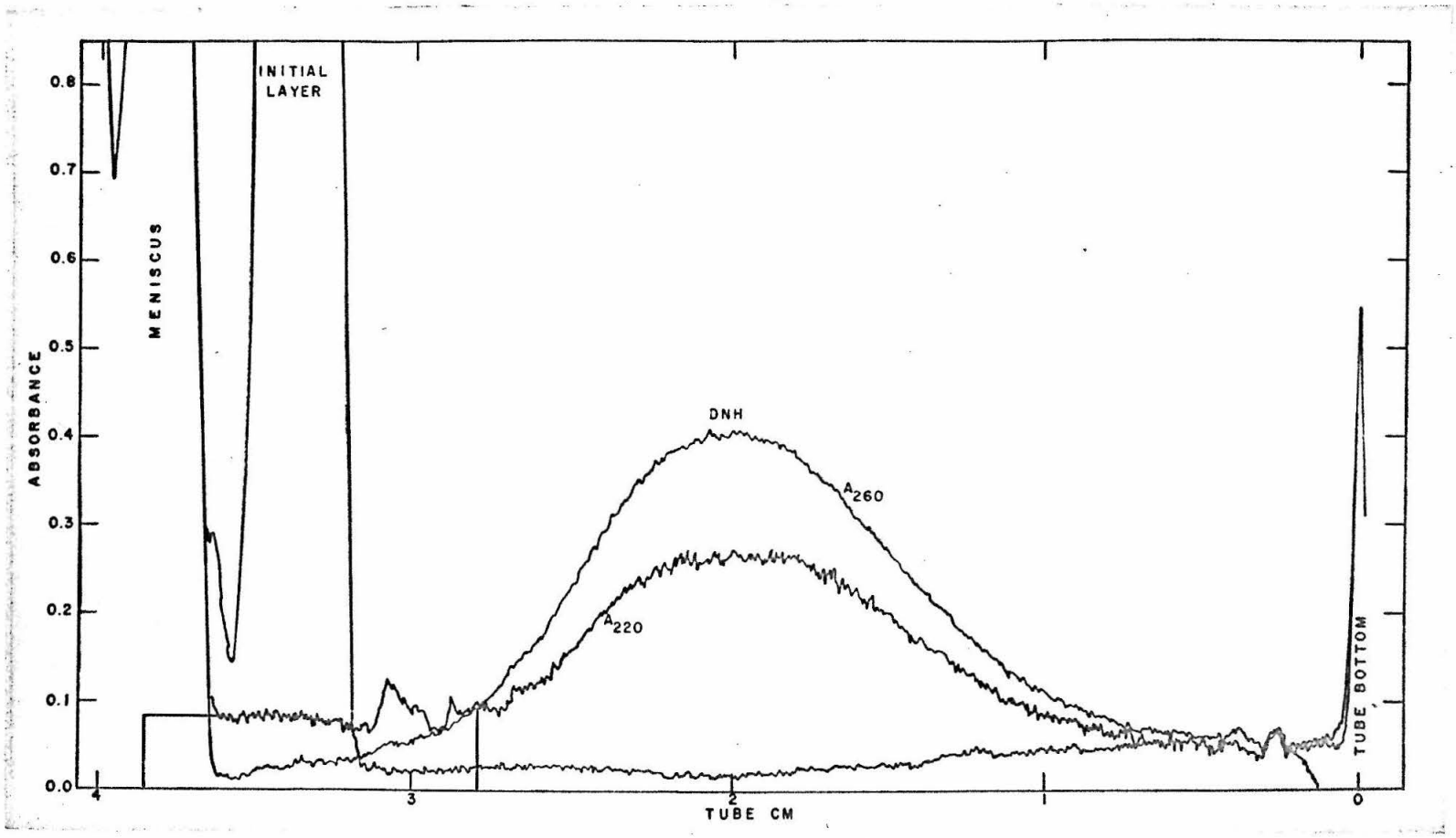
INITIAL
LAYER
MENISCUS
ABSORBANCE
0.8
0.7
0.6
0.5
0.4
0.3
0.2
0.1
0.0
DNH
A260
A220
TUBE BOTTOM
4
3
2
1
0
TUBE CM

Figure 22

When DNH IIb zones were layered on top of gradients of 0.6 F $NaClO_4$ or higher, sharp bands of H IIb were always found at the interphase of zone and gradient.

A summary of the quantitative analyses of the dissociation of DNH IIb is shown in tables VI to VIII. The data are listed in the same form as those of table V and the symbols are explained on page 243. As with DNH Ib, DNA recovery in terms of A_{260} (Line k) was close to quantitative in runs where pelletting was avoided. Recovery of histone IIb (Line q) was almost quantitative in those runs in which the salt concentration of the D_2O gradient exceeded 0.5 F and most of the recovered histone was present in a characteristic band (Line s), indicating that dissociating was sharp and essentially complete.

In contrast, those runs with gradients containing uniform $NaClO_4$ concentrations of 0.2 F and even 0.4 F showed no histone bands and gave only about 30 % recovery of initial histones in the solution above the pellet (Line q). Most of this material was found in the upper part of the tubes (Line r) and may be due to slight degradation of the DNH on standing for periods of 16 to 47 days (Line c). A run with freshly prepared DNH IIb in 0.4 F $NaClO_4$ did not show any analyzable material in the scans and the DNH must all have sedimented to the tube bottom.

Table VI

Reconstituted Calf Thymus Nucleohistone IIb

Sucrose Density Gradients

a) Sample	3	3	3	3	3
b) F $NaClO_4$	0.4	0.4-0.6	0.4-0.8	0.6	0.8
c) days old	16	16	0	16	0
d) S	-	70	39	9.9	13.0
e) F of pk	-	0.484	0.535	-	-
f) A_{260} init	1.86	1.86	1.258	1.86	1.258
g) A_{220} init	2.27	2.27	1.536	2.27	1.536
h) R_{220}	0.817	0.817	0.816	0.817	0.816
i) H/D	1.12	1.12	1.12	1.12	1.12
j) A_{400} init	-	-	0.074	-	0.074
k) % A_{260}rec	61.5	98.9	54.8	92.45	104.3
l) % not sed	10.7	8.2	-	-	-
m) % banded	50.8	48.2	54.8	81.0	97.1
n) % in H bd	-	27.7	-	7.45	7.2
o) % in pel	?	14.8	-	4.0	-
p) % A^{NH}_{220}	47.7	77.5	51.0	46.7	48.6
q) % A^{H}_{220}	31.2	56.1	68.5	?	?
r) % not sed	27.5	17.6	24.6	-	-
s) % banded	0	37.8	43.9	29.8	43.6
t) % in DNA	3.9	0.7	-	neg.	neg.
u) % in pel	?	-	-	neg.	neg.
v) R^{A}_{220}	1.06	1.49	2.28	3.21	2.71

Table VII

Reconstituted Calf Thymus Nucleohistone IIb

a) Sample	4	4	4	4
b) F $NaClO_4$	0.2	0.2	0.4-0.5	0.4-0.6
c) days old	27	47	47	0
d) S	-	18.5_{DNH}	17.7_{DNA}	22.5_{DNH}
e) F of pk	-	-	(0.402)	0.450
f) A_{260} init	3.560	3.512	3.512	3.15
g) A_{220} init	3.627	3.52	3.52	3.15
h) R_{220}	0.980	0.996	0.996	1.00
i) H/D	0.713	0.683	0.683	0.679
j) A_{400} init	-	-	-	-
k) % A_{260}rec	18.3	60.2	95.0	88.7
l) % not sed	2.8	3.8	-	-
m) % banded	15.5	56.4	-	67.1
n) % in H bd	-	-	-	6.88
o) % in pel	?	-	-	14.7
p) % A^{NH}_{220}rec	21.6	50.3	93.4	102.6
q) % A^{H}_{220}rec	27.5	31.0	90.5	130.5
r) % not sed	26.8	21.4	-	-
s) % banded	-	-	-	122.0
t) % in DNA	0.7	9.6	-	6.0
u) % in pel	?	-	-	1.9
v) R^{A}_{220}	1.47	1.37	-	1.445

Table VII

Reconstituted Calf Thymus Nucleohistone IIb

a) Sample	4	4	4	4
b) F $NaClO_4$	0.4-0.6	0.4-0.6	0.6	0.6
c) days old	27	47	0	27
d) S	22.0_{DNH}	13.0_{DNA}	15.0_{DNA}	14.1_{DNA}
e) F of pk	0.448	0.452	-	-
f) A_{260} init	3.560	3.512	3.15	2.965
g) A_{220} init	3.627	3.52	3.15	3.02
h) R_{220}	0.980	0.996	1.00	0.982
i) H/D	0.713	0.683	0.679	0.714
j) A_{400} init	-	-	-	-
k) % A_{260}rec	81.0	98.8	87.1	87.75
l) % not sed	-	-	-	-
m) % banded	65.4	-	73.4	74.6
n) % in H bd	5.1	-	4.0	5.7
o) % in pel	10.5	-	9.7	7.45
p) % A^{NH}_{220}rec	88.5	96.1	113.0	95.16
q) % A^{H}_{220}rec	103.5	90.8	163.4	109.45
r) % not sed	-	-	-	-
s) % banded	107.3	-	144.0	98.25
t) % in DNA	-2.8	-	17.7	8.25
u) % in pel	-1.0	-	1.7	2.95
v) R^{A}_{220}	1.565	-	1.62	1.43

In summary, we feel that the results of the nucleohistone IIb dissociation illustrate best the potential applicability of the salt gradient experiments in quartz tubes and the kinds and accuracy of information obtainable at present.

4. Reconstituted Calf Thymus Nucleohistones III and IV

The results with DNH III and DNH IV are rather incomplete and not very conclusive. This is partially due to the difficulty of preparing good samples of reconstituted DNH III and IV because these histones aggregate very easily, and partially due to the degradability of these nucleohistones during storage.

Three preparations of DNH III (R_{220} = 0.835, 0.725, 0.822) and one of DNH IV (R_{220} = 0.725) were studied. The first sample was prepared by dissolving lyophilyzed DNH III in 10^{-3} F $NaClO_4$, the others were freshly reconstituted samples.

The dissociation behavior of these materials seemed at first most erratic. At times the complex would dissociate below 0.2 F salt, at times not below 0.6 F. This behavior was found to be due to aging of the DNH III in solution. Freshly reconstituted material dissociated above 0.6 F $NaClO_4$ in a rather gradual manner, while storage of the solution for a few days at 4° C gave progressively larger amounts of non-sedimenting histone III at the initial zone position.

Figures 23 to 25 illustrate this situation. The first figure presents the A_{260} and A_{220} scans of a very fresh DNH III sample (R_{220} = 0.725) sedimented immediately after

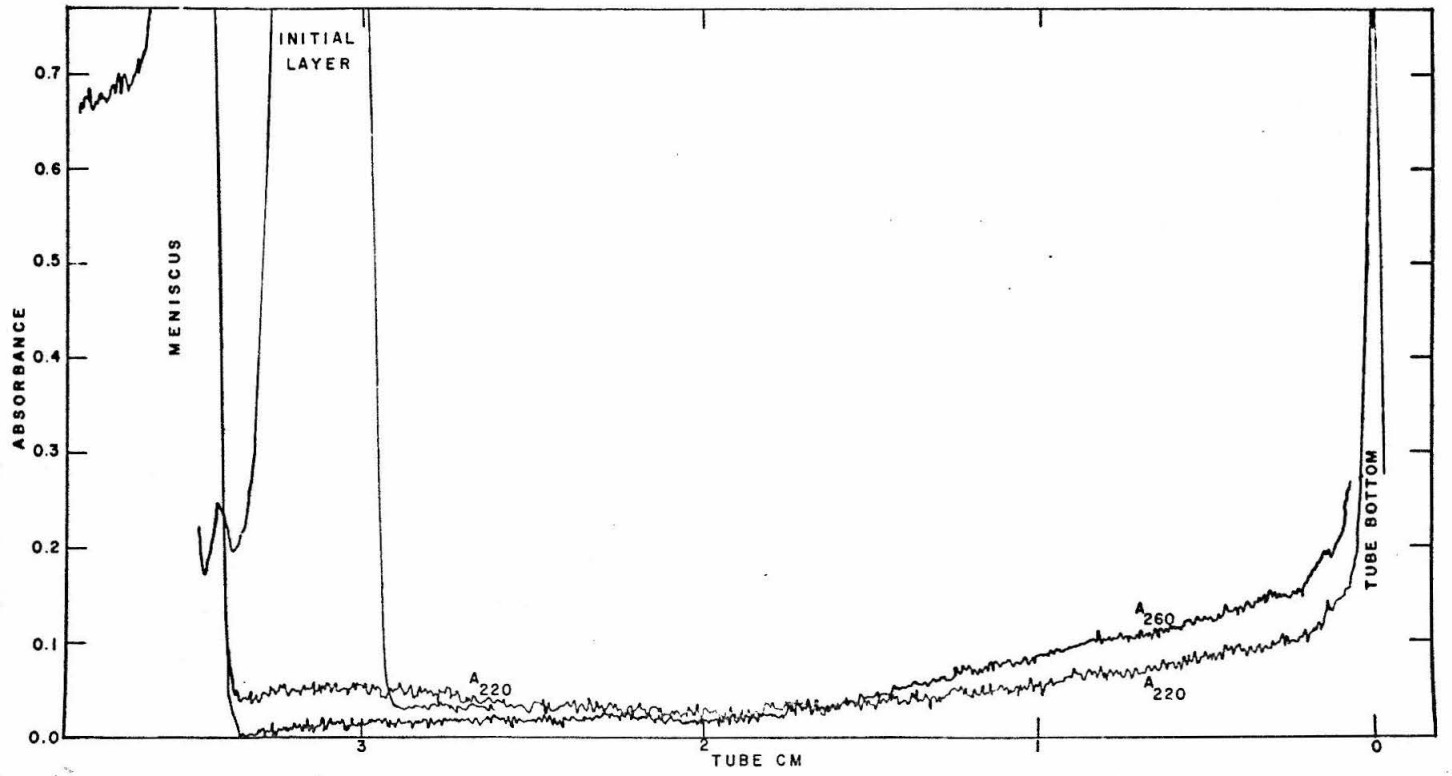

Figure 23

Quartz tube scans before and after sedimentation of a zone of freshly reconstituted calf thymus DNH III (R_{220} = 0.725; 0 days old) through a 0 to 0.2 F $NaClO_4$ gradient in D_2O. Only negligible amounts of H III were extracted. Most of the DNH is pelletted at the tube bottom.

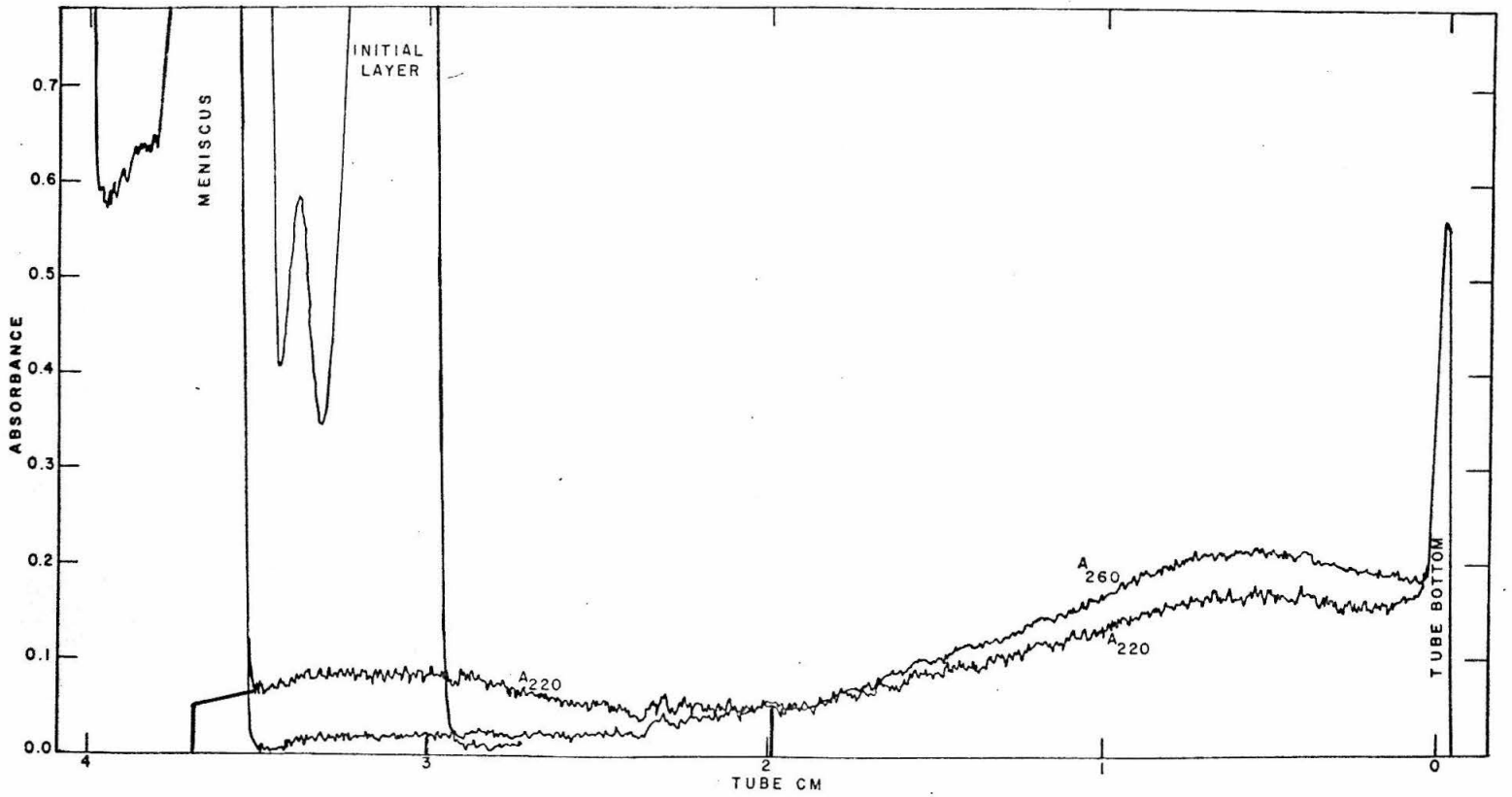

Figure 24

Same as figure 23 except that sedimentation was through a 0.2 to 0.6 F $NaClO_4$ gradient in D_2O. Again only small amounts of H III were extracted (area as outlined, corrected for DNA absorbance, corresponds to 17.3 % of the initial A^H_{220}) and most of the DNH is pelletted at the tube bottom.

reconstitution through a D_2O gradient containing 0 to 0.2 F $NaClO_4$. Figure 24 shows scans of the same material after sedimentation through a 0.2 to 0.6 F $NaClO_4$ - D_2O gradient in another tube of the same run. In both cases most of the DNH III sedimented to the tube bottom and only negligible amounts of histone III were extracted.

Figure 25 on the other hand shows the scans of a DNH III solution (R_{220} = 0.836) which had been stored for only 6 days at 4° C and then sedimented through a 0.2 to 0.6 F $NaClO_4$ gradient in D_2O. It is obvious that a large amount of histone III remained at the initial zone position, indicating that extensive dissociation or degradation had taken place during storage. Similar results were obtained after storage of other DNH III preparations. The reason for this change in behavior of DNH III during storage is not known. It points out the necessity of specifying the age of the sample, if any measurements on DNH III are to be meaningful.

For the sake of completeness, a sample of DNH IV was sedimented through gradients of 0 to 0.2 F (Fig. 26) and 0.2 to 0.8 F $NaClO_4$ (Fig. 27). In both cases the DNA (DNH?) had sedimented to the bottom of the tube leaving behind a very gradual tail of 2200 Å absorbing material. The highest absorbance was at the initial position. Because of the gradualness of the change in absorbance, quantitative esti-

Figure 25

Quartz tube scans before and after sedimentation of a zone of reconstituted calf thymus DNH III (R_{220} = 0.836) after storage for 6 days at 4° C. The gradient was 0.2 to 0.6 F $NaClO_4$ in D_2O. A large amount of H III remained at the initial position (area as outlined, corrected for DNA absorbance, corresponds to 211 % of the initial A^H_{220}) indicating substantial degradation on storage. The A_{220} baseline as measured is obviously too low (the area down to about 0.3 absorbance equals 100 % recovery of A^H_{220}). This also accounts for the low R_{220} (0.96) of the areas under the DNA peak.

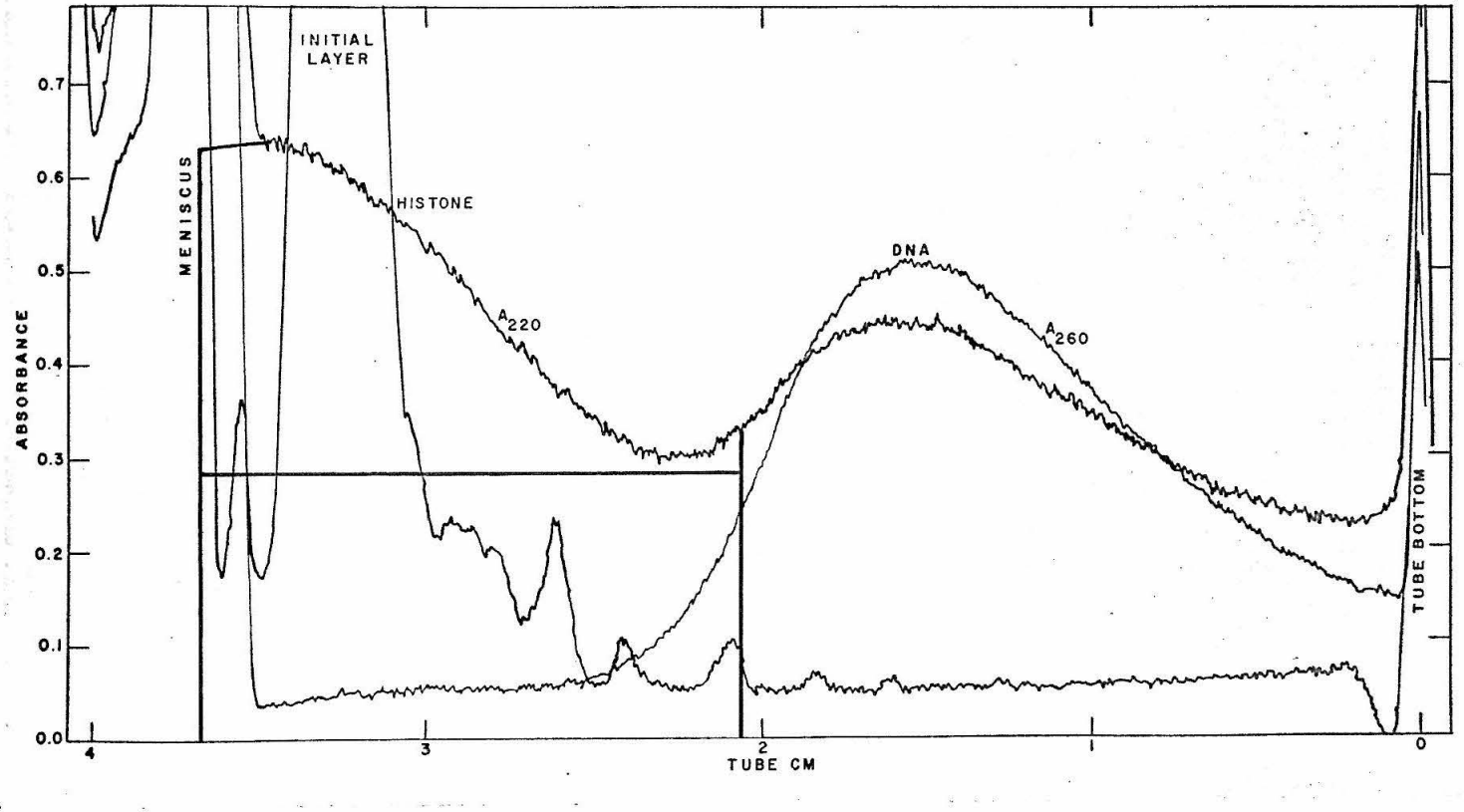
INITIAL
LAYER
MENISCUS
HISTONE
DNA
A_{220}
A_{260}
TUBE BOTTOM
ABSORBANCE
0.0
0.1
0.2
0.3
0.4
0.5
0.6
0.7
4
3
2
1
0
TUBE CM

Figure 25

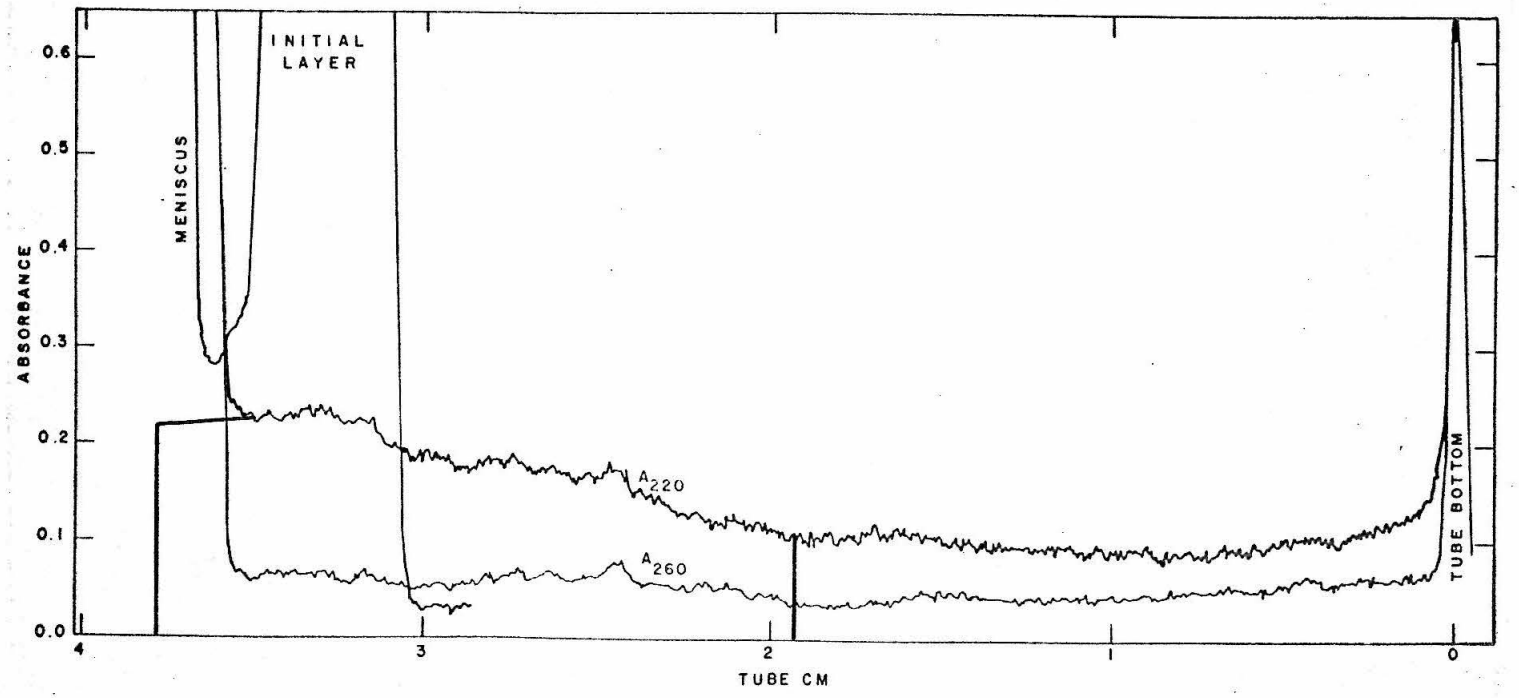

Figure 26

Quartz tube scans before and after sedimentation of a zone of reconstituted calf thymus DNH IV (R_{220} = 0.725; 2 days old) through a 0 to 0.2 F $NaClO_4$ gradient in D_2O. Some of the histone had gradually come off in the top half of the tube (area as outlined, corrected for DNA absorbance, corresponds to 92.6 % of the initial A^H_{220}), but again the baseline is probably too low. Most of the undissociated DNH has pelletted at the tube bottom.

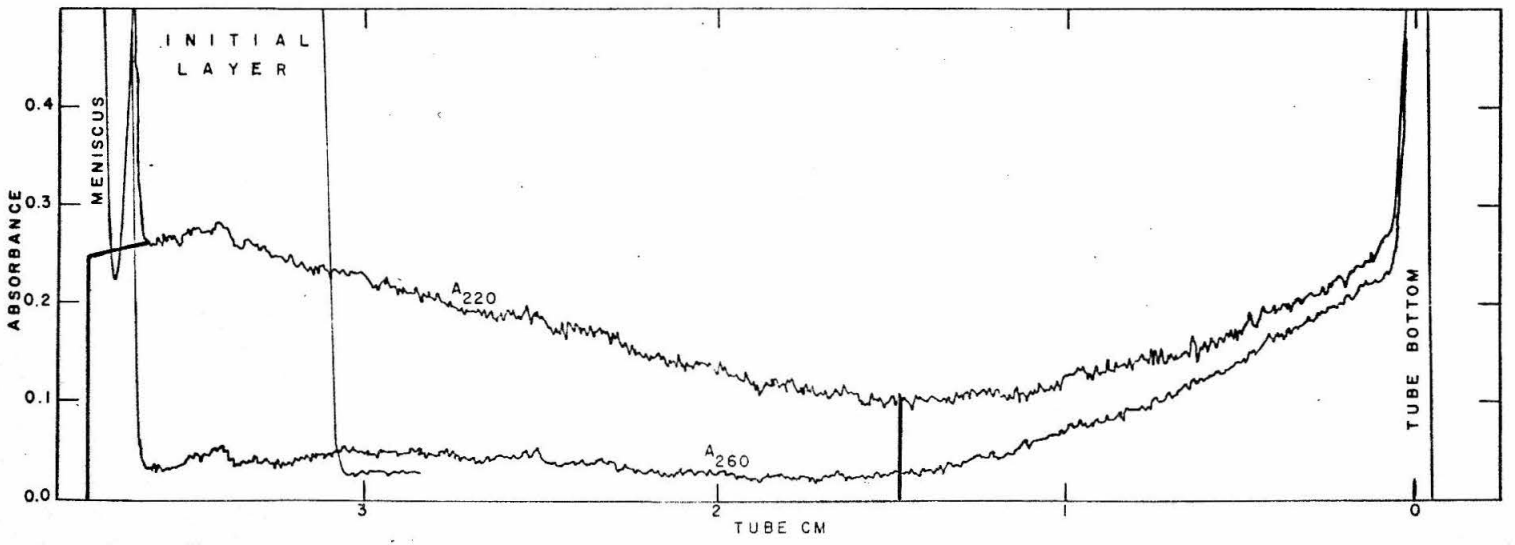

Figure 27

Same as figure 26 except that the DNH IV was 0 days old and sedimented through a 0.2 to 0.8 F $NaClO_4$ gradient in D_2O. Again considerable amounts of histones remained in the upper part of the tube (area as outlined, corrected for DNA absorbance, corresponds to 123.7 % of the initial A^H_{220}), but the baseline is again too low. Most of the undissociated DNH is pelletted at the tube bottom.

mates of the amount of material left behind are unreliable. The only conclusion that we want to draw from this fragmentary result is that no peak of histone IV was observed up to 0.8 F salt concentration.

5. Native Calf Thymus Nucleohistone

Finally, we examined the dissociation behavior of native, whole calf thymus nucleohistone. Figure 28 shows scans at 2600, 2200 and 2100 Å after sedimentation of a fresh sample (R_{220} = 0.707) through a D_2O gradient containing 0.3 to 0.5 F $NaClO_4$. Two clearly distinguishable bands are visible, the first at the interphase of the initial zone and the gradient, the second centered at 0.42 F $NaClO_4$. In gradients beginning at 0.4 F or higher $NaClO_4$ concentrations, the two bands fuse together at the top of the gradient. Figure 29 shows this situation in a salt gradient varying from 0.6 to 2.0 F $NaClO_4$ in D_2O. No further bands are observed at concentrations above 0.6 F.

Table IX lists the results of the quantitative estimates from the scans. Since the DNA was pelletted in all of the experiments, the material balance for DNA (Line k) is meaningless. (It should correspond to material sedimented to the tube wall). In regard to the amounts of histones recovered (Line q) the results are highly variable (53 to 135 %). Significant is that a large percentage of the recovered material is present in the histone bands (Line s) and that the two bands of figure 28 contain about equal quantities of material absorbing at 2200 Å (Column 1, Lines r and s).

Figure 28

Quartz tube scans before and after sedimentation of a zone of native calf thymus DNH (R_{220} = 0.707, 7 days old) through 0.3 to 0.5 F $NaClO_4$ in D_2O. Two clearly distinguishable histone bands are visible, the first at the interphase between initial zone and gradient (area as outlined, corrected for DNA absorbance, corresponds to 22.2 % of the initial A^H_{220}), the second centered at 0.42 F $NaClO_4$ (area as outlined, corrected for DNA absorbance, corresponds to 27.0 % of the initial A^H_{220}). Most of the DNA has pelletted at the tube bottom.

Figure 29

Same as figure 28 except that sedimentation was through a 0.6 to 2.0 F $NaClO_4$ gradient in D_2O. The top band of histones is due to the superposition of both bands of figure 28 (area as outlined, corrected for DNA absorbance, corresponds to 47.0 % of the initial A^H_{220} with 47.0 % remaining in the tail in the lower part of the tube). Most of the DNA has pelletted at the tube bottom. The A_{220} baseline is probably too low.

Figure 28

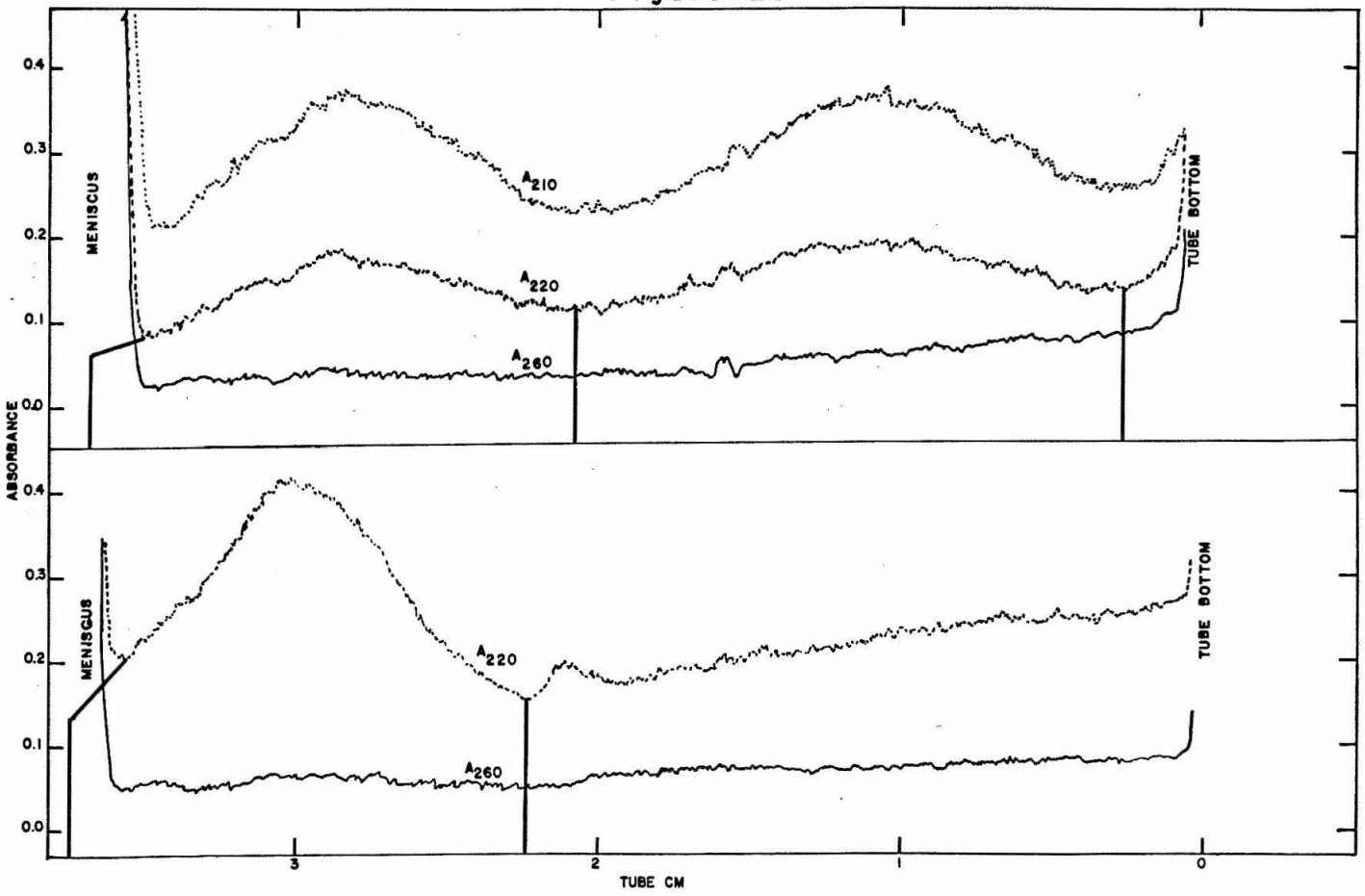

Figure 29

Table IX

Native Calf Thymus Nucleohistone

a) Sample	5	5	5	5
b) F $NaClO_4$	0.3-0.5	0.4-0.6	0.4-1.0	0.6-2.0
c) days old	7	3	0	7
d) S	-	-	-	-
e) F of pk	0.338/0.417	0.461	0.54	0.6
f) A_{260} init	3.74	1.93	1.93	3.74
g) A_{220} init	5.3	2.73	2.73	5.3
h) R_{220}	0.706	0.706	0.706	0.706
i) A_{400} init	0.38	0.227	0.227	0.38
j) H/D	1.53	1.53	1.53	1.53
k) % A_{260}rec	18.5	52.9	42.3	23.25
l) % not sed	5.85	-	-	-
m) % banded	-	-	-	-
n) % in H bd	10.1	26.4	-	8.5
o) % in tail	2.6	26.5	42.3	14.75
p) % A^{NH}_{220}	37.1	95.0	91.4	60.85
q) % A^{H}_{220}	53.4	132.1	134.5	94.0
r) % not sed	22.2	-	-	-
s) % banded	27.0	99.9	86.5	47.0
t) % in DNA	-	-	-	-
u) % in tail	4.2	32.2	48.0	47.0
v) R^{A}_{220}	-	-	-	-

From our experiments with reconstituted nucleohistones we would infer that the first band of figure 28 is due to histone I. The band centered around 0.42 F salt is most likely histone II. If any histones come off at even higher concentrations they are probably histone III.

Because of the important implications of these assignments it was necessary to verify them by actually isolating the individual histone fractions from native DNH for positive identification.

V. Discussion of the Results From Preparative Sedimentation

This chapter describes our results with salt layer and batch sedimentation and our attempts to identify the extracted histone fractions. For comparison with the data of the salt gradient experiments, approximate material balances are presented for both sedimentation procedures.

The larger scale batch sedimentation experiments offer the most conclusive proof that histones were indeed extracted in fractions which are identical with, or very similar to the histone I, II, III and IV classes obtained by Amberlite chromatography of acid extracted histones.

1. Results of Salt Layer Sedimentation Experiments

A typical result of a salt layer sedimentation experiment with native calf thymus DNH is shown in figure 30. Here the absorbance measurements of each fraction are plotted versus the fraction number, sedimentation being from left to right. The $NaClO_4$ concentrations of the individual layers are listed in the boxes in the upper part of the drawing.

The A_{260} data indicate that most of the DNA is pelletted. The absorbances at 2200 Å show a broad histone band in the 0.4 and 0.5 F $NaClO_4$ layers. Some material may be in the 0.2 and 0.3 F salt layers as well as in the 0.6 F layer, but the concentrations are considerably lower than in the main band.

Figure 31 presents the results of a similar experiment in which the sedimenting material was purified calf thymus chromatin instead of DNH. The material in the initial zone had a rather high physical density and much had sunk to about the middle of the sedimentation tube before it could be mounted and sedimented. Nevertheless, zones of dissociated histones were obtained and approximately at the expected positions for native DNH.

This result indicates that even in the much more complex aggregates which chromatin represents, the histones are quite accessible to selective salt dissociation.

Figure 30

Preparative salt layer zone sedimentation using the SW 25 rotor and plastic sedimentation tubes. Native calf thymus DNH (A_{260} = 3.937, 0 days old) in 0.016 F saline citrate was sedimented through layers of increasing D_2O concentrations and $NaClO_4$ formalities as indicated in the boxes in the upper part of the figure. The A_{220} of the fractions show a broad histone band in the 0.4 to 0.5 F $NaClO_4$ layers. Most DNA is pelletted at the tube bottom.

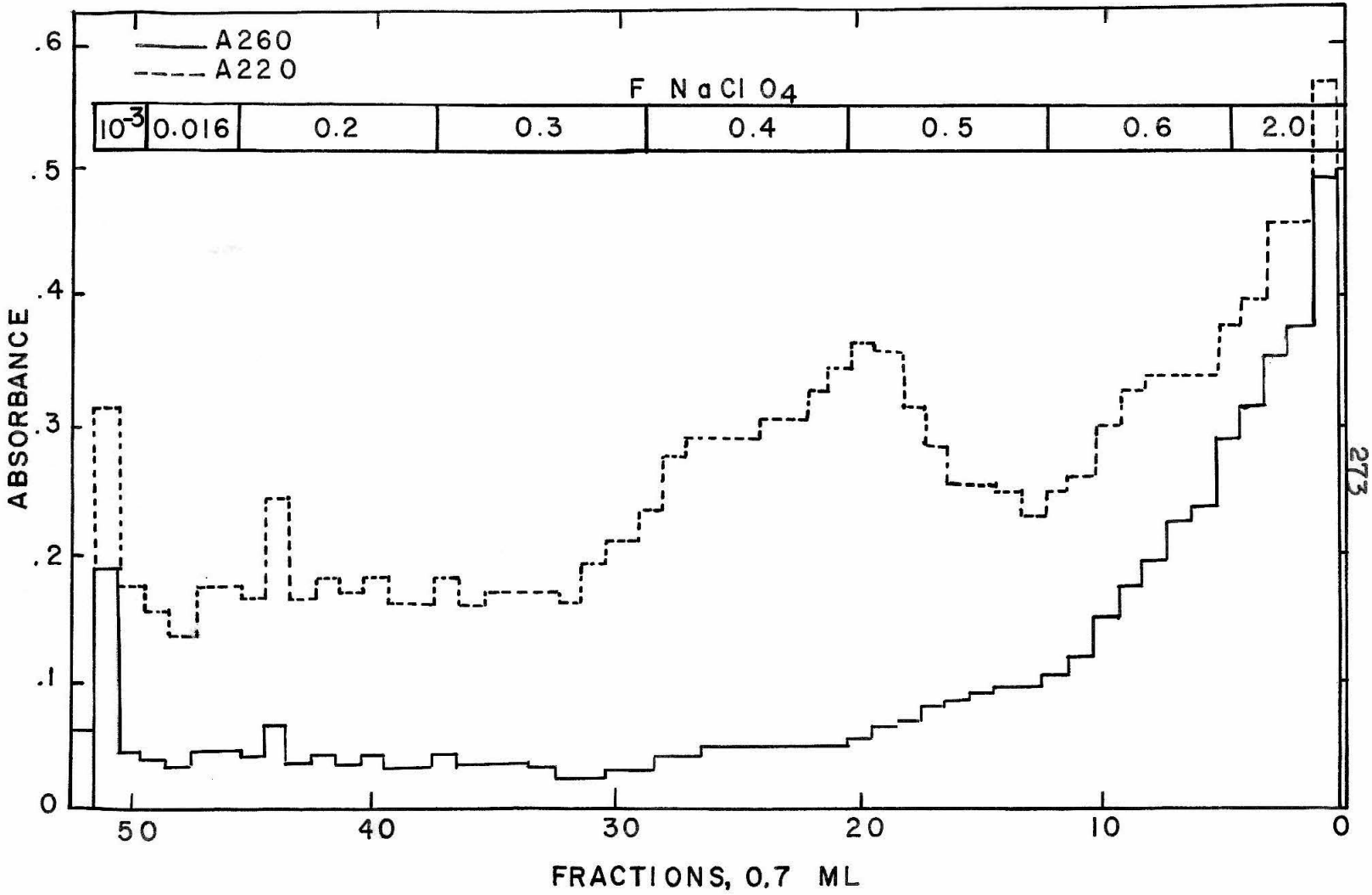
A260
A220
F NaClO4
10-3
0.016
0.2
0.3
0.4
0.5
0.6
2.0
ABSORBANCE
.6
.5
.4
.3
.2
.1
0
50
40
30
20
10
0
FRACTIONS, 0.7 ML
273

Figure 30

Figure 31

Same as figure 30 except that purified calf thymus chromatin (A_{260} = 4.109, 0 days old) was sedimented. The histone band is even broader than that of the DNH, but its general position with regard to the salt concentration is similar.

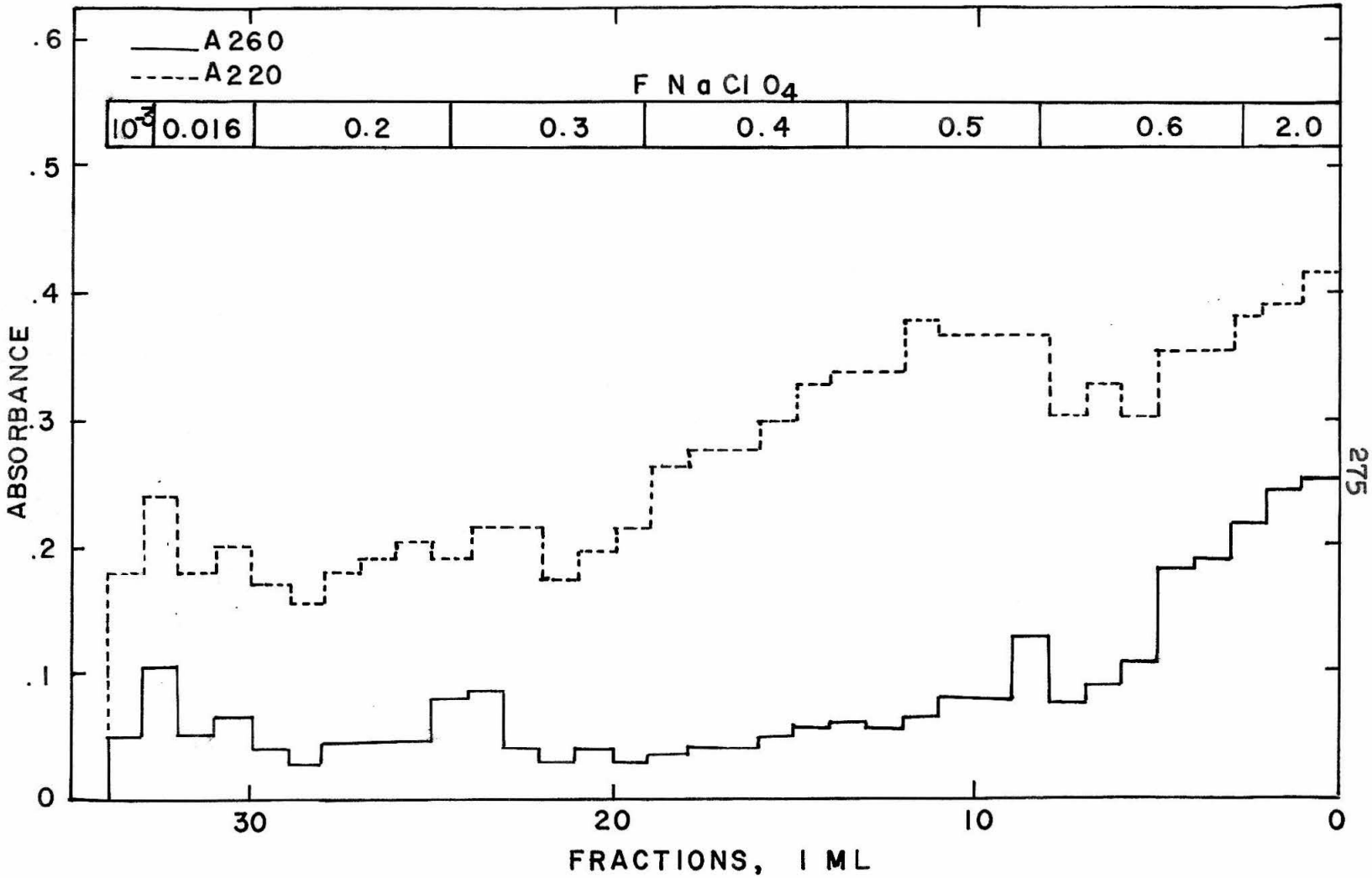
A260
A220
F NaClO4
10-3
0.016
0.2
0.3
0.4
0.5
0.6
2.0
.6
.5
.4
.3
.2
.1
0
ABSORBANCE
275
30
20
10
0
FRACTIONS, 1 ML

Figure 31

Two results of the amino acid analyses of the fractions are shown in table X. They indicate a distinct trend in the arginine to lysine ratios, with lysine rich fractions dissociating at lower salt concentrations than arginine rich fractions. However, the preliminary data were not exact enough to permit identification of the kinds of histones present in the fractions.

The reason for the poor results was the unexpected loss of most of the histone samples during desalting by dialysis against water.

Table X

Summary of Amino Acid Analyses

by the Dreyer Procedure (65)

Formality of $NaClO_4$	Mole Ratio arg/lys	
initial zone	0.366	0.405
0.2	0.275	0.325
0.3	0.292	0.326
0.3 - 0.4	0.347	0.400
0.4	0.524	0.546
0.4	0.457	0.500
0.4 - 0.5	0.513	0.568
0.5	0.575	0.587

Histone Ib	0.10
Histone IIb	0.59
Histone III	1.37
Histone IV	1.42

2. Results of Batch Sedimentation Experiments Identification of Histones by Amberlite Chromatography

The results of our batch sedimentation experiments can best be discussed in terms of the data of our Amberlite cation exchange chromatography. In these experiments histones extracted from purified calf thymus chromatin by varying concentrations of $NaClO_4$ were analyzed with regard to the number of histone classes they contained.

Figure 1 should be consulted for the elution pattern of whole calf thymus histones. Figure 32 shows that 0.27 F $NaClO_4$ extracted histones Ia and Ib, some uncharacterized run-off material, which is probably non-histone protein (70), and a small, negligible amount of material which eluted at GuCl concentrations at which histones II and III(IV) would come off the Amberlite.

Total recovery of material in the eluent represents 37.6 % of the A^{H}_{220} material present in the fractions of the supernatant which were dialyzed, lyophilyzed and applied to the column. The greatest loss occurred probably in that not all of the freeze dried material could be redissolved in 8 % GuCl.

Figure 33 gives the elution pattern of material extracted from the 0.27 F $NaClO_4$ extracted pellet by H_2SO_4 (pH 0.7).

Figure 32

Amberlite IRC-50 cation exchange chromatography. GuCl elution pattern of histones extracted by 0.27 F $NaClO_4$ from native calf thymus chromatin.
Arabic numbers give % of eluted material in the peaks; roman numbers indicate the kind of histone fraction in the peaks.

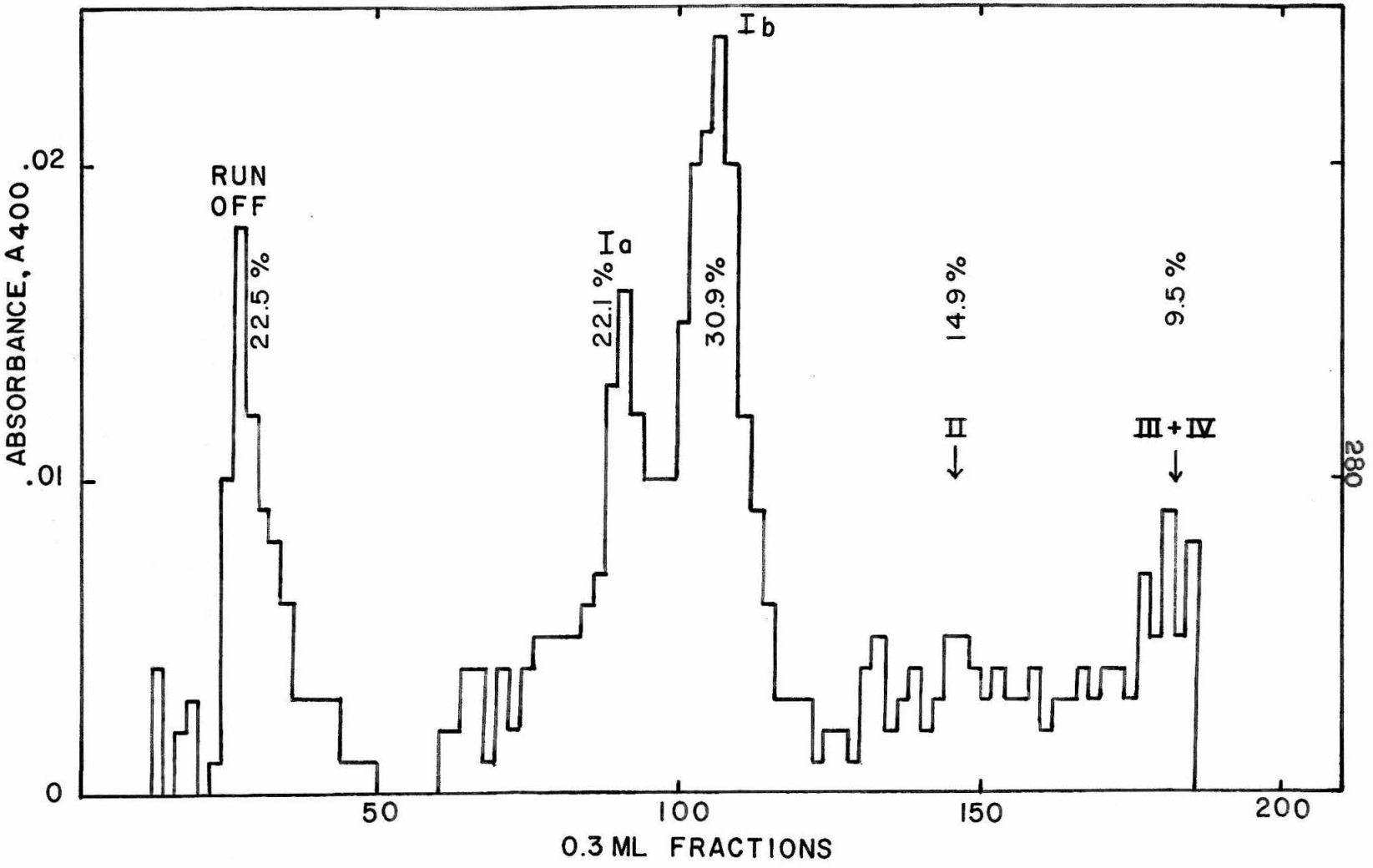
ABSORBANCE, A400
.02
.01
0
RUN
OFF
22.5 %
22.1 %
Ia
Ib
30.9 %
14.9 %
II
9.5 %
III + IV
280
50
100
150
200
0.3 ML FRACTIONS

Figure 32

Figure 33

Same as figure 32 except that here the H_2SO_4 (pH 0.7) extractable histones in the 0.27 F $NaClO_4$ extracted chromatin pellet were eluted.

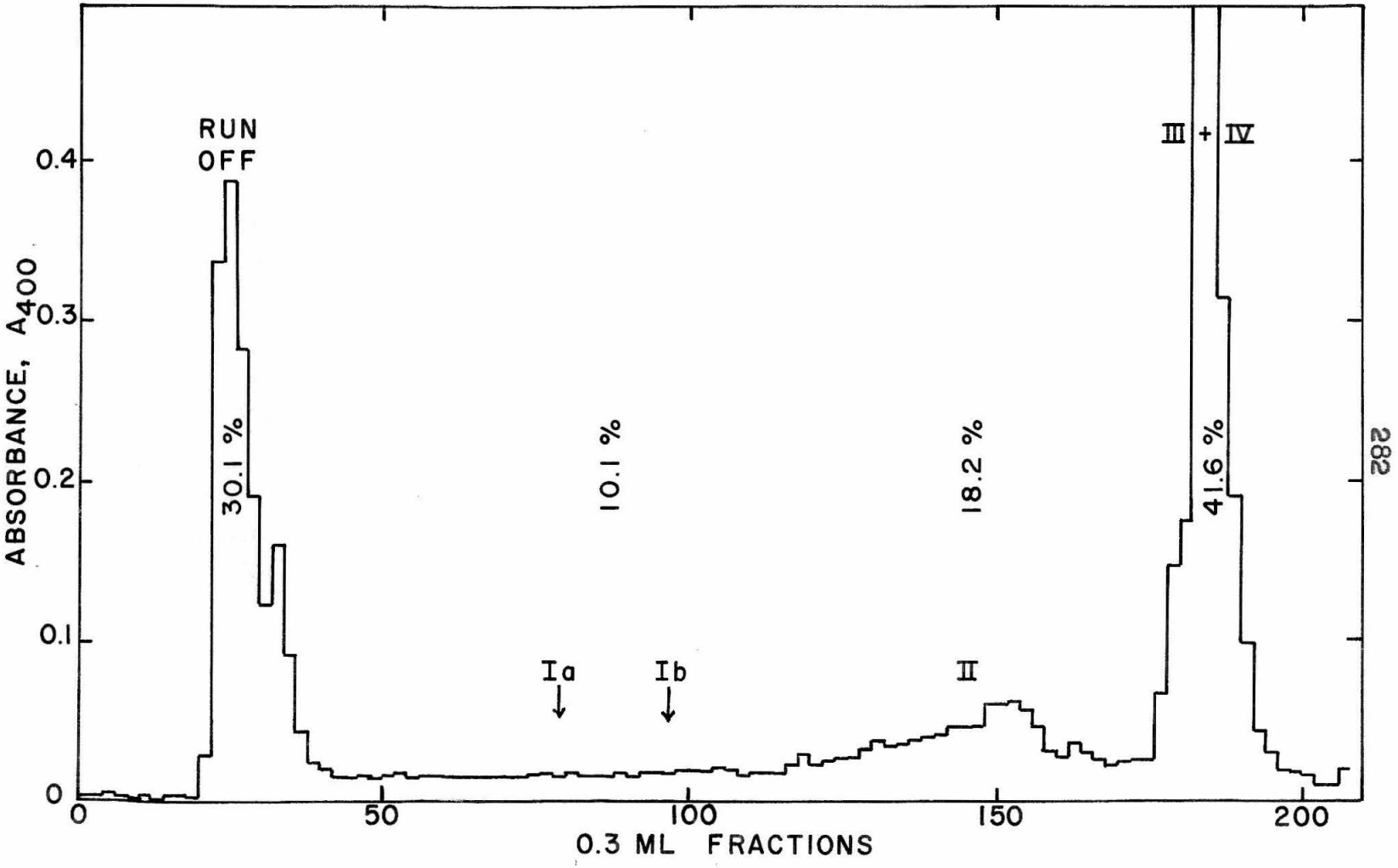
RUN
OFF
30.1 %
10.1 %
18.2 %
41.6 %
III + IV
Ia
Ib
II
ABSORBANCE, A400
0.4
0.3
0.2
0.1
0
0
50
100
150
200
0.3 ML FRACTIONS
282

Figure 33

The run-off peak is rather large, but there are no peaks at the histone Ia and Ib positions. The histone II peak is smaller than expected, if all of the remaining material had been recovered from the pellet. Histones III and IV come off as the last peak at the place where the GuCl concentration increases to 40 % as expected.

In three attempts made to determine the kinds of histones extracted by 0.36 F $NaClO_4$, we were not able to dissolve enough material in 8 % GuCl for a successful Amberlite experiment. A fourth attempt gave the results shown in figure 34. The first and largest peak is clearly run-off material. It is followed by a smaller peak which could not be classified unambiguously. It may be histone Iaa, but it seems more likely that it is additional run-off material (see discussion on page 301). The last peak is unresolved histone I. No significant amounts of histones II and III(IV) were detected in the GuCl soluble material.

Although recovery of histones from the 0.36 F $NaClO_4$ supernatant was difficult, acid extraction of the residual pellets was easy. Figure 35 shows that only histones II and III(IV) were present in the pellets as expected. There was no run-off peak.

Figure 34

Amberlite IRC-50 cation exchange chromatography. GuCl elution pattern of histones extracted by 0.36 F $NaClO_4$ from native calf thymus chromatin.
Arabic numbers give % of eluted material in the peaks; roman numbers indicate the kind of histone fraction in the peaks.

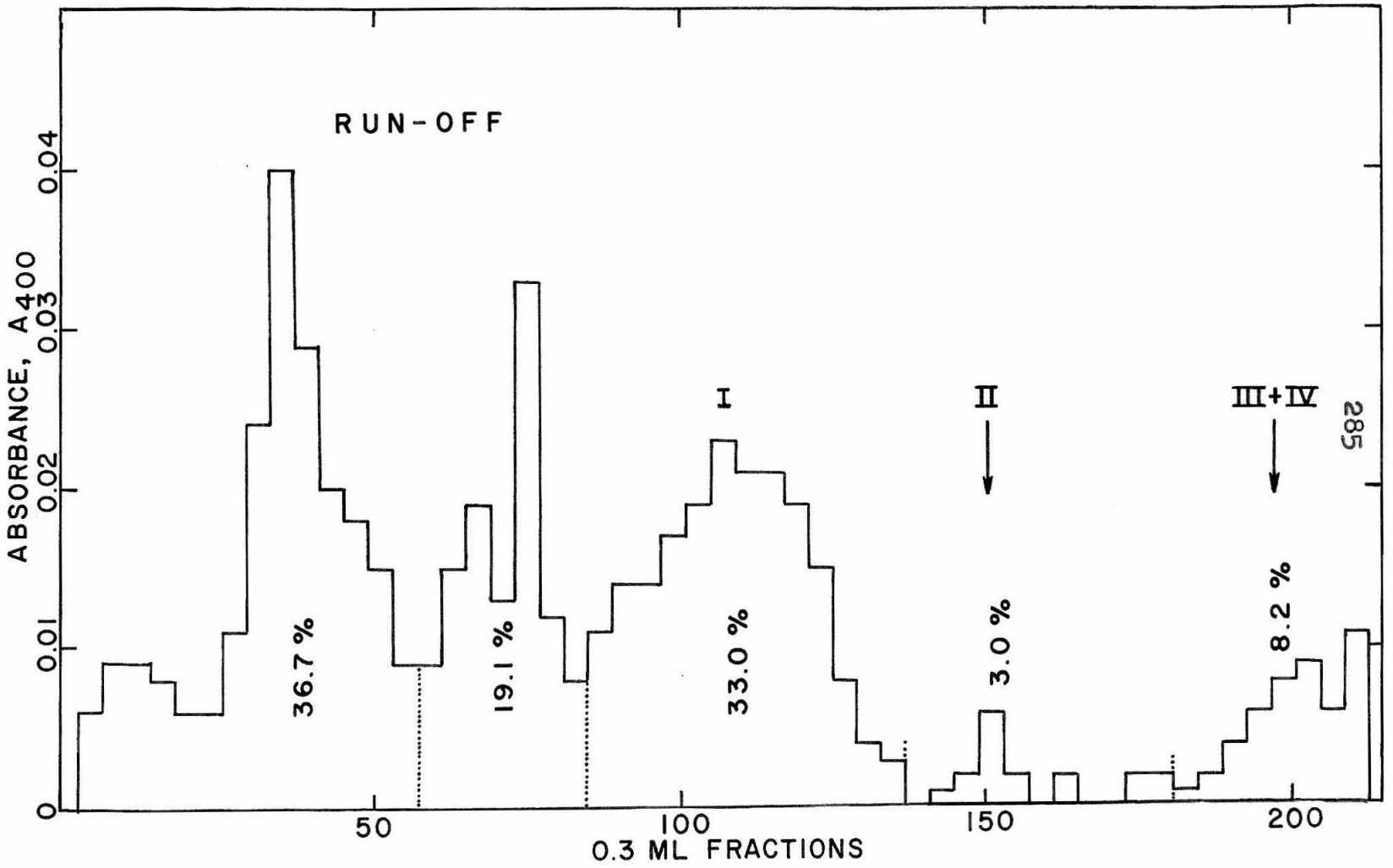
RUN-OFF
ABSORBANCE, A400
0.04
0.03
0.02
0.01
0
I
II
III+IV
285
36.7 %
19.1 %
33.0 %
3.0 %
8.2 %
50
100
150
200
0.3 ML FRACTIONS

Figure 34

Figure 35

Same as figure 34 except that here the histones were acid extracted from the 0.36 F $NaClO_4$ extracted chromatin pellet.

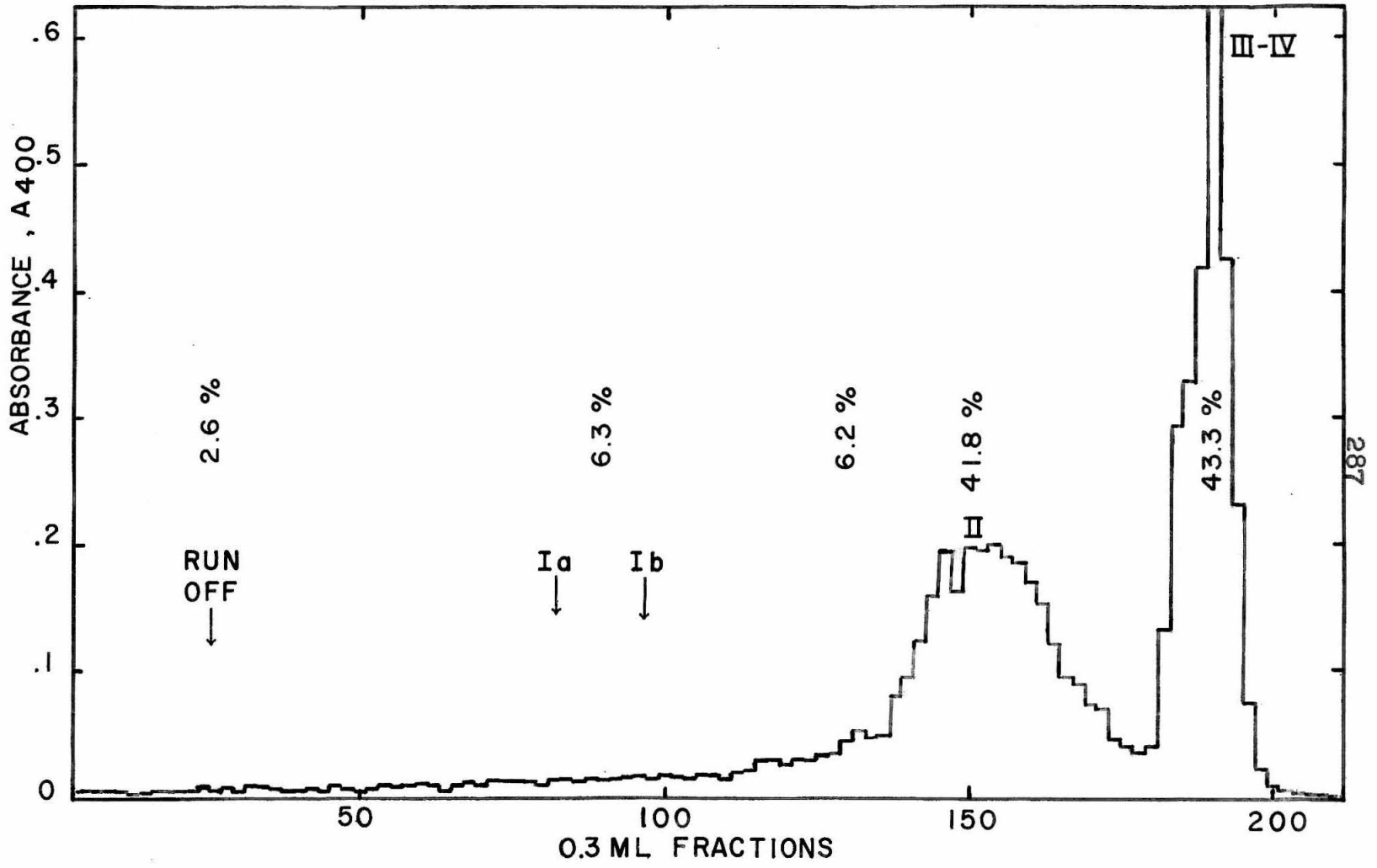
ABSORBANCE , A400
.6
.5
.4
.3
.2
.1
0
2.6 %
6.3 %
6.2 %
41.8 %
43.3 %
III-IV
II
RUN
OFF
Ia
Ib
287
50
100
150
200
0.3 ML FRACTIONS

Figure 35

Using 0.45 F $NaClO_4$, histones Ia, Ib and IIa, IIb (Fig. 36) were found in the supernatant after sedimentation plus a small amount of run-off material. No histone III(IV) was extracted. Only negligible amounts of material were recovered from the pellet by sulfuric acid treatment, not enough for a successful Amberlite experiment.

In order to summarize and correlate the Amberlite data most effectively, it is best to present the results in relative terms (Table XI). Here the assumption is made, that any "lost" material has the same average composition as the material actually eluted from the ion exchange column. The results, normalized to the total amount of eluted, TCA precipitable histones, are plotted in figure 37.

The lower half of each graph shows the distribution of histones in the supernatants, the upper half the distribution of histones in the acid extracts of the corresponding pellets. The areas of the blocks are proportional to the percentages of material eluted. Vertical blocks indicate that definite peaks were eluted, horizontal blocks indicate background absorption and no peaks. The top graph shows the elution pattern of whole, acid extracted histones for comparison.

Figure 36

Amberlite IRC-50 cation exchange chromatography. GuCl elution pattern of histones extracted by 0.45 F $NaClO_4$ from native calf thymus chromatin.
Arabic numbers give % of eluted material in the peaks; roman numbers indicate the kind of histone fraction in the peaks.

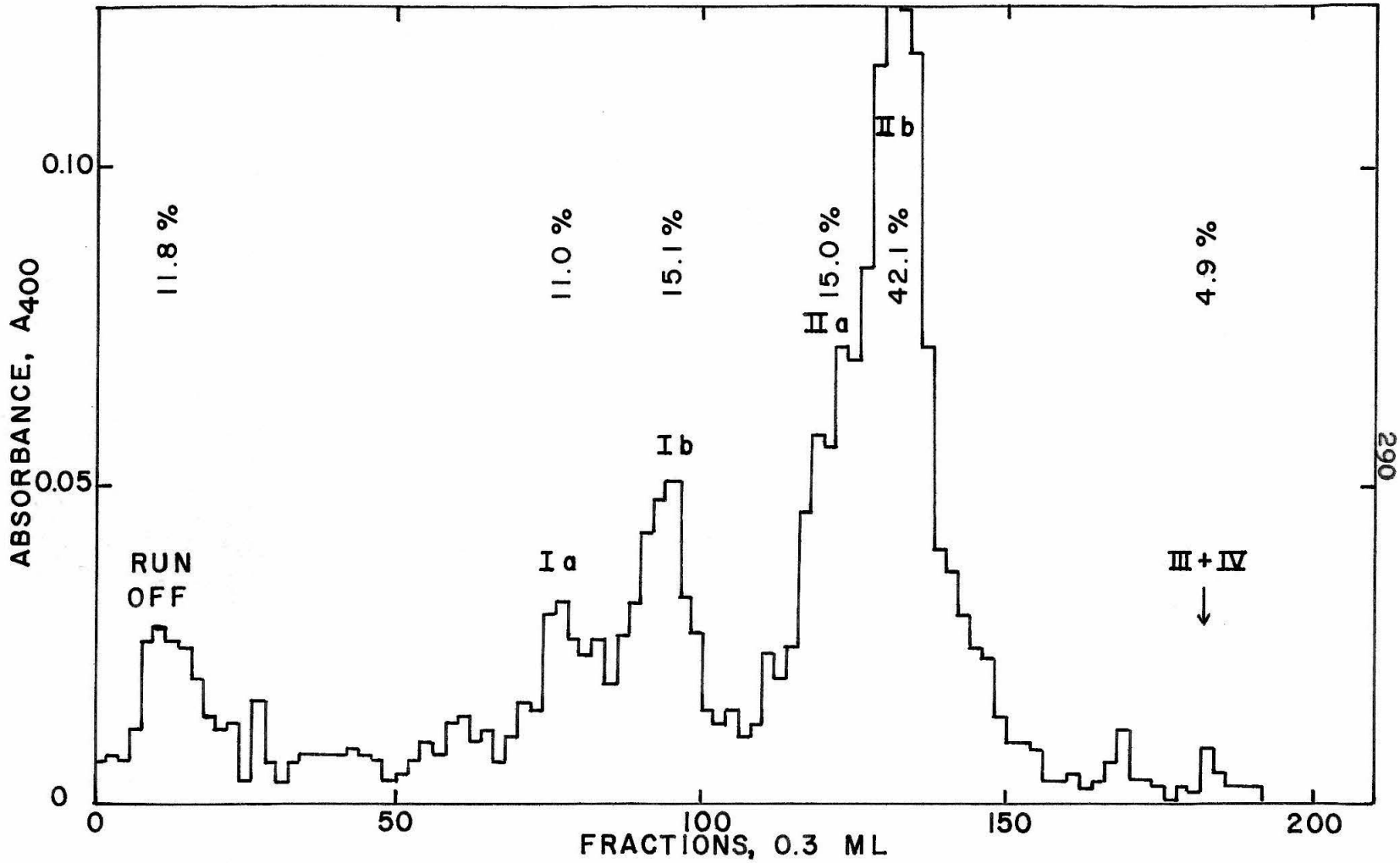
ABSORBANCE, A400
0.10
0.05
0
11.8 %
11.0 %
15.1 %
15.0 %
42.1 %
4.9 %
RUN
OFF
Ia
Ib
IIa
IIb
III + IV
0
50
100
150
200
FRACTIONS, 0.3 ML
290

Figure 36

Table XI

Percent Distribution of Histones

in the Peaks Eluted from Amberlite IRC-50

peak	0.27 F		0.36 F		0.45 F	
	super-natant	pellet	super-natant	pellet	super-natant	pellet
run-off	22.5	30.1	36.7 19.1	2.6	11.8	
Ia	22.1	10.1	33.0	6.3	11.0	
Ib	30.9				15.1	
IIa	14.9	18.2	3.0	6.2	15.0	
IIb				41.8	42.1	
III(IV)	9.5	41.6	8.2	43.3	4.9	
	99.9	100.0	100.0	100.2	99.9	

Figure 37

Summary of our Amberlite IRC-50 cation exchange chromatography experiments.
The lower half of each graph shows the distribution of histones in the supernatants, the upper half the distribution of histones in the acid extracts of the corresponding pellets. Abscissa and ordinate are not to scale, they only indicate qualitatively the relative positions and width of the peaks of the eluted material. The areas of the blocks, however, are proportional to the percentages of material eluted. The amounts of histones in the total effluent per experiment are normalized to 100 %. Tall blocks indicate that the material was present in peaks, horizontal blocks indicate that only background absorption was present and no peaks.

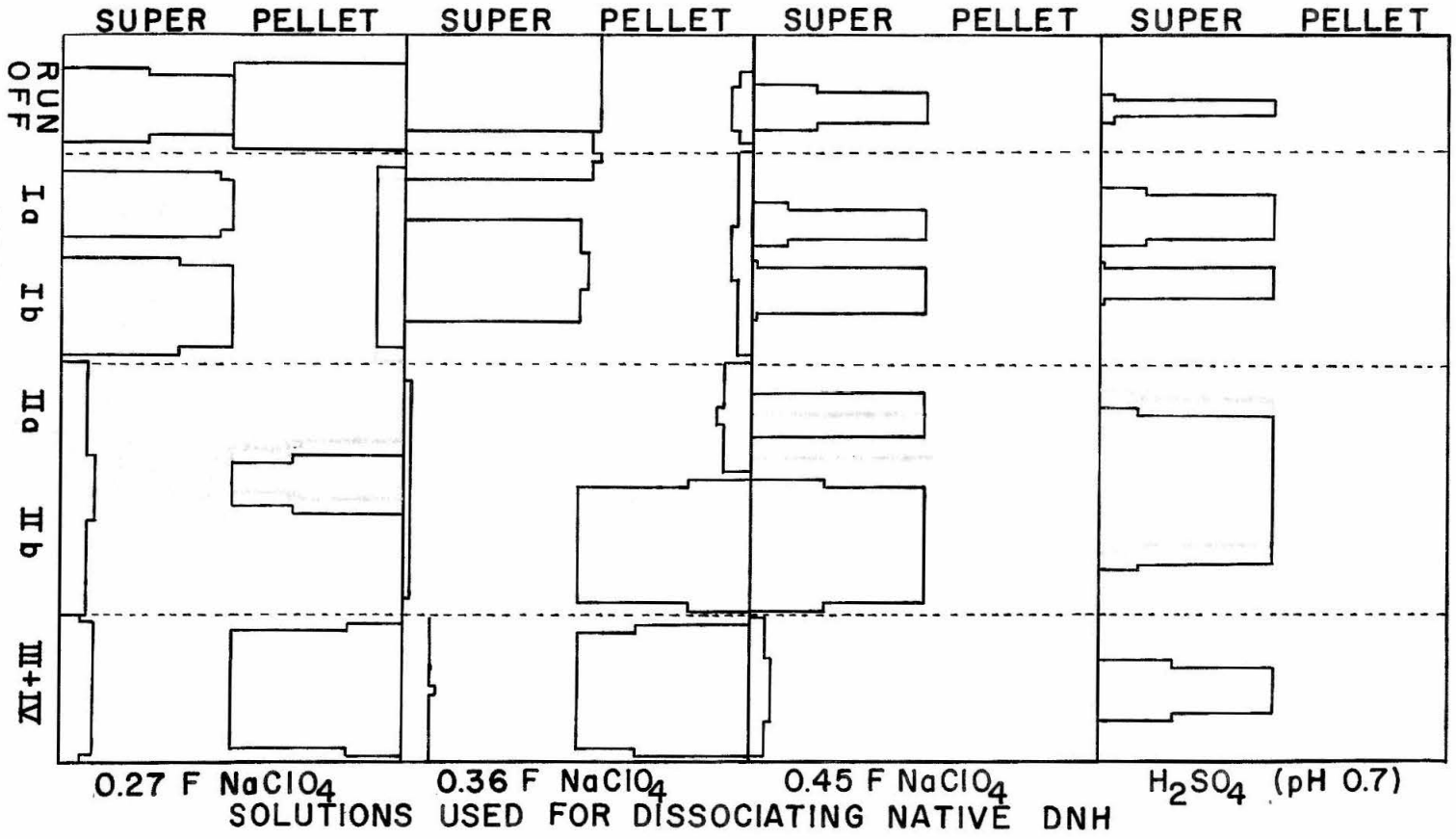
SUPER PELLET SUPER PELLET SUPER PELLET SUPER PELLET
RUN OFF
Ia
Ib
IIa
IIb
III+IV
HISTONE FRACTIONS
0.27 F NaClO4
0.36 F NaClO4
0.45 F NaClO4
H2SO4 (pH 0.7)
SOLUTIONS USED FOR DISSOCIATING NATIVE DNH

Figure 37

The figure summarizes our results most clearly: 0.27 F $NaClO_4$ extracts histones Ia and Ib and some run-off peak. The remaining pellet does not yield histone I but only histone II and III(IV) and some more run-off material. 0.36 F $NaClO_4$ extraction gave similar results, but no run-off material was obtained from the pellet. 0.45 F $NaClO_4$ extraction yielded all histones except III(IV). The material remaining on the pellet was too small for successful Amberlite chromatography, but presumably only histones III(IV) were present.

In concluding this section it must be pointed out that the nice correlation observed may be subject to some modifications. First, there is the matter of the unsatisfactory material balance, a summary of which is given in table XII. One of the difficulties in obtaining a good material balance is the high concentration of nucleohistones used in these salt extraction experiments, where the initial A_{260} was about 5 throughout the sedimentation tube. Because of the insolubility of DNH and histones at these salt concentrations much of the material aggregates and sediments to the tube bottom. Part 1 of table XII gives the amounts of histones recovered in the fractions after sedimentation.

The amounts of histones in section a) were calculated from the A_{220}'s of the fractions, assuming 0.1 mg H/ml per

Table XII

Histone Material Balance of

1) Batch Sedimentaion

Total Amount of Histones Present in the Chromatin Used				
	7570	7570	7045	7570
a) Amounts Recovered in Sedimentation Fractions				
$NaClO_4$	0.27 F	0.36 F	0.36 F	0.45 F
super-natant	535	1114	1761	1458
tail	188	356	--	1410
pellet	6852	6105	--	4706
b) Percent of Initial Amounts				
super-natant	7.05	14.7	25.0	19.2
tail	2.5	4.7	--	18.6
pellet	90.5	80.6	--	62.2
c) Percent of "Expected" Histones				
super-natant	21.7	45.3	78.5	no H II
tail	7.6	14.5	--	
total	29.3	59.8	78.5	
super-natant	plus H II	17.6	30.2	23.0
tail		5.6	--	22.3
total		23.2	30.2	45.3

Table XII

Histone Material Balance of

2) Amberlite Chromatography

Amount of Histones Used in Workup				
supernatant	535	1114	1761	1458
pellet	6852	6105	--	4706
d) Total Amounts Recovered From Amberlite Column				
$NaClO_4$	0.27 F	0.36 F	0.36 F	0.45 F
supernatant	212	192	525	973
pellet	2526	2970	--	268
e) Recovery in Percent of Amount Used in Workup				
supernatant	39.6	17.2	29.8	66.7
pellet	36.8	48.6	--	5.7

A_{220} = 1.0. The amount of histones expected in the pellets was estimated from the difference between the initial material and that found in the fractions. Section b) gives the corresponding percentages. In c) a comparison is made between the amounts of histones found and those expected if 0.27 F salt extracted run-off peak and all of histone I, 0.36 F salt did or did not extract in addition histone II, and 0.45 F salt extracted all histones except III and IV. The percentages of histones found in the fractions of Amberlite chromatography of whole, acid extracted histones (Fig. 1) were used as basis for these calculations.

It is obvious that a considerably lower percentage of histones is found in the supernatants than expected, indicating that significant amounts of these histones must have pelletted together with the partially extracted DNH. It is at present unexplainable, why these histone aggregates did not dissolve in the H_2SO_4 (pH 0.7), which was used for the extraction of the residual histones from the pellets. Only those histones which were not extracted or precipitated by the particular salt concentration used are removed from the pellets by the acid.

For the Amberlite runs only the histones in the supernatants were used, since the bottom fractions (tails) contained significant amounts of A_{260} material and were discarded. Part 2 gives the amount of TCA precipitable his-

tones which were recovered from the Amberlite column. Section d) gives the total micrograms found in the effluent and e) the corresponding percentages in terms of the amounts of histones in the supernatants or pellets. It is obvious that considerable amounts of histones are "lost" during the workup; most of it probably because not all of the salt-free histones, aggregated by freeze drying, or in the case of H_2SO_4 extraction by ethanol precipitation, are soluble in the 8 % GuCl.

We have made an attempt to dissolve the GuCl insoluble residue of the histones extracted by 0.36 F $NaClO_4$ in 10 M urea and found that even in this medium they are not completely soluble. The fraction that did dissolve was subjected to acrylamide gel electrophoresis (70) and gave a band pattern similar to that of histone II plus some small amount of histone I. It was not possible to decide whether the histone II bands were due to fraction IIa or IIb. In any event, the above result points out that the Amberlite chromatography data may be subject to some modifications depending upon how completely the histone samples are soluble in 8 % GuCl.

Second, we have observed some variation in the amounts of histones detectable by TCA precipitation in the Amberlite effluent upon storage. Figure 37a shows the change in turbid-

Figure 37a

Change in TCA precipitable material in the effluent of Amberlite IRC-50 cation exchange chromatography on standing. The elution pattern is that of histones extracted by 0.36 F $NaClO_4$ from native calf thymus chromatin (Fig. 34).
The solid line represents the turbidity if the fractions are treated with TCA immediately after collection, the dashed line that 12 hours, and the dotted line that about 30 hours after collection.
The turbidity of the run-off material decreases considerably during storage.

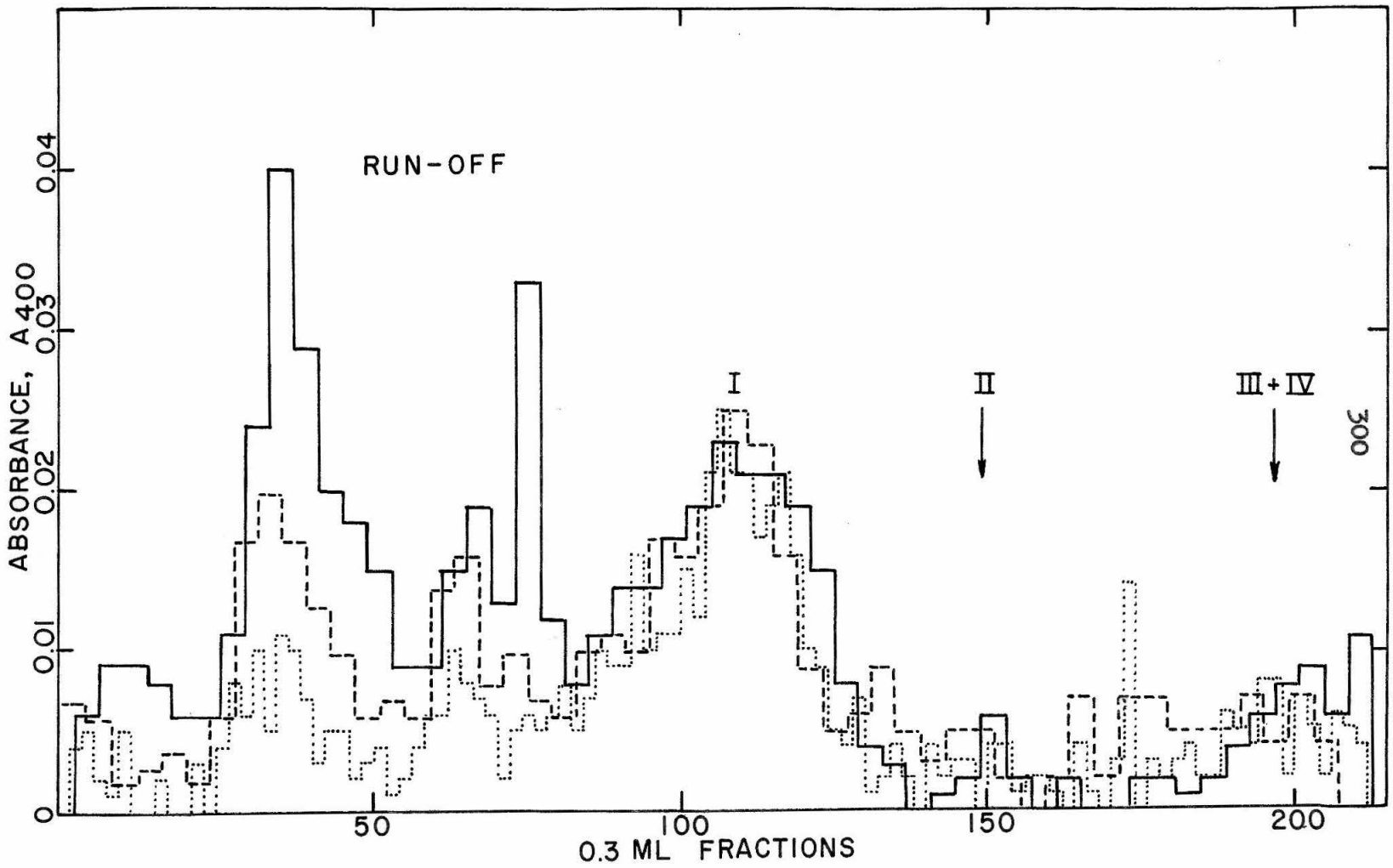
RUN-OFF
I
II
III+IV
300
ABSORBANCE, A400
0
0.01
0.02
0.03
0.04
50
100
150
200
0.3 ML FRACTIONS

Figure 37a

ity resulting when the effluent, containing histones extracted by 0.36 F $NaClO_4$, is treated with TCA immediately after collection of the fractions (solid line, see also figure 34), 12 hours after collection (dashed line) or approximately 30 hours after collection (dotted line). There is a clear decrease of turbidity in the run-off material and the peak following it, while the peak representing histone I is not affected. The degradability of the second peak being similar to that of the run-off material was the main reason why is was presumed to be run-off material rather than histone Iaa.

It is obvious that differential solubility of histone fractions and differential degradability may have distorted the Amberlite results somewhat, but it seems nevertheless quite safe to regard the overall conclusions concerning the selective extraction of histones from native DNH as correct, especially in conjunction with the data of reconstituted nucleohistone dissociation.

VI. Partially Extracted Native Calf Thymus Nucleohistones

Because of the biological implications, it is to be expected that the partially extracted, native nucleohistones will be of greater interest than the extracted histones. The following chapter considers some of the interesting biological and physical properties of the partially salt extracted DNH. The increasing activity in sustaining DNA-dependent RNA synthesis of DNH treated with increasing salt concentrations and the corresponding increase in electrophoretic mobility are discussed as confirmation of the histone extraction data. Attempts are made to interpret the low ionic strength melting curves of these materials in terms of the distribution of histones along the DNA strand.

But before discussing these results we turn our attention briefly to the problems of "contamination" of salt extracted nucleohistones with histone aggregates via reconstitution, and of "degradation".

1. Resedimentation of Extracted Nucleohistones

Since all of our partially extracted nucleohistone samples are obtained from the material that sediments to the tube bottom, it might be argued that they may be contaminated with aggregates of histones or non-histone proteins. These aggregates may, upon resuspension of the pellets in low salt media, redissolve and recomplex with the denuded DNA regions.

In order to determine the extent of such recomplexed artifacts, a number of extracted nucleohistone preparations was resedimented and the effect of such treatment was examined by electrophoresis and heat denaturation.

The experimental procedure was the following: The sedimented pellets or fractions containing high concentrations of DNA (DNH) were diluted and dialyzed into 3×10^{-4} N Na^+ EDTA (pH 6.3). Mobilities and melting curves were measured on an aliquot of these samples and the remainder was diluted with salt solutions having concentrations close to those used in the original extraction. These solutions were resedimented and the pellets were treated as above for repeat measurements.

The mobility data are listed in table XIII and show that the mobilities of the resedimented samples are only slightly faster than those taken before resedimentation.

Figures 38 to 41 show the changes in melting behavior upon resedimentation. The resedimented samples (full circles) melt at somewhat lower temperatures and show sharper transitions. The sample extracted with 0.45 F NaCl and resedimented in 0.48 F NaCl (Fig. 39) shows a more distinct two step melting profile than the original sample, suggesting that additional histones (in this case histone II) were extracted by the slightly higher salt concentration.

Resedimenting a sample, first extracted by 0.27 F NaCl, in 0.45 F NaCl gave the melting profile shown in figure 42. In this case the shift of the lower melting regions toward lower temperatures is much more pronounced than in any of the other samples, indicating that considerably more histones were extracted. Again, the two step behavior is more pronounced.

In summary, we conclude that measurements performed with resedimented preparations indicate that their properties do not change appreciably, suggesting that any histone aggregates which may be present in the pellets, do not reconstitute too easily and do not cause grossly erroneous results. In addition, the fact that histone aggregates are

Table XIII

Mobilities of NaCl Extracted Native Calf Thymus DNH

1st Sedimentation			Resedimentation		
Age of Sample	F NaCl Conc.	Mobility x 10^4 $cm^2/V\text{-}sec$	Age of Sample	F NaCl Conc.	Mobility x 10^4 $cm^2/V\text{-}sec$
4	0	1.15	10	0	1.38
(2) 5	0.27	1.39	(5) 9	0.26	1.42
(7) 9	0.45	1.53	(9) 15	0.48	1.48 0.04
			(9) 10	0.50	1.56
(0) 3	1.80	2.04	(1) 6	1.94	2.21 - 2.28

Figure 38

Heat denaturation curves of native calf thymus DNH (A_{260} = 0.732; R_{220} = 0.685) partially extracted by batch sedimentation a) with 0.27 F NaCl and b) resedimented in 0.26 F NaCl.
The samples were heated in 3 x 10^{-4} N Na^+ EDTA (pH 6.3) in the Cary.

Results	T_m °C	% H	Slope	A_{260}	R_{220}	Days Old	Δ °C
a)	74.7	39.9	3.21	1.20	0.94	(2) 8	27.7
b)	73.5	42.0	3.23	0.905	0.82	(2) (5) 10	25.7

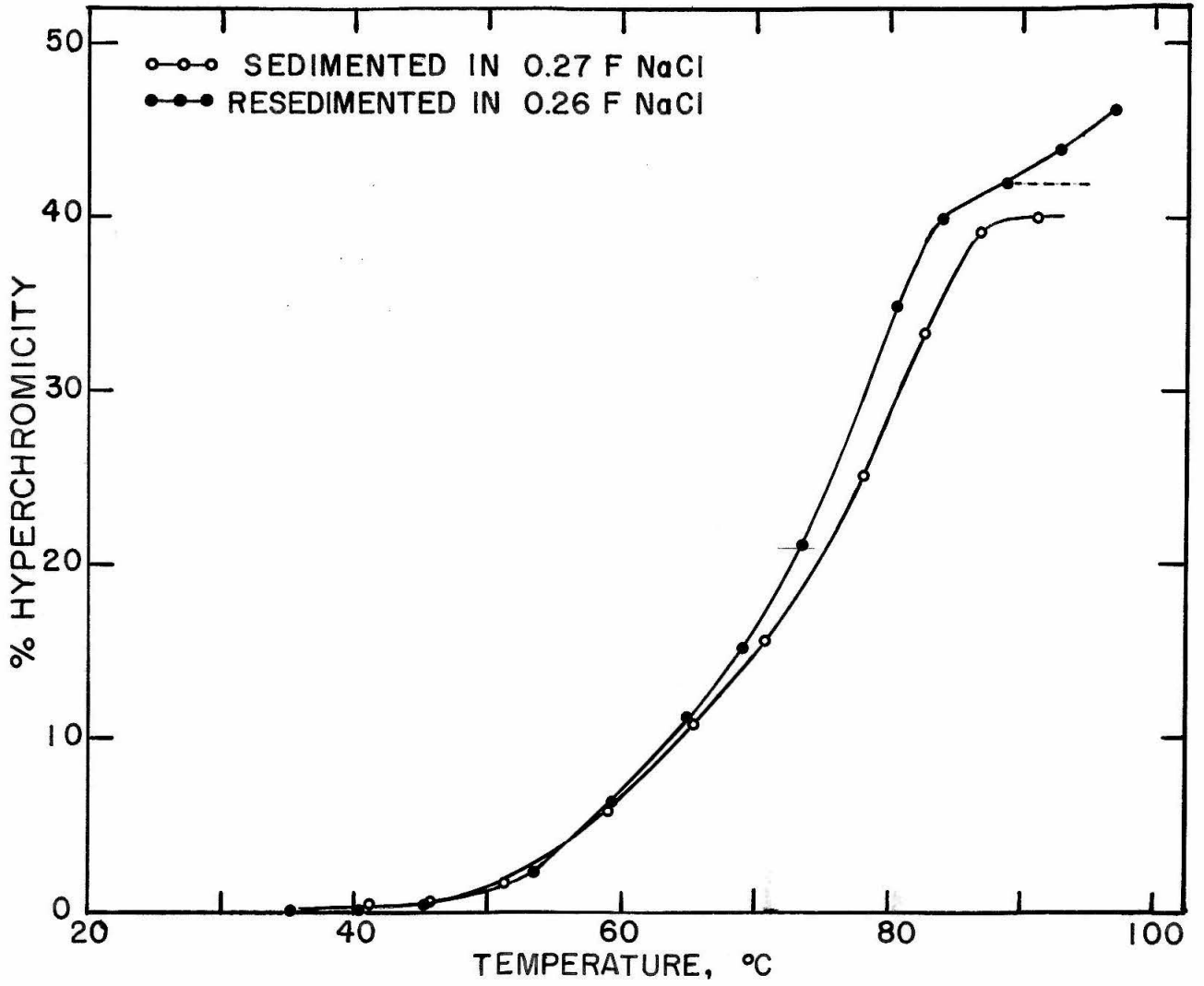
SEDIMENTED IN 0.27 F NaCl
RESEDIMENTED IN 0.26 F NaCl
% HYPERCHROMICITY
TEMPERATURE, °C
0
10
20
30
40
50
20
40
60
80
100

Figure 38

Figure 39

Heat denaturation curves of native calf thymus DNH (A_{260} = 0.732; R_{220} = 0.685) partially extracted by batch sedimentation a) with 0.45 F NaCl and b) resedimented in 0.48 F NaCl.
The samples were heated in 3 x 10^{-4} N Na^+ EDTA (pH 6.3) in the Cary.

Results	T_m °C	% H	Slope	A_{260}	R_{220}	Days Old	Δ °C
a)	69.5	39.1	2.03	0.663	0.995	(7) 12	42.0
b)	68.7	43.2	0.88	0.905	0.90	(7) (9) 15	40.0
initial	56.1	23.0	3.15				25.0
final	81.0	20.2	8.56				15.0

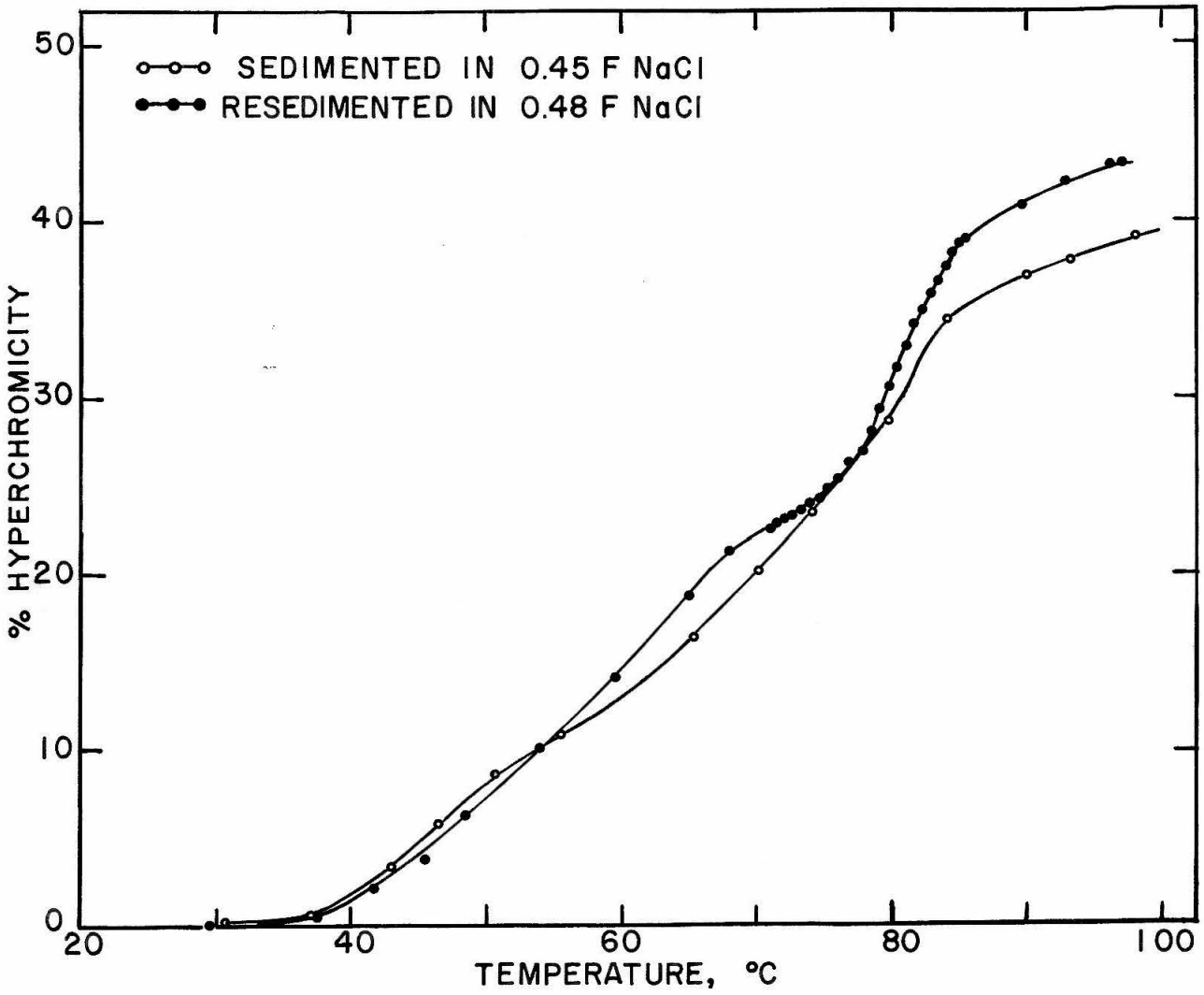
SEDIMENTED IN 0.45 F NaCl
RESEDIMENTED IN 0.48 F NaCl
% HYPERCHROMICITY
0
10
20
30
40
50
20
40
60
80
100
TEMPERATURE, °C

Figure 39

Figure 40

Heat denaturation curves of native calf thymus DNH (A_{260} = 0.760; R_{220} = 0.873) extracted by batch sedimentation with a) 1.80 F NaCl and b) resedimented in 1.94 F NaCl. The samples were heated in 3 x 10^{-4} N Na^+ EDTA (pH 6.3) in the Cary.

Results	Tm°C	% H	Slope	A_{260}	R_{220}	Days Old	Δ °C
a)	43.5	44.0	3.41	0.697	1.16	(0) 3	49.0
initial	38.9	29.0	7.72				13.5
final	75.0	15.0	2.48				35.0
b)	39.7	46.0	5.93	0.782	1.24	(0) (1) 5	58.5
initial	37.7	35.4	7.71				12.5
final	88.8	10.6	3.26				27.0

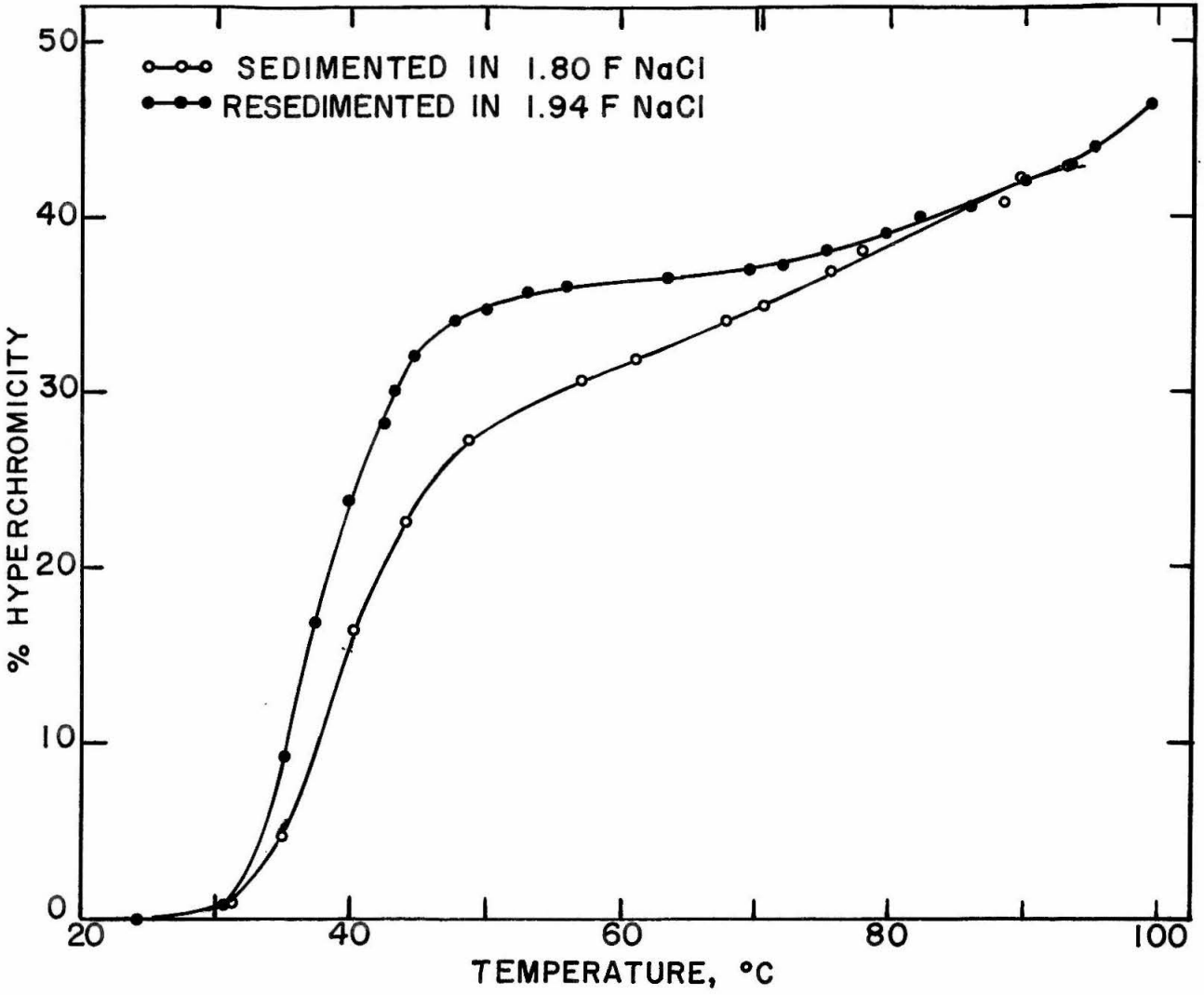
SEDIMENTED IN 1.80 F NaCl
RESEDIMENTED IN 1.94 F NaCl
% HYPERCHROMICITY
TEMPERATURE, °C
0
10
20
30
40
50
20
40
60
80
100

Figure 40

Figure 41

Heat denaturation curve of native calf thymus DNH (A_{260} = 0.760; R_{220} = 0.873) extracted by batch sedimentation with a) 1.80 F NaCl (same as Fig. 40) and b) resedimented in 1.94 F NaCl.
The samples were heated in 3 x 10^{-4} N Na^+ EDTA (pH 6.3) in the Cary.

Results	T_m °C	% H	Slope	A_{260}	R_{220}	Days Old	Δ °C
a)	43.5	44.0	3.41	0.697	1.16	(0) 3	49.0
initial	38.9	29.0	7.72				13.5
final	75.0	15.0	2.48				35.0
b)	40.6	37.2	3.92	0.873	1.32	(0) (1) 10	57.5
initial	37.2	26.0	5.62				13.0
final	82.0	11.2	1.74				42.0

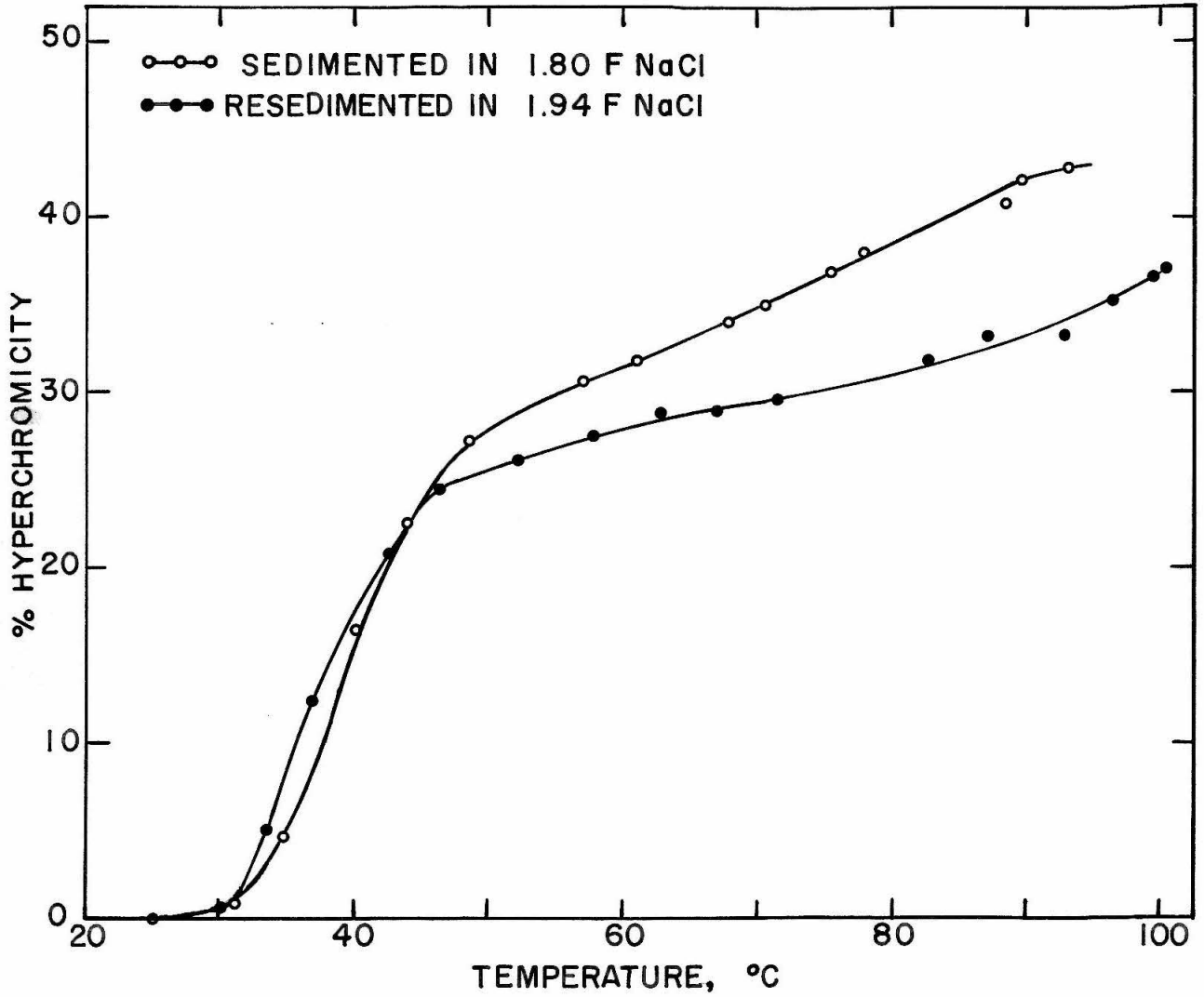
SEDIMENTED IN 1.80 F NaCl
RESEDIMENTED IN 1.94 F NaCl
% HYPERCHROMICITY
0
10
20
30
40
50
20
40
60
80
100
TEMPERATURE, °C

Figure 41

Figure 42

Heat denaturation curves of native calf thymus DNH (A_{260} = 0.732; R_{220} = 0.685) partially extracted by batch sedimentation a) with 0.27 F NaCl (same as Fig. 38a) and b) resedimented in 0.45 F NaCl.
The samples were heated in 3 x 10^{-4} N Na^+ EDTA (pH 6.3) in the Cary.

Results	T_m °C	% H	Slope	A_{260}	R_{220}	Days Old	Δ °C
a)	74.7	39.9	3.21	1.20	0.94	(2) 8	27.7
b)	68.7	38.4	1.90	1.180	0.97	(2)(9)15	43.7
initial	56.7	23.0	2.37				32.0
final	82.3	15.4	8.25				10.3

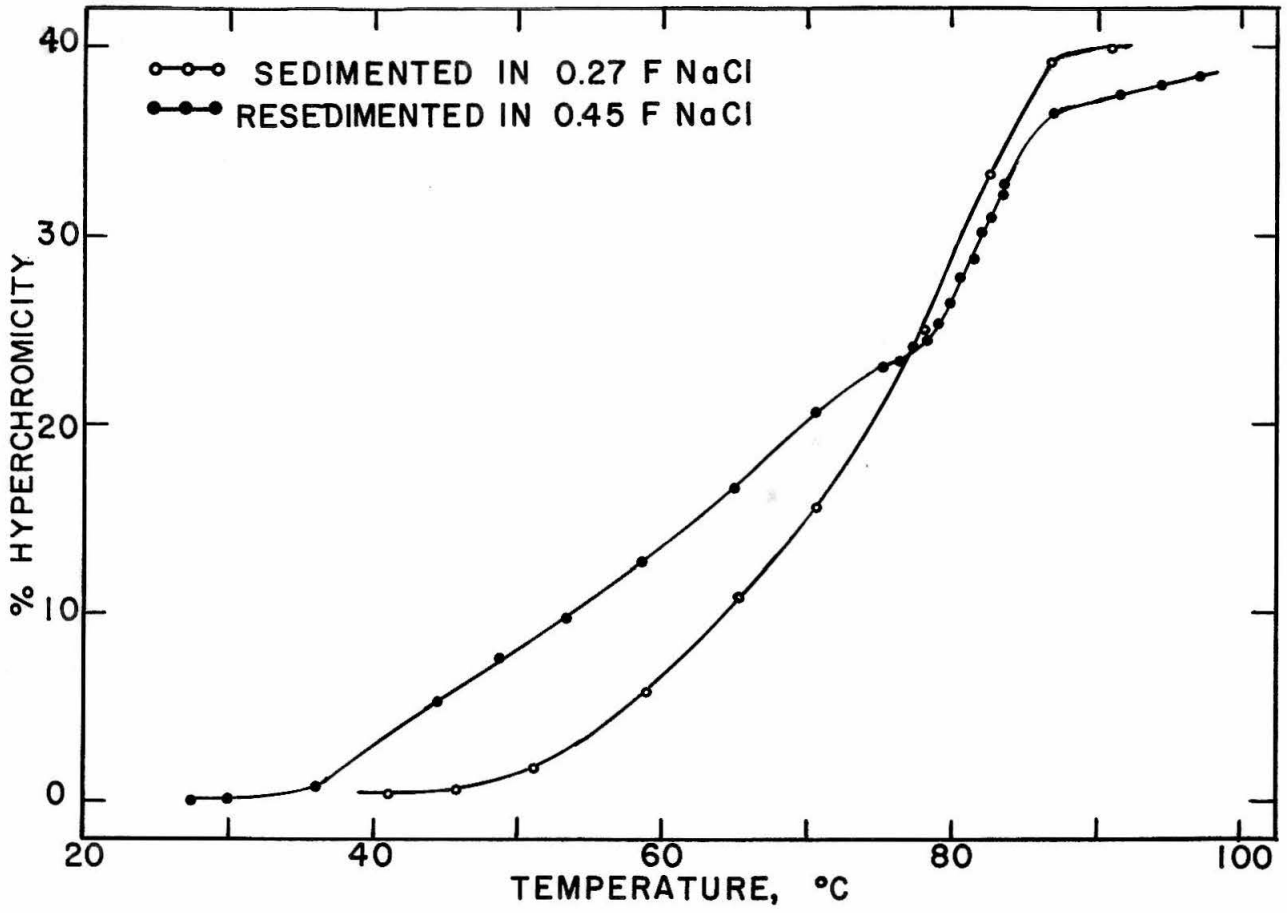
SEDIMENTED IN 0.27 F NaCl
RESEDIMENTED IN 0.45 F NaCl
% HYPERCHROMICITY
0
10
20
30
40
20
40
60
80
100
TEMPERATURE, °C

Figure 42

not very soluble even in dilute H_2SO_4, as evident from the Amberlite chromatography results, makes it unlikely that significant reconstitution occurs on dissolving the pellets. Furthermore, in contemplating resedimentation it must be remembered that nucleohistone degradation continues at an unabated rate, so that some of the changes observed may actually be due to slight degradation.

2. Degradation of Nucleohistones

Prolonged storage of nucleohistones at 4° C causes changes in their properties which seem to be mainly the results of histone degradation. A convenient way of measuring this degradation is by electrophoresis. Table XIV gives some indication as to the magnitude of the changes observed. In every case the mobility increases, either due to a loss or a lowered complexing ability of the histones of native calf thymus DNH. In addition to these increases in mobility, increases in the RNA-priming activity of stored DNH were observed.

Somewhat surprising is the fact that the melting curves of native DNH do not show very pronounced changes upon storage for similar periods of time and the Tm's do not appear very sensitive criteria for the detection of degradation of native DNH.

The most sensitive test for the extent of degradation that we have observed is the ease with which histones can be extracted by salt solutions. Figure 43 shows the absorption pattern of a layer sedimentation experiment of native calf thymus DNH which had been stored for 19 days at 4° C. Comparison with figure 30, which shows a pattern for very fresh DNH, indicates clearly the increase in the amount of

Figure 43

Effect of storage of native calf thymus DNH for 19 days at 4° C on the preparative salt layer zone sedimentation using the SW 25 rotor and plastic sedimentation tubes. The DNH (A_{260} = 1.93; R_{220} = 0.706) in 0.016 F saline citrate was sedimented through layers of increasing D_2O concentrations and $NaClO_4$ formalities as indicated in the boxes in the upper part of the figure. Most of the histones have remained at the top of the first salt layer contrary to the results with undegraded DNH (Fig. 30).

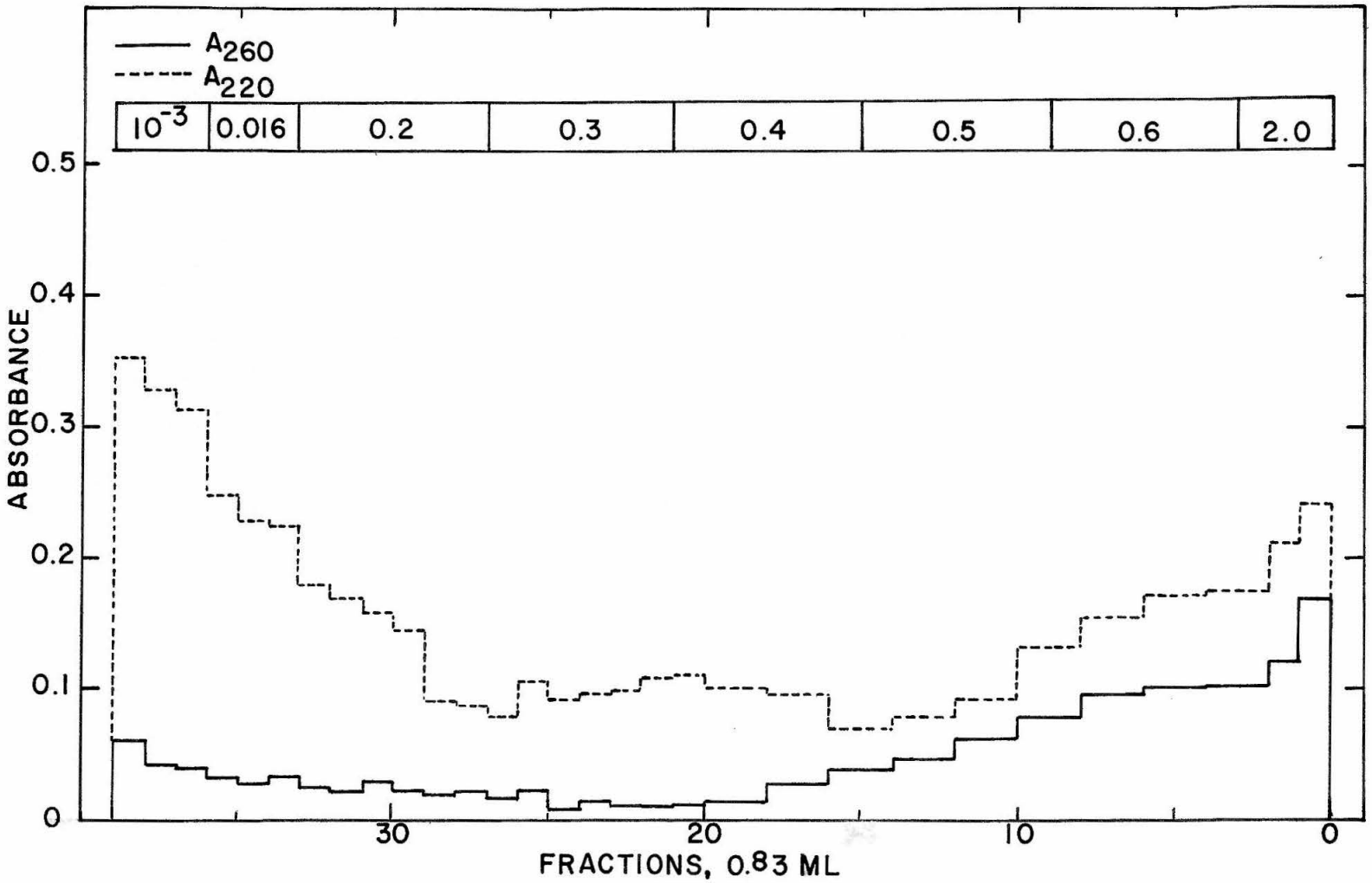
A260
A220
10-3
0.016
0.2
0.3
0.4
0.5
0.6
2.0
ABSORBANCE
0.5
0.4
0.3
0.2
0.1
0
30
20
10
0
FRACTIONS, 0.83 ML

Figure 43

histones which can be extracted or which are largely dissociated by low salt concentrations. Particularly striking are also the data with reconstituted DNH III, which were mentioned earlier (Fig. 25). In this particular case profound changes had already occurred within 6 days after preparation.

Similarly striking increases in mobility are observed if native DNH, which had been stored for extensive periods (36 days), is salt extracted (Table XIV, Sample 1). Evidently, considerably more histones become extractable by low salt concentrations.

Heating curves of DNH, extracted after varying times of storage, reflect changes in the extractability of histones as well. The melting profile is more distinctly two step (Figure 44 and 45), and low salt extracts considerably more histones if the DNH sample is older (Fig. 44). The significance of the rather low R_{220} values of both of the old DNH samples is unknown. However, the lower melting temperatures observed suggest that whatever the material is which contributes to the low R_{220} it is not stabilizing the DNA against melting.

Since there is little indication that the DNA is being degraded during storage - e. g. RNA-priming activity increases, sedimentation runs do not show degraded DNA at the initial zone position - the most probable cause for

Table XIV

Mobilities of $NaClO_4$ Extracted Native Calf Thymus DNH

Sample	nat.	0.20F	0.27F	0.30F	0.40F	0.45F	0.50F	1.0F
# 7 age	1.20* 9			1.33* (8)11	1.57* (8)11		1.84* (8) 9	
# 5 age	1.28* 1							2.05* (0) 4
# 9 age	1.33 5		1.435 (1) 8			1.91 (0) 6		
# 6 age	1.42* 21	1.56* (24)27		1.66* (24)28	1.79* (24)29			

Mobilities of NaCl Extracted Native Calf Thymus DNH

Sample	nat.	0.27F	0.45F	0.48F	0.50F	1.80F	1.94F
# 8 age	1.15 4	1.39* (2) 5	1.53* (7) 9			2.04 (0) 3	
# 8 resed. age	1.38* 10	1.42* (5) 9		1.48±.04 (9)15	1.56* (9)10		2.21-2.28* (1) 6
# 7 age	1.34 36	1.72 (37)39	1.89 (37)39			2.06 (37)44	

* Measurements by B. Olivera
Age denotes total days of storage of DNH at 4° C; the numbers in brackets indicate days of storage until salt extraction was performed.

Reproducibility of measurements was ± 2 % or better unless otherwise indicated.

Underlined data are from samples prepared by zone sedimentation. All others are from batch sedimentation.

Figure 44

Heat denaturation curves of native calf thymus DNH (A_{260} = 0.732; R_{220} = 0.685 and b) A_{260} = 0.815; R_{220} = 0.788) partially extracted by batch sedimentation with 0.27 F NaCl after different times of storage at 4° C.
The samples were heated in 3 x 10^{-4} N Na^+ EDTA (pH 6.3) in the Cary.

Results	T_m °C	% H	Slope	A_{260}	R_{220}	Days Old	Δ °C
a)	74.7	39.9	3.21	1.20	0.94	(2) 8	27.7
b)	62.3	28.2	3.21	0.762	0.663	(37) 43	40.0
initial	55.0	16.8	4.42	(A_{400} = 0.093)			24.4
final	79.5	11.4	5.49				15.0

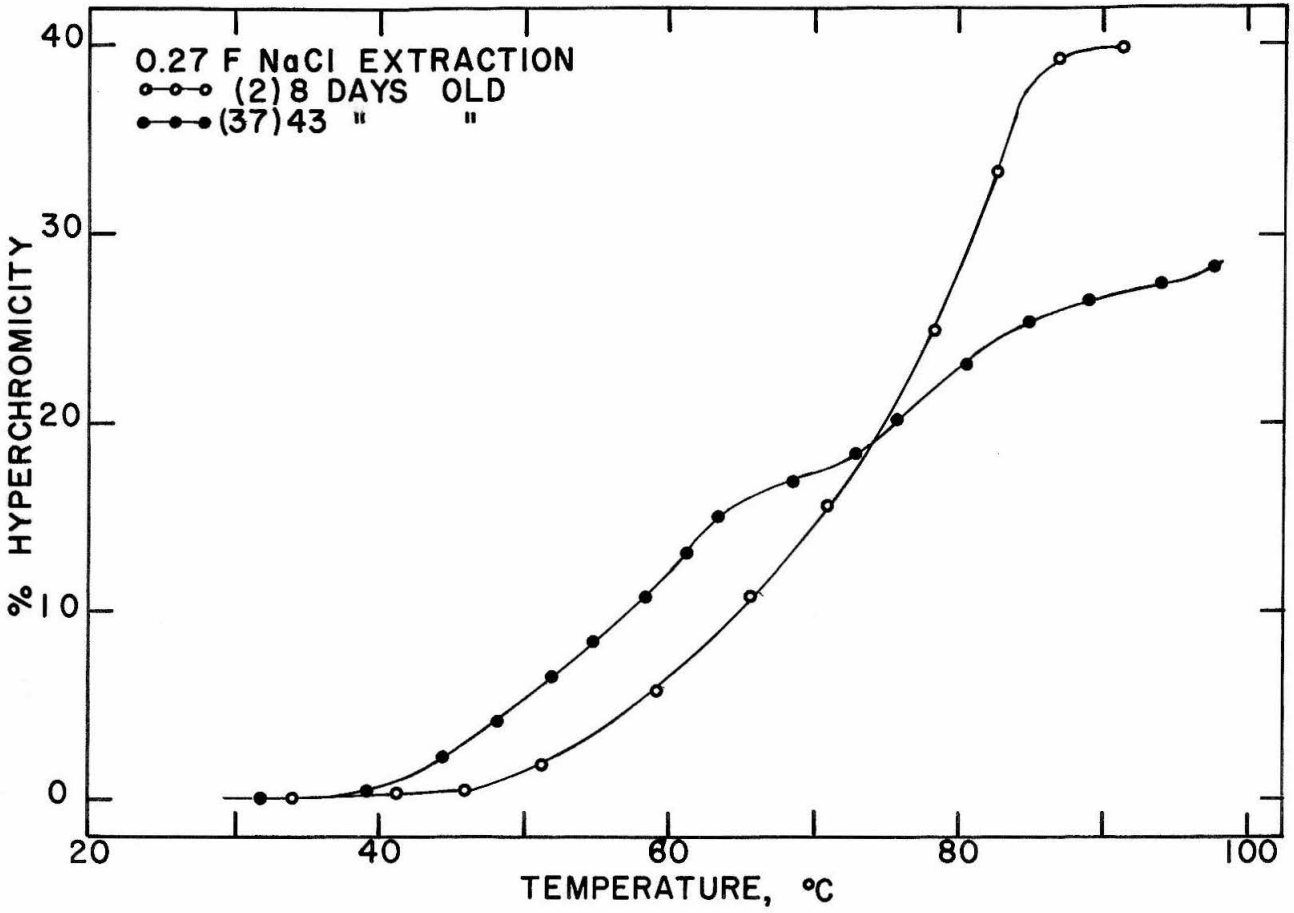
0.27 F NaCl EXTRACTION
(2) 8 DAYS OLD
(37) 43 " "
% HYPERCHROMICITY
0
10
20
30
40
20
40
60
80
100
TEMPERATURE, °C

Figure 44

Figure 45

Heat denaturation curves of native calf thymus DNH (a) A_{260} = 0.732; R_{220} = 0.685 and b) A_{260} = 0.805; R_{220} = 0.794) partially extracted by batch sedimentation with 0.45 F NaCl after different times of storage at 4° C.
The samples were heated in 3 x 10^{-4} N Na^+ EDTA (pH 6.3) in the Cary.

Results	Tm°C	% H	Slope	A_{260}	R_{220}	Days Old	Δ °C
a)	69.5	39.1	2.03	0.662	0.995	(7) 12	42.0
b)	68.8	33.6	1.84	0.667	0.667	(37) 41	39.0
initial	51.0	14.8	4.75				20.0
final	75.6	18.8	6.28				19.0

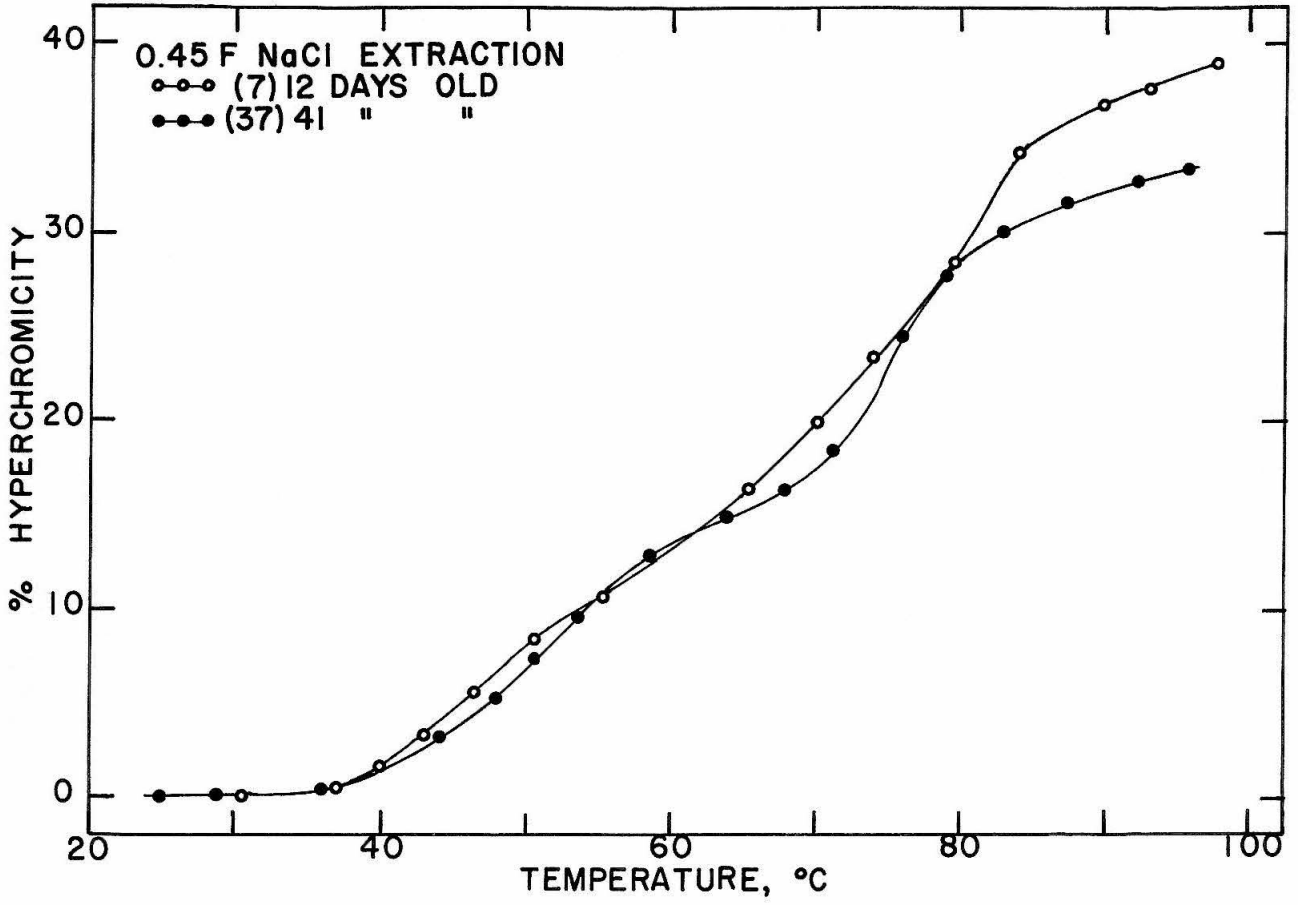
0.45 F NaCl EXTRACTION
(7) 12 DAYS OLD
(37) 41 " "
% HYPERCHROMICITY
0
10
20
30
40
20
40
60
80
100
TEMPERATURE, °C

Figure 45

the changes in the behavior of the DNH upon storage is action of enzymes on the histones. It is quite possible that some of the non-histone proteins observed in the run-off peak during Amberlite fractionations are proteolytic enzymes which could not be removed during preparation of the DNH. (71). Further experiments to clarify this point are however required.

It may be concluded from the foregoing that any results with aged, native DNH samples (say samples stored for more than 14 days) must be considered with caution. Although there probably exist differences in degradability between various DNH preparations, the age of the preparations used should always be stated in order to present meaningful data.

In the following we have adopted the convention that a number in brackets indicates the age in days at which a preparation was salt extracted. The number that follows the brackets indicates the age of the preparation at which the experiment under consideration was performed. Both ages are given, since it seems as if salt extraction decreases the rate at which the residual nucleohistone samples degrade to some extent.

3. RNA-Priming Activity

Having mentioned some of the problems that may be encountered in experiments concerning nucleohistones, we may now turn our attention to the more interesting features of these materials, for instance their ability to sustain DNA-dependent RNA synthesis.

Comparing the activity data of DNH (the measurements were made by Dr. R. C. Huang) which were normalized with respect to the DNA activity and corrected for the activity of the enzyme alone, a sharp increase in RNA priming activity after extraction with 0.2 F to 0.4 F $NaClO_4$ is obvious from figure 46.

The figure shows preliminary results of two series of activity measurements made on the same preparation of DNH. The data of curve I were obtained using the DNH sample immediately after preparation and salt extraction but a slightly aged RNA polymerase preparation. The data of curve II represent the results if the salt extraction is carried out 5 days after preparation of the DNH and a fresh preparation of RNA polymerase is used. Although it is not possible to assess whether the difference in the shape of these curves is due to the effects of storage or to the freshness of the RNA polymerase, it is clear that salt extrac-

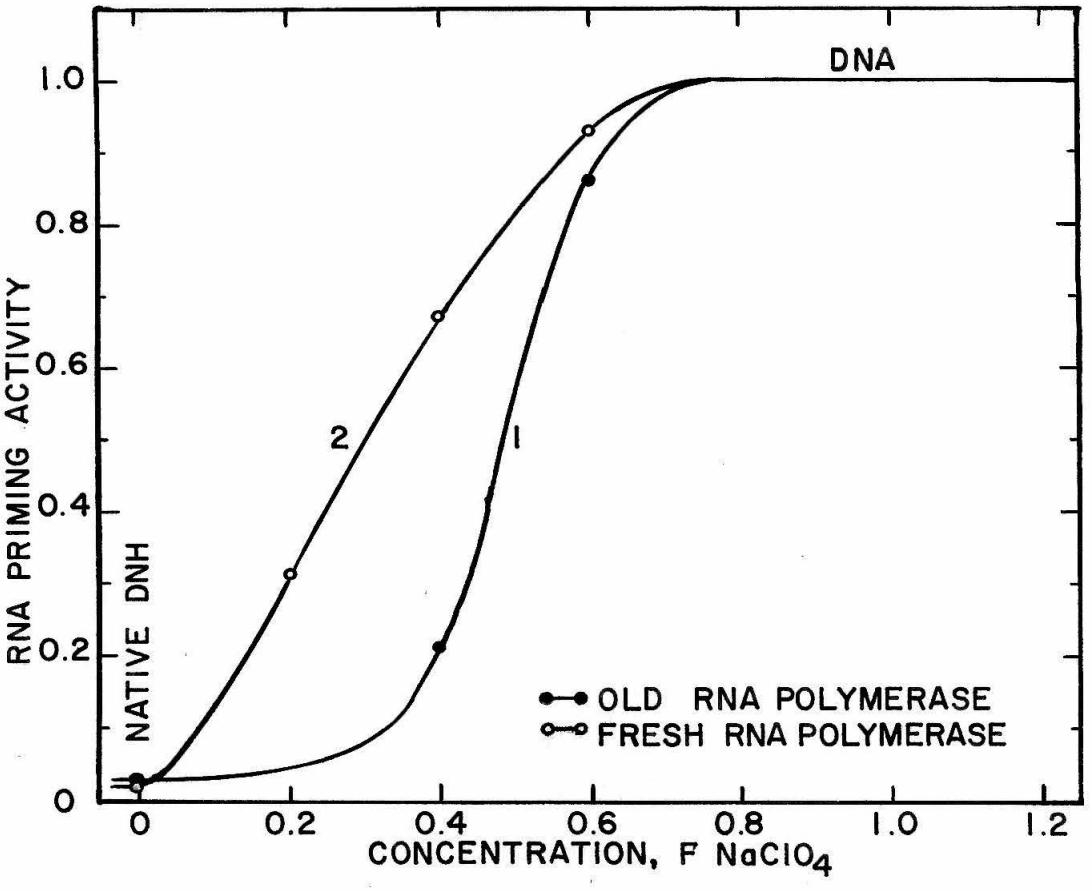

Figure 46

Preliminary results of the effects of salt extraction of histones from native calf thymus DNH on its RNA-priming activity.
Curve 1: 19.6 micrograms of DNA were used per measurement. The RNA polymerase preparation was old.
Curve 2: 8.35 micrograms of DNA were used per measurement. The RNA polymerase preparation was fresh.

tion increases the activity of the original DNH. Extraction of histones with 0.6 F $NaClO_4$ gives a pellet which has close to 90 % of the RNA-priming activity of DNA. More detailed results under standardized conditions are required to determine the contribution of the individual histone fractions more exactly.

Prof. Bonner and coworkers have investigated the possibility of whether salt extraction activates individual genes specifically by tracing the relative amounts of globulin made by salt extracted pea bud nucleohistones. Preliminary results indicate that some specific activation is indeed observed in this case (72).

4. Zone Electrophoresis of Salt Extracted Native Calf Thymus Nucleohistones

Our electrophoretic mobility measurements of partially salt extracted DNH are summarized in table XIV. The data are grouped according to $NaClO_4$ and NaCl extractions. Most samples were obtained by batch sedimentation. Those, whose mobilities are underlined, were prepared by sedimenting a 1 ml zone of DNH through solutions containing a uniform salt concentration. Only the 1.0 F $NaClO_4$ extracted DNH was obtained as a pellet from a salt gradient experiment in D_2O (0.4 - 1.0 F gradient).

The results confirm that a) extraction with increasing salt concentrations increases the total charge of the DNH by removal of the positively charged histones, and that b) NaCl is not quite as efficient as $NaClO_4$ in extracting histones from calf thymus DNH.

Furthermore, from the fact that only single, although at times somewhat broad peaks are observed (Fig. 47 a to f) shows typical bands of salt extracted DNH in comparison to native DNH) we conclude that c) the various kinds of histones must have been removed in approximately equal proportions from the individual DNH molecules.

The singlebandedness of the partially salt extracted native DNH is the most convincing evidence that gross

Figure 47

Successive position and shape of native and partially extracted DNH bands during zone electrophoresis.
Separation between markers, M, equals 3 cm actual distance traveled. Amount of current is given in arbitrary units for the final position of the bands only.

Sample	μ	days old
a) native DNH	1.33	5
b) 0.27 F $NaClO_4$ extract	1.435	(1) 8
c) 0.45 F $NaClO_4$ extract	1.91	(0) 6
d) native DNH	1.35	36
e) 0.48 F NaCl extract	1.53	(7)(9) 15
f) 1.80 F NaCl extract	2.04	(0) 3

Sample e) was resedimented.
Sample f) shows in the last scan of the band an electrophoretic anomaly, a minor artifact peak that travels faster than the main peak (see also ref. 55).

μ = mobility in 10^{-4} $cm^2/V\text{-}sec$

Figure 47

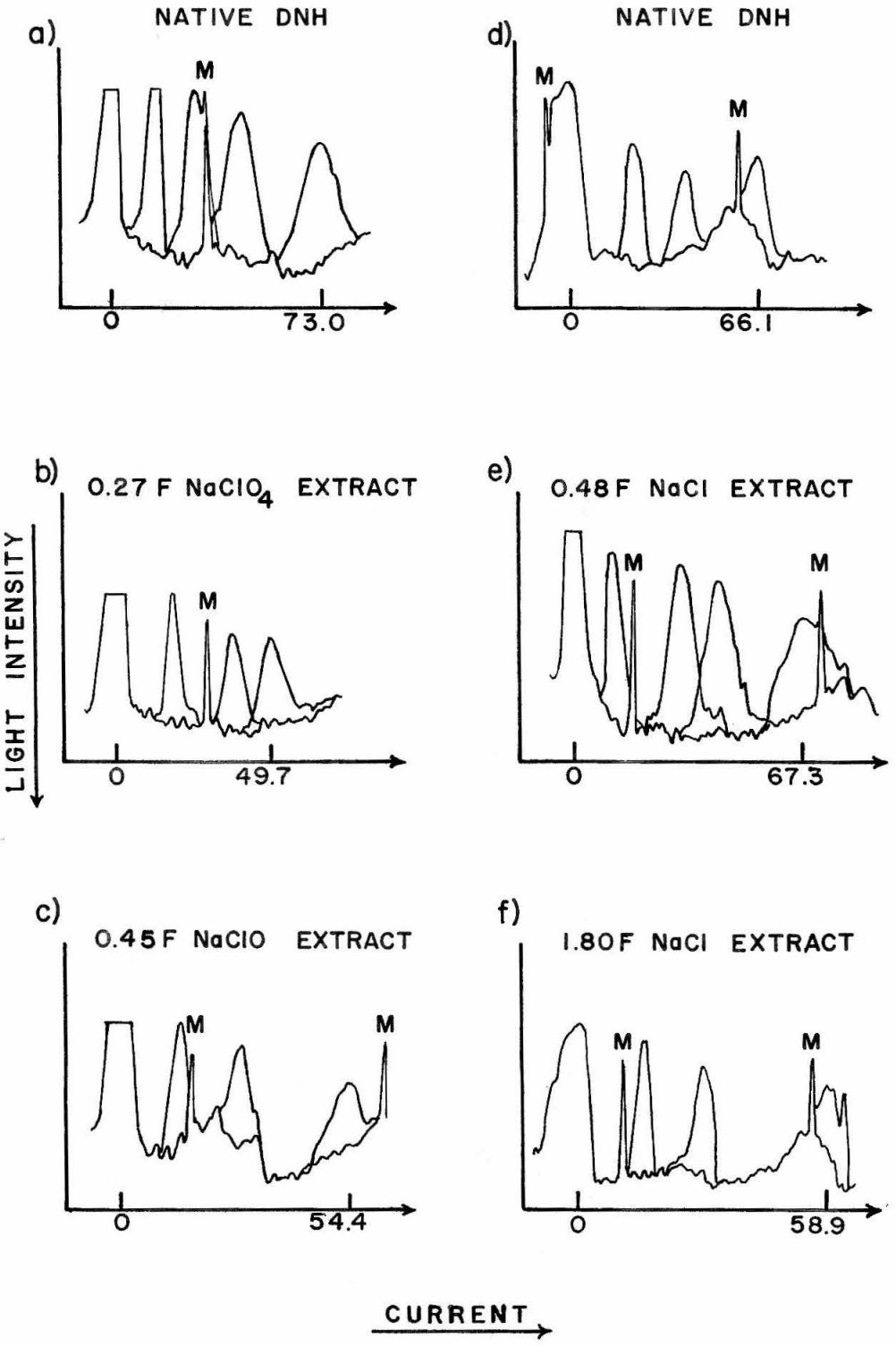
a)
NATIVE DNH
M
0
73.0
d)
NATIVE DNH
M
M
0
66.1
b)
0.27 F NaClO4 EXTRACT
M
0
49.7
LIGHT INTENSITY
e)
0.48 F NaCl EXTRACT
M
M
0
67.3
c)
0.45 F NaClO EXTRACT
M
M
0
54.4
f)
1.80 F NaCl EXTRACT
M
M
0
58.9
CURRENT

intermolecular heterogeneity does not exist. This conclusion was reached because of the results of mixing experiments performed by B. Olivera (73). He has shown that electrophoretic separation of DNA and DNH is governed by the following facts:

1. Histone II, once complexed to DNA, does not redistribute at low ionic strength (10^{-2} N) to noncovered DNA regions.

2. Histone I, reconstituted as such or as a part of whole histones to DNA, redistributes readily at low ionic strength to non-covered DNA regions, but the histone I in native DNH redistributes much more slowly under similar conditions.

3. Histone III and histone IV, once complexed to DNA, do probably not exchange at low ionic strength, but since the mobilities of even fully complexed DNH III or DNH IV is close to that of DNA, resolution of the material by electrophoresis is difficult.

The evidence for these statements comes from the successful electrophoretic separation of the following:

a) Fully complexed DNH II from DNA, DNH I, DNH III and native DNH.

b) Partially complexed DNH II from DNA.

c) Native DNH and chromatin from DNA under only slight modifications of the mobility (that of DNH is increased,

that of DNA slightly reduced) indicating a limited exchange of some mobility retarding material.

On the other hand, it was not possible to separate the following materials electrophoretically:

a) Reconstituted DNH I from DNA or partially reconstituted DNH II, and

b) reconstituted whole DNH from DNA.

Since salt extracted, native DNH, from which histones I or I and II were removed, could not be resolved into two or more bands, it must be concluded that the histone fractions are not chromosome or molecule specific (see also melting curve results).

In the following, attempts are made to correlate the observed mobility data with values calculated for a number of hypothetical situations.

Changes in the electrophoretic mobility of DNH after salt extraction of histones should be related to the overall changes in DNH charge and therefore to the amount of charge removed as histones. Using the known amino acid composition of the histone fractions, it should be possible to predict these changes in mobility, if it is assumed that changes in the friction coefficient and counterion effects due to the histone removal are negligible, i. e. if the mobility is directly proportional to the charge only.

If a mobility of 2.18×10^{-4} $cm^2/V\text{-}sec$ (74) is taken to represent DNA which is 100 % charged, then the % charge of the various nucleohistone samples can be calculated and the change in total charge upon salt extraction compared to the amount of histone removed.

Thus, an average molecular weight per amino acid residue was calculated (Table XV, Line a) from the amino acid compositions of the various histone fractions, as determined by Huang, Bonner, and Murray (75). Assuming that all of the acidic (Line c) and basic (Line b) amino acids are charged, the moles of net charge per 100 g of histone fraction were computed (Line e). From the weight percent of the histone

Table XV

Calculation of Mole % Charge of DNH

Histones	H Ib	H IIb	H III	H IV	DNA
a) av. MWT/AA	103.32	112.44	114.90	115 97	324
b) M% + AA	28.6	24.3	23.9	23.4	0
c) M% - AA	6.8	14.3	14.3	15.1	100
d) M% charge	+21.8	+10.0	+ 9.6	+ 8.3	-100
e) M% C/100g H	+.2110	+.0889	+.08355	+.07157	-.309
			+.07756		

Histones	H Iab	H IIab	H III(IV)	RUN-OFF	DNA
f) % TCA ppt.	26.4	51.1	16.4	6.1	-
g) % H fract.	28.1	54.4	17.5	0	-
h) M% C/100g H	+.0593	+.0484	+.0136		-.309
H/D = 1.5					
i) M% C/100g D	+.0889	+.0726	+.0204		-.309
H/D = 1.0					
j) M% C/100g D	+.0593	+.0484	+.0136		-.309
H/D = 0.5					
k) M% C/100g D	+.0296	+.0242	+.0068		-.309

fractions in whole calf thymus histone (Line g), as determined by Amberlite chromatography (Fig. 1), and from an assumed histone to DNA weight ratio for native DNH, the net moles of positive charge due to the individual histone fractions per 100 g of DNA were calculated (Line i - k) and compared to the negative charge of the DNA. Hypothetical mobilities can then be derived for totally covered, native DNH (Table XVI, Column 2), and for samples from which histone I (Column 3) or histones I and II (Column 4) were extracted.

A comparison of the mobility of native DNH with those calculated (Table XVII) shows that the closest agreement is obtained if the H/D is assumed to be between one and 1.5. However, the observed mobilities for extracted calf thymus DNH are in general lower than the corresponding calculated values.

This discrepancy may be due in part to the presence in the histone fractions of glutamine and aspargine instead of the negatively charged glutamic and aspartic acid, as was assumed in the calculations. If the amounts of amide found by several investigators (76) are taken into consideration (Table XVIII, Line d), then somewhat lower mobilities are calculated (Table XIX, Lines d). Again, the agreement is best with DNH having an H/D between one and 1.5, however

Table XVI

Hypothetical Mobilities

H/D = 1.5

Removed Histones	None	H I	H I&II	All
a)M% charge/100g DNA	0.1819	0.0930	0.0204	0
b) % complexed DNA	58.9	30.1	6.6	0
c) % free DNA	41.1	69.9	93.4	100
d) mobility	0.895	1.525	2.035	2.18

H/D = 1.0

Removed Histones	None	H I	H I&II	All
a)M% charge/100g DNA	0.1213	0.0620	0.0136	0
b) % complexed DNA	39.3	20.1	4.4	0
c) % free DNA	60.7	79.9	95.6	100
d) mobility	1.325	1.74	2.08	2.18

H/D = 0.5

Removed Histones	None	H I	H I&II	All
a)M% charge/100g DNA	0.0606	0.0310	0.0068	0
b) % complexed DNA	19.6	10.0	2.2	0
c) % free DNA	80.4	90.0	97.8	100
d) mobility	1.75	1.96	2.135	2.18

Table XVII

Comparison of Calculated And Observed Mobilities

Observed Mobilities DNH Samples Less Than 2 Weeks Old			Calculated Mobilities for H/D of		
Salt Conc.	$NaClO_4$	NaCl	1.5	1.0	0.5
Native DNH			Fully Covered		
0	1.15 - 1.38		0.895 <u>0.566</u>	1.325 <u>1.104</u>	1.75 <u>1.64</u>
Histone I Removed					
0.20 F 0.27 F 0.30 F	1.435 1.33	1.39	1.525 <u>1.26</u>	1.74 <u>1.57</u>	1.96 <u>1.87</u>
Histones I & II Removed					
0.40 F 0.45 F 0.50 F	1.57 1.91 1.84	 1.53 1.56	2.035 <u>1.96</u>	2.08 <u>2.04</u>	2.135 <u>2.11</u>
All Histones Removed					
1.0 F 1.8 F	2.05	 2.04	2.18	2.18	2.18

All mobilities are in units of 10^{-4} $cm^2/V\text{-}sec$.

The underlined numbers were calculated by considering mole percent of amide (Tables XVIII and XIX).

Table XVIII

Calculation of Mole % Charge of DNH

Includes Amide (76)

Histones	H Ib	H IIb	H III	H IV	DNA
a) av. MWT/AA	103.32	112.44	114.90	115.97	324
b) M% + AA	28.6	24.3	23.9	23.4	0
c) M% - AA	6.8	14.3	14.3	15.1	100
d) M% Amide	2.4	3.7	4.5	4.5	0
e) M% charge	+24.2	+13.7	+ 14.1	+12.8	-100
f) M% C/100g H	+.2343	+.1218	+ .1227	+ .1104	-.309
			+.11655		

Histones	H Iab	H IIab	H III(IV)	RUN-OFF	DNA
g) % TCA ppt	26.4	51.1	16.4	6.1	-
h) % H fract.	28.1	54.4	17.5	0	-
i) M% C/100g H	+.06584	+.06626	+.02040		-.309
H/D = 1.5					
j) M% C/100g D	+.09876	+.09939	+.03060		-.309
H/D = 1.0					
k) M% C/100g D	+.06584	+.06626	+.02040		-.309
H/D = 0.5					
l) M% C/100g D	+.03292	+.03313	+.01020		-.309

Table XIX

Hypothetical Mobilities

H/D = 1.5

Removed Histones	None	H I	H I&II	All
a) M% charge/100g DNA	0.2288	0.1300	0.0306	0
b) % complexed DNA	74.03	42.07	9.90	0
c) % free DNA	25.97	57.93	90.10	100
d) mobility	0.566	1.263	1.964	2.18

H/D = 1.0

Removed Histones	None	H I	H I&II	All
a) M% charge/100g DNA	0.1525	0.0867	0.0204	0
b) % complexed DNA	49.35	28.05	6.60	0
c) % free DNA	50.65	71.95	93.40	100
d) mobility	1.104	1.569	2.036	2.18

H/D = 0.5

Removed Histones	None	H I	H I&II	All
a) M% charge/100g DNA	0.0762	0.0433	0.0102	0
b) % complexed DNA	24.68	14.02	3.30	0
c) % free DNA	75.32	85.98	96.70	100
d) mobility	1.642	1.874	2.108	2.18

the calculated mobility for fully complexed DNH is now too low in comparison to the observed values. (Table XVII).

In summary, it seems as if changes in the net charge of DNH due to the selective extraction of histones account only qualitatively for the observed changes in mobility. Perhaps, the selective removal of individual histone fractions is not quite as quantitative as was assumed in the calculations, or as clearly differentiated into fractions as indicated by our Amberlite chromatography. On the other hand we have no guarantee that the friction coefficient remains unchanged during salt extraction of histones, so that the discrepancy between observed and calculated mobilities is due to structural changes of the DNH. Viscosity measurements on partially salt extracted DNH should clarify this point.

5. Distribution of Histones Along the DNA Helix (Heating Curve Results)

A detailed discussion of our heat denaturation experiments with partially salt extracted native DNH and partially reconstituted DNH is presented next. Possible interpretations of the results and their implications with regard to the distribution and interaction of the various histone fractions with DNA are considered.

Here the inherent complexity of the histone - DNA interaction becomes perhaps more apparent than in any of the previous sections. The individual histone fractions show not only distinctly different effects on the melting behavior of DNA, but there exists the possibility that the acid extracted histones and their complexes with DNA are not structurally identical to native DNH.

Having indicated that our electrophoresis results show that intermolecular heterogeneity of histones bound to DNA is rather unlikely, we now focus our attention on the alternative situation: the extent of intramolecular heterogeneity of histone binding. It is hoped that information concerning the distribution of histone fractions along the DNA helix might give clues to the significance of the histone - DNA interactions and to the manner in which the histones inhibit the RNA-priming ability of DNA.

a) General Considerations of Heat Denaturation

Next to direct examination of the partially salt extracted, native DNH by electronmicroscopy - a distinct possibility for future work - probably the most informative data which have bearing on this problem are those obtained from heating experiments. In a number of treatises dealing with the heat denaturation of DNA it is believed that a certain minimum number of basepairs must be broken in order for denaturation (unwinding of the strands) to proceed at a detectable rate. From 10 to perhaps 100 basepairs (77) are assumed to be involved in this "cooperative unit". It then follows that longer, for instance gene-size DNA regions extending over about 500 basepairs, would melt close to the temperature at which the pure DNA molecule melts. Similarly, large regions which are completely covered with histones would melt like DNH. However, such a situation exists only if the histones are bound irreversibly to the DNA. Only then is it possible to melt the regions selectively.

In order to get as good a resolution of these melting regions as possible, low ionic strength solutions were used for the heating experiments. To eliminate divalent ions, which are known to stabilize the DNA helix against melting (78), we used 10^{-4} F EDTA solutions (3×10^{-4} N in Na^+ , pH 6.3). B. Olivera's heating curves were done in

7.5×10^{-4} N Na^{+}-EDTA (pH 8). For the first medium the midpoint of the melting profiles (Tm) for DNA and DNH differ by 39.5° C, in the second medium the difference is about 30° C. Thus, if the extracted DNH consists of any kind of alternating sequence of gene or larger size DNA and DNH regions, we would expect a rather distinct two step melting curve with a separation of about 40° C between the two steps (30° C in the other solvent). If in the other extreme the remaining histones are randomly distributed along the DNA strand, only a broad melting curve should be observed and the Tm should decrease in proportion to the amount of histones extracted.

On the other hand, if the histone - DNA interactions are reversible and the histone molecules can migrate along the DNA, then it becomes more difficult to predict the melting behavior of the DNA. We must now consider the relative strength of histone binding to native as against denatured DNA and the possible redistribution of the histones along the DNA during heating.

If a redistribution of histones occurs during the melting of only sparsely covered DNA regions, so that the more thickly covered, still native regions are even more stabilized against denaturation, then one should expect a melting behavior similar to that observed with magnesium DNA (79). In this case the melting profile of DNA is consider-

ably broadened as small amounts (less than one equivalent of Mg^{++} per phosphate) of Mg^{++} are added to the DNA solution. The melting curve remains essentially symmetrical around Tm. This behavior was explained by the migration of Mg^{++} ions from denaturing regions to still-native regions whose stability they enhance.

Alternatively, if histones were bound more strongly to denatured DNA (an unlikely assumption if the histones are really the agents controlling the genetic activity of native DNA) then the melting curves should be similar to those observed with ribonuclease (80). Here the overall effect is a destabilization of the DNA helix at low ionic strength, which manifests itself by a decrease in the melting temperature.

b) Heating Curves of Reconstituted Calf Thymus DNH

Heating experiments with native DNH and with reconstituted DNH I, DNH IIb and DNH III(IV) rule out the possibility that any of the histone fractions bind denatured DNA more strongly than native DNA. But here ends the behavior common to all histone fractions. The interesting differences that exist between the various DNH preparations will now be discussed in turn. The experiments with reconstituted DNH were performed by B. Olivera and the interpretation of the data is the product of long hours of mutual discussion.

Figures 48 to 50 summarize Olivera's heating experiments with reconstituted calf thymus nucleohistone preparations which varied in their histone coverage as determined by R_{220}. Figure 48 shows the denaturation behavior of partially reconstituted DNH I. The curves mimic those of Mg^{++}-DNA (79): The melting profile of DNA is broadened considerably when even a little (H/D = 0.18) histone I is associated with the DNA; the profile sharpens beyond that of native DNH as the histone coverage becomes more complete. The Tm increases with increasing amounts of associated histone I until a melting temperature higher than that of fully complexed native DNH is reached.

Figure 48

Heat denaturation curves of reconstituted calf thymus DNH I compared to calf thymus DNA and native DNH. The samples were heated in 7.5 x 10^{-4} N Na^+ EDTA (pH 8) in the Gilford by B. Olivera.

Results	Tm°C	% H	Slope	A_{260}	R_{220}	H/D	Δ °C
DNA	46.7	37.6	7.66	0.848	1.66	-	13.0
rec. DNH	59.8	36.6	2.49	0.724	1.33	0.18	32.8
" "	67.5	35.7	3.33	0.744	1.17	0.38	30.4
" "	76.8	33.7	5.28	0.786	0.98	0.72	18.1
DNH	76.2	36.0	3.61	0.860	0.81	1.16	24.6

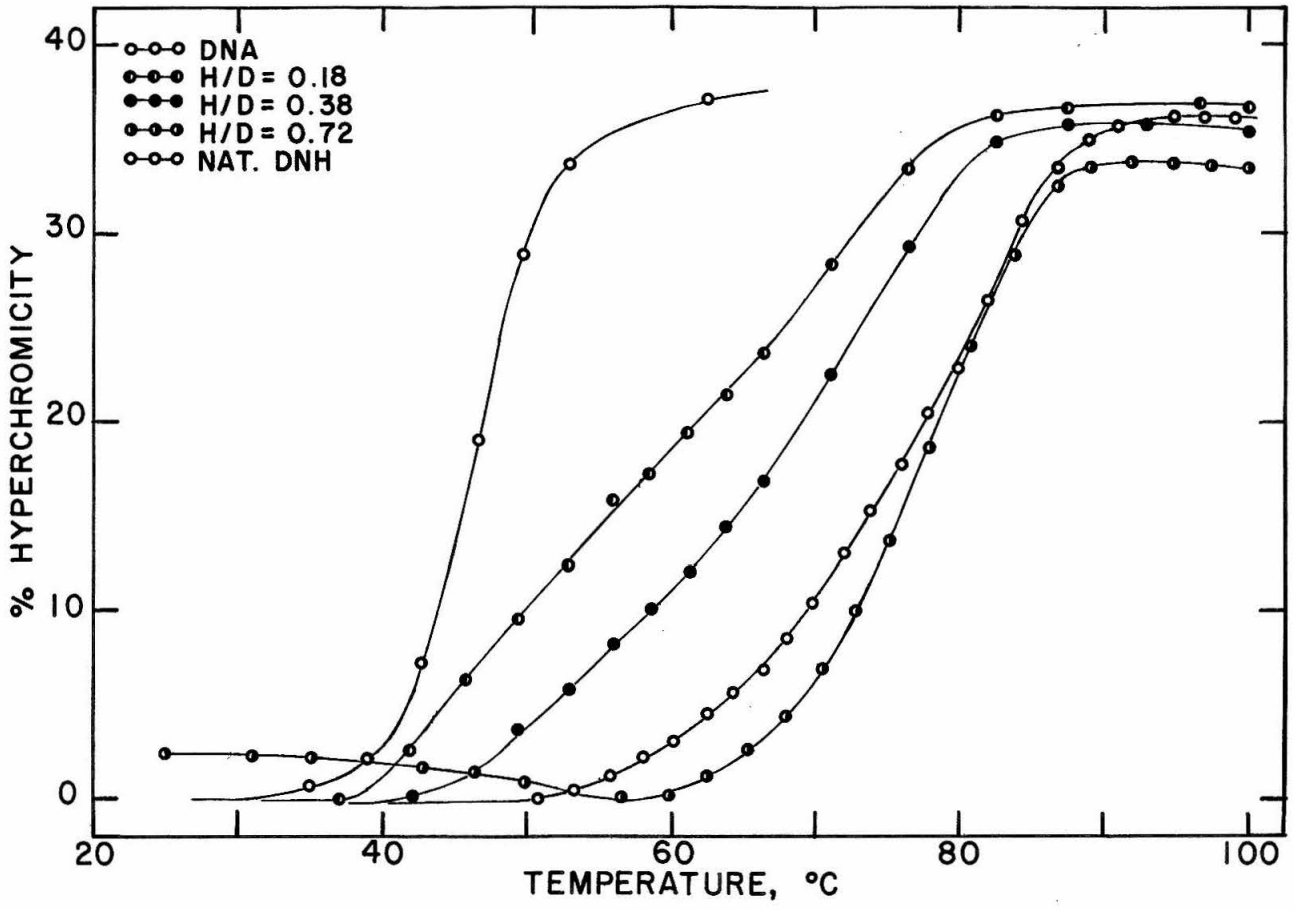
DNA
H/D = 0.18
H/D = 0.38
H/D = 0.72
NAT. DNH
% HYPERCHROMICITY
0
10
20
30
40
20
40
60
80
100
TEMPERATURE, °C

Figure 48

The results are interpreted similarly to those of Mg^{++} DNA: Histone I binds stronger to native than to denatured DNA. It is capable of traveling along the DNA strand to still-native regions as melting of partially covered regions progresses accounting for the pronounced broadening of the transition at low histone coverage. (That histone I can migrate between DNA regions and molecules has already been mentioned in the section on electrophoresis).

Reconstituted DNH IIb (Fig. 49) is not as stabilized against melting as DNH I at comparable H/D, which is most likely due to the lower net positive charge per weight of histone IIb (Table XV). The normalized slope of the curves at Tm changes only slowly with the amount of histone IIb associated with the DNA. The Tm increases in proportion to the amount of histone IIb bound to the DNA.

Figures 50 and 51 show the renaturation behavior of two DNH IIb samples differing in their H/D. For comparison a sample of DNA (Fig. 52) was renatured simultaneously with the other two samples. Aside of the previously discussed differences in Tm and the constancy of the normalized slopes at Tm of the DNH IIb samples, the most striking difference between the DNA and the DNH IIb renaturation curves is the shape of the "hysteresis" loops. The width

Figure 49

Heat denaturation curves of reconstituted calf thymus DNH IIb compared to calf thymus DNA and native DNH. The samples were heated in 7.5 x 10-4 N Na^+ EDTA (pH 8) in the Gilford by B. Olivera.

Results	Tm°C	% H	Slope	A_{260}	R_{220}	H/D	Δ °C	A_{400}
DNA	46.7	37.6	7.66	0.848	1.66	-	13.0	
rec. DNH	50.1	33.8	2.75	0.54	1.20	0.34	30.5	
" "	61.5	31.0	2.95	0.59	0.98	0.72	32.0	
" "	67.6	31.0	3.57	0.60	0.91	0.88	31.0	0.038
DNH	76.2	36.0	3.61	0.86	0.81	1.16	24.6	

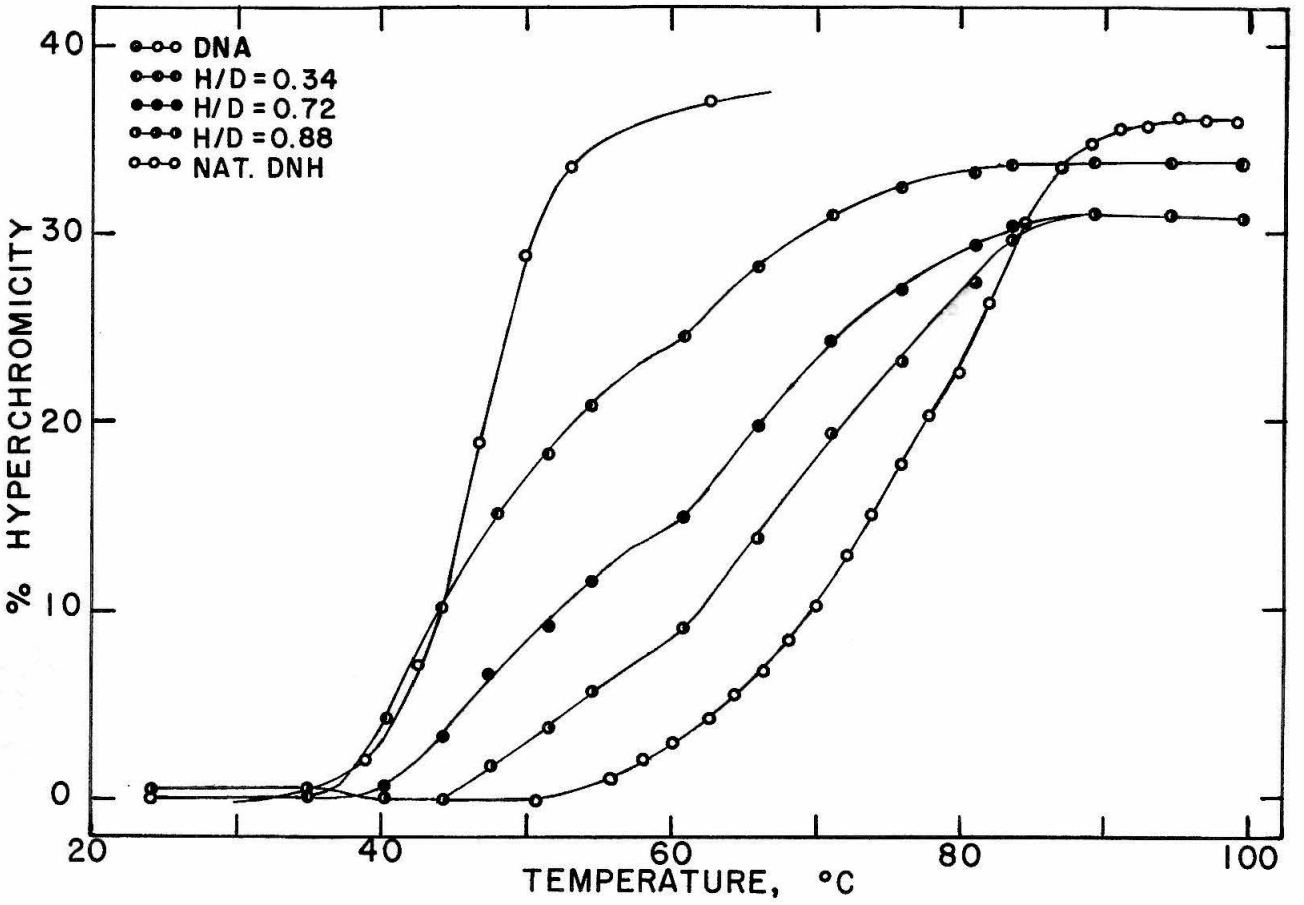
DNA
H/D = 0.34
H/D = 0.72
H/D = 0.88
NAT. DNH
% HYPERCHROMICITY
0
10
20
30
40
20
40
60
80
100
TEMPERATURE, °C

Figure 49

Figure 50

Heat denaturation and renaturation curves of reconstituted calf thymus DNH IIb in 7.5×10^{-4} N Na^+ EDTA (pH 8). Sample and heating experiment by B. Olivera in the Gilford.

Results	Tm°C	% H	Slope	A_{260}	R_{220}	H/D
Overall	48.7	35.6	2.90	0.514	1.18	0.38

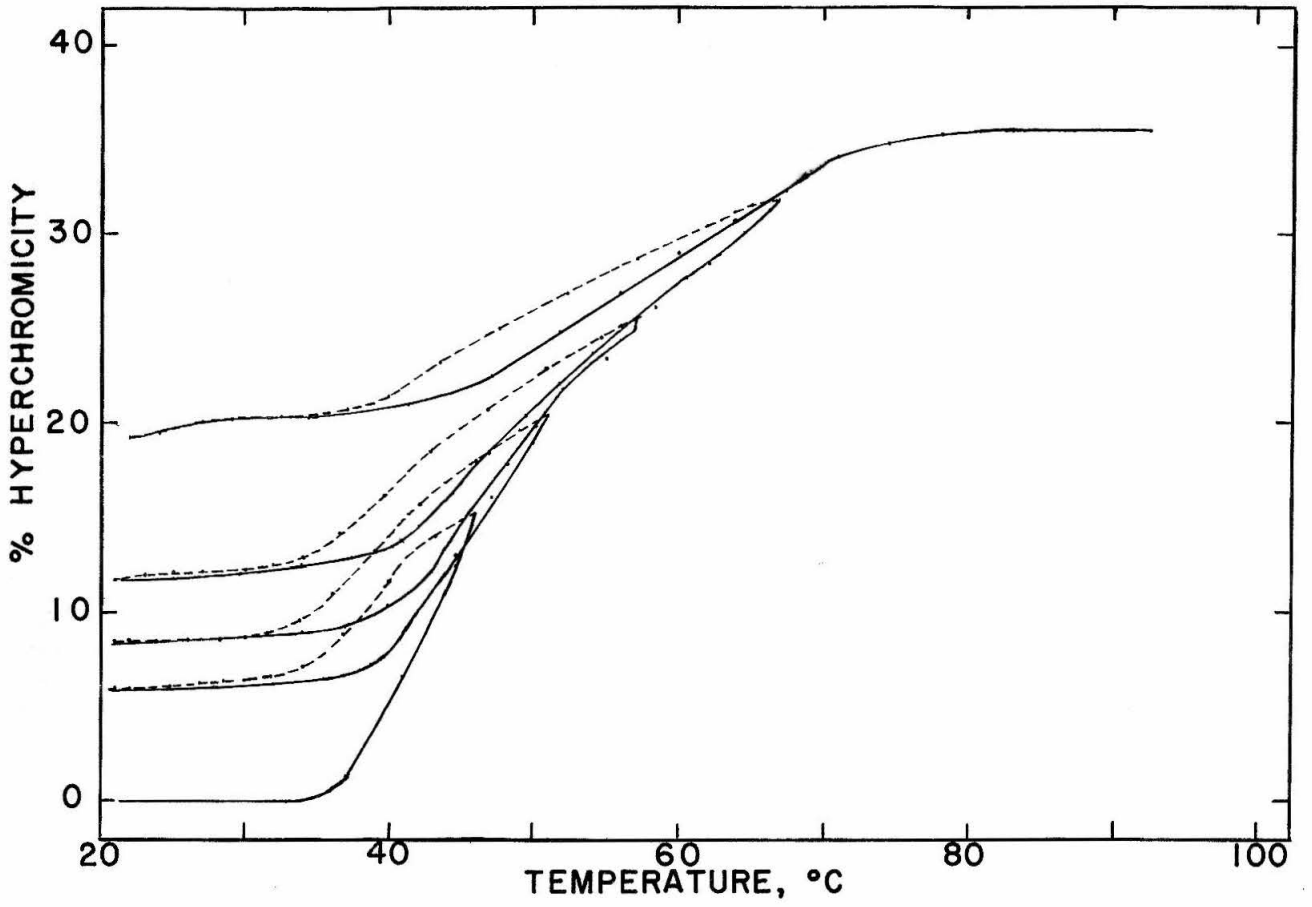

Figure 50

Figure 51

Heat denaturation and renaturation curves of reconstituted calf thymus DNH IIb in 7.5 x 10^{-4} N Na^+ EDTA (pH 8). Sample and heating experiment by B. Olivera in the Gilford.

Results	Tm°C	% H	Slope	A_{260}	R_{220}	H/D
Overall	59.2	32.6	2.67	0.536	0.994	0.69

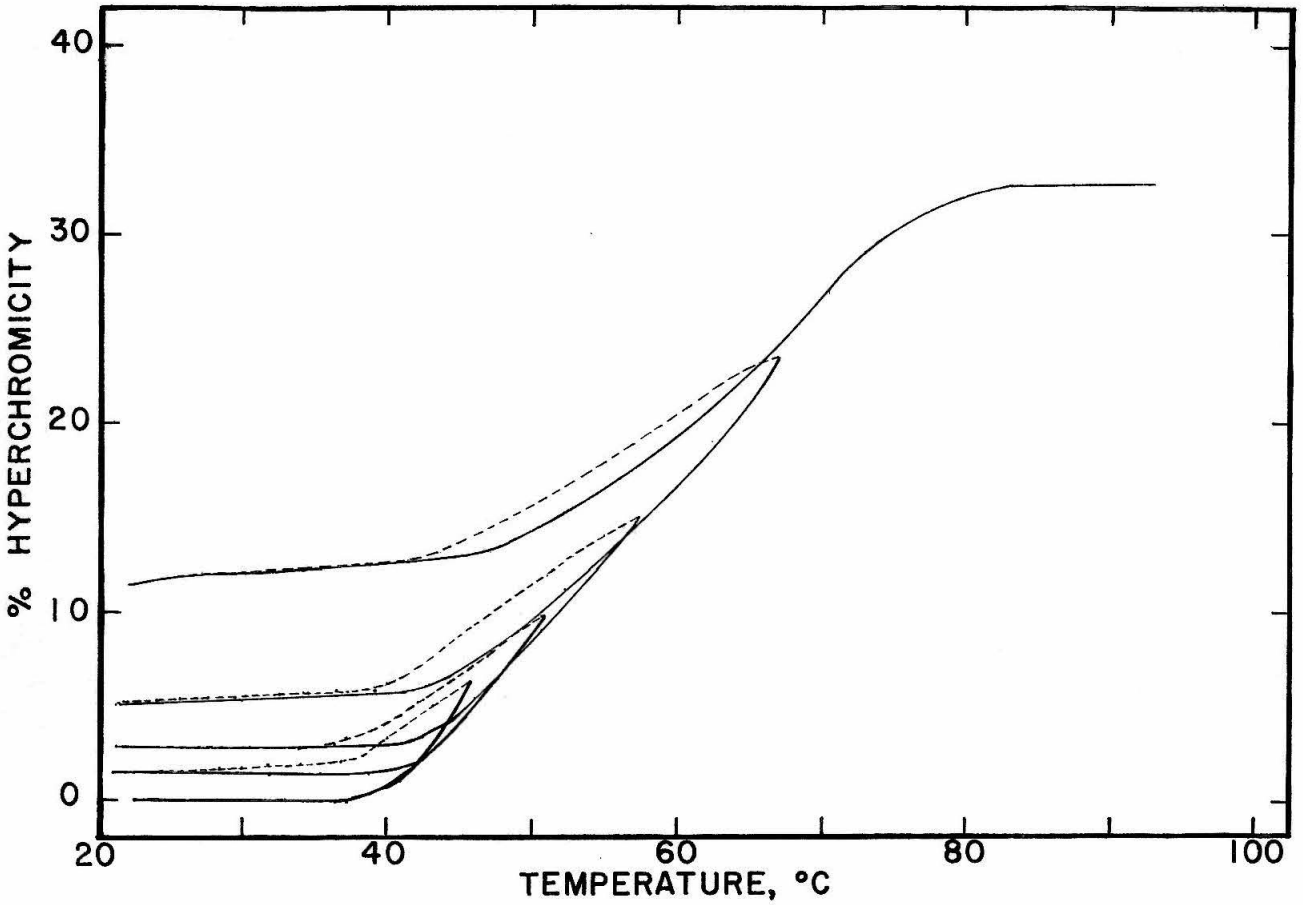

Figure 51

Figure 52

Heat denaturation and renaturation curve of calf thymus DNA in 7.5×10^{-4} N Na^{+} EDTA (pH 8). Sample and heating experiments by B. Olivera run in the Gilford.

Results	Tm°C	% H	Slope	A_{260}	R_{220}
Overall	45.7	37.2	20.83	0.485	1.58

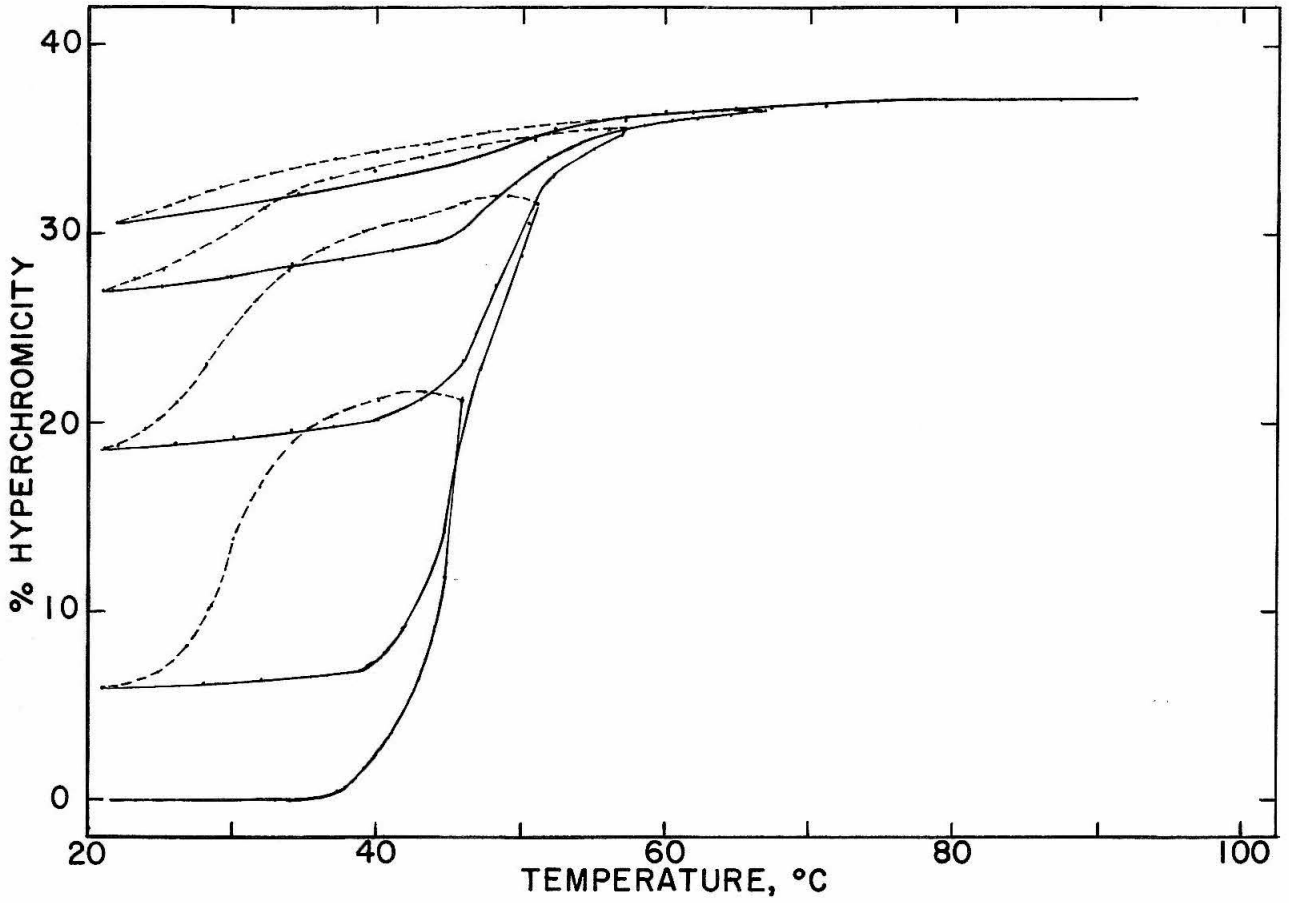

Figure 52

of these loops is obviously related to the rate of renaturation of the DNA strands. Wider loops indicate a slower renaturation rate than narrow loops.

On the molecular level we may interpret the width of the loops in terms of the length of denaturing DNA regions. Thus, it seems as if the denaturing regions in reconstituted DNH IIb are considerably shorter than those in DNA and therefore can reanneal more readily. The fact that the loops do not become larger as more of the DNH IIb is denatured suggests that histone IIb cannot migrate along the DNA strand. Since the extent of renaturation of partially denatured DNH IIb is similar to or even slightly less than that of DNA, it seems as if the histone molecules are bound to single DNA strands and remain bound even after denaturation. The lower recovery of denatured DNH IIb compared to that of DNA, which is especially noticable at higher H/D, may be due to a certain degree of interference by the histones with renaturation.

Before considering the results with reconstituted DNH III(IV) it should be pointed out that the preparation of these complexes is quite difficult because of the tendency of these materials to precipitate. The H/D values, which are based on the R_{220} of the solutions of these samples may be considerably too high since the complexes

were not separated from any non-complexed histone III(IV). From the mobility of the most highly complexed DNH III (H/D = 0.78) which is 1.8 x 10^{-4} cm^2/V-sec we would calculate that only 17.5 % of the charge of pure DNA is complexed, a result incompatible with the high H/D ratio.

In spite of these uncertainties, it is worthwhile to consider the denaturation results obtained with DNH III, for even the qualitative data are rather interesting, especially in comparison to the results with partially salt extracted, native DNH.

The melting curves of partially reconstituted DNH III (IV) (Fig. 53) are most difficult to interpret in view of what is known about the melting behavior of DNA. DNH III(IV) with low histone coverage shows a peculiar skewing of the upper parts of the melting profile towards higher temperature. Increased coverage leads to a pronounced broadening of the transition with the last melting regions even more stabilized than those of native DNH. This fact suggests that the binding of acid extracted histone III(IV) to DNA is more intimate than that of "native" histone III(IV). Perhaps, acid extraction has altered the structure of histone III(IV).

Quite unusual is the remarkable ability of DNH III(IV) to renature (Figures 54 to 56, Table XX). Already, if small

Figure 53

Heat denaturation curves of reconstituted calf thymus DNH III(IV) compared to calf thymus DNA and native DNH. The samples were heated in 7.5 x 10^{-4} N Na^+ EDTA (pH 8) in the Gilford by B. Olivera.

Results	Tm°C	% H	Slope	A_{260}	R_{220}	H/D
DNA	46.7	37.6	7.66	0.848	1.66	-
	49.9	36.0	7.58	0.530	1.32	0.18
	53.0	36.0	4.69	0.473	1.06	0.56
	63.8	36.0	2.31	0.555	0.89	0.93
DNH	76.2	36.0	3.61	0.860	0.81	1.16

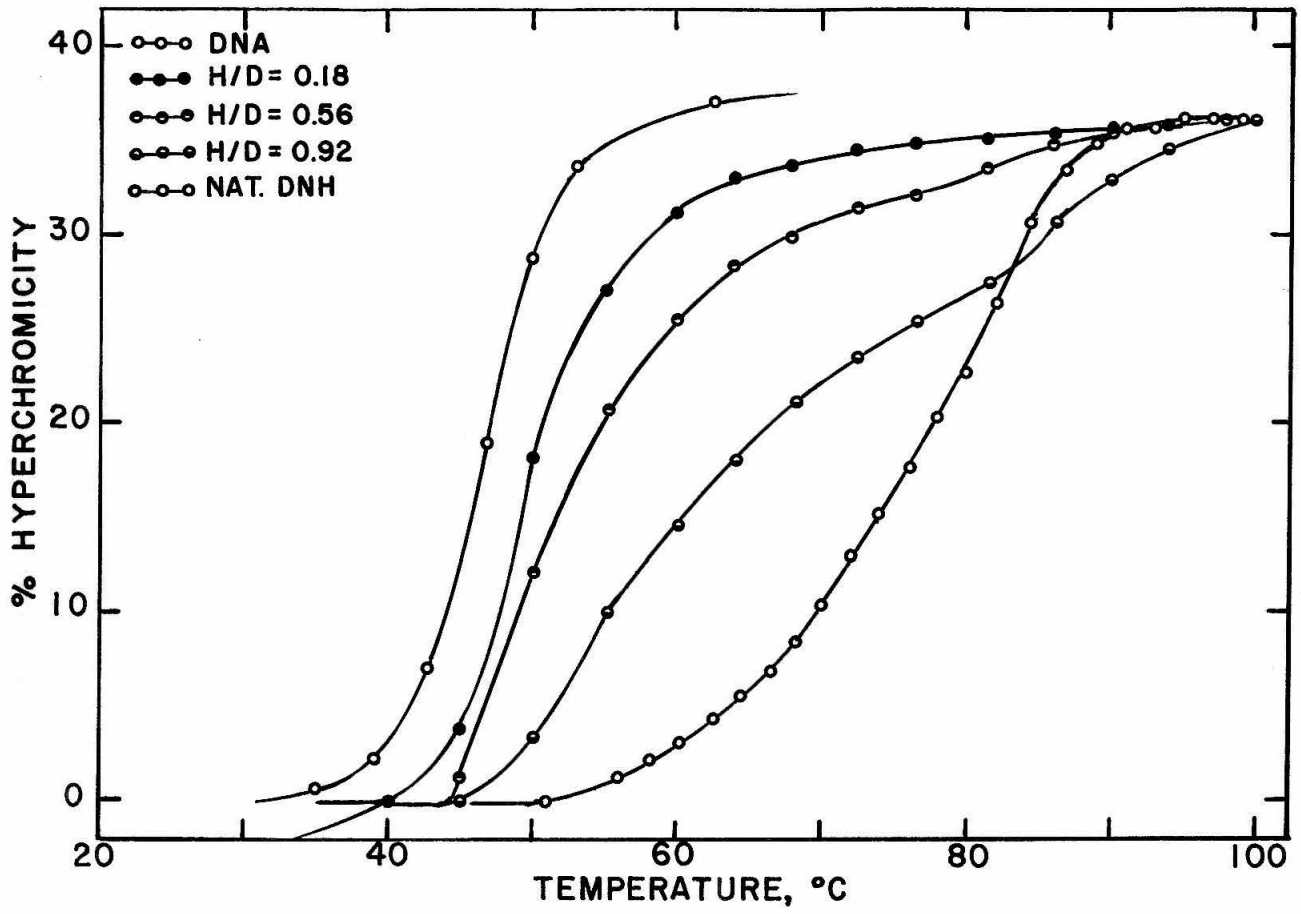
DNA
H/D = 0.18
H/D = 0.56
H/D = 0.92
NAT. DNH
% HYPERCHROMICITY
TEMPERATURE, °C
0
10
20
30
40
20
40
60
80
100

Figure 53

Figure 54

Heat denaturation and renaturation curve of reconstituted calf thymus DNH III(IV) in 7.5 x 10^{-4} N Na^{+} EDTA (pH 8). Sample and heating experiment by B. Olivera in the Gilford.

Results	Tm°C	% H	Slope	A_{260}	R_{220}	H/D
Overall	49.4	32.8	8.99	0.784	1.32	0.18

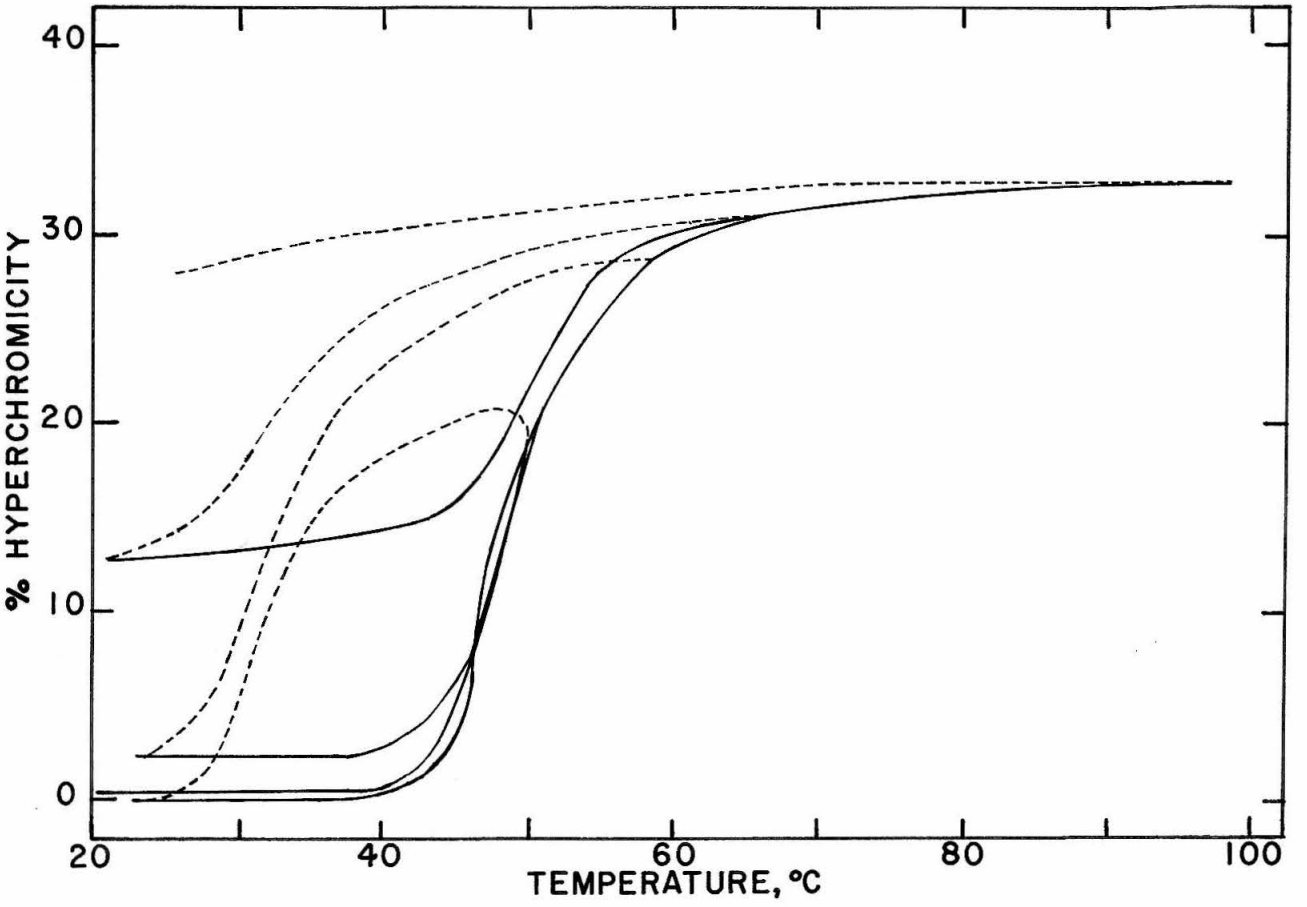

Figure 54

Figure 55

Heat denaturation and renaturation curve of reconstituted calf thymus DNH III(IV) in 7.5×10^{-4} N Na^+ EDTA (pH 8). Sample and heating experiment by B. Olivera in the Gilford.

Results	Tm°C	% H	Slope	A_{260}	R_{220}	H/D
Overall	52.3	32.5	5.62	0.832	1.06	0.56

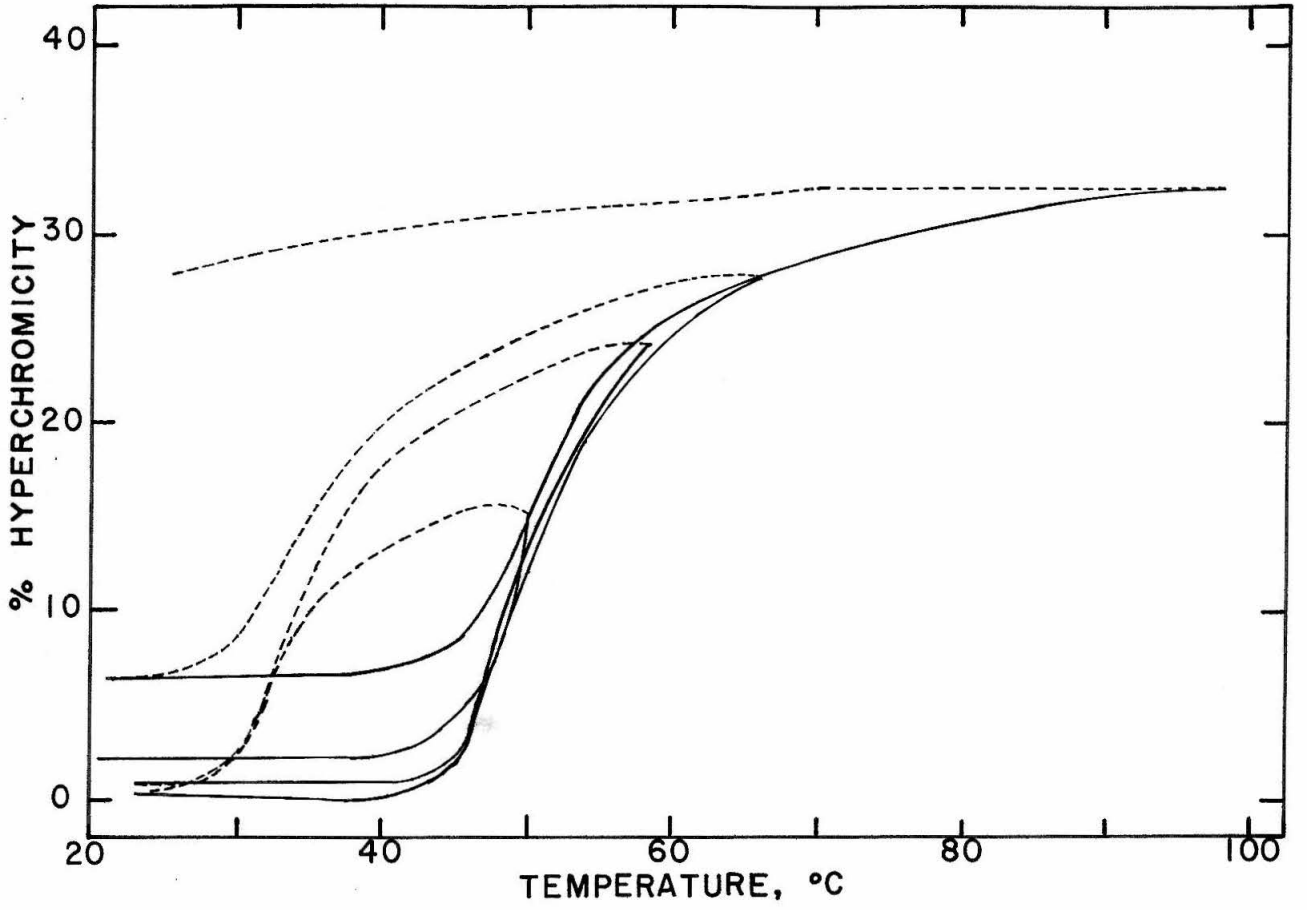

Figure 55

Figure 56

Heat denaturation and renaturation curve of reconstituted calf thymus DNH III(IV) in 7.5×10^{-4} N Na^+ EDTA (pH 8). Sample and heating experiment by B. Olivera in the Gilford.

Results	Tm°C	% H	Slope	A_{260}	R_{220}	H/D
Overall	59.7	33.6	2.69	0.789	0.94	0.81

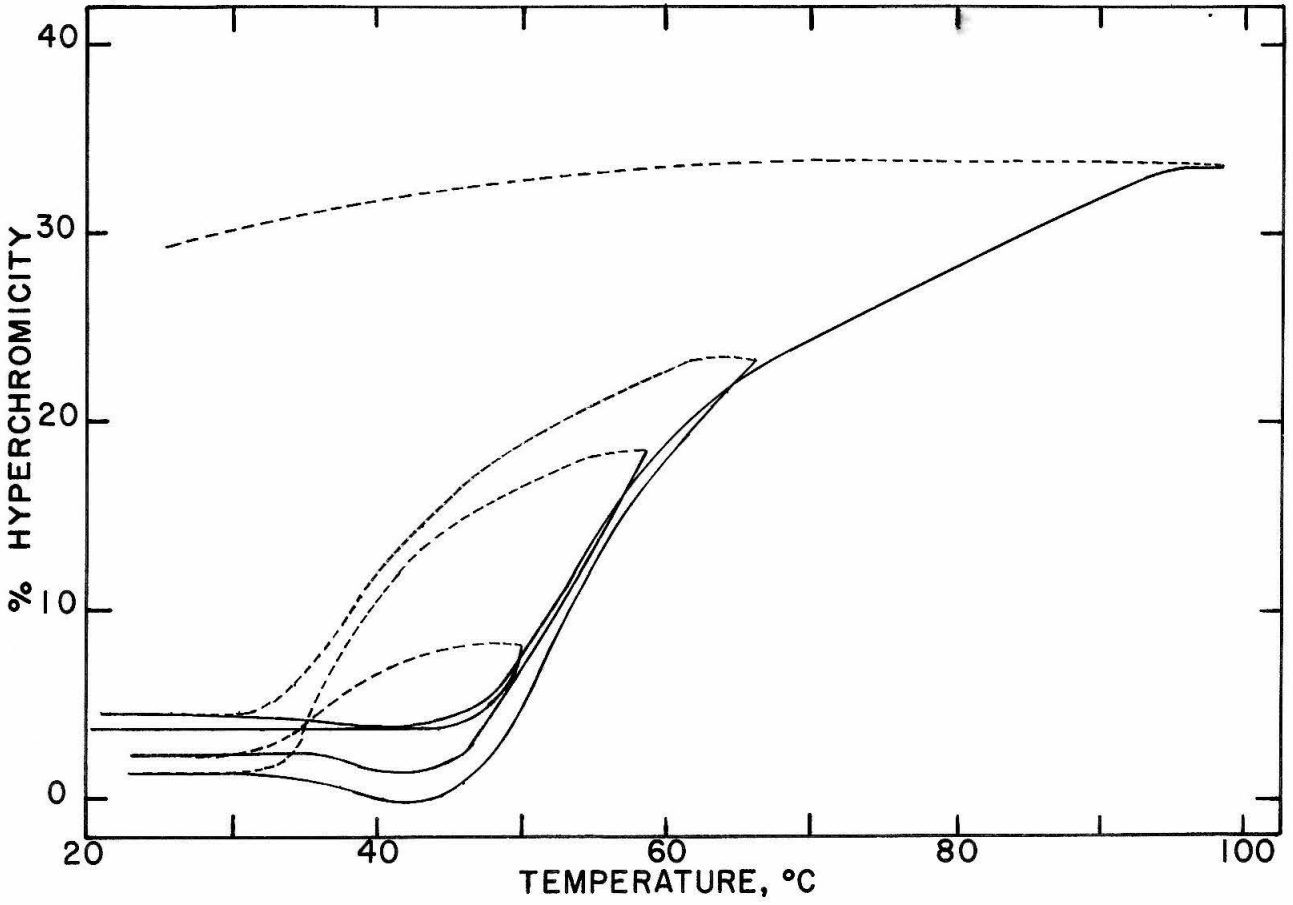

Figure 56

Table XX

Renaturation of C. T. DNA

% Denaturation	at T °C	% Renaturation
60	46	72
87	51	50
96	58	35
100	97	23

Renaturation of C. T. DNH IIb (H/D = 0.19)

% Denaturation	at T °C	% Renaturation
43	46	60
58	51	58
72	58	54
100	97	20

Renaturation of C. T. DNH III(IV) (H/D = 0.12)

% Denaturation	at T °C	% Renaturation
63	50	100
89	58.5	92
94	66	58
100	100	14

amounts of histone III(IV) are complexed to DNA (H/D = 0.18) a striking effect on the degree of renaturation is observed, even though the Tm is not increased appreciably. The recovery of the native absorbance is 100 % even after 63 % of the material has been melted. It still recovers 92 % after as much as 89 % has been melted. The contrast with the behavior of pure DNA is obvious (Fig. 52): It recovers only 72 % after 60 % are melted and only 50 % after 87 % are melted (solvents and rate of heating and cooling were of course identical).

As the histone III(IV) coverage is increased, the phenomenal recovery observed with the H/D = 0.18 material is somewhat lowered, although it is still considerably higher than DNA. This slight lowering in the effectiveness of histone III(IV) is most probably caused by the effects of the higher temperatures required to give a comparative percentage of hyperchromicity. From the unsymmetrical shape of the DNH III(IV) melting curves it may be inferred that histone III(IV) does not move along the DNA chain like histone I and from the completeness of the renaturation it can be deduced that histone III(IV) binds to both DNA strands. This tends to keep the complementary strands in register.

The width of the "hysteresis" loops, which are comparable to those of DNA (Fig. 52) indicate little if any effect of histone III(IV) on the rate of renaturation of the DNA. Thus, it seems as if the crosslinks due to histone III(IV) are rather large distances apart. Since the width of the loops does not decrease appreciably with increasing histone coverage, we conclude that the number of crosslinking units does not increase in proportion to the histone coverage. Indeed, it may be possible that additional histone molecules tend to aggregate at the same sites as the original crosslinking sites. Whether such aggregation would increase the Tm to the extend observed cannot be determined with certainty.

c) Heating Curves of Native Nucleohistones

Figures 57 to 59 show a number of typical melting curves of partially dissociated, native nucleohistone samples. The first set of curves (Fig. 57) illustrates the effect of NaCl extraction of native calf thymus DNH. All samples were prepared by batch sedimentation and resedimentation in solutions containing the indicated salt concentrations.

Figure 58 shows the effect of $NaClO_4$ extraction for comparison. It is immediately obvious that $NaClO_4$ extraction is more efficient than NaCl extraction, since comparable salt concentrations lower the Tm considerably more, if the salt is $NaClO_4$. These results support our electrophoretic observations.

Figure 59 presents heating curves obtained with partially $NaClO_4$ extracted pea bud nucleohistones. The general shape of these curves are similar to those of calf thymus DNH (Fig. 58). The Tm's are higher, since the salt concentrations were 7.5×10^{-4} N Na^+ EDTA (pH 8) rather than 3×10^{-4} N Na^+ EDTA (pH 6.3) as in figures 57 and 58.

From the shape of these heating curves it is immediately obvious that neither of the two ideal cases discussed on page 346 is applicable. Removal of histone I, e. g. by 0.27 F NaCl (Fig. 57) shows up merely as a skewing toward lower

Figure 57

Heat denaturation curves of NaCl extracted, native calf thymus DNH compared to calf thymus DNA and native DNH in 3×10^{-4} N Na^+ EDTA (pH 6.3). Extraction by batch sedimentation and resedimentation. Heated in the Cary.

Results	Tm°C	% H	Slope	A_{260}	R_{220}	Days Old	Δ °C
DNA	39.8	38.0	6.08	1.03	1.24	-	19.0
1.94 F	39.7	46.0	5.93	0.782	1.24	(0)(1) 5	58.5
initial	37.7	35.4	7.71				12.5
final	88.8	10.6	3.26				27.0
0.48 F	68.7	43.2	0.88	0.905	0.90	(7)(9)15	40.0
initial	56.1	23.0	3.15				25.0
final	81.0	20.2	8.56				15.0
0.27 F	73.5	42.0	3.23	0.905	0.82	(2)(5)10	25.7
DNH	79.3	33.2	4.97	0.89	0.72	38	19.5
				(A_{400} = 0.068)			

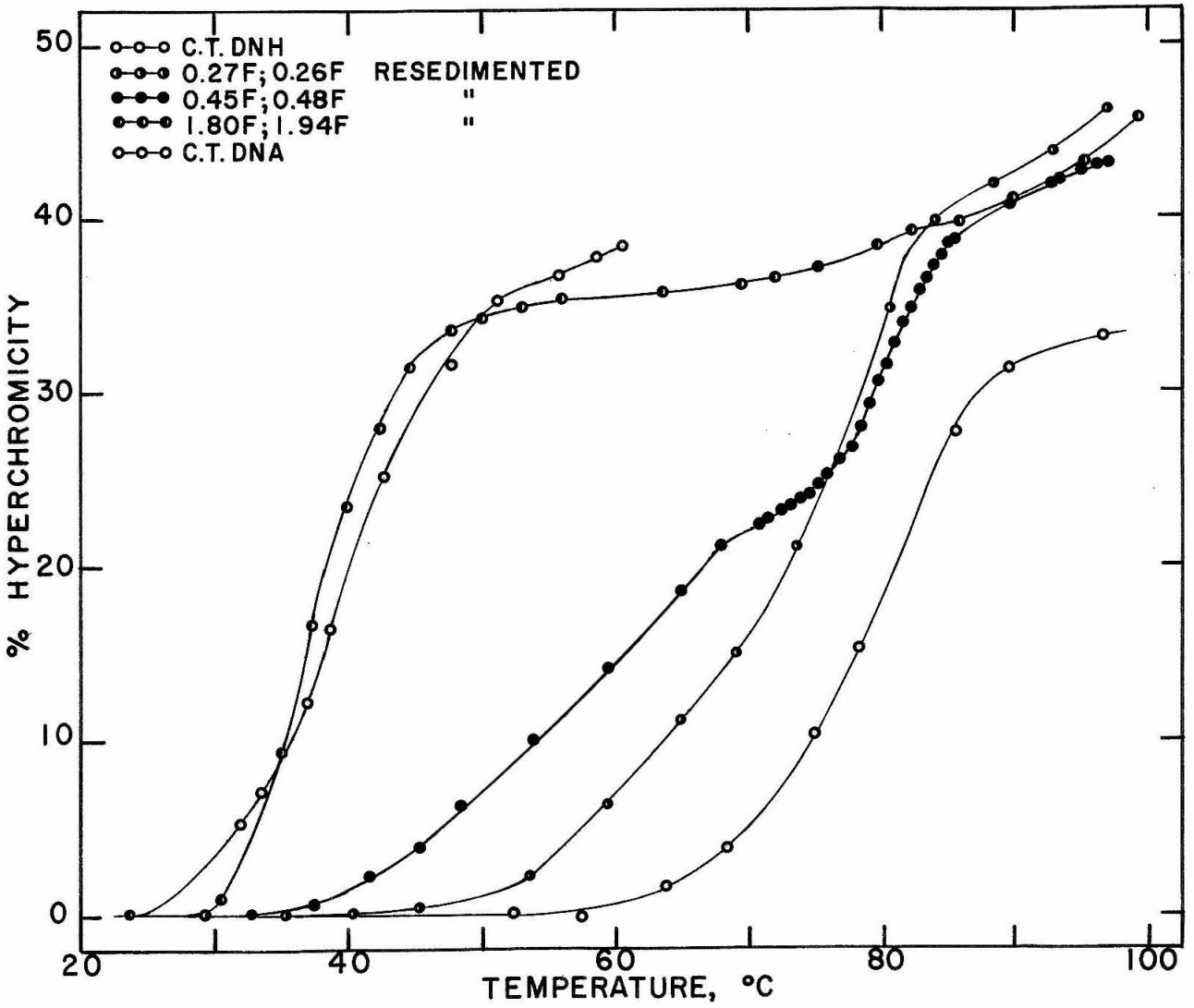
C.T. DNH
0.27F; 0.26F RESEDIMENTED
0.45F; 0.48F "
1.80F; 1.94F "
C.T. DNA
% HYPERCHROMICITY
TEMPERATURE, °C
0
10
20
30
40
50
20
40
60
80
100

Figure 57

Figure 58

Heat denaturation curves of $NaClO_4$ extracted, native calf thymus DNH compared to calf thymus DNA and native DNH in 3×10^{-4} N Na^+ EDTA (pH 6.3). Extraction by batch sedimentation and resedimentation.

Results	Tm°C	% H	Slope	A_{260}	R_{220}	Days Old	Δ °C
DNA	39.8	38.0	6.08	1.03	1.24	-	19.0
0.90 F	40.0	37.4	6.39	1.02	1.38	(0)(2) 5	21.5
initial	39.3	33.6	7.11				13.7
final	70.5	3.8	2.63				31.5
0.45 F	49.5	35.8	3.41	1.09	1.15	(0)(2) 5	34.5
initial	47.5	28.0	8.21				17.0
final	74.7	7.8	7.05				17.0
0.38 F	51.5	34.2	2.66	1.17	1.17	(0)(2) 5	40.0
initial	47.3	24.0	7.29				19.2
final	74.7	10.2	5.88				19.0
DNH	79.3	33.2	4.97	0.89	0.72	38	19.5
				(A_{400} = 0.068)			

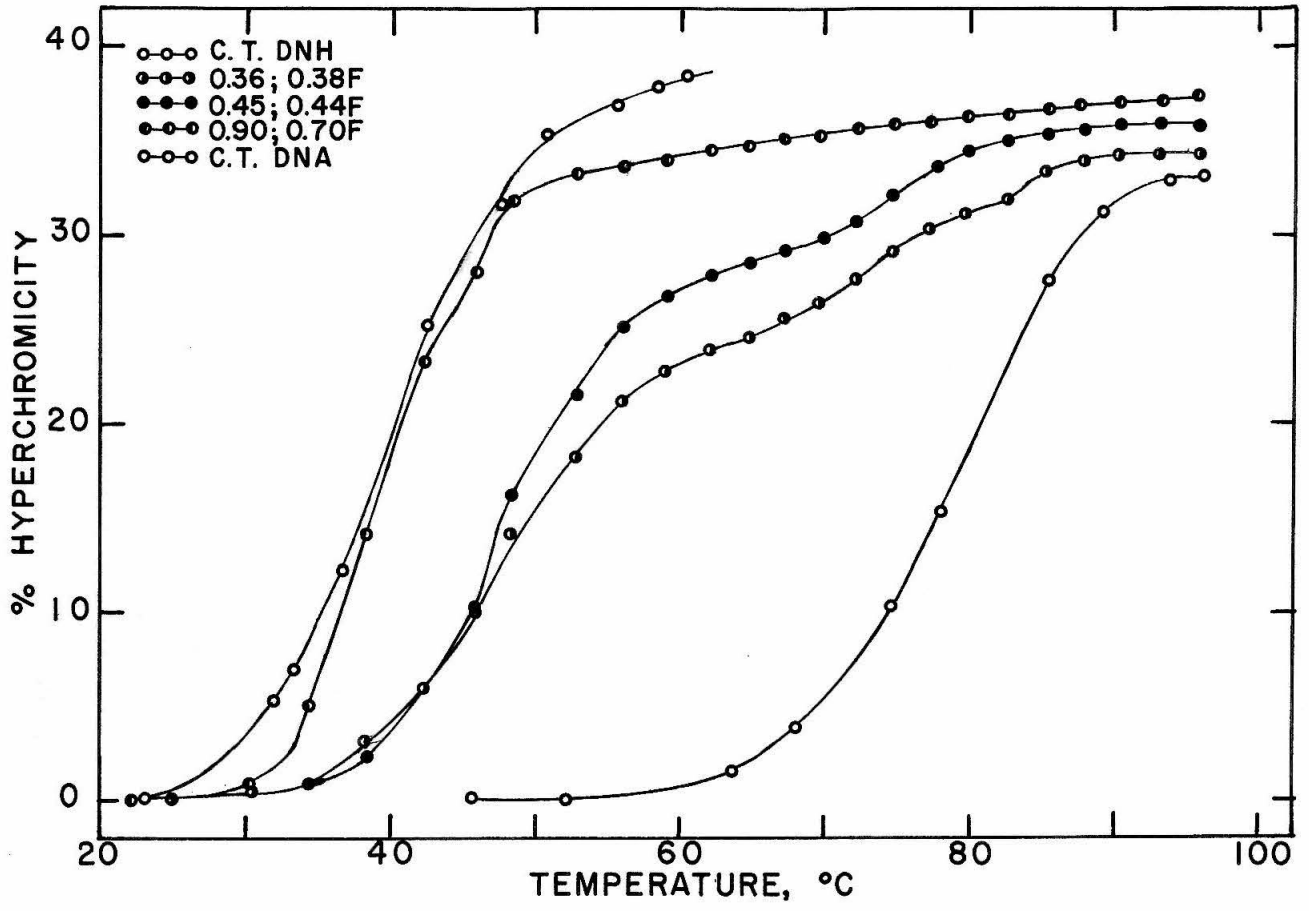
C. T. DNH
0.36; 0.38F
0.45; 0.44F
0.90; 0.70F
C. T. DNA
% HYPERCHROMICITY
0
10
20
30
40
20
40
60
80
100
TEMPERATURE, °C

Figure 58

Figure 59

Heat denaturation curves of $NaClO_4$ extracted, native pea bud DNH compared to pea bud DNH and calf thymus DNA in 7.5×10^{-4} N Na^+ EDTA (pH 8). Extraction by batch sedimentation. Heating experiments by B. Olivera in the Gilford.

Results	Tm°C	% H	Slope	A_{260}	R_{220}	Days Old	Δ°C
DNA	46.7	37.6	7.66	0.848	1.66	-	13.0
0.54 F	45.2	33.2	7.35	0.558	1.21	(4) 9	29.3
0.45 F	53.7	34.0	0.71	0.96	0.84	(2) 9	47.0
initial	43.9	17.6	7.67				11.0
final	78.3	16.4	2.12				36.0
0.36 F	65.6	33.6	1.38	0.535	1.10	(0) 9	44.2
initial	48.5	16.0	4.13				21.6
final	77.0	17.6	3.64				21.4
DNH	77.2	34.7	2.94	0.60	0.63	11	23.4

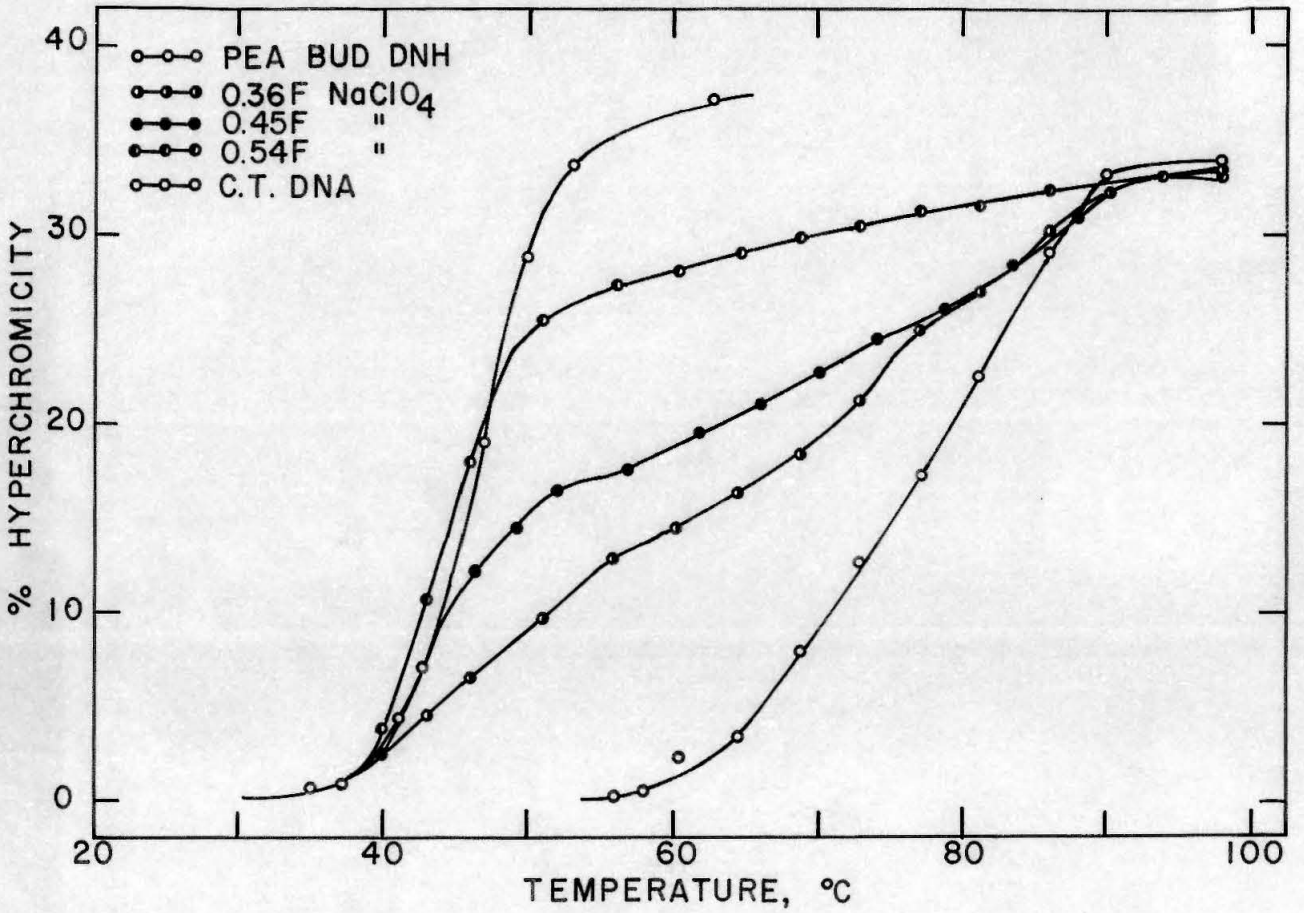
PEA BUD DNH
0.36F NaClO4
0.45F "
0.54F "
C.T. DNA
% HYPERCHROMICITY
TEMPERATURE, °C
0
10
20
30
40
20
40
60
80
100

Figure 59

temperature of the lower part of the DNH melting curve, indicating that histone I is distributed fairly evenly along the DNH. Removal of histone I and II by higher salt concentrations produces the two step profiles, while extraction with 1.94 F NaCl or 0.9 F $NaClO_4$ gives DNA-like melting as expected after total removal of histones.

The two step melting profiles are most plausibly explained by non-random distributions of the histones still associated with the DNA, i. e. histones III and IV. Since the steps are not too sharp, it is believed that the dissociated regions are either not very long, i. e. considerably shorter than the cooperative unit, or they are not completely pure DNA regions.

With regard to the nature of the differently melting regions, it is of considerable interest to investigate the renaturation behavior of partially dissociated, native nucleohistones. The renaturation behavior of a sample of pea bud DNH which was extracted with 0.36 F $NaClO_4$ is shown in figure 60. For comparison, a sample of the same material extracted with 0.54 F $NaClO_4$, which should remove histones I and II, was heated simultaneously with the above sample (Fig. 61). The renaturation behavior of the second sample is indeed very similar to that of uncomplexed calf

Figure 60

Heat denaturation and renaturation curve of 0.36 F $NaClO_4$ extracted, native pea bud DNH in 7.5×10^{-4} N Na^+ EDTA (pH 8). Heating experiment by B. Olivera in the Gilford. Age of sample: (0) 13 days.

Results	Tm°C	% H	Slope	A_{260}	R_{220}	H/D	Δ °C
Overall	63.3	30.4	0.55	0.535	1.07	0.55	43.5
1st step	41.5	11.2	0.94				16.7
2nd step	83.5	9.2	0.71				18.5

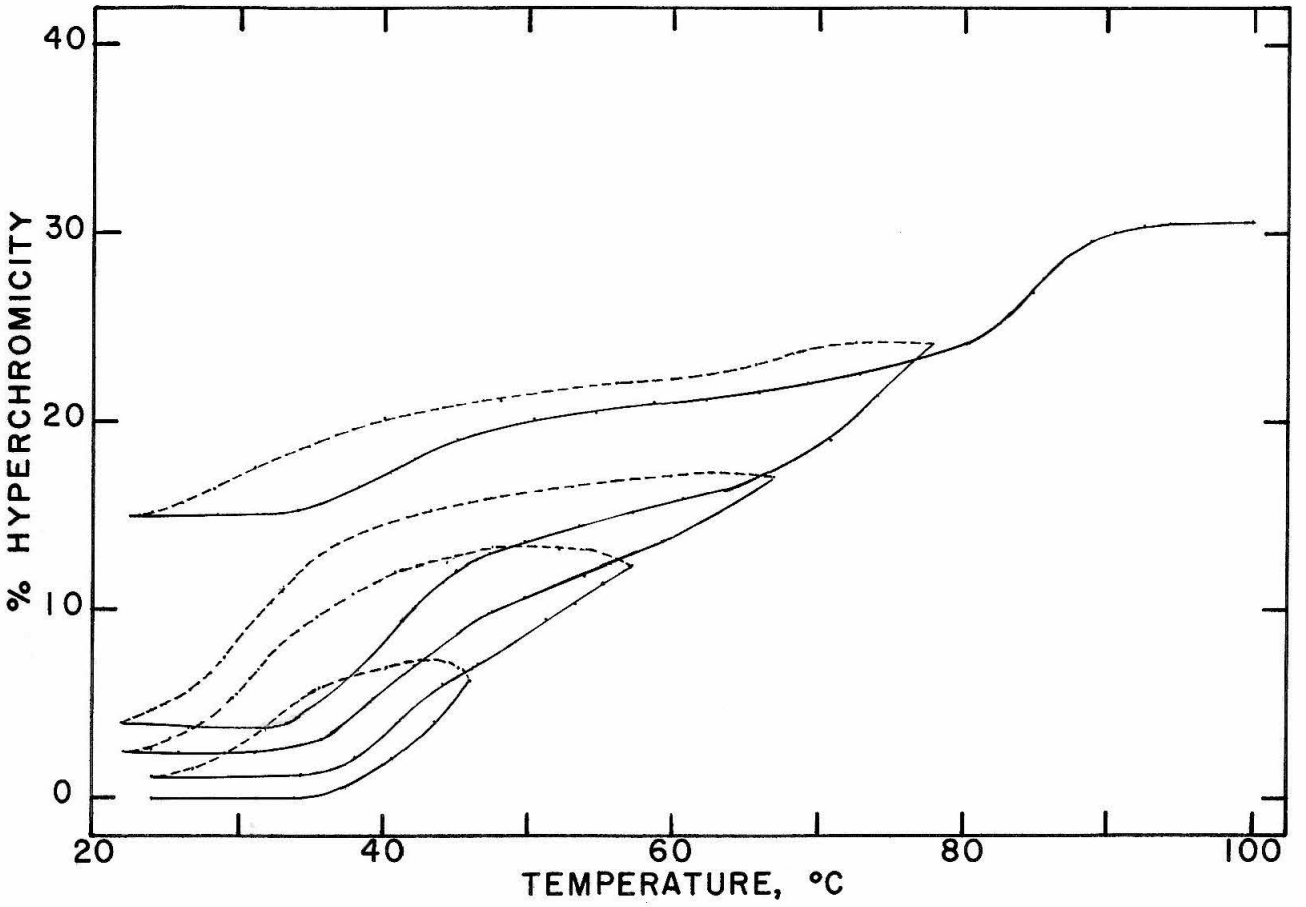

Figure 60

Figure 61

Heat denaturation and renaturation curve of 0.54 F $NaClO_4$ extracted, native pea bud DNH in 7.5×10^{-4} N Na^+ EDTA (pH 8). Heating experiment by B. Olivera in the Gilford. Age of sample: (2) 13 days.

Results	Tm°C	% H	Slope	A_{260}	R_{220}	H/D	Δ°C
Overall	44.4	32.6	3.47	0.462	1.165	0.39	15.4

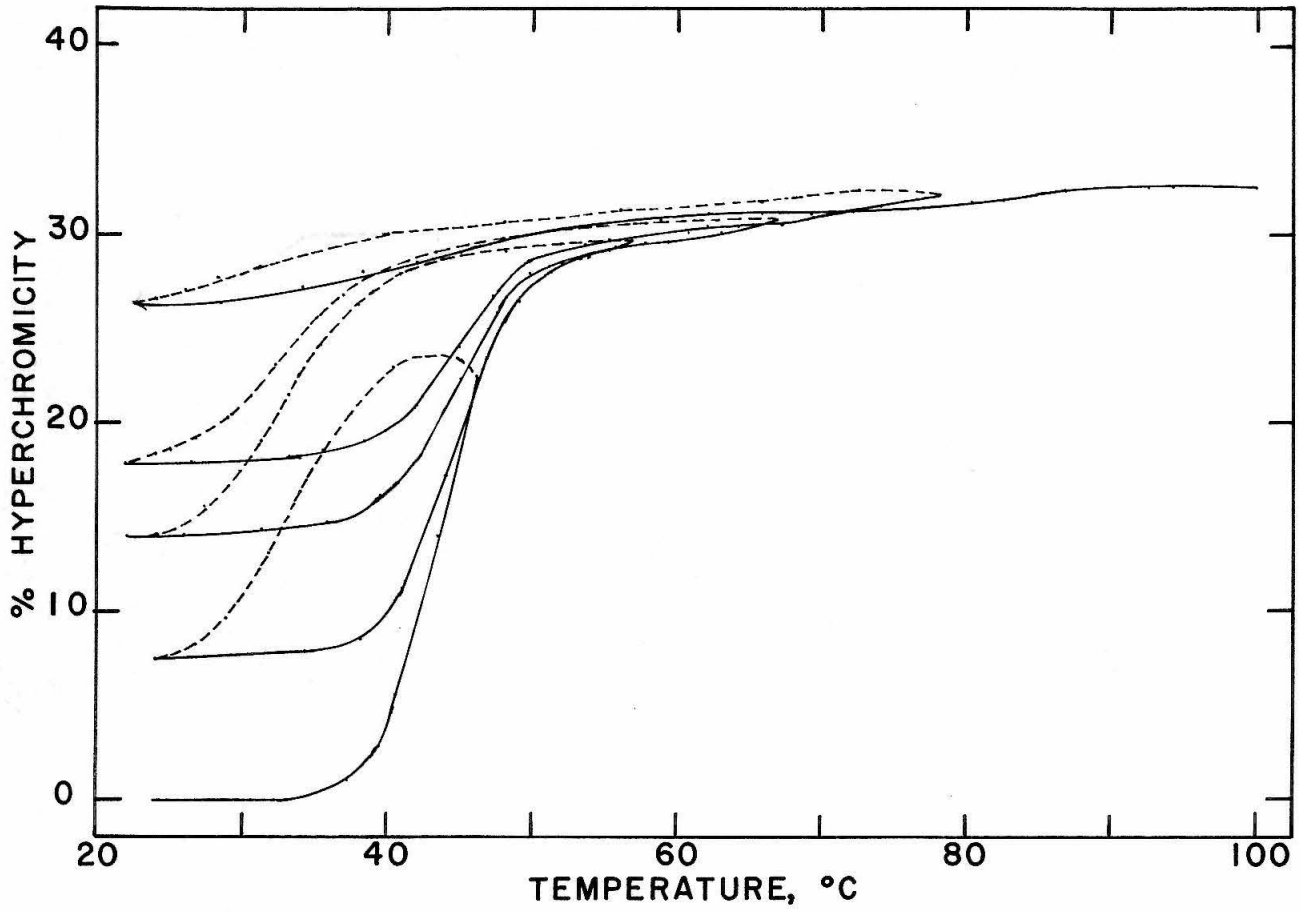

Figure 61

thymus DNA (Fig. 52). The behavior of the partially extracted material is thus unlike the behavior we have observed with our reconstituted samples: The 0.36 F $NaClO_4$ extracted sample shows clearly two differently melting regions, the first at Tm = 41.5 °C, the second at Tm = 83.5 °C, which incidentally is considerably above the Tm of whole, native DNH (Tm = 77.2 °C). This fact suggests that some of the remaining, non-dissociated histones can migrate from the denaturing regions to still-native regions, imparting to them added stability. Since these histones are mainly fractions II and III(IV), we were further surprised by the relatively poor renaturability observed here, in contrast to that found with reconstituted DNH III(IV) (Figures 54 to 56). Especially the sudden decrease in renaturation ability after the fourth heating cycle is quite striking. That the behavior is no artifact and is remarkably reproducible can be seen from figure 62, showing the results of a similarly treated pea bud nucleohistone sample.

One possible explanation for the effect is the presence of one or more single strand breaks, so that a certain amount of denaturation may cause a complete splitting off of segments making renaturation unlikely. Of course, more experiments are necessary to determine whether this contention is correct.

Figure 62

Heat denaturation and renaturation curve of 0.36 F $NaClO_4$ extracted, native pea bud DNH in 7.5×10^{-4} N Na^+ EDTA (pH 8). Heating experiment by B. Olivera in the Gilford. Age of sample: (0) 13 days.

Results	Tm°C	% H	Slope	A_{260}	R_{220}	H/D	Δ °C
Overall	66.3	33.0	0.725	0.478	1.025	0.64	45.2
1st step	40.8	9.2	0.91				10.2
2nd step	84.5	12.6	1.10				12.0

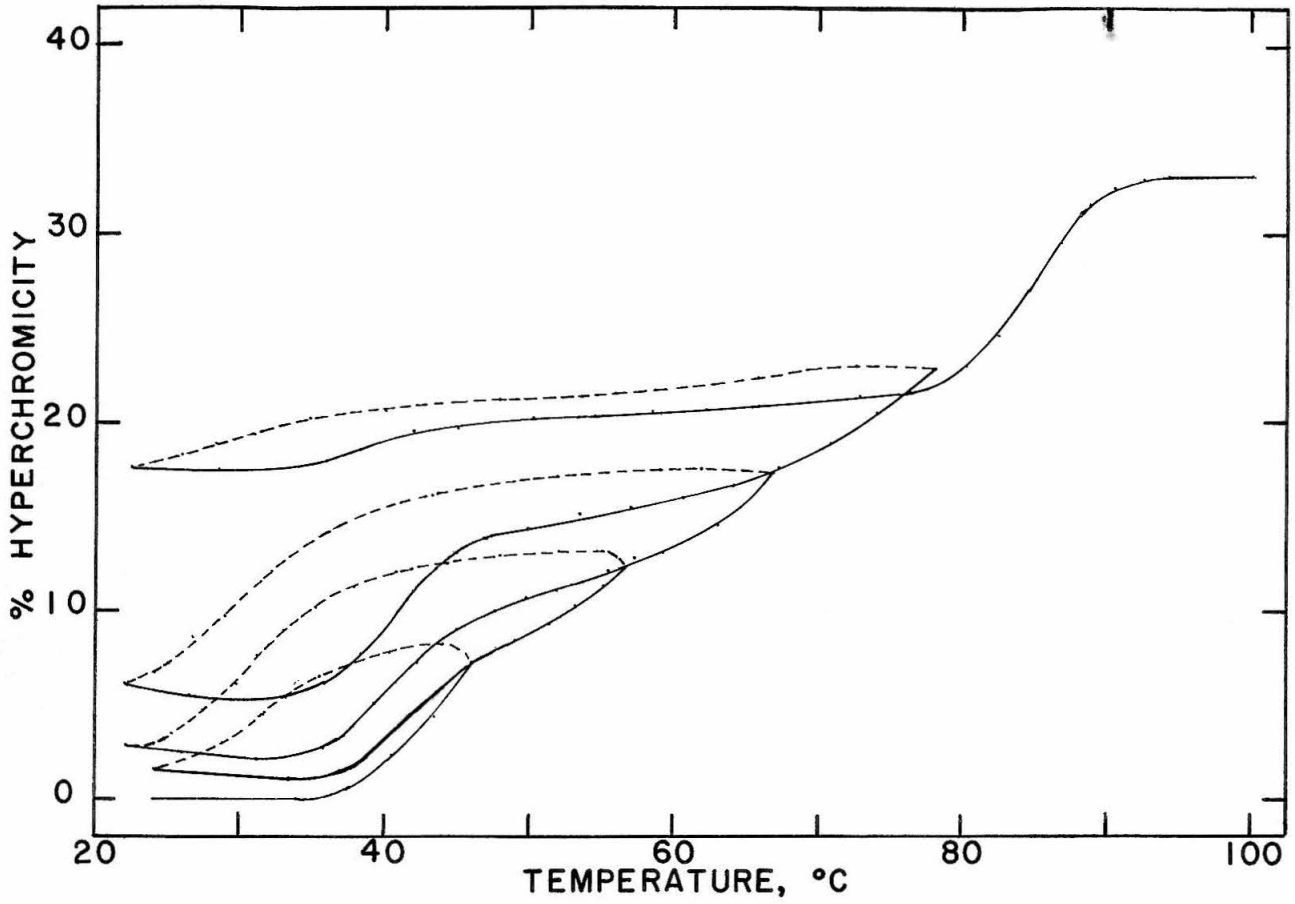

Figure 62

In retrospect the following conclusions can be drawn from the heating and renaturation experiments presented:

1) Acid extracted histone fractions when reconstituted to DNA, change its melting behavior in characteristic ways. As judged by the H/D ratio, acid extracted histone I imparts the greatest stability against melting of DNA and is capable of migrating along the DNA strand from denaturing to still-native regions. Acid extracted histones III(IV) do not seem to stabilize the DNA very much, but aid considerably in its ability to renature. Acid extracted histone IIb exhibits intermediate effects.

2) Distinct differences exist between the melting behavior of reconstituted DNH and that of partially salt extracted, native DNH. These differences must be due to different, perhaps more specific arrangements of the histone molecules along the DNA strands in native DNH as compared to reconstituted DNH as well as to differences in the histone structures of native versus acid extracted histones.

Summary

The work described in the second part of this thesis has demonstrated the following, subject to the numerous qualifications described in the text:

1. Histone - DNA complexes can be specifically dissociated by monovalent salt solutions. This specificity has been observed with reconstituted nucleohistones as well as with native nucleohistones and has been described here in terms of the behavior of three major histone fractions obtained by Amberlite chromatography: Histones Ia and Ib, histones IIa and IIb, and histones III and IV.

Just as these fractions can be successively eluted from Amberlite IRC-50 resin by increasing concentrations of GuCl, so they can be extracted from DNH by increasing concentrations of $NaClO_4$ (NaCl).(Other salts have not yet been tried, leaving interesting possibilities for future investigations.) Thus, 0.1 to 0.3 F $NaClO_4$ extracts histones I only; histones II are extracted next by $NaClO_4$ concentrations between 0.35 and 0.5 F; histones III and IV follow at concentrations above 0.5 F $NaClO_4$. Extraction by 1.0 F $NaClO_4$ gives essentially pure DNA as judged by its melting behavior.

2. One interesting feature of the nucleohistone dissociation, which was demonstrated using a novel salt gradient sedimentation technique, is the relative sharpness of the

dissociation of histone IIb from reconstituted and native DNH in comparison to the gradualness of the dissociation of histones I and III(IV). The band center of extracted histone IIb lies at 0.45 F $NaClO_4$ using reconstituted DNH IIb, and at 0.42 F $NaClO_4$ using native calf thymus DNH. The significance of this observation, especially from a biological point of view, awaits further investigations.

3. It was found that "purified" chromatin could be dissociated just as well as the nucleohistones. This indicates that the histones must be situated along the DNA of the chromatin at positions which are quite exposed to environmental influences and which permit removal of the histones in spite of its more complex structure and presence of non-histone proteins.

4. Heating experiments are presented which support the contention that the histones are non-randomly distributed along the DNA strands. However, the non-randomness does not seem to extend over consecutive DNA regions which are much larger than 50 to at most 200 basepairs even after almost 80 % of the histones (i. e. histones I and II) have been extracted.

This result is particularly surprising in view of the increased RNA-priming activity of the extracted DNH. It seems as if the non-extracted histones (mainly III and IV) do not interfere with the ability to transcribe genetic

information, although they do stabilize the DNA significantly against heat denaturation.

In order to illuminate this situation, it should be of interest to investigate the size distribution of the newly synthesized RNA as a function of the amounts of histones extracted from the DNH. With regard to the specificity of histone binding it might also be interesting to determine the base composition of the newly synthesized RNA, which should be complementary to the DNA sequences being read.

Finally a word of caution, for the fact that the DNH complexes are selectively dissociated by increasing salt concentrations should not lead to the assumption that this is the mechanism employed by the living cell. It is a convenient experimental procedure for studying polymer - polymer binding and seems promising as a standard method for the determination of the kinds of histones complexed to the DNH of various tissues.

Furthermore, the possibility of partially removing histones from native DNH without destroying its biological activity may offer interesting possibilities in studying the synthesis of specific proteins and the specificity of the regulation of gene activity by histones.

Also, it may be possible by refining the technique to extract even more selectively a number of subfractions of histones and to study their influence on the biological and physico-chemical properties of DNH. In this respect different agents may be tried which may extract histones from the DNH in a different order or with different overall compositions than those extracted by $NaClO_4$.

REFERENCES

References

1) The chromosome superstructure.

a) J. Schultz, Cold Spring Harbor Symp. Quant. Biol., 9, 55 (1941).

b) D. Mazia, T. Hayashi and K. Yudowitch, ibid., 12, 122 (1947).

c) A. E. Mirsky and H. Ris, J. Gen. Physiol., 31, 7 (1947).

d) A. E. Mirsky and H. Ris, ibid., 34, 475 (1950-1951).

e) G. Zubay and P. Doty, J. Mol. Biol., 1, 1 (1959).

f) G. Zubay in The Nucleohistones, edited by J. Bonner and P. Ts'o, Holden-Day Inc., San Francisco, London, Amsterdam, 1964, p. 95.

2) E. Stedman and E. Stedman, Nature, 166, 780 (1950).

3) R. C. Huang and J. Bonner, Proc. Natl. Acad. Sci. U. S., 48, 1216 (1962).

4) E. O. Akinrimisi, J. Bonner and P. O. P. Ts'o, J. Mol. Biol., 11, 128 (1965).

5) Nucleohistone properties at various salt concentrations.

a) A. E. Mirsky and A. W. Pollister, J. Gen. Physiol., 30, 117 (1946).

b) G. Frick, Biochim. Biophys. Acta, 3, 103 (1949).

c) E. Chargaff, C. F. Crampton and R. Lipshitz, Nature, 172, 289 (1953).

d) G. L. Brown and M. Watson, Nature, 172, 339 (1953).

e) P. F. Davison, B. E. Conway and J. A. V. Butler, Progr. Biophys. Biophys. Chem., 4, 148 (1954) p. 151.

f) C. F. Crampton, R. Lipshitz and E. Chargaff, J. Biol. Chem., 206, 499 (1954).

g) K. V. Shooter, P. F. Davison and J. A. V. Butler, Biochim. Biophys. Acta, 13, 192 (1954).

h) B. Bakay, J. J. Kolb and G. Toennis, Arch. Biochem. Biophys., 58, 144 (1955).

i) I. H. Goldberg, Biochim. Biophys. Acta, 51, 201 (1961).

j) P. M. Bayley, B. N. Preston and A. R. Peacocke, ibid., 55, 943 (1962).

k) D. M. P. Phillips, Progr. Biophys, Biophys. Chem., 12, 211 (1962) p. 240.

l) G. Giannoni and A. R. Peacocke, Biochim. Biophys. Acta, 68, 157 (1963).

m) Loc. cit. ref. 4).

6) Low solubility of DNH at moderate salt concentrations.

a to f) loc.cit. refs. 5a, 5b, 5e, 5f, 5g, 5k).

7) Degraded DNH preparations.

a to c) loc. cit. refs. 1b, 5g, 5l).

d) M. E. Maver and A. E. Greco, J. Biol. Chem., 181, 853 (1949).

e) L. G. Allgén, Acta Physiol. Scand., 22, Suppl., 76 (1950).

f) J. A. V. Butler, P. F. Davison, D. W. F. James and K. V. Shooter, Biochim. Biophys. Acta, 13, 224 (1954).

g) J. A. V. Butler and P. F. Davison, Advan. Enzymol., 18, 161 (1957).

h) E. Fredericq, Biochim. Biophys. Acta, 55, 300 (1961).

i) E. Fredericq, ibid., 68, 167 (1963).

8) DNH as crosslinked gel.

a to c) loc. cit, refs. 1e, 5g, 7h).

d) K. G. Stern, G. Goldstein, J. Wagman and J. Schryver, Federation Proc., 6, 296 (1947).

e) P. Doty and G. Zubay, J. Am. Chem. Soc., 78, 6207 (1956).

9) Reconstituted DNH aggregates.

a) W. Huiskamp, Z. Physiol. Chem., 32, 145 (1901) p. 161.

b) S. S. Cohen, J. Biol. Chem., 158, 255 (1945) p. 262.

c) M. L. Petermann and C. M. Lamb, ibid., 176, 685 (1948).

d) E. Chargaff and E. Vischer, Ann. Rev. Biochem., 17, 201 (1948) p. 202.

e) G. Schmidt, ibid., 19, 149 (1950) p. 157.

f) G. Frick, Biochim. Biophys. Acta, 8, 202 (1952).

g) C. F. Crampton, R. Lipshitz and E. Chargaff, J. Biol. Chem., 211, 125 (1954).

h) M. M. Daly and A. E. Mirsky, J. Gen. Physiol., 38, 405 (1955).

i) C. F. Crampton, J. Biol. Chem., 227, 495 (1957).

j) N. Ui, Biochim. Biophys. Acta, 25, 493 (1957).

k) C. F. Crampton and E. Chargaff, J. Biol. Chem., 226, 157 (1957).

l to o) loc. cit. refs. 1d, 5e, 5f, 7h).

10) Preparation of DNH using high salt concentrations.

a) I. Banga and A. Szent-Györgyi, Enzymologia, 9, 111 (1941).

b) A. E. Mirsky and A. W. Pollister, Proc. Natl. Acad. Sci. U. S., 28, 344 (1942).

c) K. G. Stern, S. C. Shen and P. Macaluso, Federation Proc., 4, 106 (1945).

d) K. G. Stern and S. Davis, ibid., 5, 156 (1946).

e) D. C. Gajdusek, Biochim. Biophys. Acta, 5, 397 (1950).

f) J. Shack and J. M. Thompsett, J. Biol. Chem., 197, 17 (1952).

g) Y. Khouvine, J. Grègoire and J. P. Zalta, Bull. Soc. Chim. Biol., 35, 244 (1953).

h) L. B. Smillie, A. M. Marko and G. C. Butler, Can. J. Biochem. Physiol., 33, 263 (1955).

i) H. H. Henstell, R. I. Freedman and I. Cooper, Biochim. Biophys. Acta, 16, 211 (1955).

j) K. Murray and A. R. Peacocke, ibid., 55, 935 (1962).

k to o) loc. cit. refs. 5b, 5f, 8d, 9c, 9i).

11) Preparation of histones using high salt concentrations.

a) I. Bang, Z. Physiol. Chem., 30, 508 (1900).

b) E. Hammarsten, Biochem. Z., 144, 383 (1924) p. 389.

c) R. R. Bensley, Anat. Record, 72, 351 (1938).

d) M. M. Daly, A. E. Mirsky and H. Ris, J. Gen. Physiol., 34, 439 (1950) p. 441.

e) J. Grègoire and M. Limozin, Bull. Soc. Chim. Biol., 36, 15 (1954).

f) C. F. Crampton, S. Moore and W. H. Stein, J. Biol. Chem., 215, 787 (1955).

g) J. M. Luck, H. A. Cook, N. T. Eldredge, M. I. Haley, D. W. Kupke and P. S. Rasmussen, Arch. Biochem. Biophys., 65, 449 (1956).

h) J. M. Neelin and G. C. Butler, Can. J. Biochem. Physiol., 37, 843 (1959) p. 844.

i) L. S. Wolfe and H. McIlwain, Biochem. J., 78, 33 (1961).

j to o) loc. cit. refs. 5f, 5j, 7f, 9b, 9i, 10h). see also ref. 12).

12) Extraction of lysine rich histone by salt.

a) E. Stedman and E. Stedman, Phil. Trans. Roy. Soc. London, Ser. B, 235, 565 (1950-1951).

b) P. F. Davison and J. A. V. Butler, Biochim. Biophys. Acta, 15, 439 (1954).

c) J. A. Lucy and J. A. V. Butler, ibid., 16, 431 (1955).

d) L. B. Smillie, G. C. Butler and D. B. Smith, Can. J. Biochem. Physiol., 36, 1 (1958).

e) loc. cit. ref. 51), p. 163.

13) Extraction of histones by strong acids.

A) Hydrochloric acid.

a) A. Kossel, Z. Physiol. Chem., 8, 511 (1884).

b) P. F. Davison, D. W. F. James, K. V. Shooter and J. A. V. Butler, Biochim. Biophys. Acta, 15, 415 (1954).

c) J. M. Neelin and G. E. Connell, ibid., 31, 539 (1959).

d) D. M. P. Phillips and E. W. Johns, Biochem. J., 71, 17P (1959).

e) L. Hnilica, Experiencia, 15, 139 (1959).

f) D. M. P. Phillips and E. W. Johns, Biochem. J., 72, 538 (1959).

g) E. W. Johns, D. M. P. Phillips, P. Simson and J. A. V. Butler, ibid., 77, 631 (1960).

h) L. Hnilica, E. W. Johns and J. A. V. Butler, ibid., 82, 123 (1962).

i) J. A. V. Butler, loc. cit. ref. 1f), p. 38.

j to s) loc. cit. refs. 3, 5a, 51, 7f, 10g, 11d, 11f, 11g, 11h, 12a).

B) Sulfuric acid.

a) K. Felix and A Harteneck, Z. Physiol. Chem., 157, 76 (1926).

b) N. Ui, Biochim. Biophys. Acta, 22, 205 (1956).

c) H. J. Cruft, J. Hindley, C. M. Mauritzen and E. Stedman, Nature, 180, 1107 (1957).

d) H. J. Cruft, C. M. Mauritzen and E. Stedman, Phil. Trans. Roy. Soc. London, Ser. B, 241, 93 (1957).

e) P. F. Davison, Biochem. J., 66, 703 (1957).

f) H. C. Cruft, C. M. Mauritzen and E. Stedman, Proc. Roy. Soc. London, Ser. B, 149, 21 (1958).

g) J. M. Luck, P. S. Rasmussen, K. Satake and A. N. Tsvetekov, J. Biol. Chem., 233, 1407 (1958).

h) C. M. Mauritzen and E. Stedman, Proc. Roy. Soc. London, Ser. B, 150, 299 (1959).

i) ibid., 153, 80 (1960).

j) K. Satake, P. S. Rasmussen and J. M. Luck, J. Biol. Chem., 235, 2801 (1960).

k) D. J. R. Laurence, P. Simson and J. A. V. Butler, Biochem. J., 87, 200 (1963).

l) K. Murray, loc. cit., ref. 1f) p. 23.

m to r) loc. cit. refs. 5a, 7f, 9h, 9j, 12a, 13Af).

C) Perchloric acid.

a) M. Ogur and G. Rosen, Arch. Biochem., 25, 262 (1950).

b) R. N. Feinstein and C. L. Butler, Proc. Soc. Exp. Biol. Med., 79, 179 (1951).

c) E. W. Johns and J. A. V. Butler, Biochem. J., 82, 15 (1962).

D) Trichloroacetic acid.

a) E. H. de Nooij and H. G. K. Westenbrink, Biochim. Biophys. Acta, 62, 608 (1962).

b) loc. cit. ref. 13Ai).

E) Citric acid.

a) D. M. P. Phillips, Biochem. J., 67, 9P (1957).

b) J. M. Neelin and E. M. Neelin, Can. J. Biochem. Physiol., 38, 355 (1960).

c) A. L. Dounce and R. Umaña, Biochemistry, 1, 811 (1962).

d) J. M. Neelin, loc. cit. ref 1f) p. 66.

e to g) loc. cit. refs. 7f, 11h, 12b).

F) Phosphoric acid.

a) loc. cit. ref. 7f).

14) Amberlite chromatography of histones.

a) C. F. Crampton, S. Moore and W. H. Stein, J. Biol. Chem., 225, 363 (1957).

b) P. S. Rasmussen, K. Murray and J. M. Luck, J. Mol. Biol., 1, 79 (1962).

c to j) loc. cit. refs. 9i, 11f, 11g, 11h, 13Bg, 13Bj, 13Bl, 13Ed).

15) Sephadex chromatography of histones.

a) J. Porath, Biochim. Biophys. Acta, 39, 193 (1960).

b) H. J. Cruft, ibid., 54, 611 (1961).

c) H. J. Cruft, loc. cit. ref. 1f) p. 75.

16) Carboxymethylcellulose chromatography of histones.

a) P. F. Davison, Biochem. J., 66, 708 (1957).

b) J. A. V. Butler, J. Gen. Physiol., 45, Suppl., 195 (1962).

c) L. S. Hnilica and H. Busch, J. Biol. Chem., 238, 918 (1963).

d to h) loc. cit. refs. 13Af, 13Ag, 13Ai, 13Be, 130c).

17) Other chromatographic procedures for histones.

a) loc. cit. ref. 13Ea).

18) Zone electrophoresis of histones.

a) B. M. Olivera and N. Davidson, private communications.

19) Tiselius boundary electrophoresis of histones.

a) J. L. Hall, J. Am. Chem. Soc., 63, 794 (1941) p. 797.

b) H. J. Cruft, C. M. Mauritzen and E. Stedman, Nature, 174, 580 (1954).

c) J. A. V. Butler, P. F. Davison, D. W. F. James and K. V. Shooter, Biochem. J., 57, XXIV (1954).

d) H. J. Cruft, C. M. Mauritzen and E. Stedman, Proc. Roy. Soc. London, Ser. B, 149, 36 (1958).

e) L. Hirschbein and R. Rosencwajg, Compt. Rend., 251, 1309 (1960).

f) E. H. De Nooij and J. A. Niemeijer, Biochim. Biophys. Acta, 65, 148 (1962).

g to s) loc. cit. refs. 7f, 9h, 9j, 11e, 11g, 12d, 13Ab, 13Bc, 13Bd, 13Be, 13Bh, 13Bi, 13Da).

20) Starch gel electrophoresis of histones.

a) E. W. Johns, D. M. P. Phillips, P. Simson and J. A. V. Butler, Biochem. J., 80, 189 (1961).

b) J. M. Neelin and G. C. Butler, Can. J. Biochem. Physiol., 39, 485 (1961).

c) E. W. Johns and J. A. V. Butler, Biochem. J., 84, 436 (1962).

d) K. Murray, Anal. Biochem., 3, 415 (1962) p. 423.

e to p) loc. cit. refs. 13Ac, 13Ag, 13Ah, 13Bc, 13Bk, 13Cc, 13Da, 13Eb, 13Ed, 15b, 16b, 16c).

21) Acrylamide gel electrophoresis of histones.

a) H. J. Cruft, Biochem. J., 84, 47P (1962).

b) H. C. McAllister, Jr., Y. C. Wan and J. L. Irvin, Anal. Biochem., 5, 321 (1963).

c) H. J. Cruft, loc. cit. ref. 1f) p. 72.

22) Other electrophoresis procedures used for histones.

A) Paper electrophoresis.

a to c) loc. cit. refs. 11e, p. 19, 11g, 13b, p. 417).

B) Ethylcellulose column electrophoresis.

a) loc. cit. ref. 11g).

C) Glass column electrophoresis.

a) loc. cit. ref. 9h).

23) K. Murray, loc. cit. ref. 1f) p. 15.

24) Molecular weight of histones.

a) D. M. P. Phillips, Biochem. J., 68, 35 (1958).

b) R. Trautman and C. F. Crampton, J. Am. Chem. Soc., 81, 4036 (1959).

c) D. M. P. Phillips, Biochem. J., 80, 40P (1961).

d) G. Giannoni and A. R. Peacocke, unpublished observations reported by P. M. Bayley et al., loc. cit. ref. 5j).

e) D. M. P. Phillips, Biochem. J., 87, 258 (1963).

f to u) loc. cit. refs. 5h, 7f, 9j, 11g, 11h, 13Ab, 13Af, 13Ag, 13Bb, 13Bc, 13Bf, 13Bj, 13Cc, 13Eb, 14a, 19c).

25) Cell, organ, and species specificity of histones.

a) Y. Khouvine and F. Baron, Bull. Soc. Chim. Biol., 33, 229 (1951).

b) E. J. Eadie and G. Leaf, Biochem. J., 50, XXXIV (1952).

c) H. A. Harper and M. D. Morris, Arch. Biochem. Biophys., 42, 61 (1953).

d) V. G. Allfrey, A. E. Mirsky and H. Stern, Advan. Enzymol., 16, 411 (1955).

e) E. W. Johns, Biochem. J., 84, 25P (1962).

f to r) loc. cit. refs. 2, 11d, 11h, 13Ah, 13Be, 13Bg, 13Bh, 13Bi, 14a, 16b, 19b, 20a, 20b).

26) Amberlite chromatography of histones using GuCl.

a to d) loc. cit. refs. 11g, 13Bg, 13Bj, 13Bl).

27) D. Fambrough, Jr., private communications.

28) Amino acid composition of histone fractions.

a and b) loc. cit. refs. 13Bl, 14b).

29) Proline incompatible with the alpha-helix of proteins.

a) L. Pauling and R. B. Corey, Proc. Natl. Acad. Sci. U. S., 37, 272 (1951) p. 277.

b) J. T. Edsall, J. Polymer Sci., 12, 253 (1954) p. 256.

c) H. Lindley, Biochim. Biophys. Acta, 18, 194 (1955).

d) A. G. Szent-Györgyi and C. Cohen, Science, 126, 697 (1957).

e) J. C. Kendrew, H. C. Watson, R. E. Dickerson, D. C. Phillips and V. C. Shore, Nature, 190, 666 (1961).

f) H. C. Watson and J. C. Kendrew, Nature, 190, 670 (1961).

g) D. R. Davies, J. Mol. Biol., 9, 605 (1964).

30) Molecular weight of histones by end group determination.

a to j) loc. cit. refs. 11g, 13Af, 13Ag, 13Bg, 13Bj, 13Cc, 13Eb, 24a, 24c, 24e).

31) Preparation of reconstituted DNH.

a) R. C. Huang and J. Bonner, Proc. Natl. Acad. Sci. U. S., 48, 1216 (1962).

b) J. Bonner, R. C. Huang and K. Murray, Federation Proc., 22, 353 (1963).

32) R. C. Huang, J. Bonner and K. Murray, J. Mol. Biol., 8, 54 (1964).

33) B. M. Olivera, R. C. Huang and N. Davidson, Z. Elektrochem., 68, 802 (1964).

34) Melting temperature of reconstituted DNH.

a) L. S. Hnilica and D. Billen, Biochim. Biophys. Acta, 91, 271 (1964) p. 276.

b) loc. cit. ref. 32).

35) Priming of RNA synthesis by reconstituted DNH.

a to c) loc. cit. refs. 3, 32, 34a).

Different results were obtained by

d) V. G. Allfrey, V. C. Littau and A. E. Mirsky, Proc. Natl. Acad. Sci. U. S., 49, 414 (1963).

e) G. C. Barr and J. A. V. Butler, Nature, 199, 1170 (1963).

f) J. Hindley, Biochem. Biophys. Res. Commun., 12, 175 (1963).

36) loc. cit. ref. 3).

37) loc. cit. ref. 1e). See also
A. R. Peacocke and B. N. Preston, Nature, 192, 228 (1961).

38) R. C. Huang, J. Bonner and K. Marushige, unpublished work. See also
J. Bonner and R. C. Huang, J. Mol. Biol., 6, 169 (1963).

39) Sedimentation coefficient of native DNH.
a) R. O. Carter, J. Am. Chem. Soc., 63, 1960 (1941).
b to e) loc. cit. refs. 1e, 51, 8e, 32).

40) Melting temperature of native DNH.
a) M. F. Lee, I. O. Walker and A. R. Peacocke, Biochim. Biophys. Acta, 72, 310 (1963).
b) J. Bonner and R. C. Huang, loc. cit. ref. 1f) p. 254.
c to f) loc. cit. refs. 1e, 3, 32, 38).

41) loc. cit. ref. 40b), p. 257.

42) Residual RNA in DNH.
a) R. C. Huang and J. Bonner, unpublished results. See also
b) J. A. V. Butler, P. F. Davison and D. W. F. James, Biochem. J., 54, XXI (1953).
c to e) loc. cit. refs. 1c, 51, 7f).
Little or no RNA were found by
f) K. G. Stern, G. Goldstein and H. G. Albaum, J. Biol.

Chem., 188, 273 (1951).

g) P. F. Davison and J. A. V. Butler, Biochim. Biophys. Acta, 21, 568 (1956).

h and i) loc. cit. refs. 5a, 7h).

43) Aggregation of histones.

a) G. Toennis and B. Bakay, Nature, 176, 696 (1955).

b) E. Fredericq, Biochim. Biophys. Acta, 55, 300 (1962).

c to s) loc. cit. refs. 1e, 5a, 5b, 5g, 5l, 7g, 8e, 11h, 11g, 12b, 12d, 13Ab, 13Bb, 13Bd, 13Bf, 19b, 19c). See also ref. 6).

44) Degradability of histones on standing.

a) J. P. Greenstein, J. Nat. Cancer Inst., 1, 77 (1940).

b to g) loc. cit. refs. 5g, 5h, 5l, 7e, 10e, 11h).

45) "Impurities" found in DNH.

A) RNA.

See ref. 42). Also loc. cit. refs. 5h, 5k, 13Ab).

B) Non-histone protein.

a) D. Hamer, Brit. J. Cancer, 7, 151 (1953).

b) B. Bakay, Federation Proc., 13, 178 (1954).

c) E. Fredericq, E. J. Bigwood and Cl. Wodon, Arch. Intern. Physiol. Biochim., 69, 639 (1961).

d to h) loc. cit. refs. 5a, 7h, 10b, 13Ab, 42g).

C) Lipids.

a) J. R. Baker, Quart. J. Microscop. Sci., 87, 441 (1946).

b) J. Chayen and P. B. Gahan, Biochem. J., 69, 49P (1958).

c) M. H. F. Wilkins, G. Zubay and H. R. Wilson, J. Mol. Biol., 1, 179 (1959) p. 182.

d) L. Hirschbein, Compt. Rend., 250, 222 (1960).

e and f) loc. cit. refs. 5h, 7h).

D) Enzymes.

a) loc. cit. ref. 42f).

E) Hexoses.

a) loc. cit. ref. 7h).

F) Salts.

a and b) loc. cit. refs. 5h, 42g).

46) loc. cit. ref. 5k).

47) Aggregation of histone fractions.

a) L. Ahlström, Arkiv Kemi, 24A, No. 31 (1947).

b to f) loc. cit. 10d, 13Aa, 13Ab, 13Bb, 13Bf).

Also ref. 43).

A) Aggregation by base.

a) W. L. Bloom, D. W. Watson, W. L. Cromartie and M. Freed, J. Infect. Diseases, 80, 41 (1947) p. 48.

b) W. L. Bloom, B. Codgell and G. T. Lewis, Cancer Res., 10, 205 (1950).

c) N. Ui, Bull. Chem. Soc. Japan, 27, 392 (1954).

d to j) loc. cit. refs. 5a, 5h, 9j, 13Bf, 19b, 25e, 43a).

B) Aggregation by high salt concentration.

a to e) loc. cit. refs. 5h, 9j, 12d, 13Bf, 43a).

C) Aggregation as a function of histone concentration, temperature and time.

a and b) loc. cit. refs. 13Ab, 13Bf).

48) Aggregation as a means of separating histone fractions.

a to c) loc. cit. refs. 9j, 13Bb, 13Bh).

49) Extinction coefficient of DNA and DNH.

a) E. Chargaff and R. Lipshitz, J. Am. Chem. Soc., 75, 3658 (1953).

b to i) loc. cit. refs. 1e, 5a, 5f, 5j, 7h, 8e, 10j, 40a).

50) Extinction coefficient of peptide bond.

a) A. R. Goldfarb, L. J. Saidel and E. Mosovich, J. Biol. Chem., 193, 397 (1951).

b) A. R. Goldfarb and L. J. Saidel, Science, 114, 156 (1951).

51) R. H. Jensen, private communications.

52) D. Tuan, private communications.

53) R. F. Stewart, private communications.

54) W. F. Dove, Ph. D. Thesis, California Institute of Technology, 1962, p. 27.

55) B. M. Olivera, P. Baine and N. Davidson, Biopolymers, 2, 245 (1964).

56) Beckman Instrument Co., Inc., Spinco Division, Palo Alto, Calif., Tentative Procedure "Use of Flat Bottom Quartz Tubes in SW39 Rotors", 1963.

57) J. Kaspar, private communications.

58) J. Vasilevskis, Ph. D. Thesis, California Institute of Technology, 1963, p. 11.

59) J. Vasilevskis, private communications.

60) R. C. Lief, Ph. D. Thesis, California Institute of Technology, 1964, p. 36.

61) H. K. Schachman, Ultracentrifugation in Biochemistry, Academic Press, New York, London, 1959, p. 10.

62) Approximation for the statistical average.

63) O. H. Lowry, N. J. Rosebrough, A. L. Farr and R. J. Randall, J. Biol. Chem., 193, 265 (1951).

64) S. Moore and W. H. Stein, J. Biol. Chem., 176, 367 (1948).

65) W. J. Dreyer, private communications.

66) R. C. Huang, private communications.

67) M. E. Reichmann, S. A. Rice, C. A. Thomas and P. Doty, J. Am. Chem. Soc., 76, 3047 (1954).
See also loc. cit. ref. 39a).

69) Loc. cit. ref. 61) p. 90.

70) F. Fujimura, private communications.

71) Loc. cit. ref. 14b).

72) J. Bonner and R. C. Huang, private communications.

73) Loc. cit. ref. 33a).

74) Loc. cit. ref. 55).

75) Loc. cit. ref. 32).

76) Determination of amide in histones.

a to c) loc. cit. refs. 11f, 13Af, 13Bg).

77) Cooperative melting unit of DNA.

a) C. A. Dekker and H. K. Schachman, Proc. Natl. Acad. Sci. U. S., 40, 894 (1954).

b) S. A. Rice and P. Doty, J. Am. Chem. Soc., 79, 3937 (1957).

c) S. A. Rice, A. Wada and E. P. Geiduschek, Discussions Faraday Soc., 25, 130 (1958).

d) A. R. Peacocke and I. O. Walker, J. Mol. Biol., 5, 560 (1962).

78) G. L. Eichhorn, Nature, 194, 474 (1962).

79) W. F. Dove and N. Davidson, J. Mol. Biol., 5, 467 (1962). Loc. cit. ref. 54) p. 51.

80) G. Felsenfeld, G. Sandeen and P. H. von Hippel, Proc. Natl. Acad. Sci. U. S., 50, 644 (1963).

PROPOSITIONS

Proposition I

It is proposed that the interaction of silver ions with basic proteins and polypeptides be investigated, in order to establish

1) whether arginine and lysine side chains show differences in their formation of metal complexes,

2) whether arginine-rich proteins can be selectively precipitated in proportion to their arginine content.

As has been shown in the preceding thesis, detection and characterization of individual histone fractions was rather complicated and non-quantitative due to the necessity of having to work at low concentrations in order to avoid precipitation of histones at the salt concentrations used for their dissociation from nucleohistones. In searching for a way to simplify detection and quantification of these histone fractions, several reports were found in the literature (1) stating that histidine and arginine may be precipitated selectively from a mixture of amino acids by the addition of silver ions. Histidine precipitates at pH 7, arginine at pH 9, while lysine (2) precipitates much less readily. If a similar selectivity of complex formation can be detected in the case of basic proteins, like histones, which are classified according to their arginine to lysine ratio (Table I) - their histidine concentration being small and

Table I

Amino Acid Composition of Histone Fractions From Calf Thymus in Mole %

Kenneth Murray (18)

Amino Acids	Calf Thymus Histone Fraction No.							
	Iaa	Ia	Ib	IIaa	IIa	IIb	III	IV
-N- MeLys	0	0	0	0.5	0.3	0	0.7	0.8
Lys	13.8	25.3	26.2	10.2	9.6	13.5	9.3	8.9
His	2.2	0.4	0.2	1.9	1.9	2.8	1.6	1.6
Arg	8.2	3.0	2.6	11.2	11.6	7.9	12.8	12.7
Asp	4.5	2.5	2.5	4.9	4.8	5.6	4.4	4.5
Glu	8.9	4.5	4.3	9.1	9.6	8.7	9.8	10.5
Pro	5.5	8.6	9.1	3.4	3.7	4.7	3.8	4.2
Thr	6.2	5.8	5.4	7.1	6.8	5.2	7.3	7.3
Ser	6.6	6.4	6.5	5.0	4.6	7.8	4.1	4.1
Gly	8.8	6.7	7.3	10.0	9.8	8.2	8.7	7.8
Ala	14.7	24.0	24.2	10.2	11.2	11.5	11.7	12.2
Val	5.0	4.9	4.0	6.8	6.5	6.7	5.8	5.6
Met	0.6	0.1	0.1	1.2	1.2	0.8	1.2	1.2
Ileu	3.8	1.3	1.2	5.4	5.4	4.5	5.4	5.4
Leu	8.2	5.3	5.0	8.0	8.7	8.6	8.6	8.9
Try	1.6	0.7	0.7	2.9	2.8	3.0	2.4	2.3
Phe	1.6	0.6	0.6	2.2	2.3	1.3	2.5	2.7
Cys	0	0	0	0	0	0	0	0
$\frac{Arg}{Lys}$	0.59	0.12	0.10	1.11	1.21	0.59	1.37	1.42
$\Sigma+$ AA	24.2	28.7	29.0	23.8	23.4	24.2	24.4	24.0
$\Sigma-$ AA	13.4	7.0	6.8	14.0	14.4	14.3	14.2	15.0
net + AA	10.8	21.7	22.2	9.8	9.0	9.9	10.2	9.0
MWT x 10^{-3}	~8	~8	~8	12	15	18	25	30

rather invariant - it should be possible to detect and characterize small amounts of these proteins by using radioactive silver.

Unfortunately, no binding studies of silver with basic proteins have been found in the literature, although there are numerous reports of interactions of silver with enzymes and proteins (3). In some cases the interactions have been investigated in more detail. Thus, it was found that silver ions bind stoichiometrically to the imidazole group of histidine (4), but there is some indication that other groups such as - SH (5) and probably also arginine and/or lysine participate in the silver binding as well. Since the histones do not contain cysteine, the binding capacity of silver for -SH groups does not interfere in this case.

In order to determine the likelihood of silver binding to basic amino acid residues, it may be instructive to compare the data available on amino acids and related compounds. Association constants for Ag-arginine have been reported (6), but there are no data for Ag-lysine for comparison. The only comparable data available are those of complexes with divalent Co, Cu, Mn, Ni, Zn, and Fe (Table II). Except in the case of Fe, the complexes with arginine are always somewhat stronger than with lysine, suggesting that similar observations may be expected with silver.

Table II

First Association Constants (log K_1)

20 or 25 °C

Ligand	H^+	Ag^+	Hg^{++}	Cu^{++}	Co^{++}	Mn^{++}	Ni^{++}	Zn^{++}	Fe^{++}
biguanide	13.25			11.9			9.16		
arginine	12.48	3.2		7.34	3.7	2.64	4.92	4.19	2.86
lysine	10.72			6.8	3.4	2.18	4.4	3.8	4.5
$Me-NH_2$	10.72	3.15	8.6						
$Et-NH_2$	(10.75)	3.37							
NH_3	9.61	3.4	8.8	4.25	2.1		2.8	2.4	
glycine	(9.7)	(3.45)	10.3	(8.3)	(5.0)	(3.3)	(6.5)	(5.3)	(4.)
histidine	(9.17)	6.45	7.28	(10.5)	(7.1)	3.58	(8.70)	(6.7)	5.85
imidazole	(7.1)	3.78	3.57	(4.25)	(2.3)	1.65	(3.1)	(2.7)	3.20
albumin				3.7				2.9	

underlined values = K_1K_2 ,

values in parentheses are averages over several reported values.

However, the results with free amino acids should not be strictly comparable to those with polypeptides or proteins, since in these instances only the sidechain amino or guanidino groups are expected to act as ligands, the alpha-amino and the carboxyl groups being part of the peptide chain. Steric effects may also become important in determining the strength of the binding.

A more useful comparison seems to be that of relating the basicity of the ligand to the strength of the complex formed with silver ions, as was pointed out by Larssen (7) and by Bruehlman and Verhoek (8). A linear relationship exists between the pK_{HB}, the negative logarithm of the acid dissociation constant of the ammonium ions, and log K_1, the logarithm of the first association constant of the corresponding amines with silver ions. A similar dependence of pK_{HB} and log K_{HgB} was observed by Wirth and Davidson (9) for mercury complexes. They measured the association constant for guanidinium ion with mercury and found that it fell on the straight line plot together with pyridine, primary and secondary amines. Since Hg binding is characteristically similar to that of Ag, an approximate pK_{AgGu} may be calculated by assuming that guanidinium-silver would fall on the straight line obtained by Bruehlman and Verhoek for the binding of Ag with pyridine and primary amines, i. e. $\log K_1 = 0.25_3 \log K_{HB} + 1.65 = 0.25_3 \times 13.54 + 1.65 = 5.08$.

Compared to 3.4 - a good average value for the log K_1 of complexes of silver ions with primary amines - the estimated association constant for AgGu indicates that guanidine binds silver ions 31.6 times better than a primary alkyl amine. This comparison, however, neglects the pH dependence of the binding. In order to evaluate this effect, a useful relation is that of $\log K^* = \log (K_1 / 1 + K_{HB}[H^+])$, where K^* is the effective equilibrium constant expressing the dependence of the silver complex association constant and the acid dissociation constant on the hydrogen ion concentration. Figure 1 shows plots of log K^* versus pH for arginine (ARG), guanidine (GU), primary amines (RNH_2), imidazole (IM), and histidine (HIS).

These curves indicate that the primary amines are complexed more strongly than either arginine or guanidine below pH 11; a surprising result in regard to the observed precipitation behavior. Evidently, primary amines must form stable, soluble complexes in aqueous solution, while the complexes with guanidine, although weaker, are much less soluble. If a similar behavior is observed with histones, it should be possible to precipitate histones according to their arginine content, but the silver bound would be proportional to the total amount of basic groups and not to those of arginine alone.

Of the numerous procedures available for the study of

Figure 1

Plot of log $K^* = \log[K_1 / 1 + K_{HB}(H^+)]$ versus pH for histidine (HIS), imidazole (IM), guanidine (GU), aliphatic amines (RNH_2), and arginine (ARG).
K_1 is the first association constant for the corresponding silver ion complex ($K_1 = [AgL^+]/[Ag^+] + [L]$). K_{HB} is the acid dissociation constant ($K_{HB} = ([L] + [H^+]/[LH^+])$.

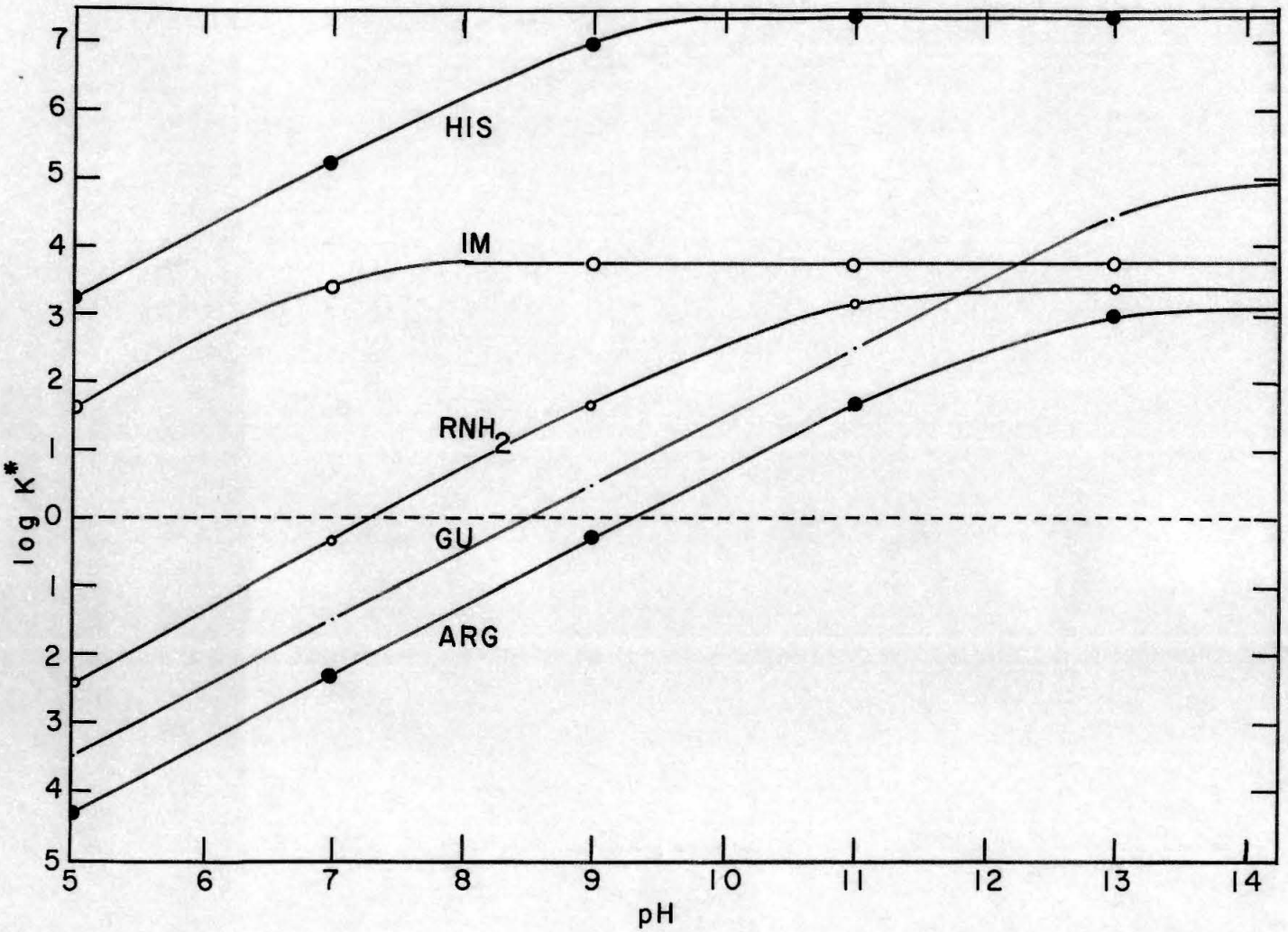

Figure 1

metal - polymer binding (10) the following procedures should be useful for histone - metal interactions:

1) Zone electrophoresis at low ionic strength. Histone mobilities in 0.01 F NaCl, buffered at pH 7.5 with 0.001 M tris buffer, range from 1.05×10^{-4} $cm^2/V\text{-sec}$ for histone fraction II to 1.52×10^{-4} $cm^2/V\text{-sec}$ for histone fraction I (11,12).

2) Ultracentrifugation. Unaggregated histones have sedimentation coefficients of 1 to 2 S (13).

3) Equilibrium dialysis (14).

4) Potentiometric titrations (15).

5) Spectrophotometric methods in cases where the complex formation results in easily measurable changes in spectral bands (16).

If silver turns out to be sufficiently selective in its complex formation, the most suitable isotope for the detection of small amounts of complex would be Ag^{110}, having a half-life of 225 days and emitting 0.7 to 1.4 Mev gamma rays and 0.4 to 1.3 Mev beta minus particles (17).

References

1) Selective precipitation of histidine and arginine by Ag.

a) Amino Acids And Proteins, Theory, Methods, Application, edited by D. M. Greenberg; C. C. Thomas, Springfield, Ill., 1951, p. 646.

b) R. J. Block, J. Biol. Chem. 133, 67 (1940).

c) H. B. Vickery and R. J. Block, ibid. 93, 105 (1931).

d) H. B. Vickery and C. S. Leavenworth, ibid. 76, 707 (1928).

e) H. B. Vickery and C. S. Leavenworth, ibid. 75, 155 (1927).

f) H. B. Vickery and C. S. Leavenworth, ibid. 72, 403 (1927).

g) H. B. Vickery and C. S. Leavenworth, ibid. 68, 225 (1926).

h) A. Kossel and S. Edlbacher, Z. Physiol. Chem. 110, 241 (1920).

i) O. Riesser, ibid. 49, 210 (1906) p. 219.

j) W. Schermesser, ibid. 41, 68 (1904) p. 89.

k) A. Kossel and F. Kutscher, ibid. 31, 165 (1900).

l) W. Gulewitsch, ibid. 27, 178 (1899).

m) A. Kossel, ibid. 25, 165 (1898) p. 179.

n) S. G. Hedin, ibid. 22, 191 (1896).

o) A. Kossel, ibid. 22, 176 (1896).

p) S. G. Hedin, ibid. 21, 297 (1896) p. 303.

q) S. G. Hedin, ibid. 21, 155 (1896).

r) S. G. Hedin, ibid. 20, 186 (1895).

2) Ag^+ lysine

a) M. Guggenheim, Die biogenen Amine, 4th edition, S. Karger Verlag, Basel, New York, 1951, p. 398.

b) A. Kossel, Z. Physiol. Chem. 25, 165 (1898) p. 179.

3) Interaction of Ag^+ with proteins and enzymes.

a) Metabolic Inhibitors, edited by R. M. Hochster and J. H. Quastel, Vol. II, Academic Press, New York, London, 1963, pp. 119 - 127, 371 - 379.

b) F. R. N. Gurd and P. E. Wilcox, Advan. Protein Chem. 11, 311 (1956) p. 370.

c) K. B. Augustinsson and G. Heimbuerger, Acta Chem. Scand. 9, 383 (1955).

d) K. Myrbaeck, Ark. Kemi. 8, 393 (1955).

e) W. H. R. Shaw, J. Am. Chem. Soc. 76, 2160 (1954).

f) A. B. Lerner, Arch. Biochem. Biophys. 36, 473 (1952).

g) W. Grassmann and D. Kusch, Z. Physiol. Chem. 290, 216 (1952).

h) C. L. A. Schmidt, The Chemistry of The Amino Acids And Proteins, 2nd. edition, C. C. Thomas, Springfield, Ill., Baltimore, Md., 1944, p. 690, 772.

i) H. Schorn, Biochem. Z. 199, 459 (1929).

j) E. Heymann and F. Oppenheimer, ibid. 199, 468 (1928).

k) H. Schlee, ibid. 148, 383 (1924) p. 396.

1) W. Pauli and J. Matula, Biochem. Z. 80, 187 (1917).

4) Ag^+ histidine in proteins.

a) Salahuddin and W. U. Malik, J. Indian Chem. Soc. 41, 365 (1964).

b) Salahuddin and W. U. Malik, ibid. 39, 693, 699 (1962).

5) Ag^+ binding to RSH, arg and lys.

a) loc. cit. ref. 3a).

b) J. P. Greenstein and M. Winitz, Chemistry of the Amino Acids, Vol. I, John Wiley and Sons, Inc., New York, London, 1961, p. 646.

c) R. Cecil and J. R. McPhee, Advan. Protein Chem. 14, 255 (1959) p. 299.

d) loc. cit. ref. 3b) p. 335.

e) loc. cit. ref. 2a).

f) J. M. Kolthoff and W. Stricks, J. Am. Chem. Soc. 72, 1952 (1950).

6) L. G. Sillén and A. E. Martell, Stability Constants of Metal-Ion Complexes, The Chemical Society, London, 1964, p. 523.

7) E. Larssen, Z. Physik. Chem. 169A, 207 (1934).

8) R. J. Bruehlman and F. H. Verhoek, J. Am. Chem. Soc. 70, 1401 (1948).

9) T. H. Wirth and N. Davidson, ibid. 86, 4325 (1964).

10) Procedures to study metal - protein binding.

a) J. Steinhardt and S. Beychok in The Proteins, Composi-

tion, Structure, and Function, 2nd edition, Vol. II, edited by H. Neurath, Academic Press, New York and London, 1964, p. 250.

b) J. S. Fruton and S. Simmonds, General Biochemistry, 3rd. edition, J. Wiley and Sons, Inc., New York, 1960, pp. 100 - 112.

c) A Laboratory Manual of Analytical Methods of Protein Chemistry, edited by P. Alexander and R. J. Block, Pergamon Press, London, Oxford, New York, Paris, 1960.

d) F. Haurowitz, Chemistry and Biology of Proteins, Academic Press, Inc., New York, 1950, pp. 58 - 85.

e) loc. cit. ref. 3h) pp. 596 - 821.

11) B. M. Olivera and H. H. Ohlenbusch, unpublished results.

12) Zone electrophoresis of proteins.

a) H. Svensson, loc. cit. ref. 10c) p. 193

b) B. S. Magdoff, ibid., p. 169.

13) D. M. P. Phillips, Prog. Biophysics and Biophys. Chem. 12, 211 (1962) p. 240.

14) Equilibrium dialysis.

a) R. M. Rosenberg, loc. cit. ref. 10c) p. 141.

b) loc. cit. ref. 10b) p. 111.

c) F. R. N. Gurd and D. S. Goodman, J. Am. Chem. Soc. 74, 670 (1952).

d) D. M. Greenberg, loc. cit. ref. 3h) p. 779.

15) a) R. H. Jensen and N. Davidson, Biopolymers (1965) in press.

b) R. H. Jensen, Ph. D. Thesis, California Institute of Technology, Pasadena, Calif., 1965.

16) Spectrophotometry.

a) R. M. Rosenberg, loc. cit. ref. 10c) p. 143.

b) Loc. cit. ref. 10a) p. 254.

17) Handbook of Chemistry and Physics, edited by C. D. Hodgman, Chemical Rubber Publishing Co., Cleveland, Ohio, 1952, p. 371.

18) a) K. Murray in The Nucleohistones, edited by J. Bonner and P. Ts'o, Holden-Day Inc., San Francisco, London, Amsterdam, 1964, p. 23.

b) P. S. Rasmussen, K. Murray and J. M. Luck, J. Mol. Biol., 1, 79 (1962).

Proposition II

As has been shown in the preceding dissertation, the selective extraction of histone fractions from native DNH has made it possible to obtain partially extracted, native DNH which shows a two step melting behavior. There is good indication that partial melting of this material and its renaturation upon slow cooling results in migration of residual histones from the melting to the more resistant DNA regions with simultaneous sharpening of the two step melting profile. Thus, long, DNA-like regions must have been formed which alternate with rather fully covered DNH regions. Since zone electrophoresis of this material does not give more than one band, it is concluded that the differently melting regions exist side by side on the same DNA molecule.

It is proposed that the possibility of separating these regions by any one of the following procedures be investigated, in order to determine

1) whether it is possible to isolate unique, intact DNA regions (genes) which are active in supporting the synthesis of messenger RNA, which in turn can support protein synthesis, and

2) whether their base composition is different.

Proposed Experimental Procedure:

1. The partially salt extracted, native DNH is partially heatdenatured at low ionic strength (e. g. 10^{-4} F EDTA) and cooled slowly to allow renaturation to proceed to completion.

2. The renatured DNH, containing relatively large regions of free DNA, must be degraded either by

a) sonication (1),

b) shearing in a syringe (2), a homogenizer (3) or an atomizer (4), or

c) treatment with endo-DNAse (5).

Ideally, the DNA fragments should have a molecular weight of 300 000 to 1 000 000 daltons, i. e. they should be approximately of gene size. The effectiveness of the degradation procedure can best be determined by zone electrophoresis. Uncomplexed, free DNA regions should be easily separable from DNH regions by this procedure (6).

(Preliminary experiments have shown, that vigorous shearing of partially salt extracted DNH by passing it through a fine syringe, resulted in considerable broadening of the electrophoretic peak as compared to that of the unsheared material.)

The separated, uncomplexed DNA is then tested for its RNA priming activity by the procedure of Huang and Bonner (7). Coupling this system with a protein synthesizing system (8) makes it possible to determine, whether the iso-

lated DNA is enriched in some specific gene, which may be identified by its respective protein (e. g. pea seed globulin).

In addition, some indication of the effectiveness of the procedure may be obtained by determining the base composition of the RNA synthesized at various stages of the procedure by:

1. DNH extracted at various salt concentrations.
2. The DNH of 1) partially heated and renatured.
3. The DNH of 2) after controlled degradation.
4. The DNA and DNH fractions after electrophoretic separation.

In the last instance, a correlation between the composition of the DNA and the synthesized RNA should be observed.

The base composition of the DNA and RNA can be determined by hydrolysis of the nucleic acids and separation of the bases by electrophoresis (9). Other procedures that have been used for the determination of the guanine-cytosine content of DNA are:

a) equilibrium density sedimentation (10),

b) column chromatography (11), and

c) heat denaturation (12).

References

1) Sonication.

a) Y. Miyazawa and C. A. Thomas, Jr., J. Mol. Biol. 11, 223 (1965) p. 224.

b) O. C. Richards and P. D. Boyer, ibid. 11, 327 (1965).

c) D. Freifelder and P. F. Davison, Biophys. J. 2, No. 2, 235 (1962).

d) H. S. Rosenkranz and A. Bendich, J. Am. Chem. Soc. 82, 3198 (1960).

e) P. Doty, B. B. McGill and S. A. Rice, Proc. Natl. Acad. Sci. U. S. 44, 432 (1958).

f) C. E. Hall and M. Litt, J. Biophys. Biochem. Cytol. 4, 1 (1958).

g) A. R. Peacocke and H. K. Schachman, Biochim. Biophys. Acta 15, 198 (1954).

2) Shearing of DNA in a syringe or capillary.

a) loc. cit. ref. 1b).

b) loc. cit. ref. 1c).

c) C. A. Thomas, Jr. and T. C. Pinkerton, J. Mol. Biol. 5, 356 (1962).

d) C. Levinthal and P. F. Davison, ibid. 3, 674 (1961).

e) P. F. Davison, Nature 185, 918 (1960).

f) P. F. Davison, Proc. Natl. Acad. Sci. U. S. 45, 1560 (1959).

3) Breakage of DNA by homogenizing.

a) D. S. Hogness and J. R. Simmons, J. Mol. Biol. 9, 411 (1964) p. 420.

b) A. D. Kaiser, J. Mol. Biol. 4, 275 (1962).

c) E. Burgi and A. D. Hershey, ibid. 4, 313 (1962).

d) I. Rubinstein, C. A. Thomas, Jr. and A. D. Hershey, Proc. Natl. Acad. Sci. U. S. 47, 1113 (1961).

e) E. Burgi and A. D. Hershey, J. Mol. Biol. 3, 458 (1961).

f) A. D. Hershey and E. Burgi, ibid. 2, 143 (1960).

g) loc. cit. ref. 1d).

4) Breakage of DNA by atomizing.

a) L. F. Cavalieri and B. H. Rosenberg, J. Am. Chem. Soc. 81, 5136 (1959).

b) L. F. Cavalieri, ibid. 79, 5319 (1957).

5) Degradation of DNA by endonucleases.

a) F. W. Studier, J. Mol. Biol. 11, 373 (1965) p. 385.

b) G. Bernardi and C. Cordonnier, ibid. 11, 141 (1965).

c) loc. cit. ref. 1b).

d) P. F. Davison, D. Freifelder and B. W. Holloway, J. Mol. Biol. 8, 1 (1964).

e) G. Bernardi and C. Sadron, Biochemistry 3, 1411 (1964).

f) G. Bernardi and M. Griffé, ibid. 3, 1419 (1964).

g) D. Freifelder and P. F. Davison, Biophys. J. 3, 49 (1963).

h) G. Bernardi, M. Griffé and E. Appella, Nature 198, 186 (1963).

i) L. A. MacHattie, G. Bernardi and C. A. Thomas, Jr., Science 141, 59 (1963).

j) I. R. Lehman in Progress in Nucleic Acid Research, Vol. II, edited by J. N. Davidson and W. Cohn, Academic Press, Inc., New York, 1963, p. 83.

k) loc. cit. ref. 1c).

l) I. R. Lehman, G. G. Roussos and E. A. Pratt, J. Biol. Chem. 237, 819 (1962).

m) I. R. Lehman, G. G. Roussos and E. A. Pratt, J. Biol. Chem. 237, 829 (1962).

n) G. Bernardi and C. Sadron, Nature 191, 809 (1961).

o) V. N. Schumaker, E. G. Richards and H. K. Schachman, J. Am. Chem. Soc. 78, 4230 (1956).

6) B. M. Olivera, R. C. Huang and N. Davidson, Ber. Bunsenges. Physik. Chem. 68, 802 (1964).

7) DNA-dependent RNA synthesis.

a) R. C. Huang, J. Bonner and K. Murray, J. Mol. Biol. 8, 54 (1964).

b) R. C. Huang and J. Bonner, Proc. Natl. Acad. Sci. U. S. 48, 1216 (1962).

8) Protein synthesizing system.

a) J. Bonner, R. C. Huang and R. V. Gilden, Proc. Natl. Acad. Sci. U. S. 50, 893 (1963).

b) R. C. Huang, N. Maheshwari and J. Bonner, Biochem. Biophys. Res. Commun. 3, 689 (1960).

9) D. O. Jordan, The Chemistry of Nucleic Acids, Butterworths, Washington, 1960, p. 82.

10) Equilibrium density sedimentation.

a) S. Takashima and E. A. Arnolds, Biochim. Biophys. Acta 94, 546 (1965) p. 547.

b) loc. cit. ref. 1a) p. 233.

c) loc. cit. ref. 3a) p. 429.

d) loc. cit. ref. 2c).

e) C. L. Schildkraut, J. Marmur and P. Doty, J. Mol. Biol. 4, 430 (1962).

f) J. Marmur and P. Doty, Nature 183, 1427 (1959).

g) R. Rolfe and M. Meselson, Proc. Natl. Acad. Sci. U. S. 45, 1039 (1959).

h) N. Sueoka, ibid. 45, 1480 (1959).

11) Column chromatography of DNA.

A. Hydroxyapatite.

a) loc. cit. ref. 1a) p. 229.

B. Methyl serum albumin.

b) loc. cit. ref. 3a) p. 421.

c) N. Sueoka and T. Y. Cheng, J. Mol. Biol. 4, 161 (1962).

d) J. D. Mandell and A. D. Hershey, Anal. Biochem. 1, 66 (1960).

12) Heat denaturation of DNA

a) loc. cit. ref. 3a) p. 431.

b) J. Marmur and P. Doty, J. Mol. Biol. 5, 109 (1962).

c) loc. cit. ref. 10f).

Proposition III

It is proposed that the denaturation - renaturation behavior of DNA-dye complexes be investigated with particular emphasis on their renaturation behavior for the following reasons:

1) The melting behavior of DNA is now quite well understood and most changes in the melting profiles due to dye complexing should be explainable (see below).

2) The distribution of dyes in partially denatured and renatured DNA-dye complexes may lead to insights about the distribution of G-C (A-T) pairs of the DNA strands.

3) The renatured complexes may give clues about the process of denaturation.

Basically, there are two main features of polyion behavior:

a) Behavior explainable on purely electrostatic grounds.

b) Behavior due to other than electrostatic forces.

This division is useful, but somewhat arbitrary. It defines electrostatic forces as those which obey the Poisson Boltzmann equation. Qualitatively, electrostatic forces are those responsible for most of the effects of simple counterions such as alkali metals and of ionic strength on the melting behavior of DNA.

Since the behavior of DNA due to non-electrostatic interactions is generally regarded as of greater intrinsic interest, it is desirable to choose conditions such that the electrostatic effects due to simple counterions are either minimized or are used to swamp out electrostatic interactions of the bases, so that the non-electrostatic effects may be observed separately.

The choice of experimental conditions will depend upon the strength of the complexes formed:

1) The binding to DNA of dyes which are not charged should be relatively independent of the counterion concentration. Melting studies of these complexes would be useful for gaining knowledge about purely non-electrostatic effects (1).

2) The binding of charged dyes to DNA may be either strong or weak.

a) Strong binding may be defined as binding which is sufficiently strong so that the dyes are bound at salt concentrations high enough to swamp out most electrostatic effects. Any change in the melting behavior at these salt concentrations should then be due mainly to non-electrostatic interactions of dyes and DNA.

b) Weak binding may be defined as binding which is significantly affected by variations in the ionic strength of the DNA solution. In order to study this kind of binding

it is necessary that counterion competition for the sites be minimized by lowering the ionic strength of the DNA solution as far as possible without causing spontaneous denaturation of the DNA. This will assure that the effect of dye binding on the melting behavior is maximized, due to the combined action of electrostatic and non-electrostatic forces.

Specific considerations with proflavine as model dye:

Two distinguishable types of binding of proflavine to DNA were found to exist (2). The first and strongest binding is characterized by binding of an individual dye molecule per 5 nucleotide pairs. It is the binding of greatest interest and has been explained in terms of intercalation (3).

The second type of complex was studied extensively in the case of acridine orange (4). It is due to weaker binding and involves stacking of dye molecules presumably along the phosphate groups on the outside of the DNA and is regarded as less interesting from a biological point of view.

All studies concerning the proflavine - DNA interaction indicate that the binding is reversible.

Turning now to the effect of the strong binding on the melting behavior of DNA at equilibrium, it should be possible to confirm:

1) the reversibility of the binding, and

2) to determine the relative binding ability of native versus denatured DNA.

Reversibility of binding can be tested by adding uncomplexed DNA to a solution containing the DNA-dye complex. If the melting profile of the mixture shows one step only, the binding is reversible. A two-step behavior will indicate non-reversible binding and should not be observed with proflavine-DNA.

If native DNA binds more strongly than denatured DNA, the melting curves should be broader than those of uncomplexed DNA, for the dyes will migrate from the denatured regions to regions which are still native.

If denatured DNA binds more strongly than native DNA, the melting profile should be steeper than that of uncomplexed DNA and the Tm should be lower than that of pure DNA. Should the binding to denatured DNA be very strong, it may be possible to denature the DNA merely by increasing the dye concentration.

With regard to renaturation and especially partial denaturation and subsequent renaturation, it has not yet been possible to develop a rigorous theory because of the complexity of the phenomenon and the lack of detailed studies. Nevertheless, some conclusions may be reached

from previous work with pure DNA. The two fundamental parameters which are of interest in renaturation studies are:

1) the completeness of renaturation, and

2) the rate of renaturation.

In order to obtain meaningful renaturation results, it is important that chemical changes during denaturation (depurination, phosphate bond breakage etc.) are prevented or at least determined by independent measurements. It has been reported, that dye binding may increase the susceptibility of DNA to degradation (5).

Furthermore, the rate of heating and cooling of the DNA solution should be slow enough to assure that no further changes in the extent of helix-coil transitions occur at the temperature at which readings are taken. If the rates towards helix-coil equilibrium are very slow, extrapolation to infinite time may have to be made for each recorded temperature.

It is known that renaturation can be significantly enhanced by lowering the temperature some 10 to 20 degrees below that used for denaturation. However, under these circumstances renaturation is not an equilibrium process and a hysteresis curve of absorbance versus temperature is obtained (Fig. 1). It may be possible to use the width of the hysteresis loop under standard cooling rates as an

Figure 1

Heat denaturation and renaturation curve of calf thymus DNA in 7.5 x 10^{-4} N Na^{+} EDTA (pH 8). Sample and heating experiment by B. Olivera run in the Gilford.

Results	Tm°C	% H	Slope	A_{260}	R_{220}
Overall	45.7	37.2	20.83	o.485	1.58

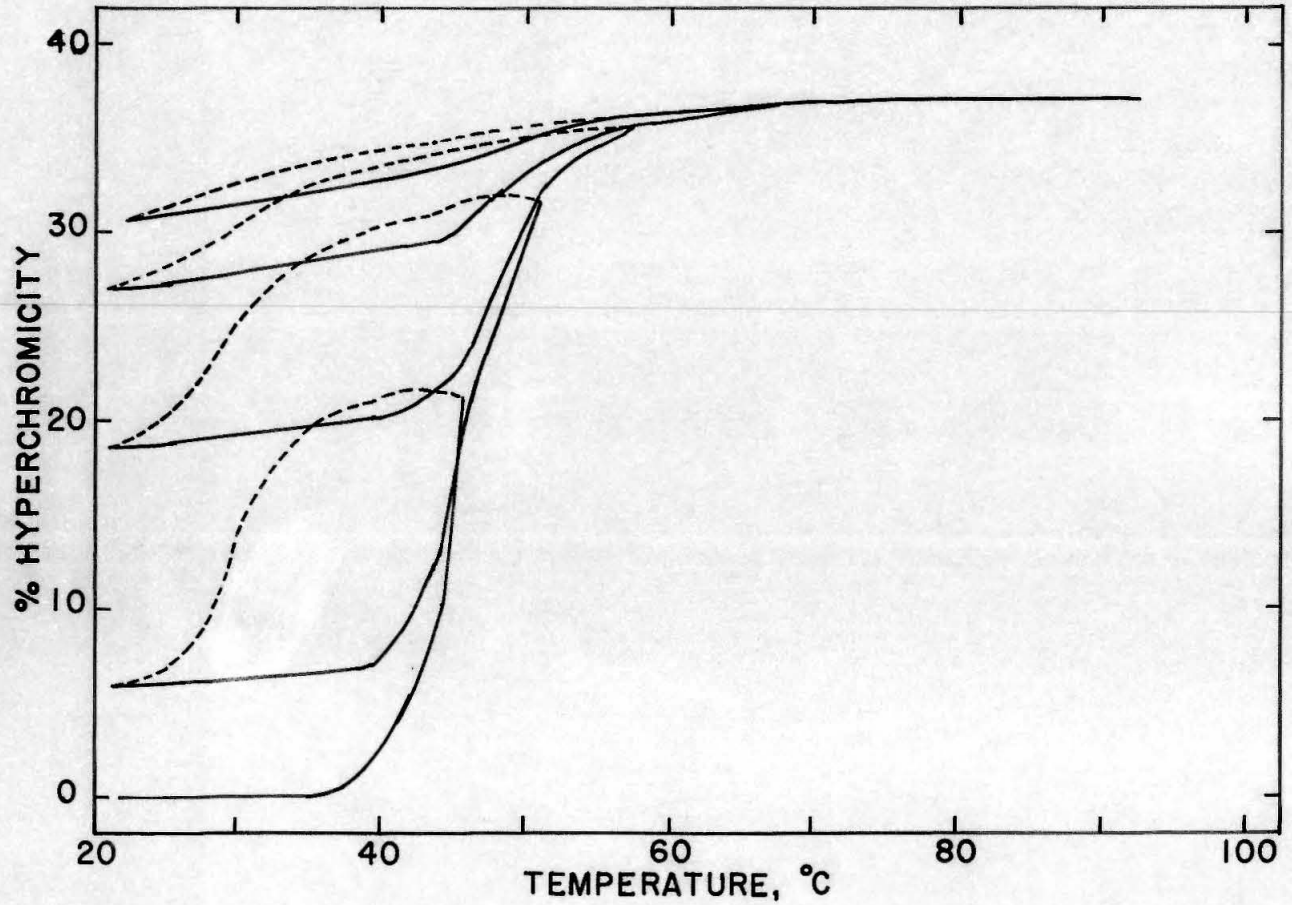

Figure 1

empirical parameter for the rate of renaturation, if appropriate calibration experiments can be performed or if a theoretical relation can be found between the rate of cooling, the loop width, and the rate of renaturation.

In whichever way the rate and extent of renaturation are determined, they will permit valuable conclusions about the interactions of dye molecules and DNA:

If the rate of renaturation of DNA is significantly increased by dye complexing, it can be concluded that the dye either crosslinks the DNA strands or maintains a structure in the denatured regions which makes reannealing more favorable.

The effects on renaturation of crosslinking of DNA strands by chemical means has been investigated by Geiduschek (6). If dyes act in a similar way, as would be expected if the intercalation model by Lerman were correct (Fig. 2) (7), fast reannealing rates should be observed with DNA-dye complexes. They should correspond to those of chemically linked DNA. Of course, fast reannealing rates will only be observed, if the DNA-dye complex is not completely denatured, for in contrast to covalent binding, the non-covalent dye-DNA interactions would then be destroyed. If crosslinks between non-complementary pairs have formed either before or after denaturation, they will reduce the completeness of the renaturation. The effect on the rate may depend greatly upon the detailed mode of crosslinking.

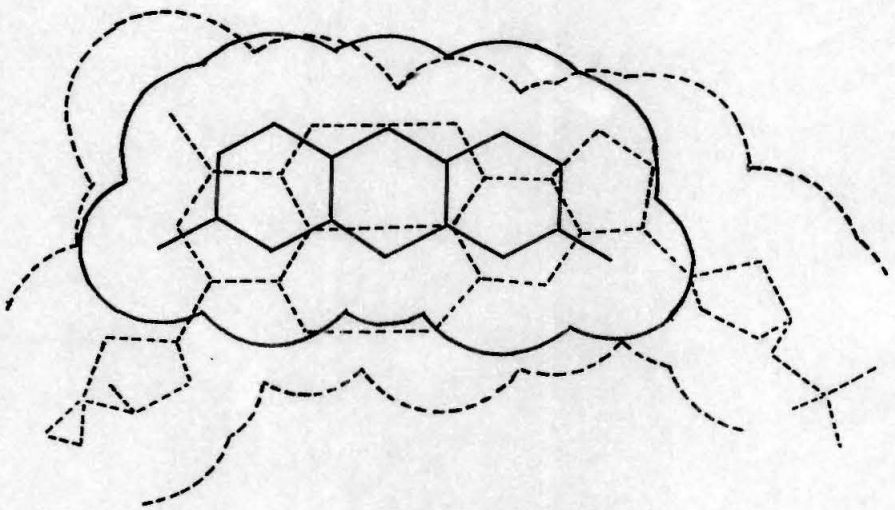

Figure 2

A molecule of proflavine superimposed over a nucleotide pair with the deoxyribose phosphate chain in the extended configuration (L. S. Lerman (3b)).

Interpretation of the renaturation results will become more difficult, if dye binding is base pair specific. In native DNA there are 16 distinguishable arrangements of neighboring basepairs. After denaturation the bases may come together in any of 256 different quartets, for it is conceivable that the dyes may have special affinities for non-Watson-Crick base pairing. In order to determine the degree of specificity under these circumstances, binding studies with model DNA molecules seem absolutely essential.

If the dye binding is specific for any particular base pairing, it may be possible by electron microscopy to determine regions along the DNA which consist of sequences of these basepairs. Should the selective binding be stronger to denatured DNA, it may be possible by partial denaturation to denature the strongly binding base pairs first and, by investigating the DNA after progressive stages of denaturation, to determine their distribution along the strand.

Similar denaturation - renaturation experiments with dyes which bind more strongly to denatured regions, should permit "freezing" of early denaturing regions, since dye complexing should prevent their reannealing. Thus, it should be possible to observe whether denaturation can start in the middle of DNA strands at particularly heat labile regions or only at the ends.

References

1) Non-electrostatic binding: Actinomycin - DNA.

a) M. Gellert, C. E. Smith, D. Neville and G. Felsenfeld, J. Mol. Biol. 11, 445 (1965).

b) L. F. Cavalieri and R. G. Nemchin, Biochim. Biophys. Acta 87, 641 (1964).

c) E. Kahan, F. Kahan and J. Hurwitz, J. Biol. Chem. 238, 2491 (1963).

d) W. Kersten, Biochim. Biophys. Acta 47, 610 (1961).

2) A. R. Peacocke and J. N. H. Skerrett, Trans. Faraday Soc. 52, 261 (1956).

3) Intercalation Model:

a) L. S. Lerman, J. Mol. Biol. 3, 18 (1961).

b) L. S. Lerman, J. Cellular Comp. Physiol. 64, Suppl. 1, 1 (1964).

c) L. S. Lerman, Proc. Natl. Acad. Sci. U. S. 49, 94 (1963).

4) A. L. Stone and D. F. Bradley, J. Am. Chem. Soc. 83, 3627 (1961).

5) D. Freifelder, P. F. Davison and E. P Geiduschek, Biophys. J. 1, 389 (1961).

6) E. P. Geiduschek, Proc. Natl. Acad. Sci. U. S. 47, 950 (1961).

7) loc. cit. ref. 3 b).

Proposition IV

Because of their biological and industrial importance, phosphorus and its compounds have been investigated by biologists and chemists alike (1). Many interesting phenomena have been studied, such as hydrolysis reactions in the presence and without enzymes, complex formation with metals, proteins and organic compounds, reactions of phosphorus halides, metal phosphides etc.

One problem, however, seems not to have been considered in great detail at all: The extent of stereospecific complex formation of phosphates with other compounds. There have been innumerable reports of specific metal ion binding to phosphates (2), of the ability of phosphates to precipitate macromolecules like proteins (3), and of the ability of nitrogen bases to precipitate polyphosphates (4), but whether these interactions are primarily ionic or influenced by stereospecific interactions is not known.

In the following, a system and procedure are proposed by which the existence of stereospecific interactions between nitrogen bases and phosphates may be investigated. In particular, the interaction between the guanidinium group and phosphates should lead to stereospecific orientation according to the scheme shown in figure 1 (5).

Figure 1

Proposed stereospecific orientation of a guanidinium group with a phosphate ion. The numbers indicate bond length in Angstrom. The N-C-N and O-P-O angles are both 123 degrees.

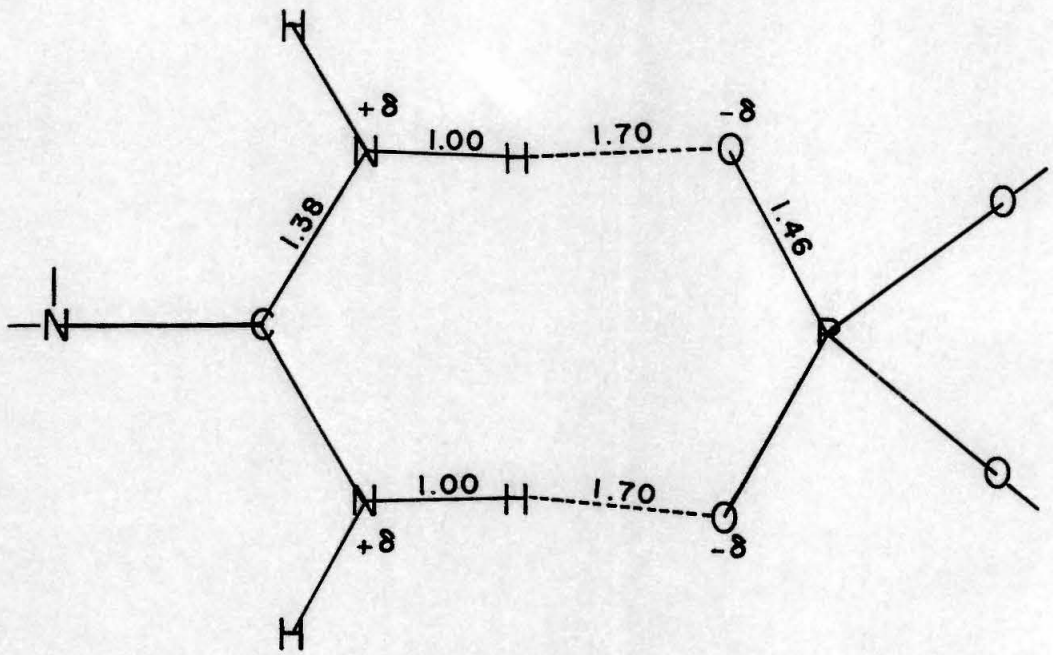

Figure 1

The resonance theory predicts (6) that both $-NH_2$ groups of the guanidinium residue, and both singly-bonded oxygen atoms of the phosphate are equivalent and that considerable pi-bonding stabilizes these ionized groups. (In fact, the stability of these groups is such, that the N-P bond in phosphagens (7) constitutes a rather high energy state with regard to its hydrolysis products, making these compounds the prime energy storage compounds of the animal kingdom.)

As the above figure illustrates, the bond distances and angles of guanidinium and phosphate complement each other such that it might be conceivable that their interactions, although probably mainly ionic, lead to considerable stereospecific alignment of the charged groups with respect to each other. If such alignment can be demonstrated in the case of monomers, its effect on polymeric substances should be cumulative and may be of profound biological importance.

It is suggested, therefore, that the nuclear magnetic resonance spectra of NaH_2PO_4 and similar phosphates (8) be studied in relation to changes in the concentration of arginine-N^{15} or creatine-N^{15} in aqueous solution. Splitting of the NMR band of phosphorus should be an indication of strong, partially covalent linking of P^{31} to N^{15}. A 1:2:1 triplet would result. The N^{15} peaks would be split into

two equal peaks each. However, spin-spin coupling may not be very likely. The strongest interactions that may be observed will probably cause only broadening and perhaps shifting of the phosphorus band due to restrictions in the rotation of the interacting moieties (9).

In order to determine whether there exists a preferred stereospecific interaction between guanidinium and phosphate, the observed shifts should be compared to shifts obtained with compounds containing only an ammonium group instead of a guanidinium group.

References

1) Reviews of phosphorus chemistry.

a) Acides Ribonucléiques et Polyphosphates; Structure, Synthèse et Fonctions, Colloq. Intern. Centre Natl. Rech. Sci., Strasbourg (France), 1961.

b) E. Thilo, Chemie der Polyphosphate, loc. cit. ref. 1a) p. 491.

c) G. Drews, Cytochemistry of Polyphosphates, loc. cit. ref. 1a) p. 533.

d) J. R. Van Wazer, Phosphorus and Its Compounds, Vol. I, "Chemistry", Interscience Publishers, Inc., New York, 1958.

e) ibid., Vol. II, "Technology, Biological Functions, and Applications", 1961.

f) Phosphoric Esters and Related Compounds, edited by G. W. Kenner and D. M. Brown, Symposium at the Chemical Society Anniversary Meeting, Cambridge Apr. 9 - 12, 1957, Chemical Society London, 1957.

g) Phosphorus Metabolism, edited by W. D. McElroy and B. Glass, J. Hopkins Press, Baltimore, 1952.

2) Binding of metal ions to phosphates.

a) H. A. Lardy, loc. cit. ref. 1g) Vol. I, p. 477.

b) J. R. Van Wazer and D. A. Campanella, J. Am. Chem. Soc. 72, 655 (1950).

c) O. H. Warburg, Heavy Metal Prothetic Groups and Enzyme Action, Clarendon Press, Oxford, 1949.

d) L. B. Rogers and C. A. Reynolds, J. Am. Chem. Soc. 71, 2081 (1949).

e) C. Neuberg and J. Mandl, Arch. Biochem. 23, 499 (1949).

3) Precipitation of proteins by phosphates.

a) G. Perlmann, Advan. Protein Chem. 10, 1 (1955).

b) D. M. Greenberg, Amino Acids and Proteins, Theory, Methods, Application, C. C. Thomas, Springfield, Ill., 1951, p. 464.

c) G. Perlmann, J. Biol. Chem. 137, 707 (1941).

d) G. Perlmann and H. Herrmann, Biochem. J. 32, 926 (1938).

e) H. Herrmann and G. Perlmann, Nature 140, 807 (1937).

4) Precipitation of polyphosphates by nitrogen bases.

a) C. Singh, Indian J. Chem. 2, 67 (1964).

b) J. P. Ebel and J. Colas, Bull. Soc. Chim. Biol. 37, 445 (1955).

5) loc. cit. ref. 1d) p. 672.

D. J. Cram and G. S. Hammond, Organic Chemistry, McGraw-Hill, New York, Toronto, London, 1959, p. 112.

6) Resonance theory.

a) B. J. Katchman, loc. cit. ref. 1e) p. 1418.

b) P. Oesper, loc. cit. ref. 1g) p. 534.

c) P. Oesper, Arch. Biochem. 27, 255 (1950) pp. 258, 265.

d) H. M. Kalckar, Chem. Rev. 28, 71 (1941) p. 126.

7) Phosphagens.

a) N. G. Thoai and J. Roche, Biol. Rev. 39, 214 (1964).

b) B. J. Katchman, loc. cit. ref 1e) p. 1317.

c) A. H. Ennor and J. F. Morrison, Physiol. Rev. 38, 631 (1958).

d) F. Lipmann, loc. cit. ref. 1g) p. 521.

e) P. Oesper, loc. cit. ref. 1g) p. 533.

8) NMR spectra of phosphates.

a) E. Fluck, Ber. 94, 1388 (1961).

b) E. Schwarzmann and J. R. Van Wazer, J. Am. Chem. Soc. 83, 365 (1961).

c) J. A. Pople, W. G. Schneider and H. J. Bernstein, High-resolution Nuclear Magnetic Resonance, McGraw-Hill, New York, Toronto, London, 1959, p. 346.

d) C. F. Callis, J. R. Van Wazer, J. N. Shoolery and W. A. Anderson, J. Am. Chem. Soc. 79, 2719 (1957).

e) J. R. Van Wazer, C. F. Callis, J. N. Shoolery and R. C. Jones, ibid., 78, 5715 (1956).

9) J. M. Jackman, Application of Nuclear Magnetic Resonance Spectroscopy in Organic Chemistry, Pergamon Press, New York, London, Oxford, Paris, 1959.

Proposition V

Ozone is one of the more economic and specific oxidizing agents (1) and it is surprising that it is not being used more widely for the many oxidations required in organic reactions. The only major application for ozone so far has been the result of its high specificity for the carbon-carbon double bond (2). Any ozonides which may be formed in inert solvents are generally not isolated due to their relative instability and are reduced with Zn and mineral acid or hydrogen and Pt to aldehydes or ketones (3). In reactive solvents, however, like water or alcohols, ozonides do not form and one obtains the peroxides or alcoxy-peroxides by addition of solvent molecules to the intermediate peroxy zwitterion (4).

In comparison to the unsaturated carbon bond, the solvents most generally used for ozonolysis are rather inert to ozone attack. Nevertheless, they do get oxidized if no olefins are present. In particular, primary alcohols have been found to give the corresponding aldehydes and acids (5). Hydrogen peroxide is almost always detected in the reaction mixture. Secondary and tertiary alcohols have not been studied in regard to their susceptibility to ozone attack in any great detail, which is surprising in view of what is known about their ease of oxidation by other oxidiz-

ing agents. Thus, secondary alcohols are readily converted by many oxidizing agents (e. g. $K_2Cr_2O_7$ in dil. H_2SO_4, aluminum t-butoxide etc.) into ketones in good yield (6). Since ozone is reactive enough so that it does not require metal ion catalysts, it is capable of being a very "clean" oxidizing agent. Regretfully, many of its reactions are still not very well understood.

There have been very few quantitative studies to compare relative reactivities of various organic groups towards ozone. Spectroscopic data about possible intermediates formed during ozonolysis are rare (7), and more work is required to gain an understanding of the mechanism of oxidation by ozone.

In particular, I should like to propose that the reactivity of secondary alcohols with regard to ozone be investigated and that the quantitativeness of conversion of these alcohols to ketones (and maybe other products) be determined. The effects of solvents on the course of ozonization should also be studied.

With regard to the mechanism of ozone reactions with secondary alcohols several possibilities exist:

a) Ionic mechanism:

In heterolytic oxidations of alcohols two related mechanisms have been considered which are elimination reactions involving the removal of the hydrogen atom of the

C-H bond together with a pair of electrons. The first scheme resembles the base-catalysed decomposition of hydroperoxides in that the oxidant is initially attached to the oxygen atom of the alcohol, i. e. (8)

$$B: + H-\overset{|}{\underset{|}{C}}-O-Ox \longrightarrow (BH)^+ + \overset{|}{\underset{|}{C}}=O + Ox^- \quad . \qquad (1)$$

In the absence of B:, the electron movement may occur in the reverse direction as "hydride transfer", i. e.

$$Ox + H-\overset{|}{\underset{|}{C}}-O-H \longrightarrow Ox-H + \overset{|}{\underset{|}{C}}=O + H^+ \quad . \qquad (2)$$

In many reported cases these electron transfers occur within cyclic intermediates or complexes (9).

If ozonization proceeds via this heterolytic process it would follow process (2) which may be represented as

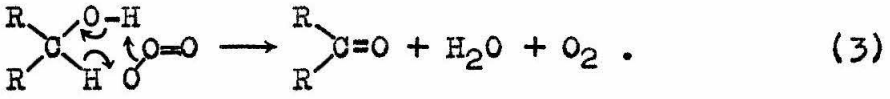

(3)

By replacing the C-H by C-D one could determine whether rupture of the C-H is involved in the rate determining step of the oxidation. Furthermore, it would be expected that the rate of reaction can be influenced by varying the nature of the R-groups. More strongly electron donating groups should favor the reaction.

If O_2 and $\rangle C=O$ can be identified in the early stages of the reaction, they may be regarded as evidence for the ionic mechanism.

b) Free radical mechanism:

It is conceivable, on the other hand, that the reaction proceeds via a free radical mechanism by abstraction of a hydrogen atom rather than a hydride ion (similar to autoxidation with O_2 (10)). The course of the reaction would then be determined by the ease with which the free radical disproportionates to give ketone by expulsion of another hydrogen atom, in relation to its reactivity toward free radical scavengers (O_2, I_2, quinones etc.) that may be added to the solution.

References

1) Application and reactions of ozone.

a) Ozone Chemistry and Technology, Advances in Chemistry Series No. 21, edited by American Chemical Society Applied Publications, American Chemical Society, Washington, D. C., 1959.

b) C. E. Thorp, Bibliography of Ozone Technology, Vol. I, "Analytical Procedures and Patent Index", Armour Research Foundation of the Illinois Institute of Technology, Technology Center, Chicago 16, Ill., 1954.

c) ibid., Vol. II, "Physical and Pharmacological Properties", 1955.

d) R. A. Worstell, J. Chem. Educ. 9, 291 (1932).

e) E. Fonrobert, Das Ozon, Enke Verlag, Stuttgart, 1916.

2) Ozone and the carbon-carbon double bond.

a) R. Criegee, loc. cit. ref. 1a) p. 133.

b) W. A. Mosher, ibid., p. 140.

c) R. Criegee, A. Kerckow and H. Zinke, Ber. 88, 1878 (1955).

d) R. Criegee and G. Lohaus, Ber. 86, 1 (1953).

e) R. Criegee, Ann. 583, 1 (1953).

f) E. Fonrobert, "Ozonide" in Methoden der Organischen Chemie, Vol. III, J. Houben, Verlag G. Thieme, Leipzig, 1930, p. 406.

g) C. Harries, Ann. 374, 288 (1910).

h) C. Harries, Ann. 343, 311 (1906).

3) Reduction of ozonides.

a) R. Pummerer and H. Richtzenhain, Ann. 529, 33 (1937).

b) F. C. Whitmore and J. M. Church, J. Am. Chem. Soc. 54, 3710 (1932).

c) F. G. Fischer, Ann. 464, 69 (1928) p. 83.

4) Addition of solvent to peroxy zwitterion.

a) R. Criegee, loc. cit. ref. 1a) p. 133.

b) N. A. Milas and J. T. Nolan, Jr., ibid., p. 136.

c) G. Lohaus, Ann. 583, 6 (1953) p. 8.

5) Primary alcohols and ozone.

a) F. G. Fischer, Ann. 476, 233 (1929).

b) loc. cit. ref. 1e) pp. 130, 155.

c) loc. cit. ref. 2g) p. 315.

d) M. Otto, Chem. Zentr. 1898, I, 307.

6) Oxydation of secondary alcohols.

a) G. O. Schenck and H. D. Becker, Angew. Chem. 70, 504 (1958).

b) E. P. Oliveto, H. Q. Smith, C. Gerold, R. Rausser and E. B. Hersberg, J. Am. Chem. Soc. 78, 1414 (1956).

c) N. Brown, M. J. Hartig, M. J. Roedel, A. W. Anderson and C. E. Schweitzer, ibid. 77, 1756 (1955).

d) N. Brown, A. W. Anderson and C. E. Schweitzer, ibid. 77, 1760 (1955).

7) Infrared spectroscopy of ozonization

a) H. C. Beachell and S. P. Nemphos, loc. cit. ref. 1a) p. 168.

b) E. Briner, ibid., p. 184.

8) W. A. Waters, Mechanism of Oxidation of Organic Compounds, J. Wiley and Sons, Inc., New York, 1964, p. 49.

9) Electron transfer within cyclic intermediates

a) D. G. Hoare and W. A. Waters, J. Chem. Soc. 1962, 965.

b) I. R. L. Barker, W. G. Overend and C. W. Rees, Chem. Ind. (London) 1961, 558.

c) C. G. Swain, R. A. Wiles and R. F. W. Bader, J. Am. Chem. Soc. 83, 1945 (1961).

d) R. Stewart and R. Van der Linden, Discussions Faraday Soc. 29, 211 (1960).

e) D. J. Cram and G. S. Hammond, Organic Chemistry, McGraw-Hill Book Co., Inc., New York, Toronto, London, 1959, p. 280.

f) P. D. Bartlett and J. D. McCollum, J. Am. Chem. Soc. 78, 1441 (1956).

10) Free radicals in autoxidation.

a) loc. cit. ref. 8) p. 6.

b) E. G. E. Hawkins, Organic Peroxides, D. Van Nostrand Co., Inc., Princeton, N. J., Toronto, New York, London, 1961, p. 355.

c) P. S. Bailey, Chem. Rev. 58, 925 (1958) p. 977.

d) R. Criegee, Fortschr. Chem. Forsch. 1, 508 (1950)

e) C. E. Frank, Chem. Rev. 46, 155 (1950).

f) E. Briner, Ch. El-Djabri and H. Paillard, Helv. Chim. Acta 21, 95 (1938).